H24/3615

MONASH UNIVERSITY
THESIS ACCEPTED IN SATISFACTION OF THE
REQUIREMENTS FOR THE DEGREE OF
DOCTOR OF PHILOSOPHY
ON..... 23 March 2004 .....
.....[redacted].....
Sec. Research Graduate School Committee

Addendum

(PhD thesis "The Behaviour of Very High Strength (VHS) Members and Welded Connections" by Mr. Hui Jiao)

- Page xix, add the following notation:

k_p^A Curvature at point A of the supplemental Figure 5.2-1 corresponding to M_p

k_p^B Curvature at point B of the supplemental Figure 5.2-1 corresponding to M_p

- Page 1, Table 1.1-1, replace "composites" by "composition
- Page 20, last paragraph, line 3, replace "0.2% proof stress … the yield stress." by the following text:

  "Since there is no yield plateau on the stress-strain curves of VHS tubes, 0.2% proof stress is adopted as the yield stress of VHS tubes according to section 14.3 of AS1391 (1991)."
- Page 34, Table 3.5-1, symbol "e_u" in column five refers to "uniform elongation"
- Page 40, Table 3.5-4, symbol "ε_u" in column three refers to "ultimate strain"
- Page 64, replace Figure 4.6-1 by the following figure

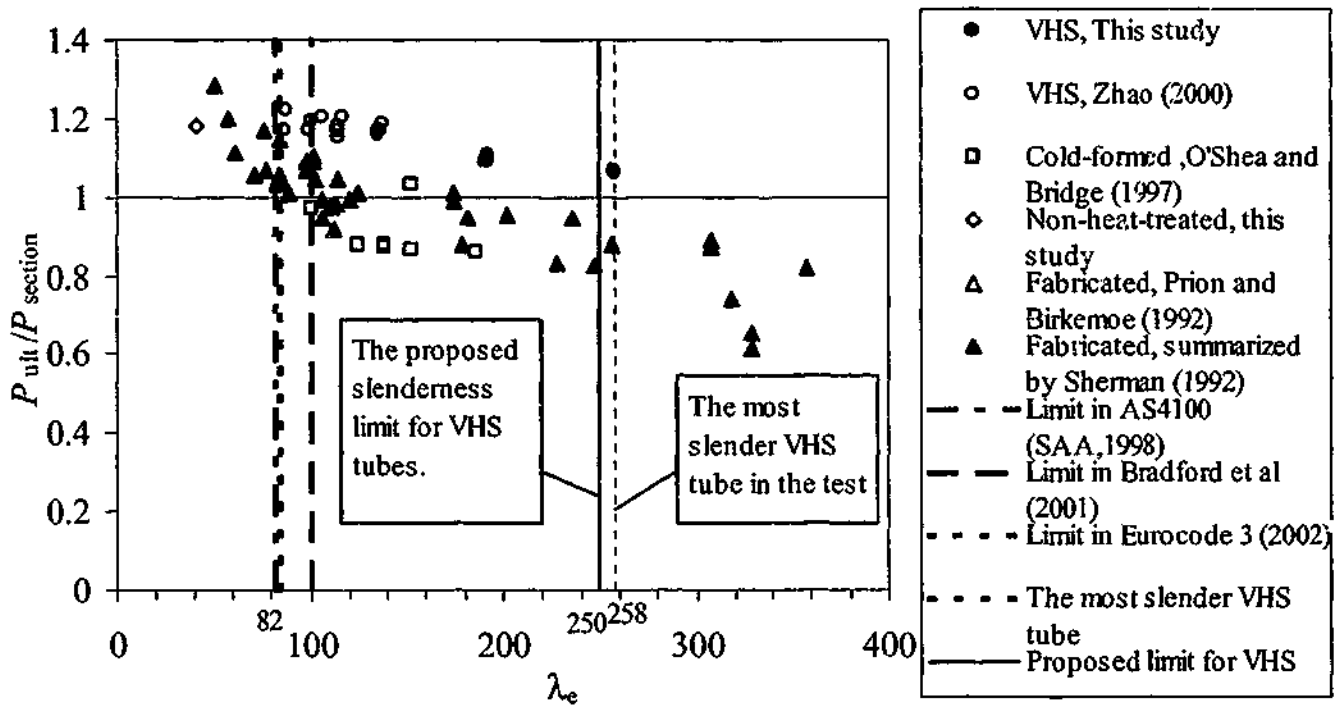

Figure 4.6-1: Element slenderness versus $P_{ult}/P_{section}$

- Page 65, line 4 to line 5, replace the sentence "According to the element …258 can be proposed" by the following text:

  "The most slender tube in the test series has an element slenderness of 258. Therefore the yield slenderness limit is at least 258. A rounded figure of 250 is

proposed in the thesis as the new limit. A value of 300 or even higher might be justified by further testing. "

- Page 65, line 9, replace "258" by "250"
- Page 65, line 9, replace "3.15" by "3.2"
- Page 65, replace Figure 4.6-2 by the following figure:

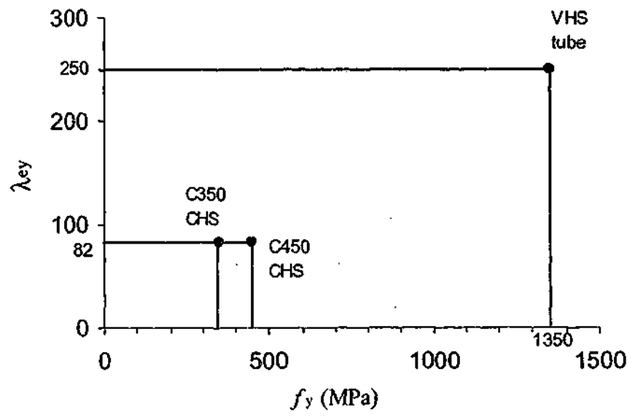

- Page 65, line 14, replace the sentence "More research is needed … rather than that (f_y/250) used in Eq.(4.1-1)." by the following text:

  "There is a knowledge gap for tubes with yield stress between 450 MPa and 1,350 MPa. Therefore, the relationship between slenderness limit and yield stress is unknown. Future test results are needed to be plotted on Figure 4.6-2 to determine the relationship between slenderness limit and yield stress. In addition to yield stress, geometrical imperfections and residual stress may affect the section slenderness. These factors may be considered for inclusion in the slenderness definition of Eq. 4.1-1 in the future."
- Page 66, line 5, replace "3.1" by "3.2"
- Page 66, Figure 4.6-3, replace "3.1" by "3.2"
- Page 67, 3rd paragraph, line 2, replace "258" by "250"
- Page 67, 3rd paragraph, line 3, replace "3.1" by "3.2"
- Page 71, section 5.2.2, 2nd paragraph, line 2, add the following text:

  "This moment-rotation relationship was first introduced by Korol and Hudoba (1972) in analyzing square hollow sections in bending. Later this section rotation definition was used by a number of researchers in analyzing square, rectangular and circular hollow sections (Hasan and Hancock 1989; Kuhlmann 1989; Stranghoener et al. 1994; Stranghoener and Sedlacek 1996)."
- Page 71, add the following figure as the supplemental Figure 5.2-1:

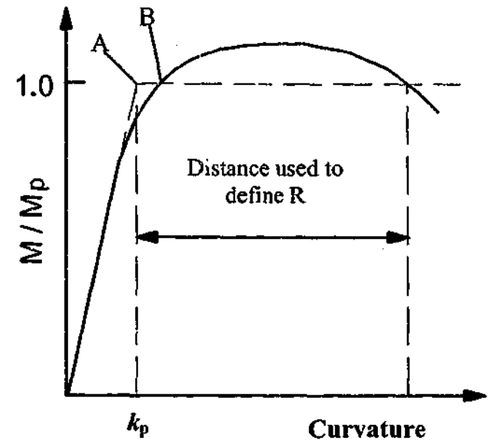

Supplemental Figure 5.2-1 M/Mp versus Curvature

- Page 72, line 13, replace "squire" by "square"
- Page 73, line 6, replace "redial" by "radial"
- Page 75, line 2, replace "The part of the specimen outside the pure bending range is treated as straight element, as observed during test." by the following text:

  "The part of the specimen outside the pure bending range is treated as straight element. This is based on casual visual observations during the test and photos in Figure 5.3-3 and Figure 5.3-5. The same treatment was taken by other researchers when deriving bending moment from pure bending test rigs (Hasan and Hancock 1989; Zhao and Hancock 1991; Cimpoeru 1992; Zhao and Hancock 1992; Stranghoener et al. 1994; Wilkinson and Hancock 1998; Zhao and Grzebieta 1999; Elchalakani et al. 2001a; 2001b; 2002a; 2002b)."
- Page 79, section 5.3.2, line 6 to line 7, delete ", were not found on tested VHS tubes,", and add the following text:

  "Localization is normally expected to occur in post-buckling deformations in shells (Rotter 1998; Teng and Rotter 2004). No special device was utilized to catch the wave-like multiple ripples before the collapse of the VHS tube. It is likely that very small wave-like displacements variations happened before the collapse of the tube. However they were not observed because their life was very limited."
- Page 80, above Table 5.3-2, add the following text: "The ratio of M_u/M_p versus element slenderness is shown in the supplemental Fig 5.3-1. It can be seen from the supplemental Fig 5.3-1 that the actual slenderness limit could be about 240 when M_p is attained according to the regression line of the tested VHS tubes. A rounded slenderness limit of 210 can be proposed for VHS tubes at the bending

moment of *Mp* based on a 10% reduction to the projected value of 240. Further testing is needed to justify this limit."

- Page 80, add the following supplemental Fig 5.3-1:

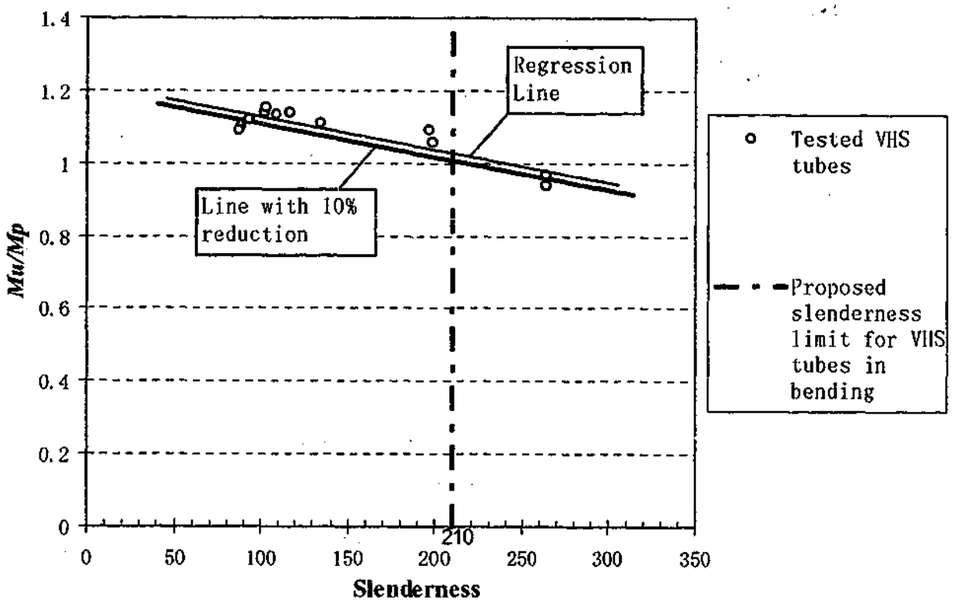

Supplemental Fig 5.3-1: M_u/M_p versus Element slenderness

- Page 82, line 5, replace "from the moment-curvature curves)" by "from point A rather than point B on the moment-curvature curves as shown in the supplemental Figure 5.2-1)."
- Page 82, line 7 to line 9, replace "It can be seen that... ovalisation on the tube section." by the following text:

"The measured curvature k_p is smaller than the calculated k_p'. This may be due to the influence of the section ovalisation during bending, which may affect the measurement of the inclinometers. Table 5.3-4 shows the comparison of k_p and k_p'. The difference between k_p and k_p' is 9.6% on average."

- Page 82, line 9, replace the last sentence "The normalized *M-k* curves... k_p'is used." by the following text:

"The normalized moment-curvatures curves are shown in Figure 5.3-7 where the calculated curvature k_p' is used in Figure 5.3-7 (a) and the measured curvature k_p is used in Figure 5.3-7 (b). Due to the measured k_p was smaller than the calculated k_p', the elastic stiffness of all sections appears to be slightly higher than the straight line drawn through the origin and the point (k_p/k_p'=1; M/M_p=1). The situation seems better when k/k_p is used as shown in Figure 5.3-7 (b) (Specimens BS8 and BS12 are not included, since M_p was not reached and the value of k_p is not applicable)."

- Page 82, below Figure 5.3-6, add the following text, table and figure:

"The moment versus curvature curves for all specimens (except BS8 and BS12) are plotted in the supplemental Fig 5.3-2 where the curvatures at point A and point B corresponding M_p are also illustrated for BS4 and BS11. It can be seen from the supplemental Fig 5.3-2 that the curvature in the plastic range for some specimens is several times larger than the curvature in the elastic range. The curvatures at the plastic moment (M_p) corresponding to point A (k_p^A) and point B (k_p^B) of the tested specimens are listed in the Supplemental Table 5.3-5. The ratio of k_p^B to k_p^A is 1.34 on average."

Supplemental Table 5.3-1: Measured curvatures at point A and point B

Specimen Label	κ_p^A (1/m)	κ_p^B (1/m)	κ_p^B/κ_p^A
BS1	0.46	0.49	1.065
BS2	0.49	0.65	1.327
BS3	0.53	0.74	1.396
BS4	0.47	0.61	1.298
BS5	0.44	0.54	1.227
BS6	0.42	0.56	1.333
BS7	0.29	0.38	1.310
BS9	0.53	0.73	1.377
BS10	0.41	0.56	1.366
BS11	0.27	0.46	1.704
Mean			1.340
COV			0.073

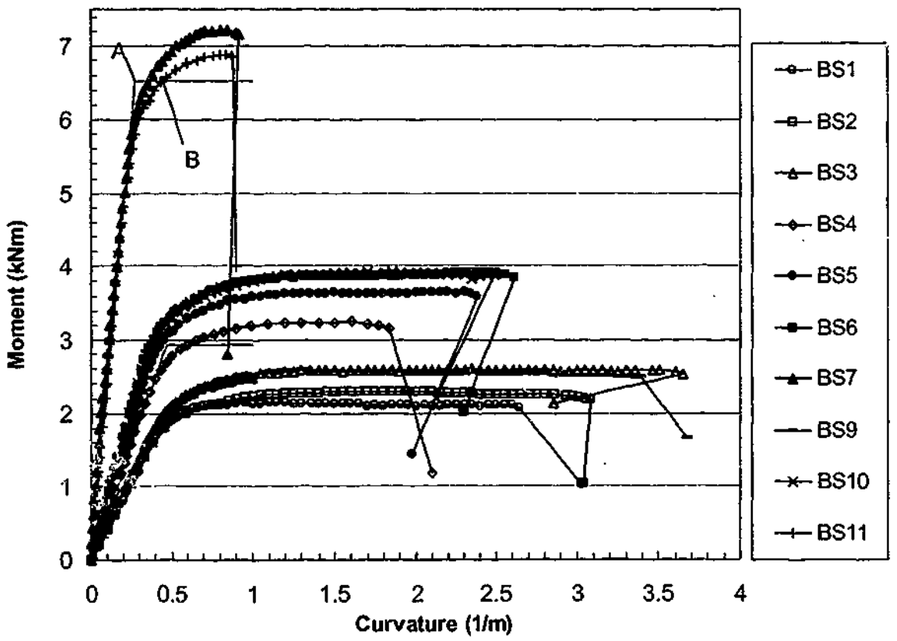

Supplemental Fig 5.3-2 Moment-curvature curves of VHS tubes

- Page 83, replace Figure 5.3-7 by the following two figures (Figure 5.3-7 (a) and Figure 5.3-7 (b)):

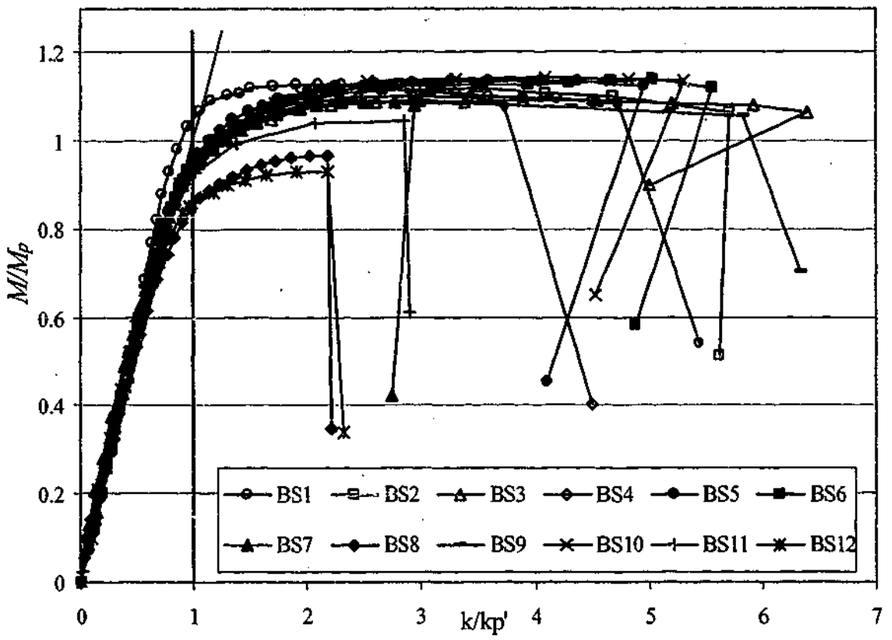

Figure 5.3-7 (a): Curves of M/M_p versus k/k_p'

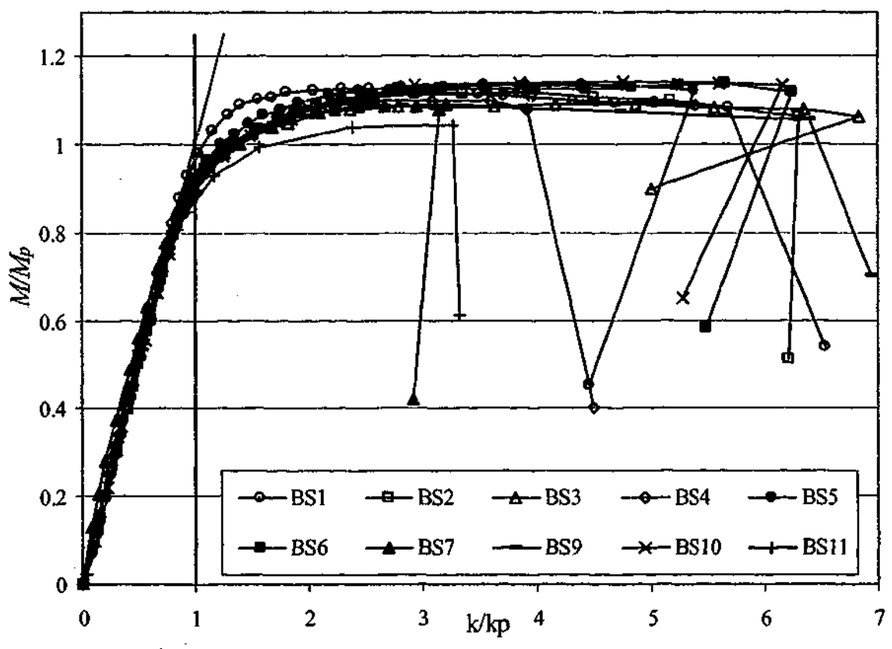

Figure 5.3-7 (b): Curves of M/M_p versus k/k_p

- Page 83, replace Table 5.3-4 by the following table:

Specimen Label	κ_p (1/m)	κ_p' (1/m)	κ_u (1/m)	κ_u/κ_p-1	$\kappa_u/\kappa_p'-1$	$(\kappa_p'-\kappa_p)/\kappa_p'$ (%)
BS1	0.46	0.56	2.64	4.73	3.74	17.4
BS2	0.49	0.54	3.07	5.26	4.65	9.6
BS3	0.53	0.57	3.65	5.89	5.38	7.3
BS4	0.47	0.49	1.84	2.91	2.77	3.6
BS5	0.44	0.48	2.38	4.41	4.00	7.5
BS6	0.42	0.47	2.61	5.22	4.58	10.4
BS7	0.29	0.31	0.91	2.15	1.93	6.9
BS8	-	0.24	0.52	0.00	0.00	
BS9	0.53	0.58	3.39	5.40	4.89	7.9
BS10	0.41	0.47	2.49	5.07	4.32	12.4
BS11	0.27	0.31	0.88	2.26	1.82	13.4
BS12	-	0.24	0.52	0.00	0.00	
Mean						9.6
COV						0.387

- Page 84, replace Figure 5.4-1 by the following figure:

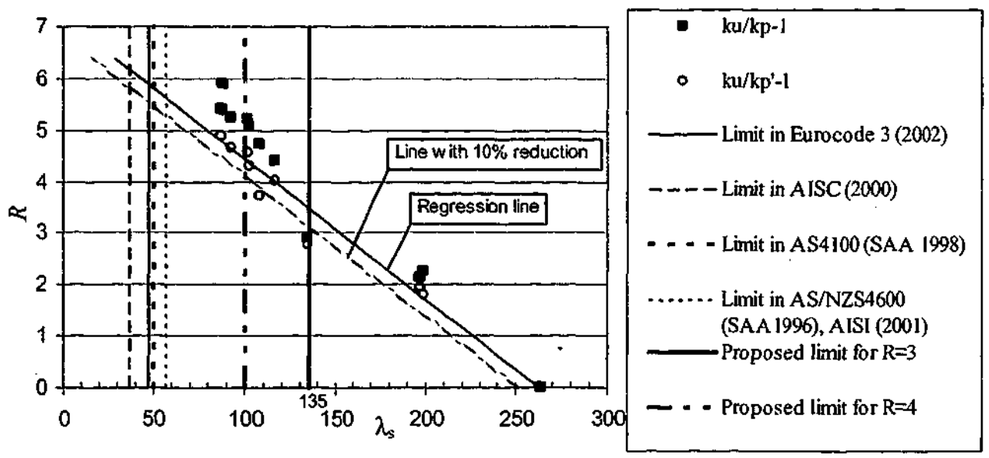

Figure 5.4-1: The rotation capacity R versus λ_s

- Page 85, line 2, replace "The plastic slenderness limits of 117 and 153 were obtained at R=4 and R=3." by the following text:

  "A reduction of 10% is applied to the regression line. The rounded plastic slenderness limits of 100 and 135 at the rotation capacity of 4 and 3 are obtained. The proposed slenderness limits are shown in Figure 5.4-1."

- Page 85, replace Figure 5.4-2 by the following figure:

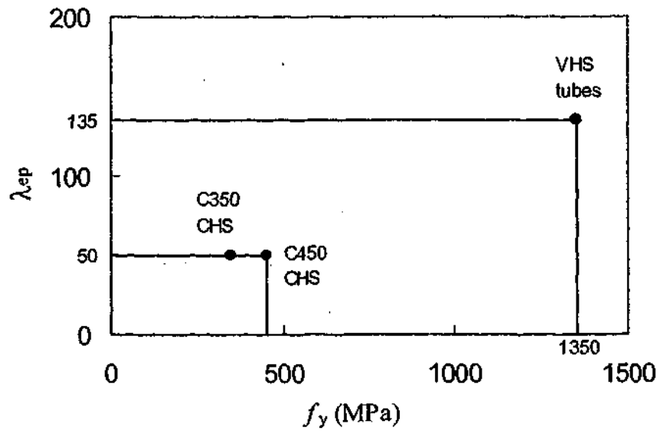

- Page 86, in the legend of Figure 5.4-3, replace "153" by "135", replace "117" by "110"
- Page 87, line 2, replace "117" by "110"
- Page 87, line 3, replace "153" by "135"
- Page 87, section 5.5, line 3, replace the sentence "The yield moment was achieved … and 85 in Eurocode 3 (2002)." by the following text:

"The yield moment was achieved for all the tested VHS tubes. A rounded yield slenderness limit of 260 can be proposed, which is very close to the limit in AISC (2000), AS/NZS4600(SAA 1996) and AISI (2001) when f_y of 1350 MPa is used, but much higher than the limit of 120 specified in AS4100 (SAA 1998) and 85 in Eurocode 3 (2002). According to the trend in Figure 5.5-1, the actual yield slenderness limit for VHS tubes in bending could be in the region around 370. Further tests are needed to adjust this value."

- Page 87, section 5.5, line 8, replace "258" by "250"

- Page 88, replace Figure 5.5-1 by the following figure:

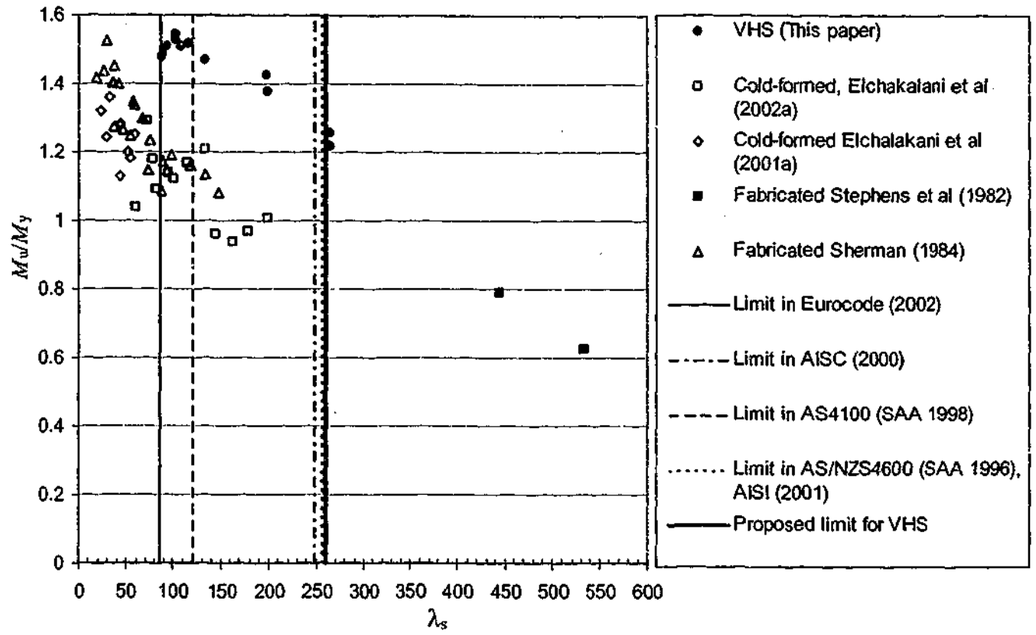

Figure 5.5-1: Ratio of the ultimate moment to the yield moment versus λ_s

- Page 89, line 9, replace "117" by "110"
- Page 89, line 9, replace "153" by "135"
- Page 89, line 9, replace "197" by "210"
- Page 89, last line, replace "264" by "260"
- Page 160, 5th dot point, line 1, replace "258" by "250"
- Page 160, 5th dot point, line 2, replace "3.1" by "3.2"
- Page 161, 1st dot point, replace "198" by "210"
- Page 161, 2nd dot point, line 1, replace "117" by "110"
- Page 161, 2nd dot point, line 1, replace "153" by "135"
- Page 161, 3rd dot point, line 1, replace "264" by "260"
- Page 180, line 23, add the following reference:

Teng, J. G. and Rotter, J. M. (2004). "*Buckling of Thin Metal Shells*". London, Spon Press.

THE BEHAVIOUR OF VERY HIGH STRENGTH (VHS) MEMBERS AND WELDED CONNECTIONS

Hui Jiao

B. Eng., M. Eng.

Thesis

Presented for the Degree of
Doctor of Philosophy

Department of Civil Engineering
Monash University
Melbourne, Australia
2003

ABSTRACT

The main aim of this thesis is to investigate the strength, ductility and weldability of very high strength (VHS) circular steel tubes in order to access the suitability of VHS tubes as structural steel hollow section members. Extensive experiments were conducted in tension, compression and in bending. Tests on butt-welded and transverse fillet-welded VHS tubes were also carried out.

There has been an increasing need to use high strength steels in the automotive industry and in other engineering applications around the world. However some problems may exist in the application of high strength steels, including low material ductility and HAZ softening in welded connections.

Tension tests were conducted to investigate the strength and ductility of VHS tubes. Both tensile coupons and full section tubes were tested. The material ductility of VHS circular steel tubes was examined mainly in terms of the ultimate strength to the yield stress ratio and the percentage elongation. The fracture-to-ultimate load ratio and the ultimate strain to the yield strain ratio were also examined. During the tests, different failure modes were observed for VHS and non-heat-treated (NHT) tubes. Although the failure of the VHS tensile coupons developed along a single shear band, multi-shear bands were observed in the fracture zone of full section VHS tubes. The ultimate strength to the yield stress ratio of VHS tubes was found to be greater than some high strength cold-formed hollow sections and sheet steels, such as C450 and G500. The shear band failure mode was compared with that of other thin sheet steels.

Compression tests were performed on stub columns of VHS tubes. The out-of straightness of stub columns was measured with a feeler gauge. The residual stress of VHS tubes was measured by the slicing method. The aim of these measurements was to examine their influence on the buckling and strength of VHS tubes in compression. The out-of-straightness was found about $L/6800$ on average, where L was the length of the stub column. Both VHS tubes and non-heat-treated tubes (NHT) had a similar level of geometrical imperfections. The measured residual stress was found approximately 4% on average of the yield stress, with the outside surface in compression and the inside surface in tension. The residual stress pattern obtained for

non-heat-treated tubes was very different from that of VHS tubes. Eight stub columns were tested with the element slenderness ratio ranging from 135 to 258. New element slenderness limit (λ_{ey}) of 258 and non-dimensional local buckling parameter limit of 3.1 were proposed for VHS tubes. The very large value of λ_{ey} was obtained partly because of the very large yield stress used in the definition of element slenderness and partly because of the very low residual stress in the section. The stub columns of non-heated-treated (NHT) tubes were also tested in the same manner. The results were compared with those of the VHS tubes.

The bending behaviour of VHS tubes was studied under 4-point-bending and pure bending tests. A total of 12 specimens, with the nominal diameter ranging from 31.8 to 75mm and the tube thickness between 1.6 to 2.0mm, were tested. Large bending deflection was achieved for VHS tubes with the diameter to thickness ratio up to 24. Full plastic moment was reached for tubes with the section slenderness of 197 or less. New plastic slenderness limits of 117 and 153 were proposed based on the beam plastic rotation capacity of 4 and 3. A yield slenderness limit of 264 was proposed for VHS tubes.

Tension tests were carried out to examine the tension capacity of VHS tubes after welding. Two types of welded connections were used in the study: (1) complete penetration butt-welded VHS tubes, (2) VHS tubes fillet welded to a steel plate along the whole perimeter of VHS tubes. Both butt welded connections and transverse fillet welded connections failed in the heat-affected-zone (HAZ). The failure modes were compared with those of welded cold-formed C350 and C450 square hollow sections. Significant strength reduction was observed in HAZ compared with the strength of VHS tubes. A strength reduction factor was proposed to modify the existing design rules in Australian standards and American specifications for VHS tubes. The FOSM (First Order Second Moment) reliability analysis method was used to calibrate the reduction factor. The issue of matching between the base metal and weld metal was also discussed.

The CFRP (Carbon Fibre Reinforced Plastics) strengthening technique was used to recover the strength loss in HAZ of butt-welded VHS tubes. Three types of epoxy resins with different lap shear strength were adopted. Tests were conducted to

determine the lap shear strength between CFRP and VHS steel tube. A total of twenty-one butt-welded VHS tubes strengthened with CFRP were tested in axial tension. Three kinds of failure modes, i.e. adhesive failure, fibre tear and mixed failure of CFRP break and adhesive failure were observed. The suitable epoxy adhesive for strengthening VHS tubes was recommended. A significant strength increase was achieved using CFRP-epoxy strengthening technique. A theoretical model was developed to estimate the load carrying capacity of butt-welded VHS tubes strengthened using CFRP.

A number of future research topics were identified, including the shear band formation of VHS tubes during axial tension, finite element analysis of VHS tubes in compression and in bending, ovalisation simulation of VHS tubes, post-weld-heat-treatment of welded VHS tubes and the load transfer mechanism of CFRP strengthened VHS tubes.

The main conclusions of this thesis are: VHS tubes satisfy the ductility requirements specified in AS/NZS4600 for thin-walled hollow sections in terms of the percentage elongation and the ultimate strength to the yield stress ratio. In addition, VHS tubes can be connected by welding method, however, a strength reduction factor needs to be applied when using the design rules in current steel design standards. VHS tubes have prospective potential to be used as structural steel hollow section members in either normal buildings or temporary structures for the purpose of emergency or in military applications.

PREFACE

This thesis is submitted to Monash University, Melbourne, Australia, for the degree of Doctor of Philosophy. The work described herein was carried out by the candidate in the Department of Civil Engineering, Clayton Campus at Monash University. The period of candidature was from February 2000 to August 2003. The candidate was supervised by Professor Xiao-Ling Zhao.

Under the Regulations of Monash University relating to the requirements for the Degree of Doctor of Philosophy, the candidate declares that the work presented in this thesis contains no material that has been accepted for the award of any other degree at another university or institution. To the candidate's best knowledge, the thesis contains no work written or published by another person, except where due reference is made in the text.

During the candidature, nine papers, based on the work presented in this thesis, have been jointly written with Professor Xiao-Ling Zhao. They are:

Journal Papers:

Jiao, H. and Zhao, X. L. (2001) "Material ductility of very high strength (VHS) circular steel tubes in tension", *Thin-Walled Structures*, 39(11): 887-906.

Jiao, H. and Zhao, X. L. (2002) "Imperfection, residual stress and yield slenderness limit of very high strength (VHS) circular steel tubes", *Journal of Constructional Steel Research*, 59(2): 233-249.

Jiao, H. and Zhao, X. L. (2003) "Tension capacity of very high strength (VHS) circular steel tubes after welding", *Advances in Structural Engineering-An International Journal*, (under review).

Jiao, H. and Zhao, X. L. (2003) "Section slenderness limits of very high strength circular steel tubes in bending", *Thin-Walled Structures*, (under review).

Conference Papers

Jiao, H. and Zhao, X. L. (2001) "Strength of butt welds and transverse fillet welds in very high strength (VHS) circular steel tubes". *The Six Pacific Steel Structure Conference*, Beijing, China. 775-780.

Jiao, H. and Zhao, X. L. (2002) "Design of butt welds and transverse fillet welds in very high strength (VHS®) circular steel tubes". *17th Australian Conference on the Mechanics of Structures and Materials*, Gold Coast, Queensland, Australia. 583-587.

Jiao, H. and Zhao, X. L. (2002) "Shear band orientation of very high strength (VHS) circular steel tubes". *The Third Australasian Congress on Applied Mechanics*, Sydney, Australia.

Jiao, H. and Zhao, X. L. (2002) "Strengthening tests of butt-welded very high strength (VHS) circular steel tubes". *IABSE Symposium (The International Association for Bridge and Structural Engineering)*, 11-13 September, Melbourne, Australia.

Jiao, H. and Zhao, X. L. (2003) "Tests of very high strength (VHS) circular steel tubes in bending". *Advances in structures, ASSCCA'03*, G. J. Hancock, M. A. Bradford, T. Wilkinson, B. Uy and K. J. R. Rasmussen (eds.), Sydney, Australia, A.A. Balkema Publishers. 157-161.

[redacted]

Hui Jiao

August 2003

ACKNOWLEDGMENTS

I am sincerely grateful to my supervisor, Professor Xiao-Ling Zhao, for his expert advice, clear guidance and invaluable support throughout the candidature. I thank him for his constant encouragement and assistance both on and off campus during my candidature at Monash University.

I am also grateful to those who provided financial support to this project. My main scholarship was a Monash Graduate Scholarship (MGS) supplemented by a Monash Departmental Scholarship (MDS). The project was sponsored by Australian Research Council and OneSteel Market Mills, Australia.

Test specimens were provided by OneSteel Market Mills, Australia. Thanks are due to Mr. Tony Gunn for the arrangement of visiting the workshop where VHS tubes are produced and for the delivery of VHS tubes. Thanks to Mr. Hayden Dagg for his comments and information about the project. Thanks are also due to Mr. Paul Calcinai at Crossline Engineering Pty. Ltd. for welding VHS specimens and to Mr. Fred Cassis at Vantico Pty. Ltd. for supplying epoxy samples.

I am indebted to all workshop staff for their assistance in performing the experiments. Thanks are due to the manager of the Strong Floor Laboratory, Mr. Graeme Rundle, for his arrangement of using the testing facilities. Thanks are given to Mr. Roger Doulis and Mr. Kevin Nievaart for setting up the test machine and providing suggestions on the operation of Baldwin universal testing machine. I am also grateful to Mr. Roy Goswell for making measurement devices. Lots of thanks to Mr. Don McCarthy for the assistance in editing photos and capturing video frames.

Thanks are due to other staff members in Civil Engineering Department and Engineering Faculty, especially Mrs. Jenny Manson, who has provided assistance since the beginning of my PhD enrolment. I am also grateful to Mrs. Jane Moodie for helping me write English in his thesis. Mr. Rob Alexander created some good quality diagrams for the published papers and some figures in this thesis.

I thank all my friends and colleagues for their encouragement and friendship during my research. Thanks are given to Prof. Greg Hancock, Prof. Don Sherman, Prof. Mark Bradford, Prof. Wai-Fah Chen and Prof. Jin-Guang Teng for provision of references on this research topic. Thanks are due to Prof. Russell Bridge and Mr. Mohamed Elchalakani for their comments on the published papers. I am also grateful to the visiting scholar, Associate Professor Tao Zhong from FuZhou University, China, for his suggestions and comments on the finite element analysis of VHS tubes.

I would like to give my sincerest gratitude and greatest respect to my father, ZhongTang Jiao, who passed away during my application for PhD candidature. His hope, support and encouragement have been with me to overcome any difficulties in my life. He would have been pleased and excited about having the first doctor in the family. I thank my mother, ChuanXian Meng, my brother, Wei Jiao, for their love and encouragement during my candidature.

To my wife, XiaoLin Li, thank you for your assistance and support of my study. I owe a lot to my daughter, ZiWei, and my little son, Frank. Thank you for your patience and those weekends that should have been spent on playgrounds or in swimming pools during the last three and a half years.

[redacted]

Hui Jiao

August 2003

CONTENTS

NOTATION

The following symbols are used in this thesis, and are defined when they first appear in the text. The interpretation of a symbol will be evident from the context if more than one meaning is assigned to the symbol.

A	Cross-sectional area of full section VHS or NHT steel tube
A_c	Cross-sectional area of tensile coupon
b	Width of tensile coupon
d	Diameter of the support in 4-point-bending
D	Outside diameter of VHS or NHT tube
D_l, D_s	Diameter of deformed tube in bending
d_e	Effective diameter of circular steel tube
DL	Dead load
D_m	Mean dead load
D_n	Nominal dead load
e	Axial deflection
E	Young's modulus of elasticity
e_0	Percentage elongation over $5.65\sqrt{A}$ mm gauge length including fracture
e_{200}	Percentage elongation over 200mm gauge length including fracture
e_{30}	Percentage elongation over 30mm gauge length including fracture
e_{50}	Percentage elongation over 50mm gauge length including fracture
e_u	Percentage elongation over 50mm gauge length excluding fracture
f_{HAZ}	Ultimate strength of heat affected zone of VHS steel tube
F_m, M_m, P_m	Mean value of dimensionless random variable reflecting uncertainty in "fabrication", "material strength", and "professional model"
f_u	Ultimate tensile strength
f_{un}	Nominal ultimate tensile strength
f_y	0.2% proof stress of full section tube
f_{yn}	Nominal yield stress
f_{yt}	0.2% proof stress of tensile coupon

I	Second moment of area
k_f	Form factor in AS4100
L	Overall length of specimen
L'	Distance between the loading point and the support in 4-point-bending test
L_0	Original gauge length
l_1	Shorter bond length in the test of shear strength between CFRP and VHS
l_2	Longer bond length in the test of shear strength between CFRP and VHS
L_c	Distance from the maximum out-of-straightness to the near end of the tube
l_e	Effective CFRP bond length
LL	Live load
L_m	Mean live load
L_n	Nominal live load
L_r	Gauge length for imperfection measurement
l_o	Applied CFRP bond length (from one end of CFRP to the center of the weld)
M	Bending moment
M_p	Plastic bending moment
M_u	Ultimate bending moment
M_y	Yield bending moment
n	Number of CFRP layers
N_s	Nominal section capacity in compression
P	Axial load
P'	Load perpendicular to the beam in 4-point-bending
P_{CFRP}	Load carried by CFRP composite
$P_{CFRP\text{-}bonded}$	Load carrying capacity of CFRP strengthened welded connections
P_f	Fracture load in tensile test
P_{HAZ}	Load carrying capacity of HAZ in a welded connection
P_{max}	Maximum load
$P_{section}$	Full effective section capacity
P_{ult}	Measured ultimate load
P_{VHS}	Load carrying capacity of VHS steel member
$P_{VHS\text{-}d}$	Nominal design capacity of VHS steel member ($0.85 f_u A_s$)

$P_{VHS\text{-}u}$	Ultimate load carrying capacity of VHS steel member ($f_u A_s$)
$P_{VHS\text{-}y}$	Load carrying capacity of VHS steel member at yielding ($f_y A_s$)
r	Tube radius
Q_m	Mean load
R	Rotation capacity
R_m	Mean resistance
R_n	Nominal resistance
S	Plastic section modulus
t	Wall thickness of VHS or NHT tubes
U	Load combination
V	Lap shear strength between CFRP and VHS steel
V_D	Coefficient of variation of dead load
V_e	Effective lap shear strength between CFRP and VHS steel with the effective CFRP bond length
V_F, V_M, V_p	Coefficient of variation of dimensionless random variable reflecting uncertainty in "fabrication", "material strength", and "professional model"
V_L	Coefficient of variation of live load
V_Q	Coefficient of variation of load
V_R	Coefficient of variation of resistance
Z	Elastic section modulus
α	Non-dimensional local buckling parameter
α_c	Non-dimensional local buckling parameter limit
β	Reliability index
$\beta_{0.25}$	Reliability Index at $D_n/(D_n + L_n)$ of 0.25
ΔW_o	Measured imperfection
ΔD	Difference in tube diameter of ovalled tube in bending
ε_u	Ultimate strain corresponding to the ultimate strength
ε_y	Yield strain corresponding to the yield stress
Φ	Capacity factor
γ_D, γ_L	Dead load and live load factors
κ	Tube curvature

κ_l	Tube limit curvature
κ_p	Tube curvature at the plastic moment during test
$\kappa_{p'}$	Calculated tube curvature at the plastic moment
κ_u	Tube curvature at the local buckling
λ	Section slenderness
λ_e	Element slenderness
λ_{ep}	Plastic section slenderness limit
λ_{ey}	Element yield slenderness limit
μ	Maximum initial out-of-straightness
θ	Angle at the loading point in 4-point-bending
θ_1, θ_2	Measured angles of the inclinometers
θ_u	Beam rotation angle at the local buckling
θ_y	Beam rotation angle at the yield moment
ρ	Tube bending radius
σ_{rs}	Residual stress
ψ	Reduction factor in the design of welded VHS tubes

Chapter 1

INTRODUCTION

1.1 BACKGROUND

There has been an increasing demand in automotive and building industries for steel members that are light-weight, high-strength, and with sufficient ductility. High strength cold-formed thin-walled steels have been widely used today such as C450 RHS (nominal yield stress f_{yn}=450MPa) (Zhao and Hancock 1991), DuraGal RHS (f_{yn}=450MPa) (Zhao and Mahendran 1998), G500 (f_{yn}=500MPa) and G550 (f_{yn}=550MPa) (Rogers and Hancock 1997). Other steels with yield stress over 600MPa have also been introduced, such as Bisalloy 80 steel (f_{yn}=650MPa) in Australia (Rasmussen and Hancock 1992) and 700Q steel (f_{yn}=700MPa) in Canada (Sivakumaran and Yuan 1998).

The very high strength (VHS®) circular steel tubes have been produced by OneSteel Market Mills, Australia since the late 1990s. VHS tube is a quenched and tempered circular hollow section. It has a yield stress of around 1350MPa and ultimate strength of 1500MPa (Zhao 2000). The high strength property of VHS tubes is achieved due to both the chemical composites and the production process.

According to the chemical composites and the production process, VHS tube may be classified as quenched and tempered high strength low alloy steel. Its chemical composites consist of minor addition of alloy elements that are shown in Table 1.1-1.

Table 1.1-1: Chemical composites of VHS tube (%)

C	P	Mn	Si	S	Ni	Cr	Mo	Cu	Al	Ti	Nb	V
0.2	0.012-0.019	1.08-1.11	0.2	0.04-0.008	0.018-0.023	0.021-0.025	0.19-0.21	0.008-0.26	0.029-0.03	0.019-0.023	0.001-0.004	0.003-0.005

The chemical composite values shown in Table 1.1-1 were taken from actual tests. Therefore they are typical values instead of minimum to maximum. The range in values represents that different amounts of alloy elements were put in tubes with different thickness in order to achieve the same properties.

VHS tubes are produced from sheet steel coils. Firstly, the steel sheets are cold-formed into circular steel tubes. The seams are formed by electric resistance welding method. Then the cold-formed tubes are heat treated by elevating the temperature to 950°C, quenching the steel in 20°C cold water, followed by tempering at 230°C for 15 minutes.

Currently VHS tubes are mainly used in automotive industry as door intrusion beams, stabiliser bars, drive shafts, axles and other automotive components. According to the manufacturer's report (BHP Steel 2002), the advantages of VHS tubes over traditional steel elements are:

- VHS tubes can absorb more crash energy per kilogram, therefore to provide additional protection for vehicle occupants.
- The low weight and high strength allow vehicle weight to be reduced, therefore to make vehicles energy efficient and environment protective due to low vehicle emissions.

VHS tubes may also have some advantages over traditional structural steel members in civil engineering due to the high strength and low weight properties. For example, the section load carrying capacity can be increased without increasing the section dimensions, a saving on material costs. The financial benefits can also be realized through reduced transport and lifting costs. The reduced dimension or material thickness can also save the welding costs. The structural foundation costs may be reduced due to lower dead weight of steel structures.

Although VHS tubes may bring these financial benefits to civil engineering projects, no application of VHS tubes can be found in other industries except those used in automotive industry today. This may be due to the ductility concern of VHS tubes, since it is generally believed that the higher the strength the lower the ductility. Another concern is the weldability of VHS tubes. The heat-affected-zone (HAZ)

softening might be a problem in welding of high strength steels. Little research can be found on very high strength steels.

1.2 OBJECTIVES OF THE THESIS

This research project aims to investigate the strength, ductility and weldability of VHS tubes in order to access the suitability of VHS tubes to be used as structural steel hollow section members. Detailed objectives are:

1) To review the application and development of high strength steels;
2) To examine the ductility of very high strength (VHS) circular steel tubes in terms of the percentage elongation and the ultimate strength to yield stress ratio. To compare the ductility of VHS tubes with other high strength traditional structural steel members, such as high strength cold-formed steel members;
3) To investigate the section capacity and yield slenderness limit of VHS tubes subject to compression load. To examine the geometrical imperfection and the residual stresses of VHS tubes;
4) To study the bending behaviour of VHS tubes. To examine the yield and plastic slenderness limits of VHS tubes in pure bending;
5) To investigate the weldability of VHS tubes. To examine the tension capacity of VHS tubes after welding. To provide design reference for welded connection of VHS tubes based on current steel design standards;
6) To apply feasible strengthening techniques suitable for strengthening steel structures on welded VHS tubes if HAZ softening exists on welded VHS tubes.
7) To identify topics and provide recommendations on further research of VHS tubes

1.3 OUTLINE OF THE THESIS

The main body of this thesis consists of nine Chapters. The following tasks have been carried out in each individual Chapter to address the objectives of this research project:

Chapter 2: Development of high strength steel

- Provide a simple classification of high strength steels;
- Review historical development and application of high strength steels;
- Identify problems related to application of high strength steels.

Chapter 3: VHS tubes in tension

- Review ductility criteria of steels in steel design standards;
- Examine the failure mode and load carrying capacity of VHS tensile coupon specimens;
- Study the failure mode and load carrying capacity of full section VHS tubes;
- Examine the ductility of VHS tubes in terms of the percentage elongation and the ultimate strength to yield strength ratio;
- Discuss related factors that may affect the shear band orientation of VHS tubes.

Chapter 4: VHS tubes in compression

- Review the geometrical imperfection and residual stress measurement methods;
- Examine the geometrical imperfection and residual stress measurement of VHS tubes;
- Study the failure mode, section capacity and element slenderness limit of VHS tubes through stub column tests;

Chapter 5: VHS tubes in bending

- Review the tests of circular steel tubes in bending; introduce the rotation capacity and ovalisation of circular hollow sections;
- Discuss the failure mode and bending capacity of VHS tubes in pure bending;
- Determine the plastic slenderness limit of VHS tubes in bending;
- Determine the yield slenderness limit of VHS tubes in bending.

Chapter 6: Butt-welded and fillet-welded VHS tubes

- Determine the welding procedures of welded VHS tubes;
- Examine the failure mode and tension capacity of complete penetration butt-welded VHS tubes;
- Examine the failure mode and tension capacity of fillet-welded T-connections of VHS tubes;
- Provide design reference for design of complete penetration butt-welded and fillet-welded VHS tubes;
- Discuss the issue of matching strength of weld metal;

Chapter 7: CFRP strengthened butt-welded VHS tubes

- Review CFRP application on steel structures;
- Study the lap shear strength between CFRP and VHS tubes;
- Examine the failure mode and load carrying capacity of CFRP strengthened butt-welded VHS tubes;
- Study the effective bond length and provide a theoretical model to predict the load carrying capacity of CFRP strengthened VHS tubes;

Chapter 8: Recommended future work

- Simulate the shear band formation of VHS tubes in tension;
- Simulate the behaviour of VHS tubes in compression and in bending;

- Simulate the ovalisation of VHS tubes in bending;
- Investigate the method of post-weld-heat-treatment on welded VHS tubes;
- Study the effective bond length of CFRP strengthened VHS tubes.

Chapter 9 Conclusions

- Outline the conclusions obtained from the investigations in each Chapter;
- Summarize the topics recommended for further research on VHS tubes.

Chapter 2

DEVELOPMENT OF HIGH STRENGTH STEELS

In the history of high strength steels development, different methods have been used to enhance the strength of steels. These methods may include chemical processes, such as adding carbon or other alloy elements to plain steels, or physical processes, such as cold-forming or heat-treating. This Chapter briefly reviews the development history and engineering applications of high strength steels

2.1 CLASSIFICATION OF HIGH STRENGTH STEELS

2.1.1 Introduction

With the development of metallurgical technology over the last fifty years, the strength in high strength steels has dramatically increased. One hundred years ago, high strength steels were developed based on tensile strength alone, whereas today high strength steels are developed based on the combined consideration of strength, ductility, weldability and formability. In this development process, plain carbon steels, high strength low alloy steels and quenched and tempered high strength steels are the most important categories.

2.1.2 Plain Carbon Steels

Among the broad variety of steels, carbon steel is the most commonly used. In U.S., the traditional constructional steel for bridges and buildings before 1960 was low carbon steels that had a yield stress of about 230 MPa. In 1960, ASTM A36 carbon steel that had a yield stress of 250 MPa and a tensile strength of 400 to 550 MPa was introduced. It was used as a common structural steel until the 1970s (Fletcher 1979). The strength of carbon steels depends on the carbon content: the more carbon in steel,

the higher the strength. However the steel properties of ductility, toughness and weldability deteriorate rapidly as the carbon content of the steel is increased (Korchynsky 1984). Therefore, in order to maintain a balanced combination of these properties, the carbon content must be reduced. Thus, the strength of steel is very much restricted. The carbon content in the current ASTM standard (ASTM 2001a) is limited to a maximum of 0.29%.

2.1.3 High Strength Low Alloy (HSLA) Steels

HSLA sheet steels have been produced since the 1950s. They are low carbon steels modified with a small addition of alloy elements. Hot-rolled HSLA steels can have a yield stress up to 552 MPa. Cold rolled HSLA steels may have higher yield stress but lower ductility. HSLA steels can be produced as bars, sheets, plates, structural shapes and tubular sections using conventional cold-forming process.

2.1.4 Quenched and Tempered High Strength Steels

Quenching and tempering is a common practice to raise the strength levels of steels in combination with optimum ductility (Lankford et al. 1985). During the quenching process, martensite is formed in steels. Martensite is a very strong phase but normally it is very brittle. Therefore it is necessary to modify the mechanical properties by tempering the steel in a normal temperature range between 150-700°C (Honeycombe and Bhadeshia 1995). Most of the plain carbon steels were used without a heat treatment process (Lankford et al. 1985), but carbon steels with high carbon content were often heat treated to upgrade the mechanical properties (Honeycombe and Bhadeshia 1995). Heat-treating low alloy steels is the common method of producing high strength steel (Uwer and Dibelmeyer 1986). Steels with ultra-high strength (above 1500 MPa) and certain ductility can be achieved depending on the composition and the temperatures used in the heat treatment process (Matsuoka et al. 1979; Honeycombe and Bhadeshia 1995).

2.2 APPLICATION OF HIGH STRENGTH STEELS

Since the invention of steel, people have been using some techniques to improve the steel performance, such as strength and ductility. It was found by archaeologists that in the 13th century BC, people began using quenching and tempering techniques to sharpen tool tips and edges (Maddin 1992). However it was only in the last century that intense research on high strength steel was conducted due to the need for high performance steel during the rapid development of industries (Pearce and Painter 1977).

Developing ultra-high strength steels was first attempted by aircraft scientists. As aircraft speed increased, more consideration was given to the maximum strength of components for the lowest possible weight. Steels with the ultimate tensile strength of 1240 MPa were commonly used in the aircraft industry by the 1960s (Jackson 1962). However the use of steels with strengths above 1379 MPa was restricted by dangerous brittleness associated with ultra-high strength. This problem was solved to a certain extent by controlling the tempering temperature and modifying the steel chemical composition. By these methods, the ultimate tensile strength was increased up to 1793 MPa.

The automotive industry also made significant strides in applying high strength steels. This was in response to the increase in energy costs and consumer demand for fuel-efficient vehicles. Using high strength steels has been a major consideration for weight saving in automobiles and trucks. According to the data released by High Strength Steel Task Force (1994; 1995), the average weight of U.S. passenger cars reduced about 300kg from 1700kg in 1975 to around 1400kg in 1993 due to the extensive use of high strength steels. In the 1970s, the requirements for the yield stress of high strength steels in automotive industry were 620 to 690 MPa, whereas, in the 1980s, it was increased to 900 and 1170 MPa (Armitage and Young 1983). By 1970, high strength low alloy steels were extensively used as engine rails, reinforcements brackets, control arms, door beams, bumpers, trailing axles, truck trailer beds and beams. In addition to automotive parts, high strength steels were also used in railroad equipment and heavy construction machinery, bridges, storage tanks, linepipes, agriculture equipments and in electrical transmission towers (Dennis 1983).

In the 1970s there was also a trend to use high strength steels in the construction of high-rise buildings (Brockenbrough 1973). Many studies on high strength steels were conducted (Teoh 1983; Korchynsky 1984). In the first half of the 1980s, steel framed buildings were designed using steels of 400 and 490 MPa. However in the late 1980s, steels with 590 and 780 MPa were developed and used in the construction of high rise and large scale buildings (Nagata 2001).

Today, designers also use high strength steel in "hybrid" applications. Common examples of this practice include beams with high strength flanges and standard strength web, and steel tanks with higher strength steel for the more heavily loaded lower sections, thereby maintaining a constant wall thickness for simplified fabrication. This hybrid approach can give steel a crucial cost advantage (Ooyen 2002).

Recently, High strength steels have been studied by many researchers. For example, the high strength Duragal SHS structural steel with the yield strength of 450 MPa was investigated for use as a domestic floor system (Alikhail et al. 1998). High strength sheet steels G550 with the nominal yield stress of 550 MPa were studied under tension and compression (Rogers and Hancock 1997; 2001; Yang and Hancock 2002a; 2002b). High strength sheet steels with yield stress up to 1000 MPa were studied under fatigue load (Sperle and Nilsson 1992). The welded sections of BISALLOY 80 steel plate with a yield stress of 690 MPa were studied under compression (Rasmussen and Hancock 1992).

In summary, the world is experiencing a need for high strength steels in the automotive industry and other engineering applications. However the current steel design standards only cover steels with a yield stress up to 690 MPa. In this study, very high strength steel tubes with a yield stress of 1350 MPa and an ultimate strength of 1500 MPa were studied under tension, compression and bending. Detailed descriptions can be seen from Chapter 3 to Chapter 5.

2.3 DUCTILITY

Ductility is one of the major concerns in the applications of high strength steels, since it is generally believed that the higher the yield stress, the lower the ductility. Here, the ductility refers to the material ductility, i.e. the ability of a steel member to deform plastically before fracture (ASTM 1998). Due to concerns about the low ductility, the use of high strength steel is very much restricted in structural applications.

One of the principal functions of ductility is to reduce or eliminate the effect of stress concentrations in connections and other geometric discontinuities, such as holes or cracks. For ductile materials, stress concentrations can be redistributed. Ductility also permits the cold forming of a steel member by preventing the impairment to its subsequent structural behaviour.

Two commonly used parameters for measuring steel's ductility are the percentage elongation and the ultimate strength to the yield strength ratio. Figure 2.3-1 and Figure 2.3-2 show the minimum ductility requirements of some carbon and high strength low alloy steels specified in ASTM and Australian standards (ASTM 2000a; ASTM 2000b; ASTM 2001b; ASTM 2001c; ASTM 2001d; SAA 1991b; SAA 1993a) together with some ultra-high strength steels produced in Australia (Bisalloy steels Pty. Ltd 2003) and Japan (Kashima et al. 1992).

It can be seen from Figure 2.3-1 and Figure 2.3-2 that the steel's ductility decreases with the increase of the yield stress for carbon and HSLA steels. However, some quenched and tempered high strength steels do not follow this trend. Although current steel standards only cover steels with a yield stress up to 690 MPa, ultra-high strength steels with a yield stress over 700MPa has been used in transport equipment, high rise buildings, bridges, mining equipment and military applications (Shah Khan et al. 1998; Tanabe et al. 1995; Bisalloy steels Pty. Ltd 2003). The ductility of VHS steel tubes will be addressed in Chapter 3.

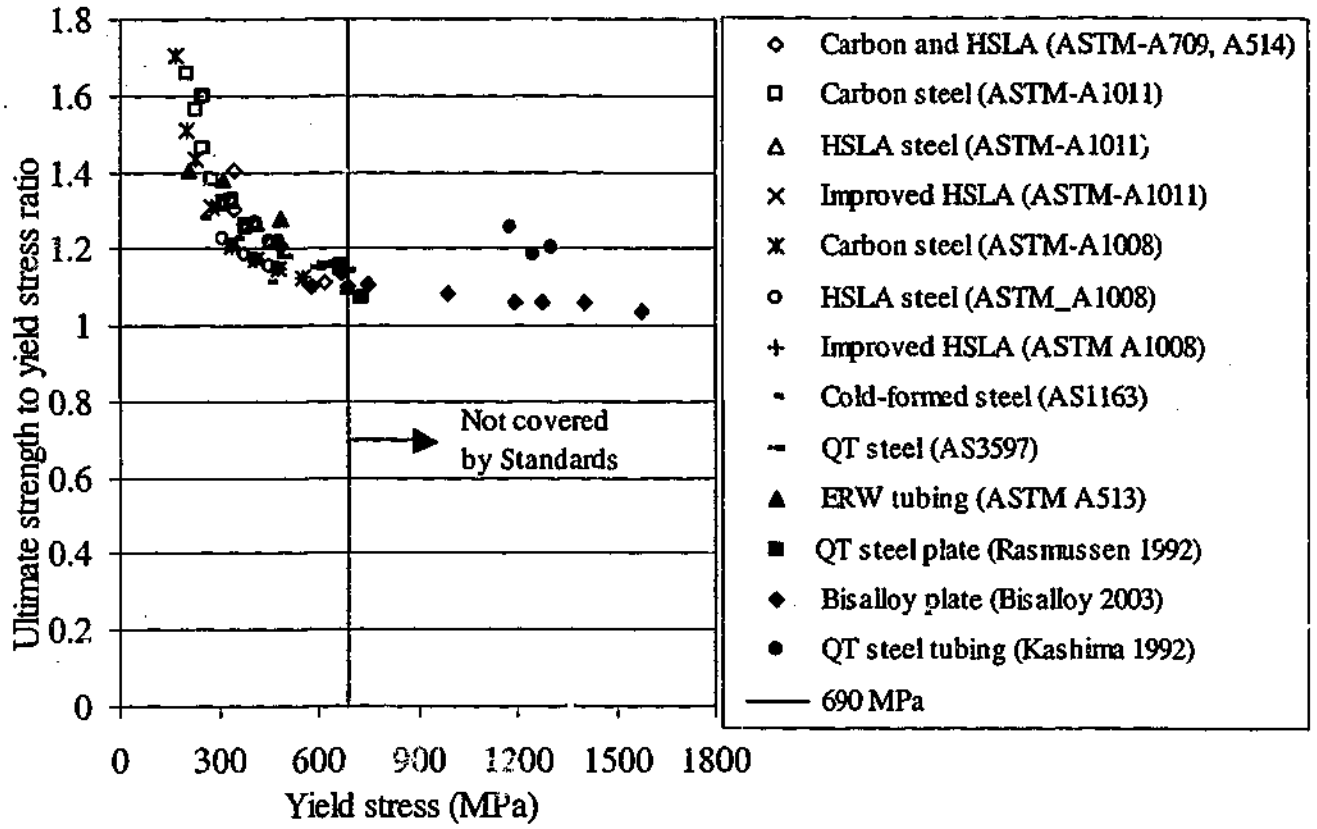

Figure 2.3-1: Ultimate strength to yield stress ratios versus yield stress of some steels

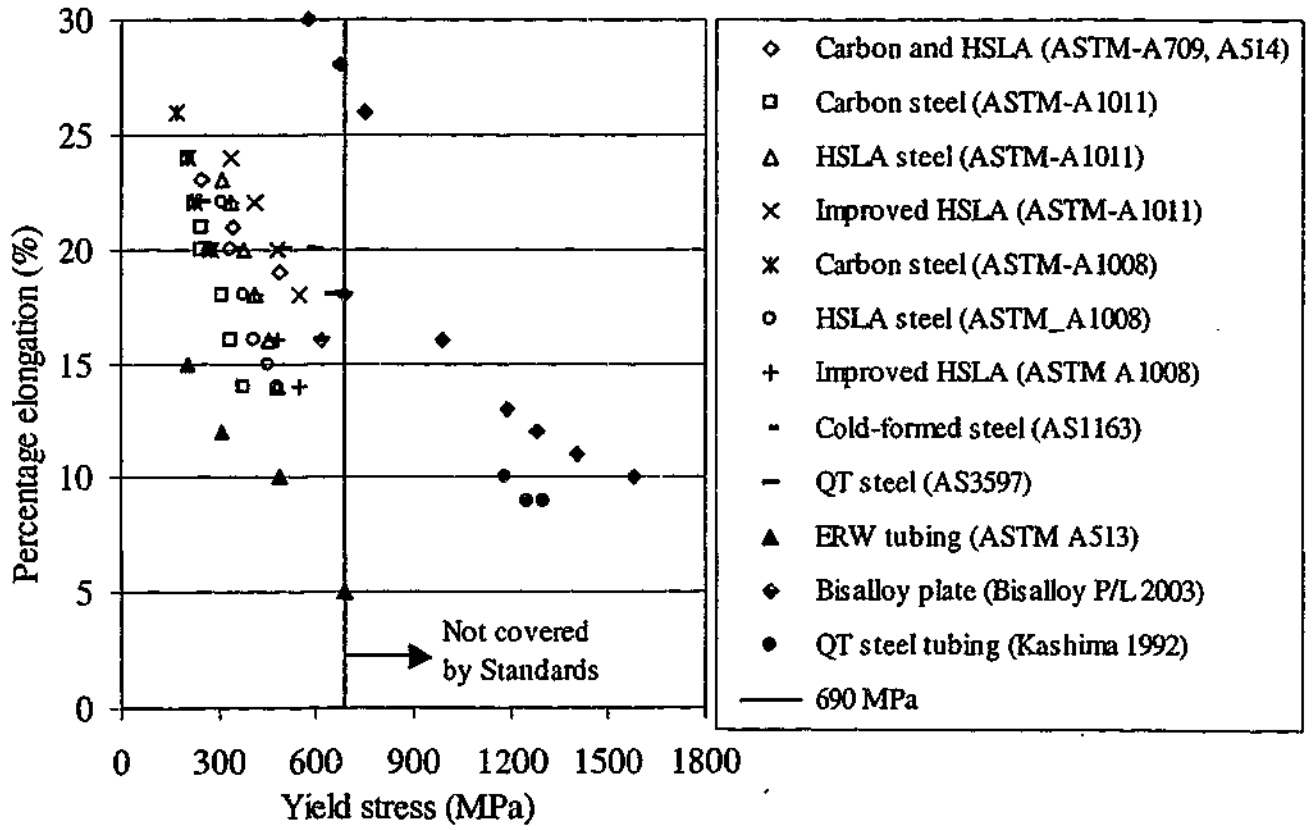

Figure 2.3-2: Percentage elongation versus yield stress of some steels

2.4 WELDED CONNECTION OF HIGH STRENGTH STEELS

Welding is the most common means of connection method. Over 80% of high strength steels applications involve welding (WTIA 1996). The heat affected zone softening caused during a fusion weld may be a key problem for welding high strength steels.

2.4.1 Heat Affected Zone (HAZ) Softening

The heat-affected zone (HAZ) in a weld connection is the region directly adjacent to the weld. It experiences a thermal cycle ranging from the unaffected parent metal to the melting boundary of the fusion weld. The HAZ softening in welded connections of high strength steels, especially quenched and tempered steels, is a drawback in the structural application of high strength steels. The micro-structural change in HAZ may incur a detrimental effect on the base metal strength (Martukanitz et al. 2000).

The influential factors on HAZ strength include joint preparation, welding procedures, selection of weld metal, preheating, heat input, welding technique and post weld heat treatment (Vuceric 1987). Particular attention needs to be paid to the control of the hydrogen content in order to minimize the risk of HAZ cracking. Careful clearness and dryness of the joint preparations and the use of hydrogen controlled welding metals may help reduce the hydrogen content. Post-weld heat treatment may be conducted for hydrogen dissolution and to improve the mechanical properties of welds (Olabi and Hashmi 1996). Limitations on both preheating and heat input are necessary to ensure that the HAZ cools at an appropriate rate and that the correct microstructure is achieved. A slow cooling rate can result in a soft HAZ and thus a loss of tensile properties. A rapid cooling rate produces a hard HAZ that may cause the loss of ductility. Therefore cooling is controlled by a balance between preheating and heat input. The strength reduction may be predicted based on the heat input and the cooling rate (Akselsen et al. 1989).

Some methods may be used to strengthen the HAZ. It has been pointed out that increasing the HAZ strength by heat treatment without adjustment in composition may increase the chance of cracking (Cullison 1995). An effort has been made in Japan to produce a HAZ softening-resistant steel tube with a tensile strength of 780MPa. The

method used in the steel production process was to refine the steel chemical content and to apply a thermo-mechanical control process (TMCP) (Tanabe et al. 1995a). The steel tube was used in automotive industry as propeller shaft. Fatigue torsion tests on the arc or friction welds showed that high fatigue strength was obtained in the HAZ.

Groove-welded butt joints and fillet-welded T-joints of VHS tubes were explained in detail in Chapter 6. The strengthening of butt-welded VHS tubes using CFRP-epoxy strengthening system was used in this study.

2.4.2 Strengthening of Butt-Welded VHS Tubes

CFRP material has been widely used to strengthen concrete structures (Teng et al. 2002). The application of CFRP material in strengthening metallic structures has been increasing rapidly in recent years due to its advantages over traditional strengthening materials, including high strength to weight ratio, resistance to corrosion and environmental degradation, and ease and speed of handling during construction (Tumialan et al. 2002; Cederquist 1999; Moy 2001).

Some examples of these applications include the strengthening of cast iron beams of underground structures (Moriarty and Barnes 1998), retrofitting of steel bridge beams or steel bridge piers (Sen et al. 2001; Miller et al. 2001; Tavakkolizadeh and Saadatmanesh 2003a; 2003b; Tani et al. 2000) and repair of fatigue damage for riveted connections (Bassetti et al. 1998). However studies on the strengthening of HAZ softening in welded high strength steels are very limited.

In this study, one kind of CFRP material and three kinds of epoxy resins will be used in the strengthening of butt-welded VHS tubes. Detailed descriptions can be found in Chapter 7.

2.5 SUMMARY

In this chapter, the historical development of high strength steels was briefly reviewed. The high strength steels were classified based on chemical composites and production methods. Only the most popular categories of high strength steels were addressed. Questions regarding the engineering application of high strength steels, i.e. the low ductility and the heat affected zone softening in a welded connection were discussed.

There is an increasing need to use high strength steels in the automotive industry and in other engineering applications around the world. Some problems may exist in the application of high strength steels, including low material ductility and HAZ softening in weld connections. Currently, there is no Australian Standard for the design of structural elements utilizing high strength quenched and tempered steels. The steel structures design code AS4100 (SAA 1998) may be used for the design of structures in steel grades up to 450 MPa, beyond which the general provisions of this code are not applicable. The American specifications for structural steel buildings (AISC 1999) covers steels with a yield stress up to 690 MPa.

The very high strength (VHS) circular steel tubes produced in Australia have a yield stress about 1350 MPa and an ultimate tensile strength about 1500 MPa. Therefore VHS steel tubes need to be studied in detail in order to examine if it can be used as structural steel members.

Chapter 3

VHS TUBES IN TENSION

3.1 INTRODUCTION

Chapter 2 described the key problems regarding the application of high strength steels, including low ductility and HAZ softening. This chapter reports an investigation on the material ductility of VHS tubes under static tension load. The tensile tests were conducted in accordance with the Australian Standard for tensile testing of materials (SAA 1991a). In order to compare the test results of VHS tubes with those of the cold-formed circular hollow sections, some non-heat-treated steel tubes (NHT) were also tested. A total of 15 VHS tensile coupons and 12 full section VHS tubes plus 2 coupons and 5 full section tubes of NHT steel were tested. The tested tubes had a diameter ranging from 31.8mm to 75mm with wall thickness ranging from 1.6mm to 2.0mm. The test results were compared with the ductility requirements of various design codes. The ultimate strength to the yield stress ratio of VHS tubes is compared with that of various cold-formed and hot finished steels such as C250, C350 and C450 specified in AS1163-1191 (SAA 1991b), G250 to G550 specified in AS1397-1993 (SAA 1993b), Bisalloy steel (Rasmussen and Hancock 1992; Bisalloy steels Pty. Ltd 2003) and 700Q (Sivakumaran and Yuan 1998). The percentage elongation over different gauge lengths was obtained for VHS tubes.

3.2 DUCTILITY CRITERIA OF STEEL

3.2.1 Literature Review

Percentage elongation obtained in a tensile test was used as a parameter for steel ductility as early as the beginning of last century (Unwin 1903; 1910). The total elongation consists of two parts. One is the general extension or uniform extension that is assumed to take place uniformly along the specimen, and is proportional to the gauge length. The other part is the local extension that occurs after the maximum load has been reached. It is independent of the gauge length (Oliver 1928). Ray et al. (1994) attempted to develop other parameters from a tension test for the ductility of steel, but the percentage elongation is accepted as one of the parameters for steel ductility in the current steel design standards.

The percentage elongation on a certain gauge length may be different for different steels. With an original gauge length of 50mm, for example, the elongation could be over 60% for stainless steels with a yield stress of around 300 MPa (Mathew et al. 1985), whereas the ductility was only about 5% for sheet maraging steel with a yield stress of around 850 MPa (Mazhar et al. 1988). There was an argument on what amount of ductility is required for a steel to be considered suitable for structural application (Gillett 1940). In 1970s, Dhalla and Winter (1974a; 1974b) studied low carbon cold-reduced sheet steels. They suggested that a steel was adequately ductile for cold-formed construction if the percentage elongation on 50mm gauge length was greater than 7% plus a minimum ultimate strength to yield stress ratio of 1.05. They pointed out that it was essential to use the ultimate strength to yield stress ratio as a second parameter for steel ductility. These suggestions have formed the base for specifying the ductility criteria in current cold-formed steel design standards, which is outlined in the next section.

3.2.2 Ductility Criteria in Current Steel Design Standards

Certain ductility requirements are stipulated in current design standards for different methods of structural analysis.

Examples of the requirements of some standards are given below.

(1) AS/NZS 4600 (SAA 1996)

For high strength cold-formed steels (yield stress higher than 450MPa),

(i) $f_u/f_y \geq 1.08$

(ii) $e_{50} \geq 10\%$, or $e_{200} \geq 7\%$

(2) Eurocode 3 (2002)

Requirements for application of plastic analysis method:

(i) $f_u/f_y \geq 1.2$

(ii) $e_0 \geq 15\%$

(iii) $\varepsilon_u/\varepsilon_y \geq 20$

(3) AS4100 (SAA 1998)

(i) $f_u/f_y \geq 1.2$

(ii) $e_0 \geq 15\%$

(iii) the steel exhibits a strain-hardening capacity

(iv) the length of yield plateau $\geq 6\varepsilon_y$

Here, f_u is the ultimate tensile strength; f_y is the yield stress; e_{50} represents the percentage elongation over 50mm gauge length including fracture; e_{200} is the percentage elongation over 200mm gauge length including fracture; e_0 refers to the percentage elongation over $5.65\sqrt{A}$ mm gauge length including fracture (A is the section area of a specimen in mm^2); ε_u is the ultimate strain corresponding to the ultimate strength f_u; ε_y is the yield strain corresponding to the yield stress f_y.

3.3 COUPON TENSILE TESTS

3.3.1 Test Setup and Test Results

A total of 15 VHS tensile coupon specimens were cut from VHS tubes with diameters of 38, 57.4 and 75mm, and thicknesses of 1.6, 1.8 and 2.0mm. The dimensions of the coupon specimens are given in Table 3.3-1. The diameter D of the tube, the thickness t and the width b of the coupon are defined in Figure 3.3-1. Due to the high strength of the material, the laser cut method was adopted to avoid changes being made to the material properties. The laser cut method can be used on quenched and tempered steels with a thickness up to 10mm. It is more accurate with the small kerf and heat-affected zone achieved with low levels of excess heat (WTIA 1996). Since the laser beam was normal to the tube surface, the following formula was used to calculate the cross-sectional area of the tensile coupons:

$$A_c = \frac{1}{4}\arcsin\left(\frac{b}{D}\right)\left[D^2 - (D-2t)^2\right] \tag{3.3-1}$$

where D is the outside diameter of a tube, t is the tube thickness and b is the width of a tensile coupon as shown in Figure 3.3-1. A_c is the cross-sectional area of the coupon.

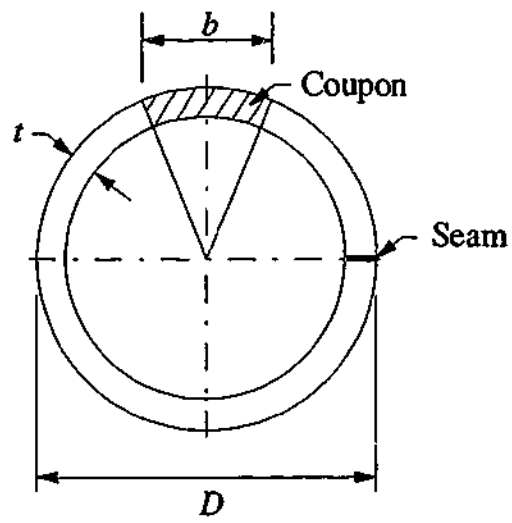

Figure 3.3-1. Cross-sectional dimensions of a tensile coupon

Table 3.3-1: Dimension of tensile coupons

Tube Type	Specimen Label	D (mm)	t (mm)	b (mm)	A_c (mm^2)
VHS	TS1A	38.3	1.64	19.77	32.67
	TS1B	38.3	1.62	19.76	32.28
	TS1C	38.3	1.65	20.07	33.35
	TS2A	38.3	1.86	19.85	36.87
	TS2B	38.3	1.85	19.51	36.11
	TS2C	38.3	1.87	19.77	36.89
	TS3A	38.3	2.07	19.79	40.62
	TS3B	38.3	2.04	19.69	40.00
	TS3C	38.3	2.05	19.68	40.07
	TS4A	57.4	1.61	19.23	30.62
	TS4B	57.4	1.63	18.48	29.74
	TS4C	57.4	1.60	18.47	29.3
	TS5A	75.4	1.59	19.06	29.93
	TS5B	75.4	1.60	19.79	31.36
	TS5C	75.4	1.58	19.41	30.3
NHT	TS6A	38.1	1.65	12.34	20.75
	TS6B	38.1	1.65	12.32	20.72

In order to compare the VHS properties with the properties of the original cold-formed material, two coupons were made from non-heat-treated (NHT) tubes. All coupons were cut at 90° to the seam welds on tubes in accordance with ASTM E8M (ASTM 1999a). The original gauge length and width of the specimens met the requirements of AS 1391 (SAA 1991a). All tests were performed in a 500kN universal testing machine with a strain rate of 1.4×10^{-4}/s.

The results are listed in Table 3.3-2. The first letter in the labels refers to tension test (T) followed by section number (S1-S4). The last letter refers to the repeated samples (A-C). 0.2% proof stress was used to determine the yield stress. Two strain gauges were mounted on each specimen to offset the influence of residual stress on Young's

modulus of elasticity. Both ends of each specimen were flattened so that they could be easily gripped.

From Table 3.3-2 it can be seen that the average yield stress of non-heat-treated steels was 433 MPa, whereas the average yield stress of VHS material was 1365 MPa, and the average ultimate strength was 1520 MPa. The Young's modulus of elasticity was about 200 GPa for both non-heat-treated tubes and VHS tubes.

Table 3.3-2: Test results of tensile coupons

Tube Type	Specimen Label	P_{max} (kN)	P_f (kN)	P_f/P_{max}	f_u (MPa)	f_y (MPa)	f_u/f_y	E_s (GPa)
VHS	TS1A	50.9	43.9	0.862	1558	1402	1.111	190.9
	TS1B	49.5	42.5	0.859	1533	1392	1.101	195.1
	TS1C	51.7	44.9	0.868	1550	1400	1.107	190.7
	TS2A	55.8	46.4	0.832	1513	1361	1.112	198.3
	TS2B	54.3	46.6	0.858	1507	1360	1.108	204.4
	TS2C	55.3	46.3	0.837	1499	1362	1.101	197.6
	TS3A	60.0	48.1	0.802	1477	1328	1.113	195.6
	TS3B	59.8	47.7	0.798	1495	1329	1.125	197.1
	TS3C	59.6	47.1	0.790	1487	1332	1.117	200.2
	TS4A	46.1	37.5	0.813	1506	1346	1.118	203
	TS4B	44.8	39.6	0.884	1506	1365	1.103	194.2
	TS4C	44.5	36.4	0.818	1519	1368	1.110	197
	TS5A	46.1	37.0	0.803	1540	1363	1.130	195.2
	TS5B	48.3	40.5	0.839	1540	1370	1.125	196.7
	TS5C	47.5	39.4	0.829	1568	1399	1.120	203.7
	MEAN	-	-	0.833	1520	1365	1.113	197.3
	COV	-	-	0.033	0.017	0.018	0.008	0.020
NHT	TS6A	10.4	1.3	0.125	501	433	1.157	193.6
	TS6B	10.4	0.9	0.087	502	432	1.162	198.4
	MEAN	-	-	0.106	502	433	1.160	196.0
	COV	-	-	0.182	0.001	0.001	0.002	0.012

3.3.2 Failure Modes

The VHS steel and its original non-heat-treated steel (NHT) had completely different failure modes. The VHS material showed a kind of shear failure with an oblique shear band (Figure 3.3-2). The angle between the shear band and the loading direction was around 62.5°, similar to the failure angle observed for G550 steel when loaded in longitudinal direction (Kennedy 1996). By contrast, the non-heat-treated material showed diffuse necking when it entered into the plastic range (See Figure 3.3-3). Typical stress-strain and load-displacement curves are shown in Figure 3.3-4 and Figure 3.3-5 for VHS tensile coupons. It is interesting to observe that the strain reduces from point P1 to P2 and P3 in Figure 3.3-4 due to the release of elastic energy. However, the axial displacement increases from Point P1 to P2 to P3 in Figure 3.3-5 due to the physical separation of the tensile coupon. During the test, a video camera was used to record the progressive failure. By matching synchronously the video shown in Figure 3.3-6 with the load-displacement and stress–strain data, it can be observed that when strain reached the maximum point P1, shear band began to develop, then the strain in sections away from the shear band began to decrease until it reached the failure point P3, then the specimen split into two pieces (Figure 3.3-6).

Figure 3.3-2: VHS tensile coupons

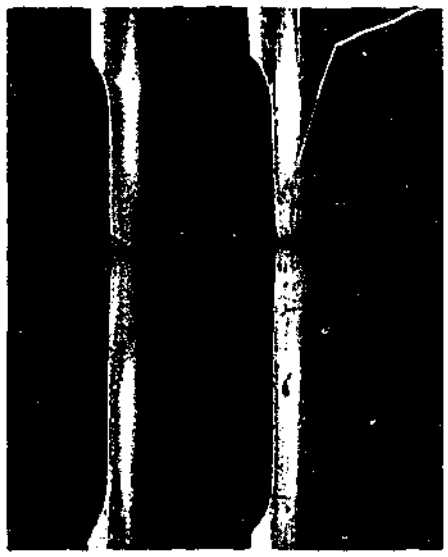

Figure 3.3-3: NHT tensile coupons

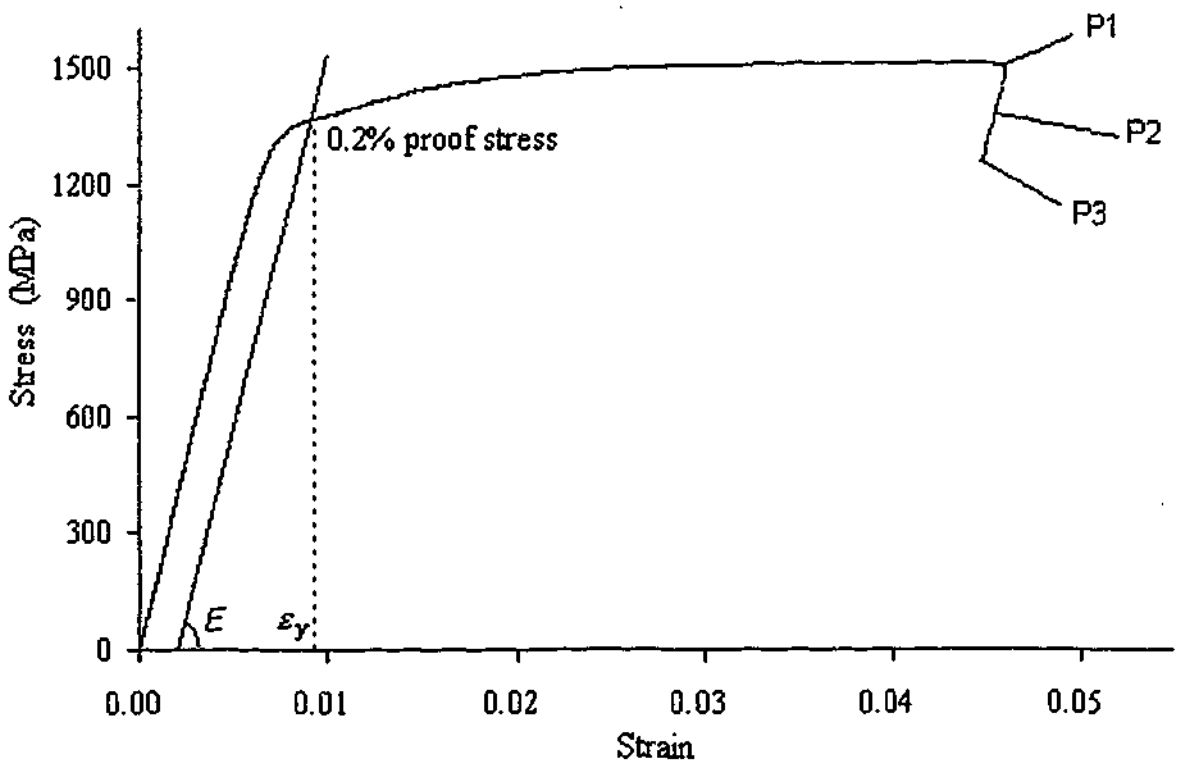

Figure 3.3-4: Typical stress-strain curve of VHS coupons (TS2A)

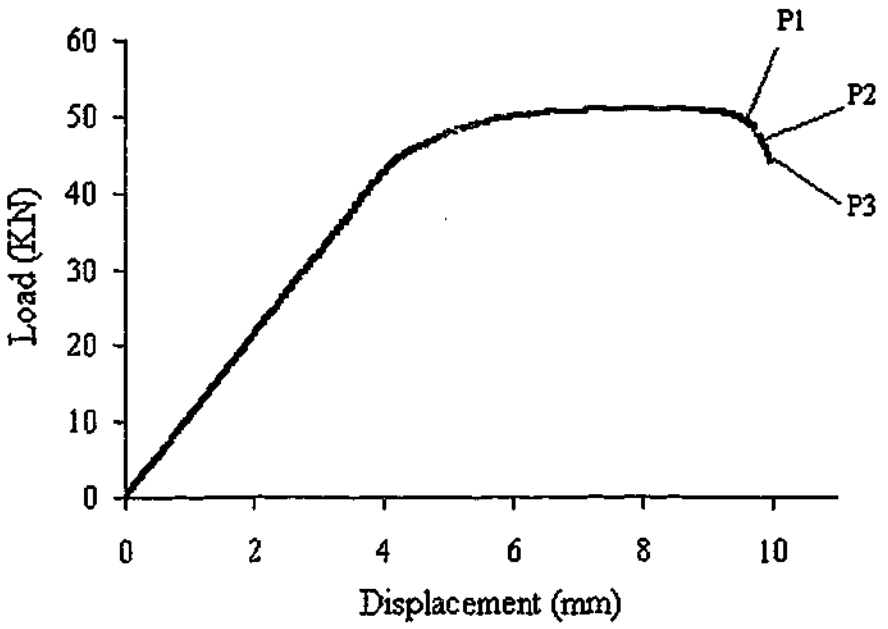

Figure 3.3-5: Typical load-displacement curve of VHS coupons (TS2A)

(P1)

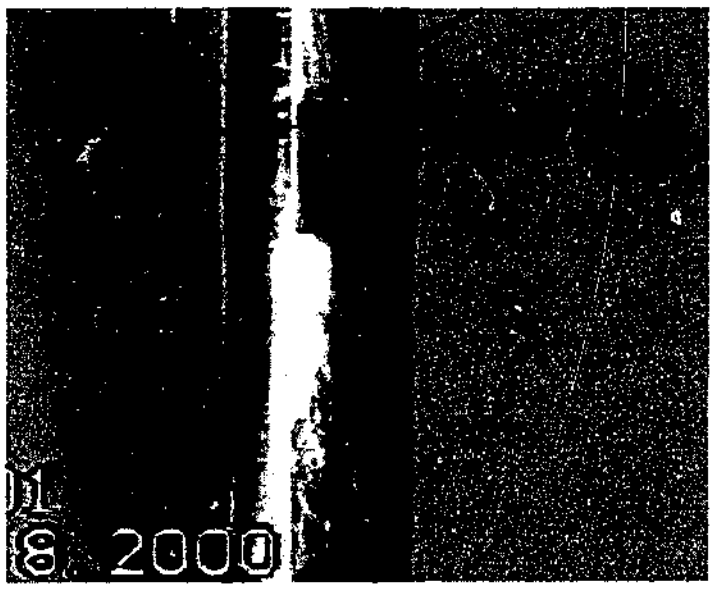

(P2)

(P3)

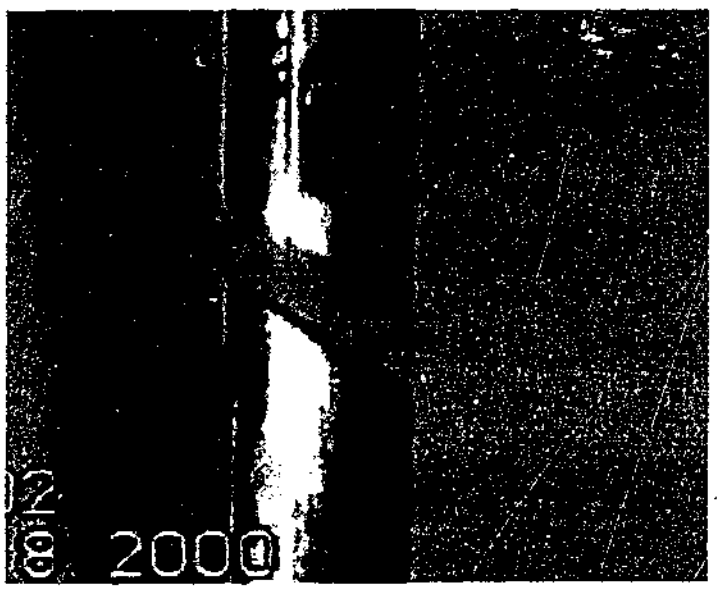

Figure 3.3-6: Typical failure process of VHS tensile coupons. (P1) A Shear band appeared. (P2) The shear band developed. (P3) The fracture occurred.

3.4 FULL SECTION TENSILE TESTS

3.4.1 Test Setup and Test Results

A total of twelve full section VHS steel tubes and five non-heat-treated tubes were tested. The test setup was the same as that for the coupon test except that steel plugs were put in both ends of each specimen to enable the tube to be gripped. The free length between each grip face was 320mm. All tests were performed under a strain rate of 1×10^{-4}/s. The specimen dimensions were listed in Table 3.4-1. The first two letters (FT) in the labels refer to full section tensile tests followed by section number (S1-S6). The last letter refers to two samples (A and B). The letter N is used to identify non-heat-treated tubes.

Table 3.4-1: Section dimensions of full section tubes

Tube Type	Specimen Label	t (mm)	D (mm)	A (mm^2)
VHS	FTS1A	2.058	38.225	233.83
	FTS1B	2.057	38.260	233.95
	FTS2A	1.842	38.280	210.86
	FTS2B	1.873	38.212	213.83
	FTS3A	1.622	38.317	186.99
	FTS3B	1.623	38.282	186.92
	FTS4A	2.042	31.913	191.63
	FTS4B	2.070	31.925	194.15
	FTS5A	1.845	32.017	174.88
	FTS5B	1.842	32.035	174.72
	FTS6A	1.660	31.915	157.78
	FTS6B	1.658	31.888	157.46
NHT	FTS1NA	1.580	38.073	181.14
	FTS1NB	1.567	38.020	179.45
	FTS2NA	1.773	38.020	201.90
	FTS2NB	1.773	38.033	201.97
	FTS3NA	1.987	37.987	224.72

The test results are listed in Table 3.4-2. The measured average yield stress for VHS tubes was 1327MPa, whereas the measured average yield stress for non-heat-treated tubes was 465MPa.

Table 3.4-2: Full section tensile test results

Tube Type	Specimen Label	P_{max} (kN)	P_f (kN)	P_{max}/P_f	f_u (MPa)	f_y (MPa)	f_u/f_y	E (GPa)
VHS	FTS1A*	352.3	322.62	0.916	1506	-	-	-
	FTS1B	350.7	323.40	0.922	1499	1332	1.125	198.6
	FTS2A	316.0	302.97	0.959	1484	1329	1.116	201.2
	FTS2B	312.8	297.50	0.951	1463	1311	1.115	192.8
	FTS3A	284.0	271.83	0.957	1519	1356	1.121	200.4
	FTS3B	283.6	263.26	0.928	1517	1353	1.121	202.5
	FTS4A	292.6	271.07	0.926	1527	1359	1.124	195.6
	FTS4B	291.4	279.70	0.960	1501	1340	1.120	193.1
	FTS5A	253.6	232.90	0.918	1450	1289	1.125	191.4
	FTS5B	251.8	232.42	0.923	1441	1279	1.127	192.1
	FTS6A	231.1	214.30	0.927	1465	1324	1.106	189.5
	FTS6B	232.2	214.55	0.924	1474	1329	1.110	190.9
	MEAN			0.934	1487	1327	1.119	195.3
	COV			0.017	0.018	0.277	0.006	0.023
NHT	FTS1NA	88.2	5.10	0.058	487	455	1.070	201.1
	FTS1NB	88.5	13.80	0.156	493	463	1.065	201.3
	FTS2NA	103.5	16.20	0.157	513	462	1.109	198.2
	FTS2NB	104.3	18.90	0.181	516	466	1.109	194.1
	FTS3NA	118.5	24.10	0.203	527	481	1.095	198.1
	MEAN			0.151	507	465	1.090	198.6
	COV			0.330	0.030	0.019	0.017	0.013

Note: * The strain gauge was damaged for FTS1A during the test.

3.4.2 Failure Modes

VHS coupons were put on top of full section tubes after testing as shown in Figure 3.4-1. The VHS full section steel tubes showed similar shear failure mode to the coupon specimens, and the same shear angle was observed. The failure of full section non-heat-treated steel tubes, however, was quite different from their coupon specimens. Figure 3.4-2 shows the typical progressive failure of the non-heat-treated steel tubes. The typical load-displacement curve is plotted in Figure 3.4-3. Since the seam weld is more brittle than the base metal of the tube, when the load applied reached the maximum load (Point (a) in Figure 3.4-3), numerous small necking gradually appeared along the seam weld, which was also observed by Zhao et al (1996) for C350 RHS members. When the load reached point (b), a crack appeared on the seam; then the crack tip developed horizontally into the whole tube section (See (c) and (d) in Figure 3.4-2). As the crack developed, the load began to decrease dramatically until the specimen was broken into two parts (Point (c) and (d) in Figure 3.4-3). This observation confirmed that the strength and ductility of a coupon cut from a tube might not accurately represent the tube's strength and ductility properties (ASTM 1999a).

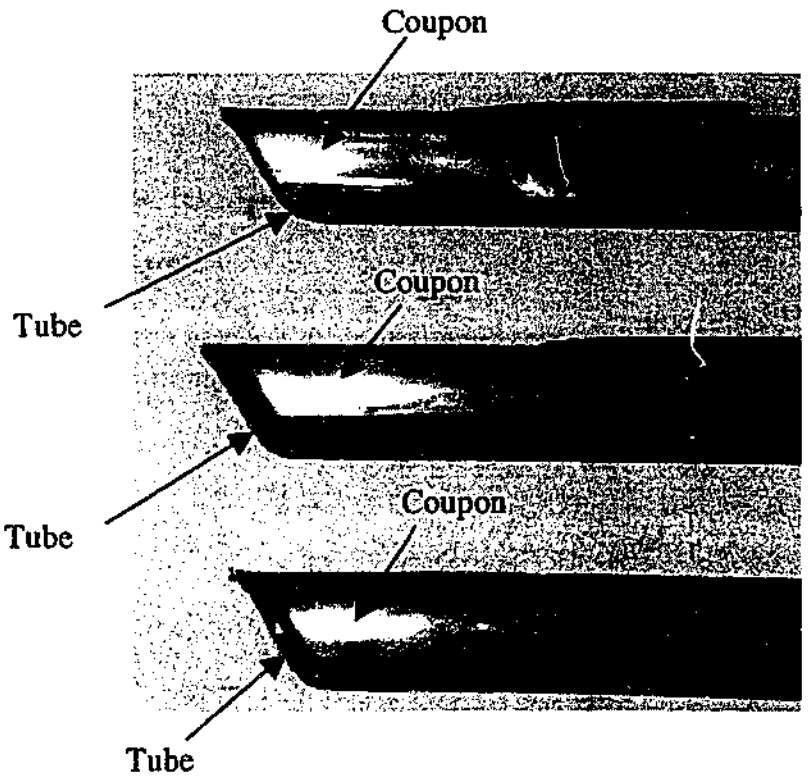

Figure 3.4-1: Comparing of failure angle between VHS coupons and full section tubes (Coupons were put on top of the full section tubes.)

(a)

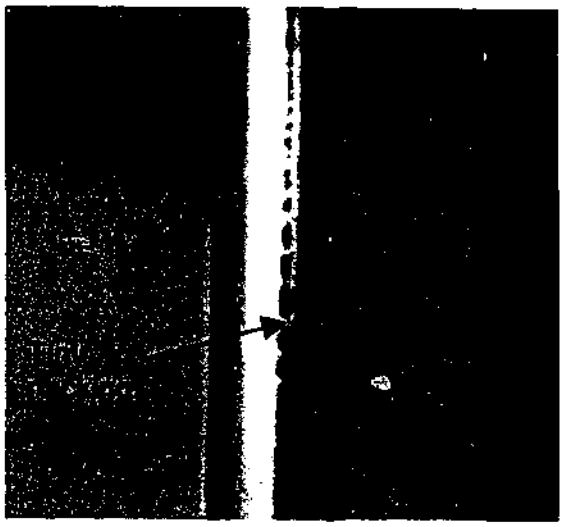

(b)

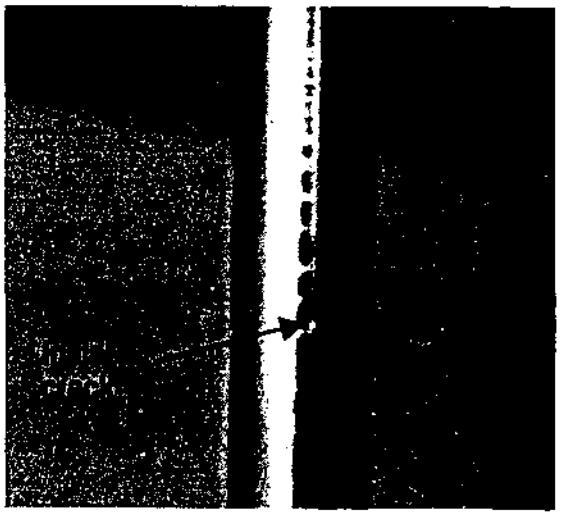

(c)

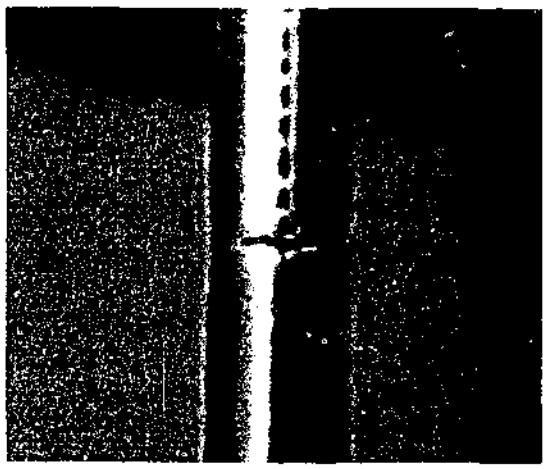

(d)

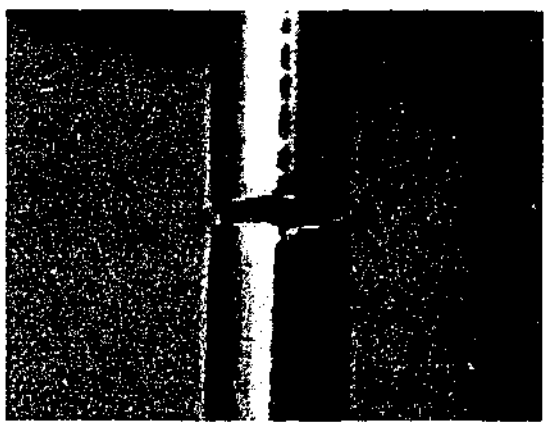

Figure 3.4-2: Typical failure mode of non-heat-treated full section tubes. (a) Tiny necking; (b) Initial crack; (c) Developed crack; (d) Crack across the whole section

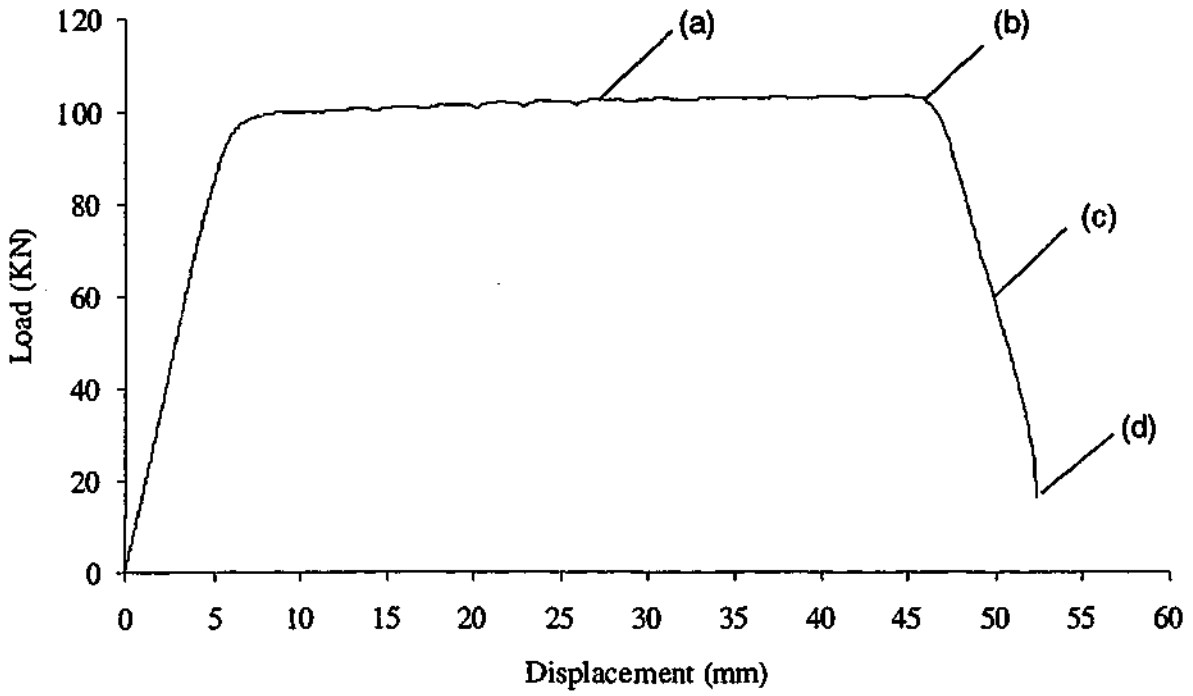

Figure 3.4-3: Typical load-displacement curve of non-heat-treated full section tubes

3.5 MATERIAL DUCTILITY OF VHS STEEL

3.5.1 Ultimate Strength to Yield Stress Ratio

It is commonly believed that cold-working of a metal results in an increase in strength and a decrease in ductility, i.e. the higher the strength, the lower the ductility. As mentioned in Chapter 2, the ultimate strength to the yield stress ratio is an important parameter in assessing the ductility. This ratio is plotted in Figure 3.5-1 based on nominal values of various cold-formed products. This ratio is also plotted against the yield stress in Figure 3.5-2 based on measured values from several studies. Three types of products are included: (i) cold-formed hollow sections (C250, C350, C450 and non-heat-treated tubes), (ii) sheet steels (G250 to G550), (iii) quenched and temped steels (Bisalloy 80, 700Q and VHS). As shown in Figure 3.5-1, for cold-formed steel hollow sections and sheet steels, the ultimate strength to yield stress ratio decreases as the yield stress increases. The ratio approaches 1.0 when the yield stress approaches 550MPa. This explains why fracture may occur prior to the desired shape if cold working on steel is excessive (Dieter and Bacon 1988). It seems that heat-treated steels do not follow the trend for cold-formed hollow sections and sheet steels. The ratio f_{un}/f_{yn} is 1.14 for 700Q, 1.15 for Bisalloy 80 and 1.16 for VHS tubes. It can be seen from Figure 3.5-2 that the same trend remains for cold-formed steel hollow sections and sheet steels when measured values are used. Similar to the nominal f_{un}/f_{yn} ratios, the ratios ranging from 1.06 to 1.16 are obtained for heat-treated steels when measured values are used.

Figure 3.5-2 also illustrates that there is very little difference in the ratios of f_u/f_y between full section tubes and coupon specimens for VHS material, with an average value of 1.119 for full section tubes, which is close to the previous testing result of 1.117 in Zhao (2000), and an average of 1.113 for tensile coupon tests. This implies that due to the heat treatment process the material properties of VHS tubes become uniform around the section. On the other hand, the f_u/f_y ratio for non-heat-treated steel tubes is on average 1.16 for tensile coupons and 1.09 for full section tubes. The lower f_u/f_y ratio for full section non-heat-treated tubes may be caused by the lower ductility of the seam weld.

From the above discussion, it can be seen that the ratio f_u/f_y for VHS tubes meets the minimum requirement of $f_u/f_y \geq 1.08$ specified in AS/NZS4600 (SAA 1996). However the ratio is about 7% less than the minimum requirement of $f_u/f_y \geq 1.2$ specified in Eurocode 3 (2002) and AS4100 (SAA 1998).

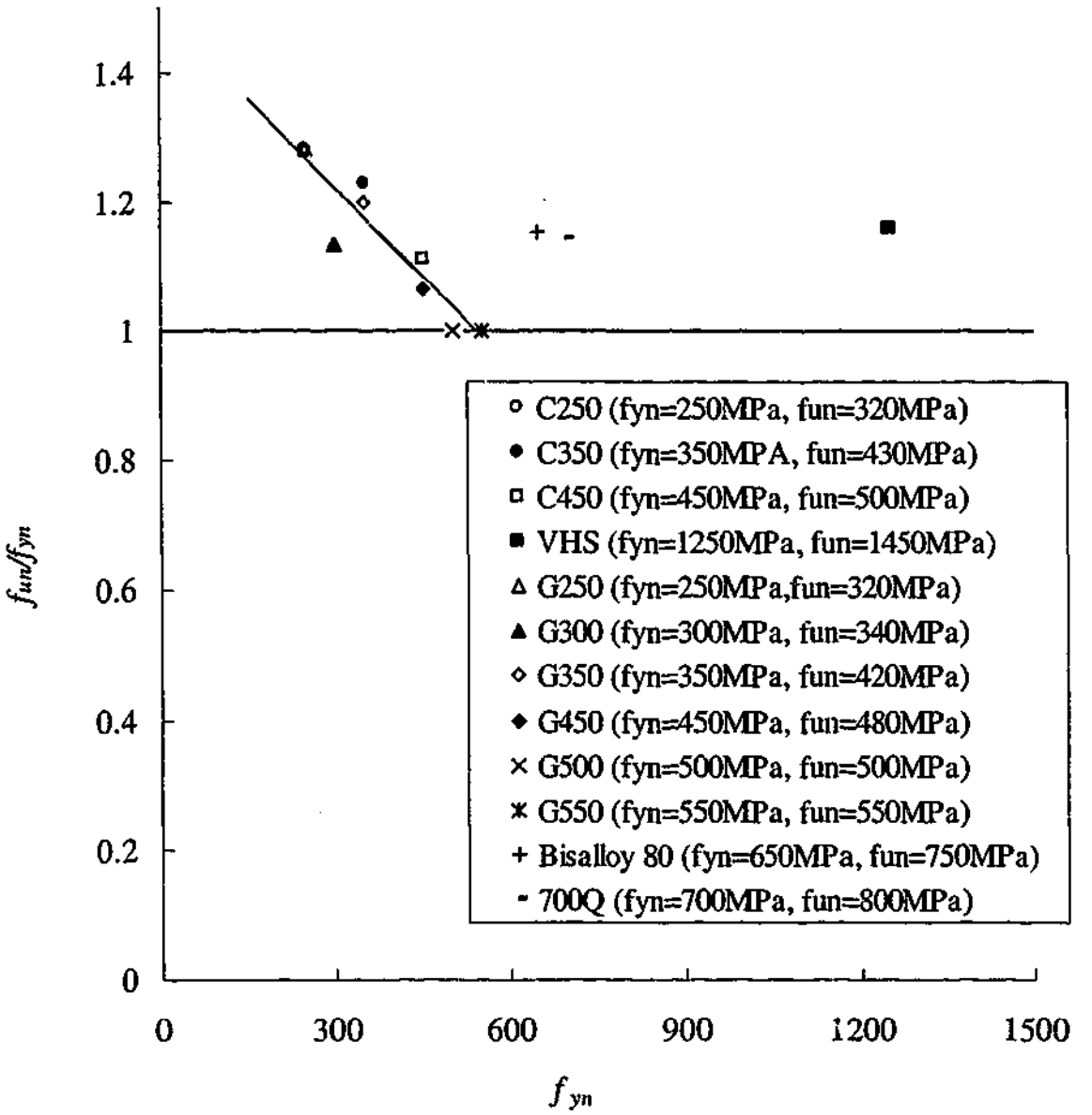

Figure 3.5-1: Nominal f_{un}/f_{yn} versus f_{yn}

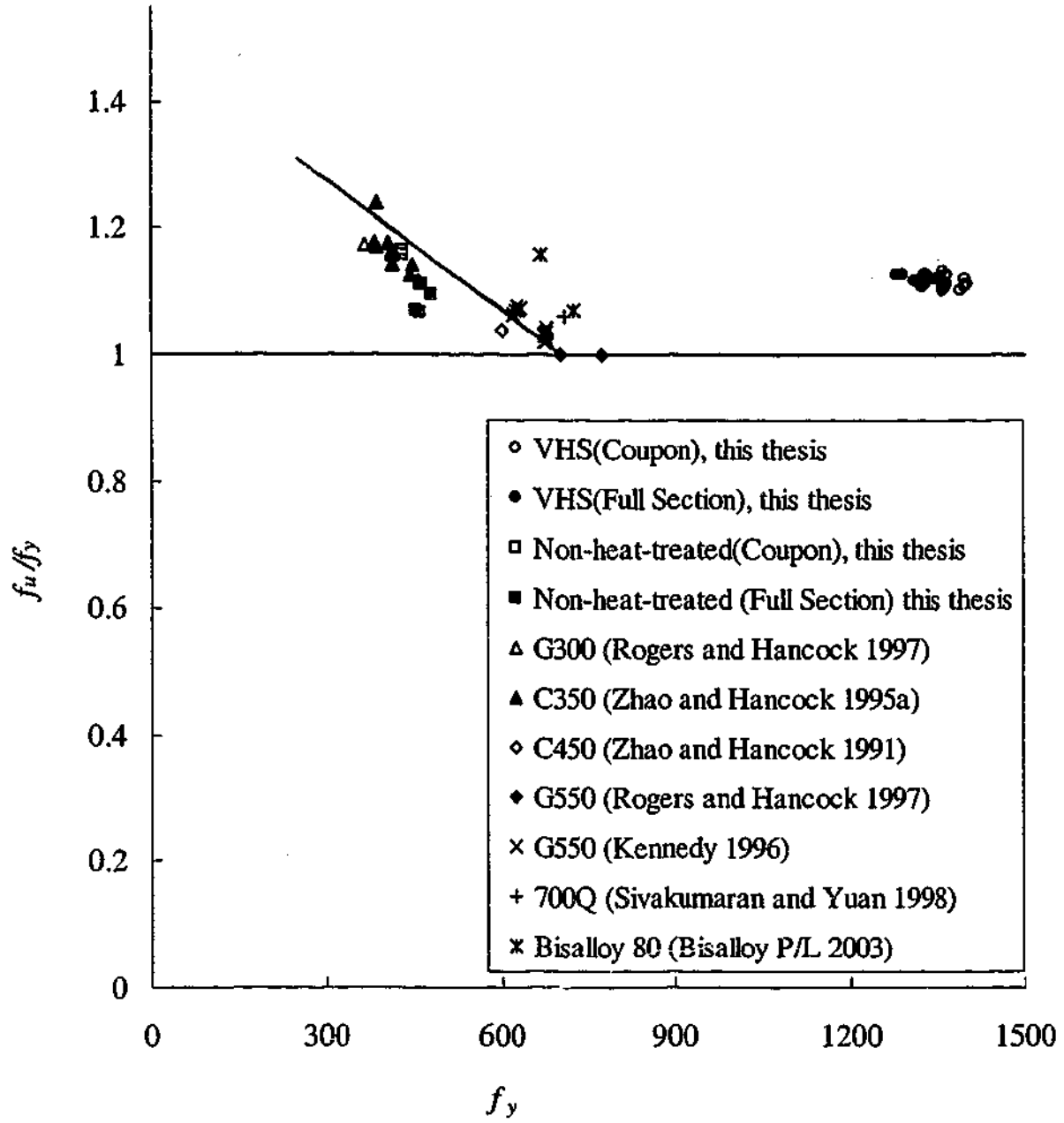

Figure 3.5-2: Experimental f_u/f_y versus f_y

3.5.2 Percentage Elongation

3.5.2.1 Coupon Specimens

Before testing, quick-drying ink was painted on each test specimen and scribed lines were marked at 2.5mm intervals. A line parallel to the longitudinal axis was also marked on each specimen. After testing, two broken test pieces were firmly fitted together so that percentage elongation after fracture could be measured. An optical

magnifier was used to assist the reading. The measured percentage elongations are listed in Table 3.5-1. The elongation on the standard original gauge length of $5.65\sqrt{A_c}$ was obtained by converting the measured values (e_{50}) in accordance with the equation given by ISO (1984):

$$e_0 = \frac{e_{50}}{1.25\left(\frac{\sqrt{A_c}}{50}\right)^{0.127}} \qquad (3.5\text{-}1)$$

Table 3.5-1: Percentage elongation of coupon specimens

Tube Type	Specimen Label	Percentage elongation			
		e_{30} (%)	e_{50} (%)	e_u (%)	e_0 (%)
VHS	TS1A	9.00	7.40	3.75	7.80
	TS1B	9.33	6.80	2.38	7.17
	TS1C	10.33	7.80	2.67	8.21
	TS2A	10.67	7.40	3.25	7.74
	TS2B	10.67	7.60	3.50	7.96
	TS2C	9.67	7.78	3.38	8.13
	TS3A	10.33	7.80	3.13	8.11
	TS3B	10.67	8.00	2.88	8.32
	TS3C	10.67	7.80	2.75	8.11
	TS4A	9.80	6.92	2.5	7.32
	TS4B	8.17	5.58	1.72	5.91
	TS4C	8.80	6.26	1.88	6.64
	TS5A	10.47	7.30	3.08	7.73
	TS5B	9.43	7.30	2.86	7.71
	TS5C	10.97	8.10	2.30	8.58
	MEAN	9.93	7.32	2.80	7.70
	COV	0.08	0.09	0.20	0.09
Non-heat-treated	TS6A	33.67	27.60	17.14	29.93
	TS6B	33.00	26.20	14.86	28.42
	MEAN	33.34	26.90	16.00	29.17
	COV	0.01	0.03	0.07	0.03

As can be seen from Table 3.5-1, the percentage elongation of the non-heat-treated material is at least three times larger than that of the VHS material. The average elongation on 50mm gauge length for VHS material is 7.32%, which does not meet the minimum requirement of 10% for high strength steels in AS/NZS 4600 (SAA1996). The average elongation on the standard original gauge length is 7.7%, which is much less than the requirement of 15% specified in Eurocode 3 and AS4100 for plastic design. It should be noted that the conversion method does not apply to VHS tubes because the formula is obtained from a statistical assessment of international test results that do not include tests on quenched and tempered steels. The average percentage elongation on 50mm gauge length for the non-heat-treated tubes is 26.9%, which is far greater than the standard requirement of 10%. A mean value of 29.17% was obtained on the standard original gauge length of $5.65\sqrt{A_c}$ for non-heat-treated tubes, which is larger than the requirement of 15% in Eurocode 3 and AS4100.

3.5.2.2 Full Section Tubes

The full section tubes were marked with lines at intervals of 10mm using the same method. The measured percentage elongations are summarized in Table 3.5-2 for VHS tubes and in Table 3.5-3 for non-heat-treated tubes. The same formula was used to calculate the elongation on the standard original gauge length of $5.65\sqrt{A}$ in accordance with ISO (1984) (To replace the cross-sectional area of tensile coupon (A_c) with the cross-sectional area of full section tube (A) in Eq. (3.5-1)).

For VHS tubes, multi-shear bands were observed in the fracture zone of the tubes (Figure 3.5-3), which caused the percentage elongation on 50mm original gauge length to be around 3% larger than that of the tensile coupon specimens. A mean value of 10.96% was achieved for e_{50}, which meets the requirement of 10% specified in AS/NZS4600. The elongation on the standard original gauge length (e_0) of 10.32% is larger than that of 7.7% for coupons. It seems that that measured elongations (e_{50} and e_0) for coupons under-estimate those of full section VHS tubes.

For non-heat-treated tubes, because a crack always started on the seam weld (see Figure 3.4-2) and final fracture occurred at the position opposite the seam weld, the specimen bent towards the seam weld (see Figure 3.5-4). Therefore, the percentage elongation was measured along both the seam weld and the side opposite the seam weld. Table 3.5-3 shows that the measured percentage elongation, e_{50}, along the seam weld is about half that along the side opposite the seam weld. Both e_{50} values are larger than the requirement of 10% specified in AS4600. It is interesting to observe that the elongation e_{50} along the opposite side is about the same as the elongation e_{50} of 27% for NHT coupons.

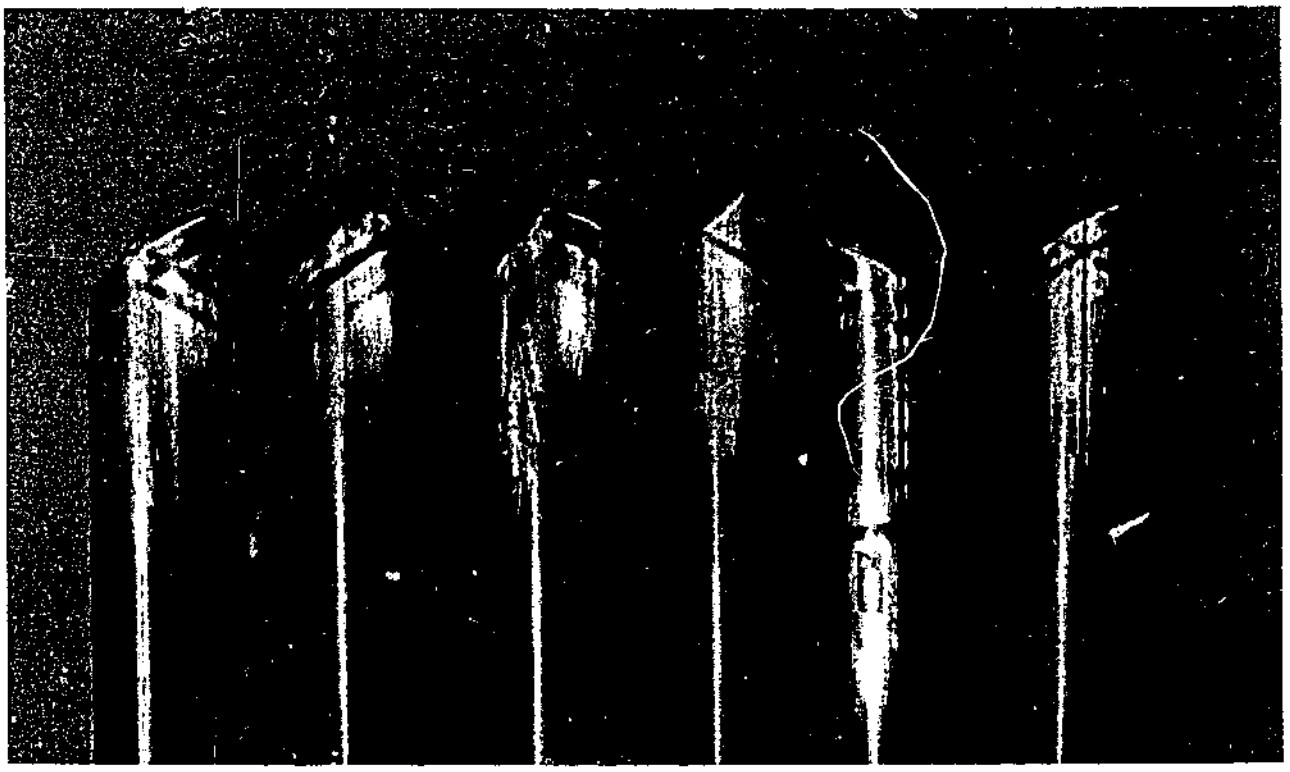

Figure 3.5-3: Multi-shear bands on full section VHS tubes

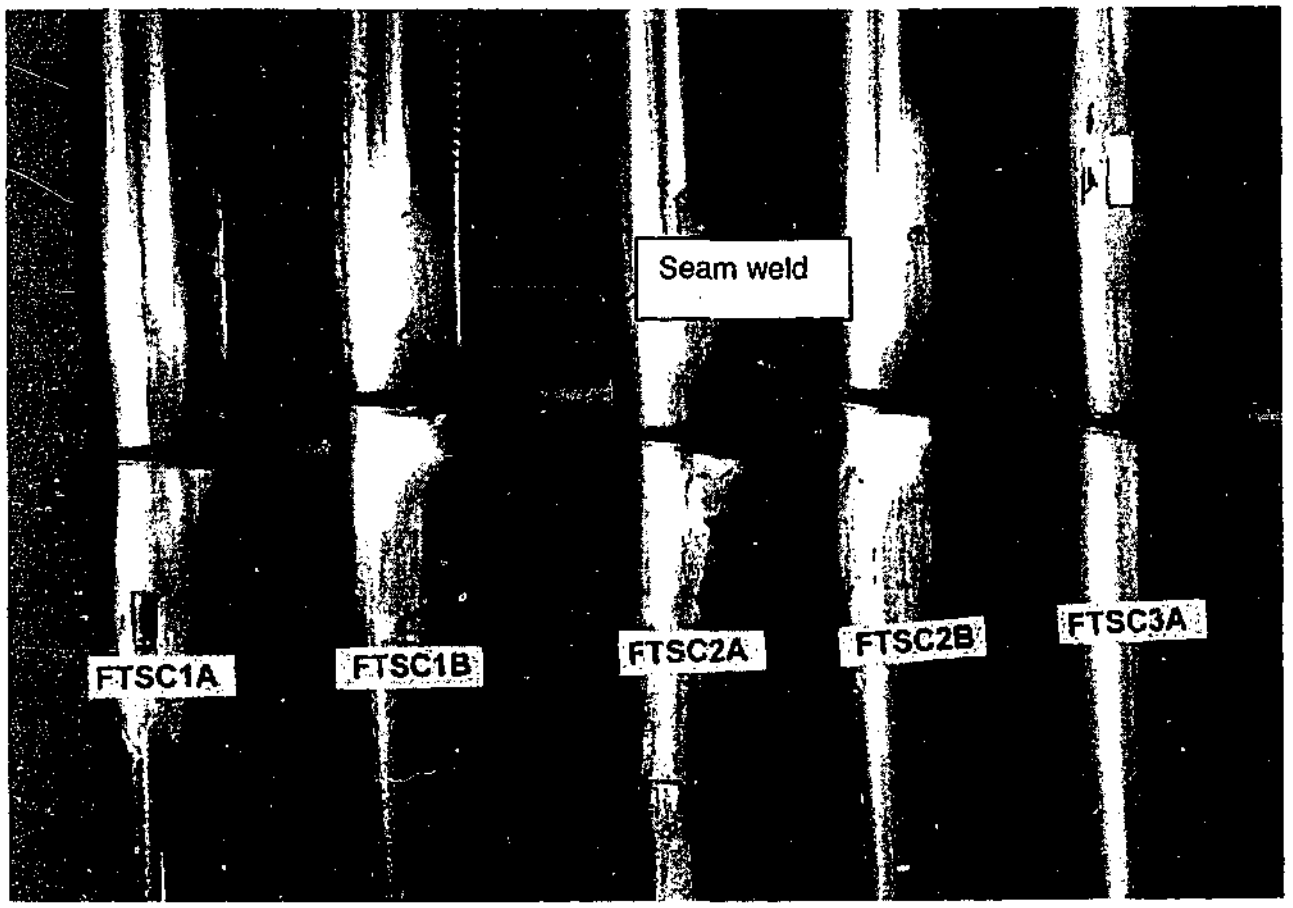

Figure 3.5-4: Failure of full section non-heat-treated tubes (from left to right: FTS1NA, FTS1NB, FTS2NA, FTS2NB, FTS3NA)

Table 3.5-2: Percentage Elongation of full section VHS tubes

Specimen Label	Percentage elongation			
	e_{50} (%)	e_{200} (%)	e_u (%)	e_0 (%)
FTS1A	13.40	6.25	2.7	12.46
FTS1B	13.20	5.05	2.5	12.27
FTS2A	10.00	5.35	2.9	9.36
FTS2B	9.80	4.70	2.75	9.16
FTS3A	11.80	5.75	2.7	11.13
FTS3B	10.40	5.45	2.36	9.81
FTS4A	10.80	4.80	2.8	10.17
FTS4B	9.00	5.20	2.9	8.47
FTS5B	10.40	5.25	3.5	9.85
FTS6A	10.60	5.30	2.4	10.11
FTS6B	11.20	5.10	2.2	10.68
MEAN	10.96	5.29	2.70	10.32
COV	0.1187	0.0776	0.1237	0.1148

Table 3.5-3: Percentage Elongation of full section non-heat-treated tubes

Specimen Label	Percentage elongation			
	Seam weld		Opposite to weld seam	
	e_{50} (%)	e_{200} (%)	e_{50} (%)	e_{200} (%)
FTUS2A	12.20	8.10	26.60	12.10
FTUS2B	13.10	9.75	28.40	13.70
FTUS3B	13.60	12.57	26.40	16.50
MEAN	13.00	10.10	27.10	14.10
COV	0.0447	0.1820	0.0331	0.1294

3.5.3 Fracture -to-Ultimate Load Ratios

The ratio of fracture-to-ultimate load, P_f/P_{max}, was used to indicate a material's ductility by Rogers and Hancock (1997). They stated that the lower the P_f/P_{max} ratio, the greater the degree of ductility. A summary of P_f/P_{max} ratios is given in Table 3.3-2 for coupons and Table 3.4-2 for full section tubes. The measured P_f/P_{max} values are plotted against the measured yield stress in Figure 3.5-5 together with the P_f/P_{max} ratios measured by Rogers and Hancock (1997). The ratio is 0.833 on average for VHS coupons and 0.934 on average for VHS full sections, and these ratios are similar to those obtained by Rogers and Hancock (1997) for G300 and G550 sheet steels, and are much larger than those (0.106 and 0.151) for non-heat-treated coupons and tubes. The low average P_f/P_{max} value of 0.106 for non-heat-treated coupons shows that it is much ductile than VHS steel.

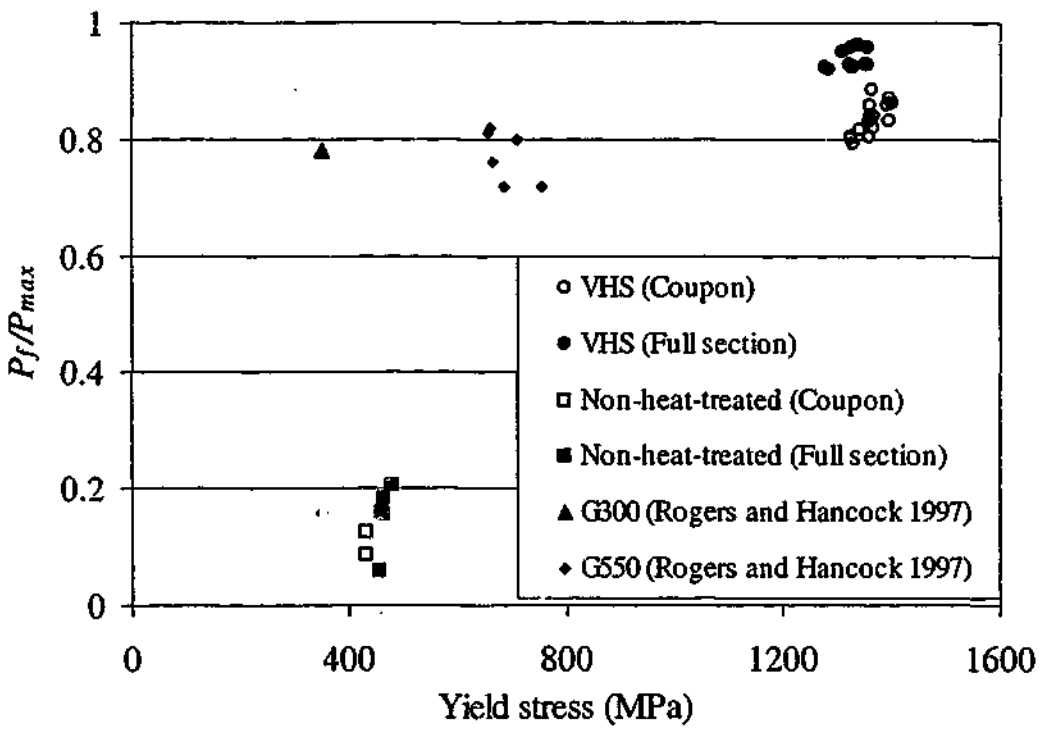

Figure 3.5-5: Fracture-to-ultimate load ratios versus yield stress

3.5.4 Ratio of ε_u to ε_y

Table 3.5-4 shows the yield strain ε_y and ultimate strain ε_u of VHS coupons and full section tubes obtained from the stress-strain curves. The average $\varepsilon_u/\varepsilon_y$ ratios are 4.057 for coupons and 4.613 for full section tubes. They are far smaller than the minimum requirement of 20 in Eurocode 3 (2002) for the method of plastic design, whereas the average $\varepsilon_u/\varepsilon_y$ ratio for non-heat-treated coupons is 29.64 (See Table 3.5-5), which is larger than this requirement. Since the ultimate strain ε_u is not uniform around the section of non-heat-treated tubes, their $\varepsilon_u/\varepsilon_y$ ratios are not summarized. Because no yield plateau is exhibited on the stress-strain curves for both VHS and non-heat-treated steel, the test results cannot be compared to the yield plateau requirement in AS4100.

Table 3.5-4: Yield strain and ultimate strain of VHS coupons and full sections

Specimen Label (1)	ε_y (%) (2)	ε_u (%) (3)	$\varepsilon_u/\varepsilon_y$ (4)
TS1A	0.914	4.248	4.648
TS1B	0.918	3.005	3.274
TS2A	0.887	4.200	4.733
TS2B	0.902	3.974	4.408
TS3B	0.877	3.272	3.731
TS4A	0.864	3.626	4.197
TS4B	0.909	2.910	3.200
TS4C	0.906	3.250	3.588
TS5A	0.901	3.960	4.398
TS5B	0.900	3.964	4.406
TS5C	0.897	3.625	4.043
MEAN	0.898	3.639	4.057
COV	0.017	0.124	0.126
FTS2A	0.871	3.663	4.204
FTS3A	0.883	4.250	4.813
FTS4A	0.895	4.261	4.760
FTS5B	0.870	4.580	5.268
FTS6A	0.902	3.623	4.018
MEAN	0.884	4.075	4.613
COV	0.014	0.091	0.097

Table 3.5-5: Yield strain and ultimate strain of non-heat-treated coupons

Specimen Label (1)	ε_y (%) (2)	ε_u (%) (3)	$\varepsilon_u/\varepsilon_y$ (4)
TS6A	0.425	12.200	28.706
TS6B	0.423	12.930	30.575
MEAN	0.424	12.565	29.640
COV	0.002	0.029	0.032

3.6 SHEAR BAND ORIENTATION

This section identifies different shear band orientations for different types of tubes or sheet steels. It intends to explore the possible reasons behind the phenomenon, such as:

- Anisotropy of steels,
- Rotation of steel crystals during plastic deformation,
- Material properties, manufacturing process,
- geometrical effects.

Very similar shear band orientations were observed for G550 sheet steel (62°) (Benham et al. 1996) and cold-formed C450 circular hollow sections (60°) (Hatherly and Malin 1984). However, completely different shear orientation or failure mode was also found for some other thin walled steels, such as maraging steel (38°) (Kusnierz 1994) and non-heat-treated steel (ductile failure, no shear band). Table 3.6-1 shows the yield stress (f_y), specimen width (b), thickness (t) and the manufacturing processes of these steels. Some failure modes are shown in Figure 3.6-1. Research is needed to explain the phenomenon observed in this section.

Table 3.6-1: Steels with different shear band

Steel Name	f_y (MPa)	t	b	b/t	Orientation Angle	Manufacturing process	Reference
VHS	1350	1.6	12	8	62.5	heat treated	This thesis
G550	658	0.4	13	30	62	cold reduced	Benham et al. (1996)
C450 CHS	450	2.0	11	6	60	cold formed	Hatherly and Malin (1984)
Maraging steel	1750	4.0	19	5	38	hot rolled	Kusnierz (1994)
NHT	430	1.6	12	8	0	cold formed	This thesis
C350	350	1.6	11	7	0	cold formed	Rogers and Hancock (1997)

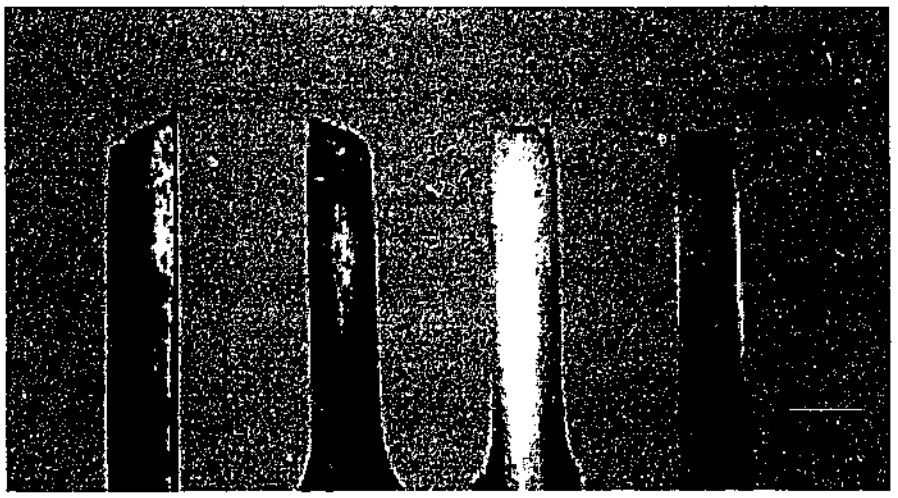

Figure 3.6-1: Failure modes of some steel coupons

3.6.1 Anisotropy of Steels

According to the maximum shear stress yield criterion (Benham et al. 1996), the shear orientation should be 45° to the principal stress for isotropic steel. The final orientation of 62.5° that was measured in the current investigation may indicate that VHS tubes become anisotropic before failure. The anisotropy of steels may be caused by different manufacturing processes, such as cold-rolling process (Hatherly and Malin 1984; Kusnierz 1994). During cold-rolling, the randomly distributed grains in a metal may orient towards a certain direction. As a result, initially isotropic steel may become anisotropic after the plastic deformation. For example, the tensile yield stress of G550 sheet steel along the direction perpendicular to the rolling direction was about 13% greater than that parallel to the rolling direction (Rogers and Hancock 1997). Similar to the mechanical process, the sequence of heat treatments may also cause grains of a steel to re-crystallize to a final texture (Anand and Spitzig 1980).

3.6.2 Rotation of Steel Crystals During Plastic Deformation

The anisotropy of steels may also form during a plastic deformation. For example, when hexagonal single crystals are stretched in tension, the base planes gradually turn towards a position parallel to the load direction. The grains of a polycrystal steel will rotate towards a limiting orientation (Hill 1998). Some of the quantitative analyses of shear band formation were based on the constitutive equations of continuum mechanics (Tvergaard 1999; Needleman and Tvergaard 1992). Hill's bifurcation theory (Hill 1958; Hill and Hutchinson 1975) was adopted to calculate the onset of the instability of a solid under static load (Tomita 1994; Okazawa and Usami 2000). It is very likely that the 62.5° (rather than 45°) shear band formed because of the rotation of the steel crystals during the plastic deformation as pointed out by Hill (1998).

3.6.3 Material Properties And Manufacturing Process

All of the steels listed in Table 3.6-1 are thin walled and in a plane stress status under axial tension. However, the chemical contents and manufacturing processes for these steels were different, and therefore the mechanical properties, such as the yield stress, ductility and failure mode may be different. For example, the maraging steel (Anand and Spitzig 1980) was a kind of ultra-high strength steel that had a measured 0.2%

proof yield stress of around 1750MPa. The shear band was formed at a tensile strain of 0.034. It was manufactured by hot rolling at 1091°C and then normalized at 900°C for 30 minutes, whereas VHS steel is produced by elevating the temperature to 950°C, quenching the steel in 20°C cold water, and then tempering at 230°C for 15 minutes. Since VHS steel and the maraging steel have different chemical contents and are manufactured in different ways, the amounts of precipitate particles in the martensite matrix, that are responsible for the ultra-high strength property of such steels (Anand and Spitzig 1980), are different. As a result, the shear stress orientation at failure may be different (38° versus 62.5°). G550 steel is produced by hot rolling to 2.5mm in thickness, and then cold reduced to 0.42mm (Rogers and Hancock 2001). This cold-reduced process made it a kind of anisotropic steel (Rogers and Hancock 1997). Although similar shear band was observed for VHS, G550 and C450 steels, different analyses models should be adopted when conducting quantitative analyses.

It is also interesting to observe from Table 3.5-5 that materials with lower yield stress (350MPa and 430MPa) have orientation of zero, while those with higher yield stress have orientations of above 38°. This may match, to some extent, the ductile necking failure for those with lower yield stress and the more brittle failure (sudden) for those with higher yield stress.

3.6.4 Geometric Effect

It was found by Okazawa and Usami (2000) that the failure mode of tensile coupons depends on the width-to-thickness ratio (*b/t*) of the specimens. Three failure modes were identified: (1) diagonal localized necking for *b/t* of 10, (2) concentrated necking for *b/t* of 4, (3) two axial symmetric localized necking for *b/t* of 1.0. It was pointed out by Hill (1998) that "When thin strips are pulled in tension (their width being at least five times their thickness), it is observed that the neck does not form directly across the specimen, but at an oblique angle which depends on the state of anisotropy". It can be seen from Table 3.6-1 that all of the samples listed have *b/t* ≥5, but different orientation angles were observed. This may indicate that different degrees of isotropy may exist in the steels. It may be concluded that the shear band orientation depends on not only the geometric *b/t* ratio, but also on the microstructure of the steel. Further research is needed to fully understand the geometrical effect.

3.7 SUMMARY

In this chapter, an investigation of the strength and ductility of VHS tubes under static tension load was presented. The material ductility of very high strength (VHS) circular steel tubes was examined mainly in terms of the ultimate strength to the yield stress ratio and the percentage elongation. The percentage elongation and the ultimate strength to the yield stress ratio have been well established as parameters for the measurement of steel ductility. These parameters can be obtained from the axial tension test. Different ductility limits are stipulated in current steel design standards.

VHS tubes and some coupons have been tested in axial tension. The test results were compared to the non-heat-treated (NHT) cold-formed steel tubes. Fracture-to-ultimate load ratio was also examined briefly. During the tests, different failure modes were observed for VHS and NHT tubes. While the NHT steel showed diffuse necking, VHS tubes showed shear band necking. Although the failure of the VHS coupons developed along a single shear band, multi-shear bands were observed in the fracture zone of full section VHS tubes. The measured percentage elongation and the ultimate strength to the yield stress ratio were higher than some cold-formed or high strength sheet steels. Both the percentage elongation for full section VHS tubes on a gauge length of 50mm and the ultimate strength to the yield strength ratio meet the requirements stipulated in AS/NZS 4600. The ultimate strength to yield stress ratio of the VHS tubes was found to be greater than some high strength cold-formed hollow sections and sheet steels, such as C450 and G500. The shear band failure mode was compared with that of other thin sheet steels. The angle between the shear band and the loading direction of VHS tubes is 62.5°. The shear band orientation and failure mode for different steels may depend on the chemical content, manufacturing process and the geometrical dimensions of the tensile specimen.

Chapter 4

VHS TUBES IN COMPRESSION

4.1 INTRODUCTION

Chapter 3 described the material ductility of VHS tubes. This chapter presents an investigation of the section capacity of VHS tubes by means of stub column tests.

Like other thin-walled tubular steel columns under compression load, local buckling may be the major phenomenon that affects the compression strength of VHS tubes when the D/t ratio reaches a certain value.

In current Australian steel structures standard AS4100 (SAA 1998), the element slenderness λ_e is used to determine the local buckling effect. For circular hollow sections, the element slenderness is calculated as:

$$\lambda_e=\left(\frac{D}{t}\right)\left(\frac{f_y}{250}\right) \tag{4.1-1}$$

where D is the outer diameter of the tube, t is the tube wall thickness and f_y is the yield stress in MPa. A compression yield slenderness limit λ_{ey} of 82 is specified for CHS in AS4100 (SAA 1998). When λ_e is greater than λ_{ey}, local buckling may happen, and the effective diameter d_e ($<D$) is introduced to determine the ultimate compressive capacity. Slightly different definitions of λ_e are used in different design codes. When converted to the format given in Eq.(4.1-1), current codes give different values of the yield slenderness limit. A summary of these limits can be found in Bradford et al. (2001). For example, λ_{ey} becomes 84.6 for Eurocode 3 (2002), 88 for AISC-LRFD (1999) and BS5950 (BSI 2000), and 89.6 for AS/NZS 4600 (SAA 1996).

It is well known that structural tubes can be manufactured by several methods. These manufacturing processes will produce different levels of residual stresses and geometrical imperfections, which will affect their structural performance. Therefore, the slenderness limit given in a design code may be suitable for certain steel tubes which are similar to those used in the calibration of the design rules, but might not be suitable for other tubular sections.

For VHS tubes, due to the high yield stress, its calculated element slenderness according to Eq.(4.1-1) becomes higher than the slenderness limit λ_{ey} in AS4100 (SAA 1998) for tubes with *D/t* ratios larger than 15. However, it was found by Zhao (2000) that the section capacity of VHS tubes with element slenderness between 87 and 138 (i.e. *D/t* between 16 and 26) reached the full yield capacity (i.e. the product of yield stress and full cross-section area). This proves that the current slenderness limit is too conservative for VHS circular steel tubes.

In order to determine the yield slenderness limit of VHS circular steel tubes, eight VHS stub columns were tested. The tested tubes have *D/t* ratios between 24 and 46 (λ_e between 135 to 258). An investigation on the geometrical imperfections and the residual stresses of VHS tubes are also presented in this Chapter in order to further understand the local buckling behaviour of VHS tubes under axial compression. Two non-heat-treated tubes were also tested to show the effect of the manufacturing process on geometrical imperfections and residual stresses.

4.2 LITERATURE REVIEW

The failure mode may be different for circular hollow sections (CHS) subjected to compression when the diameter to thickness (D/t) ratios are different. Initial imperfections and residual stress may have some influences on the buckling strength of circular steel tubes. In this section, some studies on CHS in compression and methods of imperfection and residual stress measurement are briefly reviewed.

4.2.1 Thin-Walled Shells Versus Thick Walled Columns

Different failure modes have been observed for thin-walled shells and relatively thick-walled tubes. Under axial compression, tubes with small D/t values may reach their yield capacities with an axisymmetric bulge failure mode (elephant's foot) at one end of the tube, whereas tubes with larger D/t (normally shells) may buckle elastically before yielding (Donnell and Wan 1950; Schilling 1965). The limit of the D/t value for the two failure modes also depends on the material properties. For example, Mamalis and Johnson (1983) found that the elephant foot failure mode occurred in aluminium alloy tubes with a D/t value less than 48, whereas the D/t value was found up to 220 for cold-formed circular tubes (O'Shea and Bridge 1997). It should be noticed that when D/t increased, some of the circular tubes buckled initially at one end of the tube followed by the diamond shaped collapse.

4.2.2 Methods for Measuring Geometrical Imperfections

It is generally believed that the column strength of thin-walled shells is sensitive to geometrical imperfections. Rotter (1985; 1998a; 1998b) studied the buckling strength of cylindrical steel bins and silos. He proposed three levels of imperfections for design of tubes with different manufacture qualities, as:

$$\frac{\Delta W_o}{t} \le \frac{1}{40}\sqrt{\frac{r}{t}} \qquad \text{(Class A: Excellent)} \qquad (4.2\text{-}1)$$

$$\frac{\Delta W_o}{t} \le \frac{1}{25}\sqrt{\frac{r}{t}} \qquad \text{(Class B: High quality)} \qquad (4.2\text{-}2)$$

$$\frac{\Delta W_o}{t} \leq \frac{1}{16.5}\sqrt{\frac{r}{t}} \qquad \text{(Class C: Normal)} \qquad (4.2\text{-}3)$$

where ΔW_o is the measured imperfections; r is the tube radius; t is the tube thickness.

The imperfection measurement techniques for the last fifty years were surveyed by Singer and Abramovich (1995). In his report, the probe system and LVDT scanning system were commonly used by some laboratories. In addition, there were some other methods for the measuring of initial imperfections. O'Shea and Bridges (1997) used linear displacement transducers to measure the out-of-roundness of circular steel tubes by rotating the specimens in a fixed measuring rig. A laser sensor was used by Yang et al (2002b) to measure the imperfection of thin-walled square hollow section tubes.

In this thesis, a feeler gauge was used. The detailed measurement process is described in Section 4.3.

4.2.3 Methods for Measuring Residual Stress

Residual stress is the stress that is left in a member after it is formed into a finished product. In structural steel members, residual stress may be formed by certain production procedures, such as cold-forming and heat treating. There has been a concern about the effect of residual stress on column strength. A general expression was given by Osgood (1951) to predict the buckling load of a column containing residual stress. Huber and Beedle (1954) studied the effect of residual stress on I-section columns. They found that residual stresses in the flanges were of more influence on column strength than were the residual stresses in the web.

The methods for the measurement of residual stresses on steel members can be divided into three categories: destructive, semi-destructive and non-destructive methods. One destructive method is the slicing method, in which the residual stress is released by cutting a specimen into small pieces. The residual stress is obtained based on the measured strain changes (Tebedge et al. 1973; Sherman 1969; Rasmussen and Hancock 1992). One semi-destructive method is the hole-drilling method, in which a strain gauge rosette needs to be applied around the drilled role. The most commonly used non-destructive methods of measuring residual stress are the X-ray diffraction

and ultrasound method (Runble and Sparrow 1985). In this thesis, the slicing method was used. Details are given in Section 4.4.

4.3 IMPERFECTION MEASUREMENT

The cold-forming or heat treatment process may introduce initial geometric imperfections to VHS tubes. There are two types of imperfections, namely wall imperfections and member imperfections. Wall imperfections were measured since local buckling is the concern for short columns.

During the measurement, tubes were placed on a super flat plate, and a feeler gauge (measurement ranging from 0.03mm to 1.2mm) was used to measure the gap (μ) between the tube and the plate. This method is illustrated in Figure 4.3-1 where measurements were made when the tube was rotated every 90 degree. The initial out-of-straightness of all stub column specimens were measured along the whole length and are summarized in Table 4.3-1, where L_e is the distance from the position of the maximum out-of-straightness to the near end of the tube.

It can be seen from Table 4.3-1 that the maximum initial out-of-straightness ranges from 0.03 mm to 0.07mm. The out-of-straightness is normalized with respect to the gauge length (L_r) for imperfection measurement using the following equation specified in the ECCS Buckling of steel shells: European recommendations (ECCS 1988):

$$L_r = 4\sqrt{(\frac{D-t}{2})\cdot t} \qquad (4.3\text{-}1)$$

The values of gauge length and the ratios of (μ/L_r) are given in Table 4.3-1. It can be seen that the ratio of (μ/L_r) is about 10 times less than the tolerance of 0.01 specified in ECCS (1988). This is expected since the D/t ratios of VHS tubes are relatively small (ranging from 24 to 47). It should be pointed out that the method of measurement was not exactly the same as that given in the shell buckling code (ECCS 1988), and the out-of-straightness values obtained should be viewed with caution.

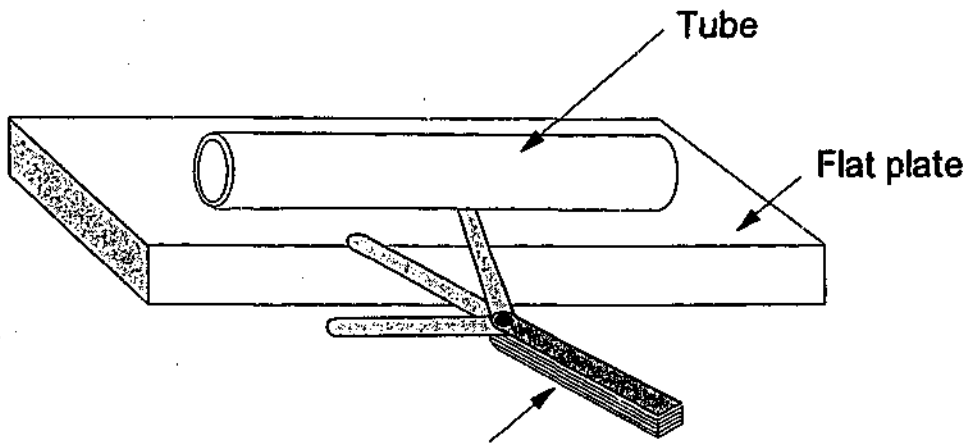

Figure 4.3-1: Imperfection measurements

Table 4.3-1. Imperfection measurements

Tube Type	Nominal Tube Size ($D \times t$) (mm)	Specimen Label	L (mm)	μ (mm)	L_e (mm)	L_r (mm)	μ / L_r
VHS	75×1.6	CS7A	299	0.03	140	30.65	0.00098
	75×1.6	CS7B	299	0.05	130	30.65	0.00163
	75×1.6	CS7C	299	0.03	100	30.65	0.00098
	57.2×1.6	CS8A	239	0.03	40	26.68	0.00112
	57.2×1.6	CS8B	239	0.03	55	26.68	0.00112
	57.2×1.6	CS8C	240	0.03	120	26.68	0.00112
	38×1.6	CS9A	140	0.07	0	21.59	0.00324
	38×1.6	CS9B	140	0.05	60	21.59	0.00232
		MEAN	-	0.04	-	-	0.00157
		COV	-	0.3536	-	-	0.52094
Non-heat-treated	38×1.6	CSNA	140	0.03	50	21.59	0.00139
	38×1.6	CSNB	140	0.03	70	21.59	0.00139
		MEAN	-	0.03	-	-	0.00139
		COV	-	0	-	-	0

4.4 RESIDUAL STRESS MEASUREMENT

The residual stress for both VHS and non-heat-treated tubes was measured by the slicing method. This method was used by former researchers on plate specimens (Rasmussen and Hancock 1992; Tebedge et al. 1973) and on tubular members (Sherman 1969; Key and Hancock 1985) to determine residual stresses.

A total of 24 strain gauges were mounted on each specimen as shown in Figure 4.4-1. Half of the strain gauges were placed along the longitudinal direction while the other half along the transverse direction. Eight strain gauges were mounted at the section located 20mm away from each end of the tube, with half of them on the inside surface and the other half on the outside surface. Four strain gauges were mounted along the longitudinal direction and four along the transverse direction on the outside surface at the mid span of the specimen in order to study the effect of cutting. No strain gauges were applied to the inner surface at middle span due to the difficulty of access.

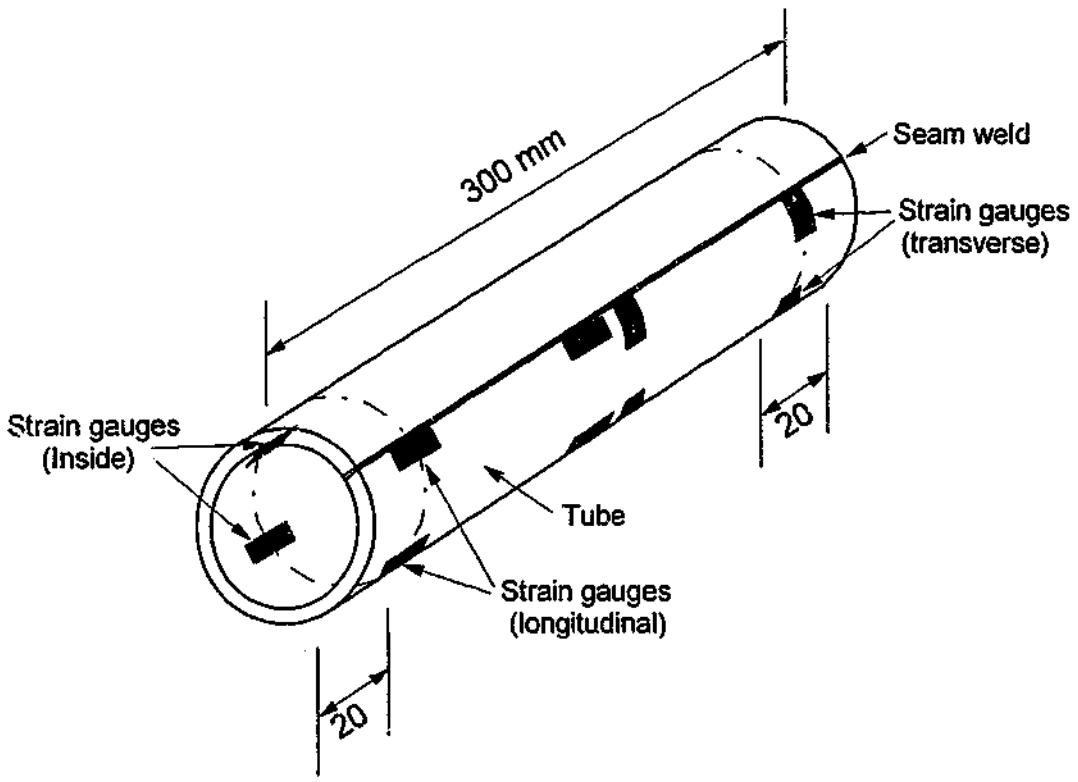

Figure 4.4-1: Measurement of residual stress

After the initial reading, cuttings were made around each strain gauge. The changes in strain were measured and the residual stress was obtained by multiplying the strain by Young's modulus (E=200GPa).

Table 4.4-1 shows the measured residual stresses for VHS and non-heat-treated tubes. The values in brackets are residual stresses measured in the middle outside surface of the tube. It can be seen that the residual stresses between the end and middle part of a tube do not differ significantly.

Table 4.4-1: Measured residual stress in MPa of VHS and Non-heat-treated tubes ($\phi 38 \times 1.6$mm)

Direction of residual stress	Tube Type	Section position	Strain gauge position from the seam (Clockwise seen from the front view of Figure 4.4-1)			
			0	90°	180°	270°
Longitudinal (MPa)	VHS	Outside	-67 (-47)	-75 (-28)	-56 (-24)	-51 (-16)
		Inside	28	41	11	24
	Non-heat-treated	Outside	303 (327)	276 (298)	213 (279)	236 (274)
		Inside	-273	-211	-194	-149
Transverse (MPa)	VHS	Outside	-60 (-110)	-47 (-61)	-34 (-31)	-49 (-28)
		Inside	49	54	39	59
	Non-heat-treated	Outside	63 (90)	55 (82)	49 (97)	72 (84)
		Inside	-108	-112	-86	-129

Note: Values in ( ) are residual stress in the middle span of 300mm tubes.

The longitudinal and transverse residual stress to yield stress ratios are plotted in Figure 4.4-2 and Figure 4.4-3 respectively. For VHS tubes, the residual stress is tensile on the inside surface and compressive on the outside surface. This tension and compression distribution pattern is similar to the pattern of the fabricated tubular columns tested by Chen and Ross (1977). The absolute average value is around 50

MPa for both longitudinal and transverse directions, which is about 4% of its yield stress. Contrary to the residual stress pattern of VHS tubes, the longitudinal residual stress of non-heat-treated tubes is compressive on the inside surface and tensile on the outside surface. The average residual stress is approximately 50% of its yield stress, which is of the same order as that of cold-formed square hollow sections tested by Key and Hancock (1985). The transverse residual stress of non-heat-treated tubes is on average about 20% of the yield stress, and thus is smaller than the longitudinal residual stress. This different residual stress distribution patterns between VHS and non-heat-treated tubes are illustrated by the cut coupons and tubes shown in Figure 4.4-4 (for the longitudinal direction) and Figure 4.4-5 (for the transverse direction). The inward bend of VHS coupons (See Figure 4.4-4) indicates that the longitudinal residual stress is compressive on the outside surface and tensile on the inside surface, whereas the outward bend of non-heat-treated coupons shows that the longitudinal residual stress is tensile on the outside surface and compressive on the inside surface. In Figure 4.4-5, the opening of the non-heat-treated tube (tensile outside and compressive inside) and the closure of the VHS tube (compressive outside and tensile inside) indicate the transverse residual stresses pattern.

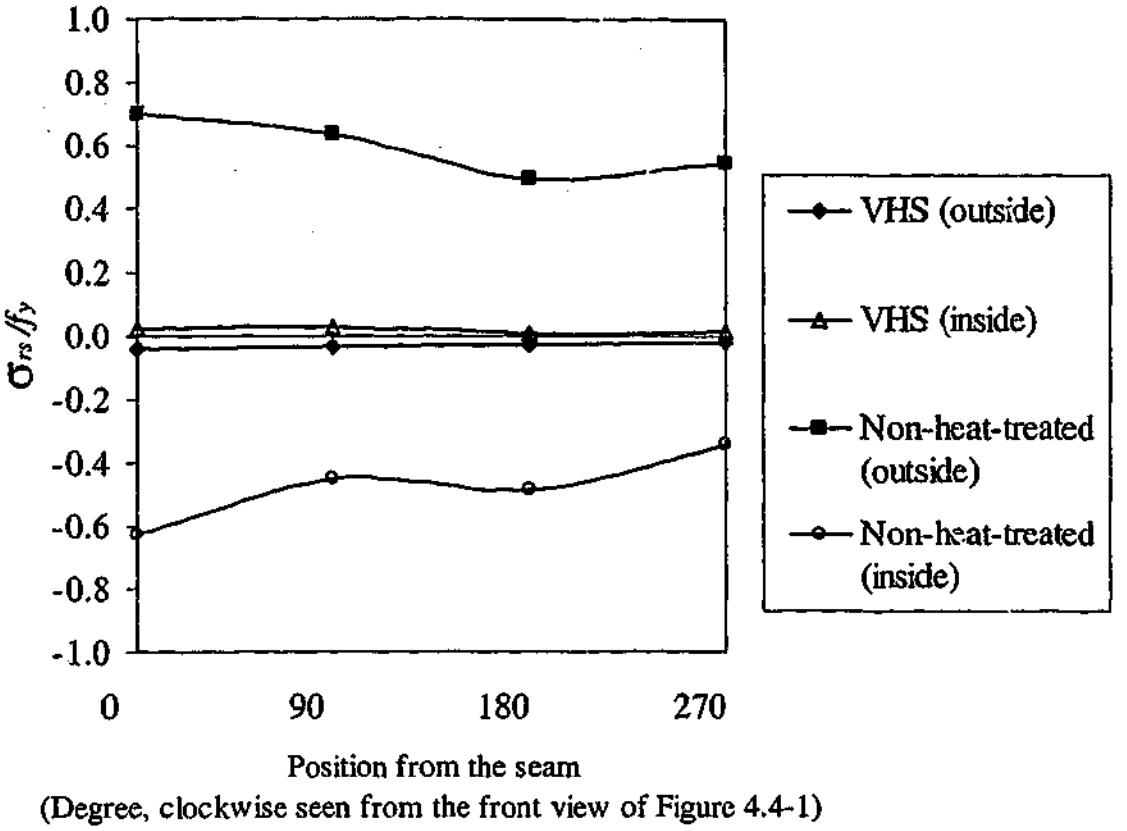

Figure 4.4-2: Longitudinal residual stress distribution

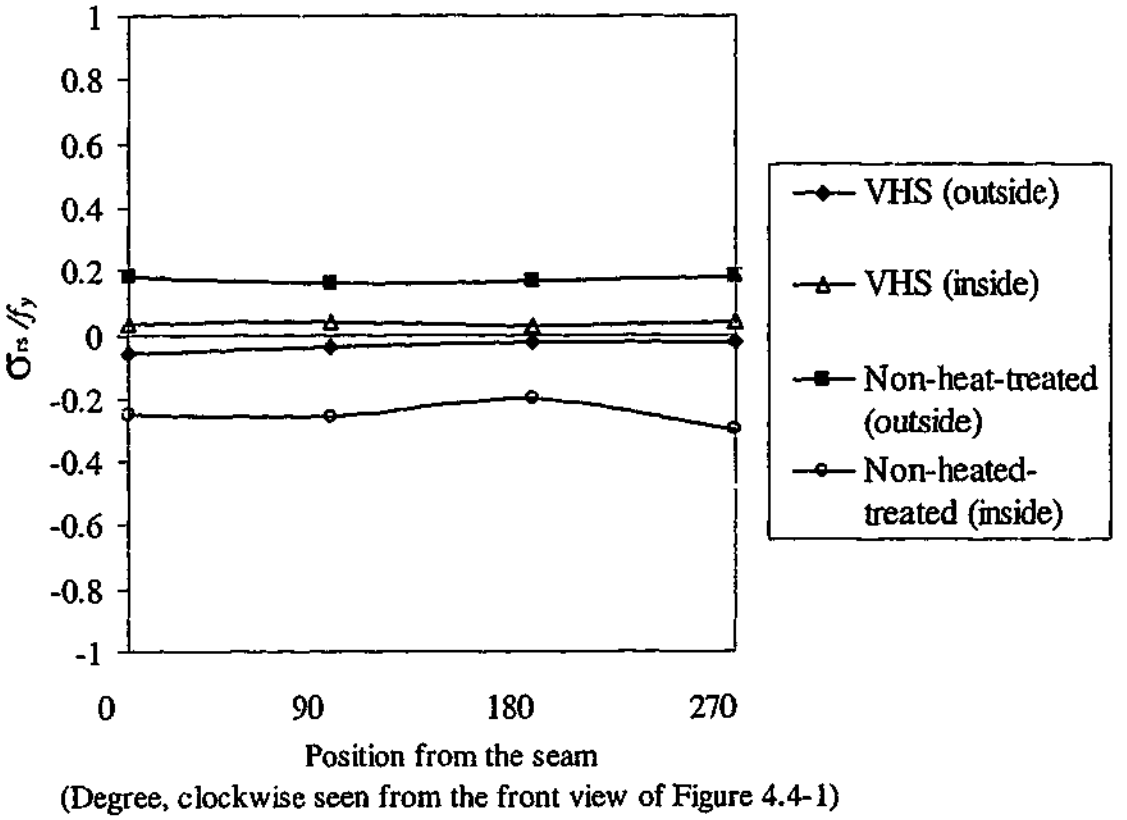

Figure 4.4-3: Transverse residual stress distribution

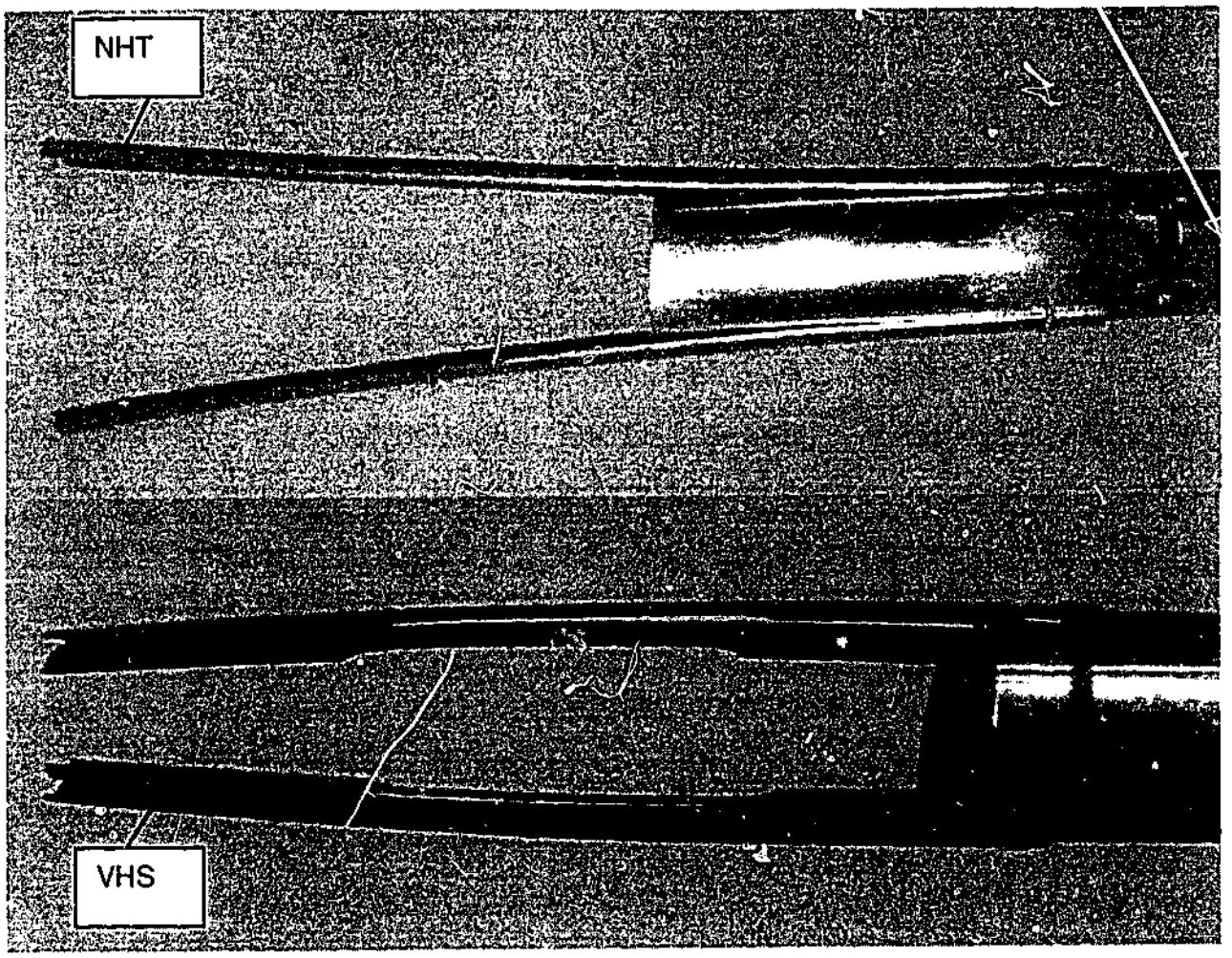

Figure 4.4-4: Tensile coupons after cutting in the longitudinal direction

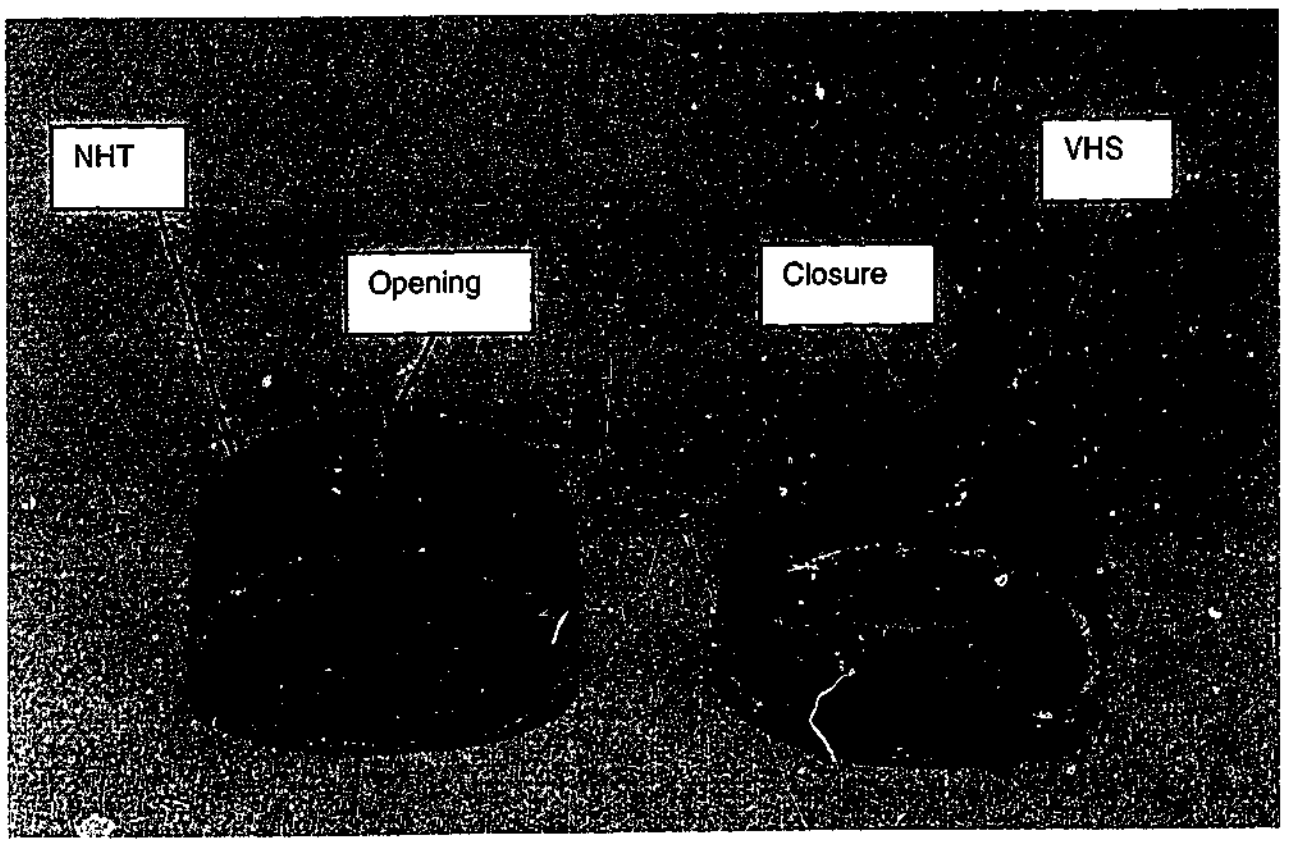

Figure 4.4-5: Release of transverse residual stress

The different production processes of VHS and NHT tubes account for the reverse residual stress distribution. The residual stress of the NHT tubes arises from the cold forming process, which prevents the tube from springing back, causing a compressive residual stress on the inside and tensile residual stress on the outside of the tube. On the other hand, the residual stress of VHS tubes may be caused by the uneven through-thickness cooling effect. Since cooling involves contraction of the section elements, the fibres that are the first to cool will end up having to contract more than strictly necessary in order to accommodate the adjacent fibres (Dowling et al. 1992), which keeps the fibres to be maintained in a state of contraction, i.e. a state of compressive stress. Because the steel fibres on the outside surface of VHS tubes will dissipate the heat faster than the inside fibres during the cooling process when tempered, the outside of VHS tubes remains in a compressive state and the inside in a tensile state.

The presence of the residual stress changes the stress-strain curves (Schilling 1965). Under a compression load, the residual compression stress causes the stress of some fibres to be equal to or larger than the yield stress. Such a partially plastic and elastic stress state makes the section enter into an inelastic state (Dowling et al. 1992; Huber and Beedle 1954). Since the measured residual stresses in VHS tubes are so small, their influence on the stub column strength would be negligible.

4.5 STUB COLUMN TESTS

4.5.1 Specimen Design and Test Setup

To study the local buckling behaviour, tubes with large *D/t* ratio need to be tested. The largest diameter of VHS tubes commercially available is 75mm with a thickness of 1.6mm. Another two sections were also selected as showed in Table 4.5-1.

Table 4.5-1: Measured dimensions of stub column specimens

Tube Type	Specimen Label	*D* (mm)	*t* (mm)	*L* (mm)	*A* (mm^2)	*D/t*
VHS	CS7A	75.42	1.61	299	373.76	46.8
	CS7B	75.51	1.62	299	374.93	46.8
	CS7C	75.31	1.61	299	372.79	46.8
	CS8A	57.42	1.64	239	287.39	35.0
	CS8B	57.47	1.63	239	285.61	35.3
	CS8C	57.42	1.63	240	286.05	35.2
	CS9A	38.20	1.58	140	181.77	24.2
	CS9B	38.18	1.58	140	181.66	24.2
NHT	CSNA	38.00	1.59	140	181.33	24.0
	CSNB	37.97	1.59	140	181.72	23.9

Other VHS tubes with smaller *D/t* ratios have been tested and reported by Zhao (2000). In order to compare the compression capacity of tubes with different residual stress distributions, two VHS tubes and their source material (non-heat-treated tubes) with the same nominal diameter of 38mm and thickness of 1.6mm were also tested. The length of stub column specimens was determined according to AS/NZS 4600

(SAA 1996), such that they are short enough (less than 20 times the radius of gyration of the section) to avoid the overall buckling and long enough (larger than 3 times the outside diameter) to eliminate end effects. Both ends of each specimen were milled flat so that the two faces are parallel to each other. The measured specimen dimensions are listed in Table 4.5-1. The specimen labels follow those adopted by Zhao (2000). The first letter in a label (C) refers to compression test, followed by section number (S7 to S9 or SN). Letter N refers to non-heat-treated tubes. The last letter (A to C) represents repeated samples. Specimens CS7A to CS8C were tested in a 5000kN capacity Amsler testing machine with a loading rate of 0.5mm/min, whereas tests of CS9A to CSNB were conducted in a 500kN capacity Baldwin machine with the same loading rate. Two strain gauges were mounted on each tube and two string-pots were used to measure the displacement in the same way as in Zhao (2000).

4.5.2 Test Results

Initial imperfections have significant influence on the strength of thin-walled shells (Donnell and Wan 1950; Calladine 1995). The effect of initial imperfection on the strength of VHS tubes seems insignificant because of the small initial out-of-straightness and the relatively small D/t ratios. All failure happened at approximately $D/5$ away from one end of the tube (see Figure 4.5-1), which shows that tubes with low D/t ratio (D/t up to 220 in (O'Shea and Bridge 1997)) will form a ring-like bulge (elephant's foot) near one of the loaded edges (Dowling et al. 1992). For VHS tubes with D/t=47, a diamond shaped inelastic local buckling was formed following the initial ring-like bulge as shown in Figure 4.5-2. A sudden load drop was observed when the tube buckled at the bottom end. The typical load-displacement curves of each section are plotted in Figure 4.5-3. During the test, a video camera was used to record the failure process. The failure of a tube can be illustrated by matching simultaneously the buckling picture with the load-displacement data. The sudden drop from point (a) to point (b) in Figure 4.5-3 corresponds to the buckling happened at the bottom end of the tube as shown in Figure 4.5-2 (a) and Figure 4.5-2 (b). In addition, when a bulge was formed at one end of a tube, the further shortening of the tube under the applied load was concentrated on the bulge, and strains of other sections away from the bulge began to release elastically. Figure 4.5-4 shows the typical stress-strain

curve determined from average readings of the two strain gauges at the middle height of the specimen. Point (a) at the maximum load in Figure 4.5-4 corresponds to the point (a) in Figure 4.5-2 and Figure 4.5-3.

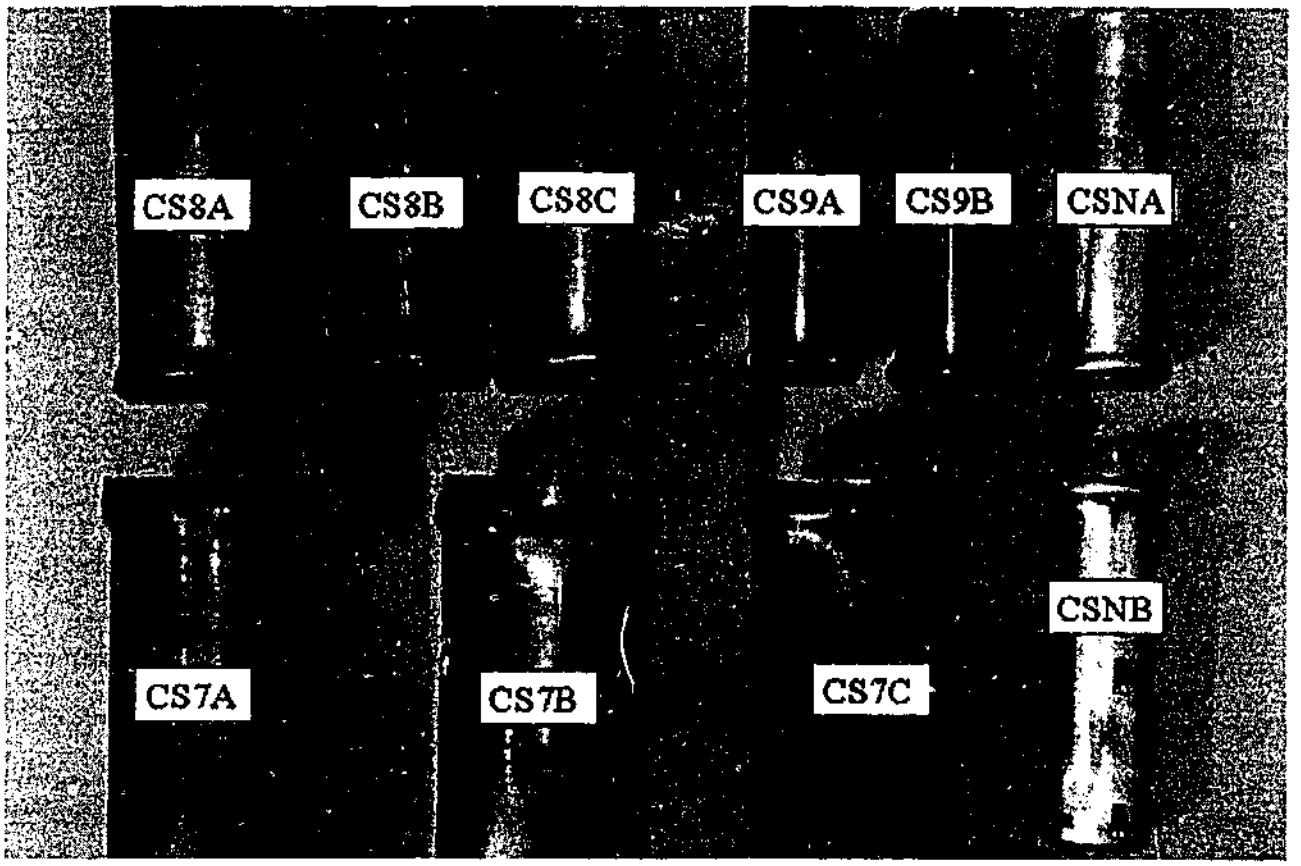

Figure 4.5-1: Failure mode of stub columns

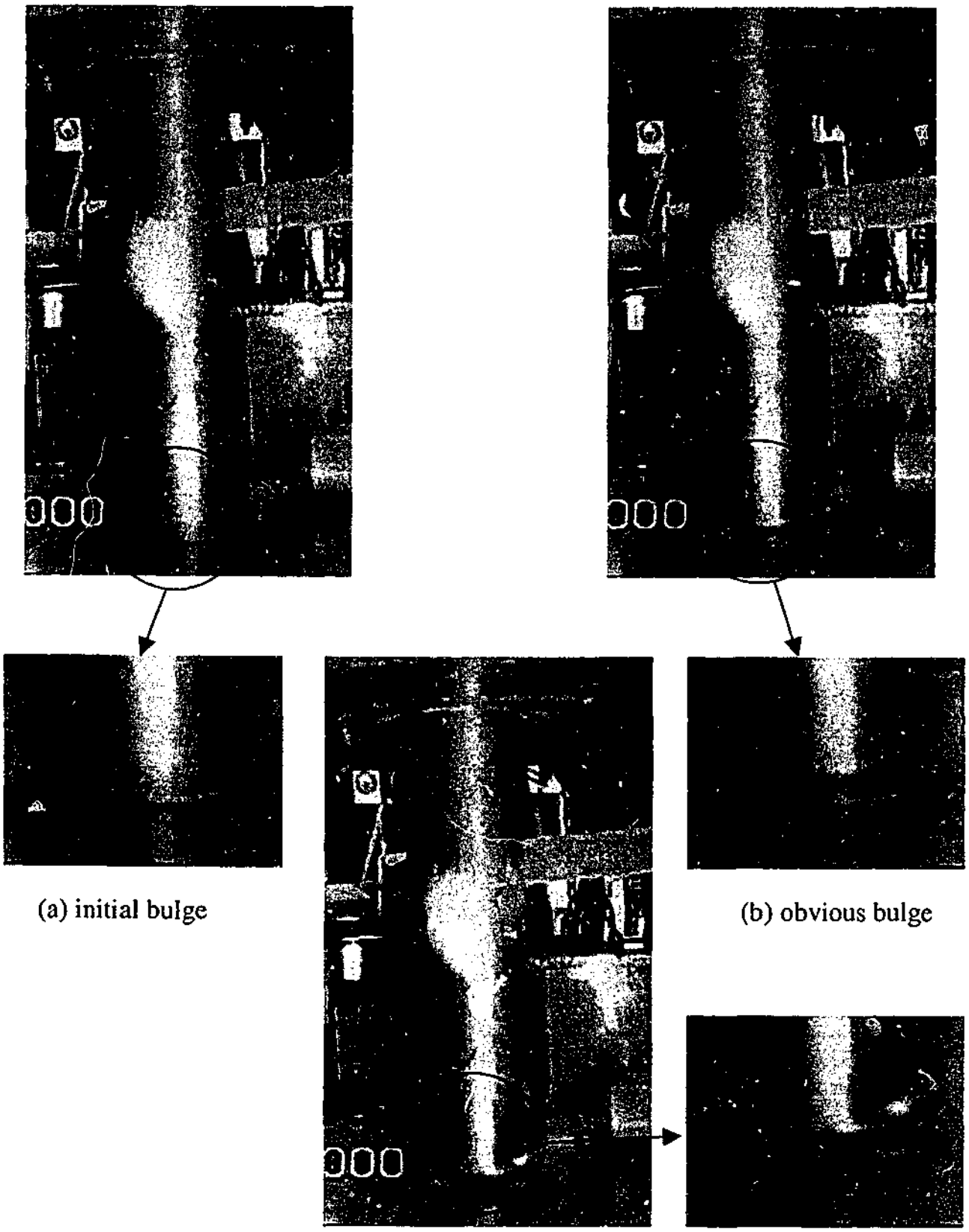

(a) initial bulge

(b) obvious bulge

(c) diamond shape

Figure 4.5-2: Failure process of CS7A. (a), (b) and (c) correspond to the letters in Figure 4.5-3.

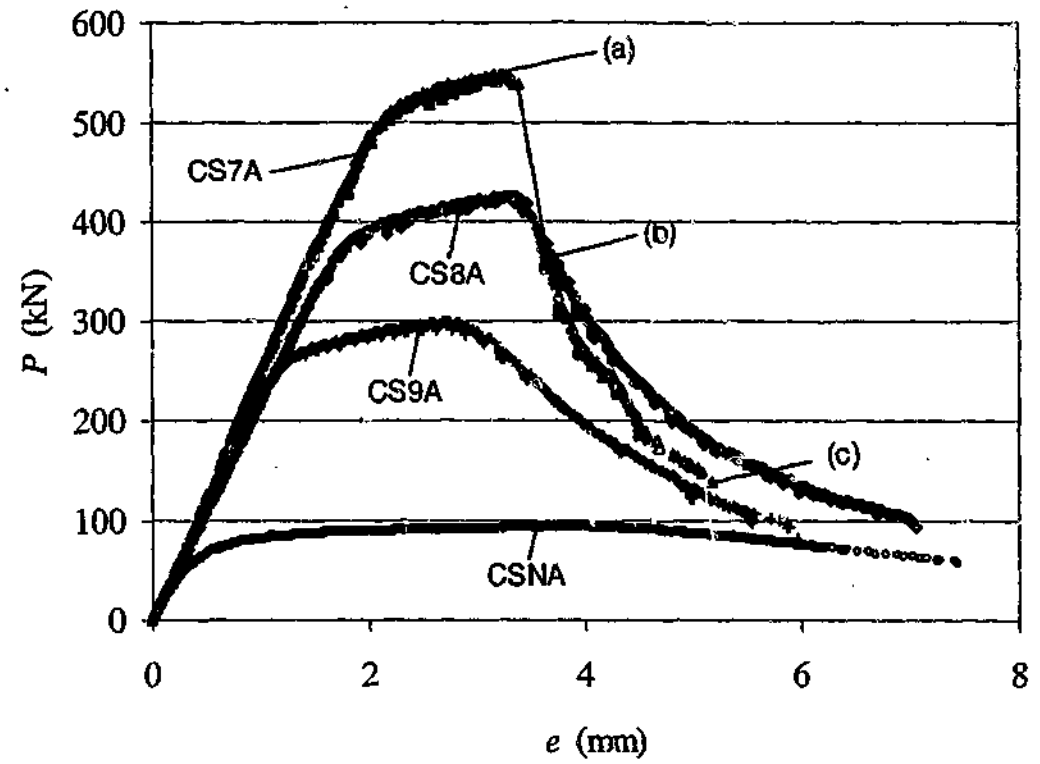

Figure 4.5-3: Typical load-displacement curves

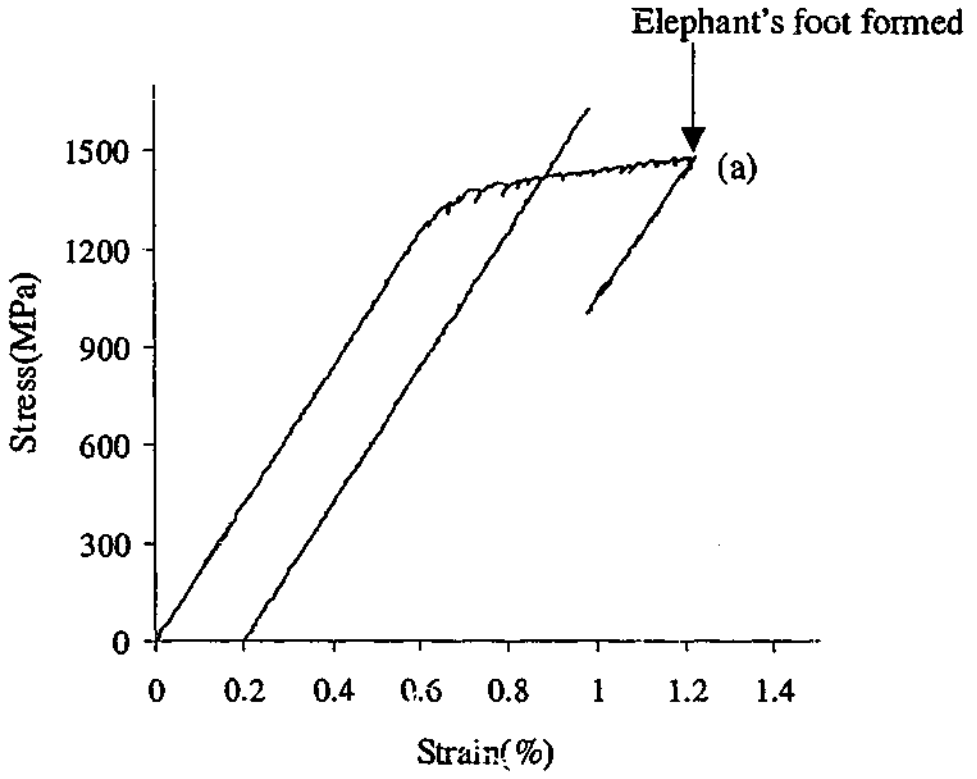

Figure 4.5-4: Typical stress-strain curve of stub column (CS7A) at the middle height

4.6 YIELD SLENDERNESS LIMIT

The measured ultimate load (P_{ult}), the calculated full section capacity ($P_{section}$) and the non-dimensional local buckling parameter (α) are shown in Table 4.6-1.

Table 4.6-1: Stub column tests results

Tube Type	Specimen Label	P_{ult} (kN)	$P_{section}$ (kN)	$P_{ult}/P_{section}$	f_{yt} (MPa)	f_u (MPa)	λ_e	α
VHS	CS7A	547	515	1.063	1377	1464	258	3.08
	CS7B	549	516	1.063	1377	1464	258	3.08
	CS7C	547	513	1.066	1377	1467	258	3.08
	CS8A	425	391	1.087	1360	1479	190	4.16
	CS8B	430	388	1.107	1360	1506	192	4.13
	CS8C	423	389	1.087	1360	1479	191	4.14
	CS9A	298	254	1.172	1398	1638	135	5.69
	CS9B	295	254	1.160	1398	1622	135	5.69
	MEAN			1.101	1376	1515		
	COV			0.0367	0.011	0.045		
NHT	CSNA	93	79	1.181	433	511	41	18.90
	CSNB	93	79	1.182	433	512	41	18.97
	MEAN			1.181	433	512		
	COV			0.0005	0	0.001		

$P_{section}$ is calculated by using the cross-sectional area and the yield stress f_{yt} (0.2% proof stress) obtained from tensile coupon tests in Chapter 3 and Zhao (2000). α is the non-dimensional local buckling parameter used in some design codes, such as AISI (1996) and AS/NZS 4600 (SAA 1996). It is defined as:

$$\alpha = \frac{E / f_y}{D / t} \tag{4.6-1}$$

λ_e in Eq.(4.1-1) can be rewritten in terms of α:

$$\lambda_e = \frac{E}{250 \cdot \alpha} \tag{4.6-2}$$

The P_{ult} /$P_{section}$ ratios of all VHS tubes tested in this thesis and in Zhao (2000) are plotted (in solid and hollow circles) against the element slenderness λ_e in Figure 4.6-1 together with some former test data on CHS (O'Shea and Bridge 1997; Prion and Birkemoe 1992; Sherman 1992). Different slenderness limits in the references (SAA 1998; Bradford et al. 2001; Eurocode 3 2002) are also illustrated.

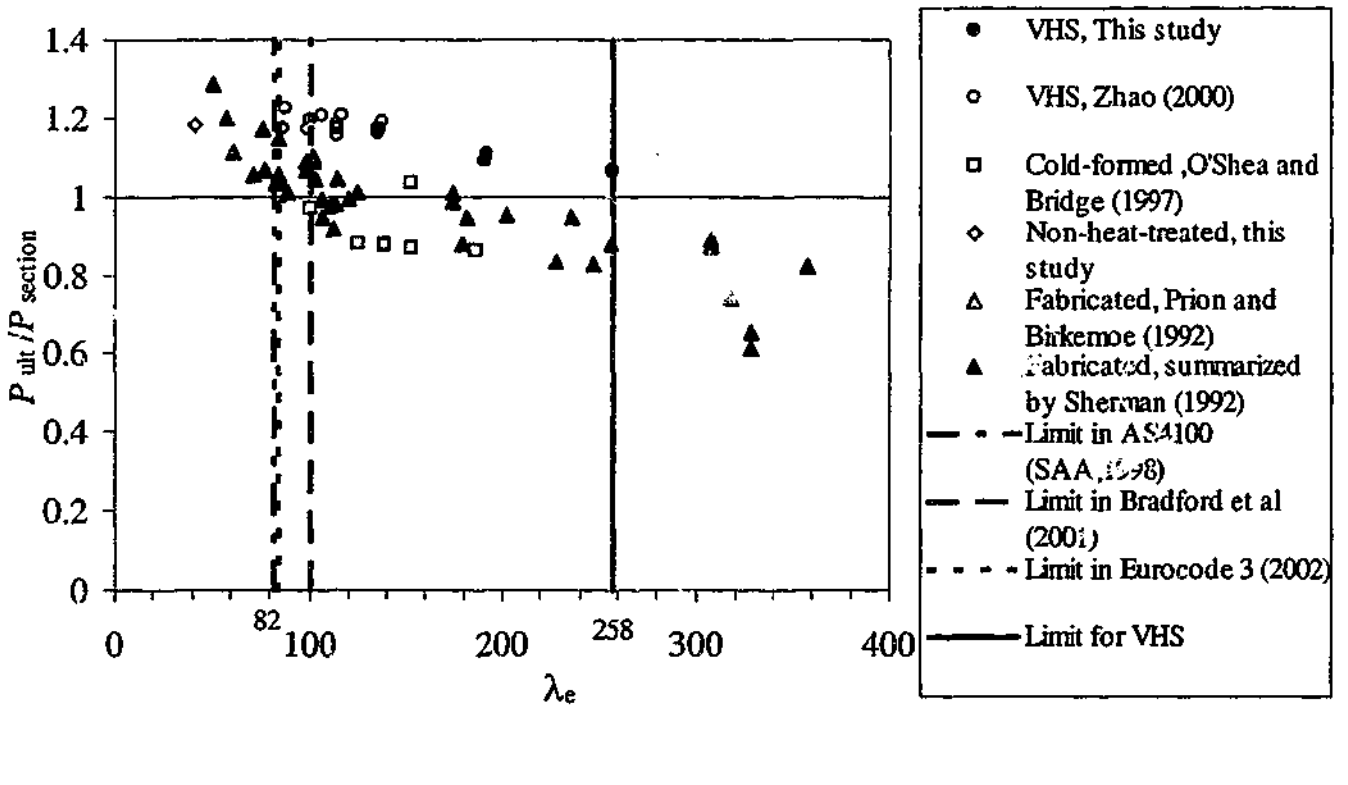

Figure 4.6-1: Element slenderness versus $P_{ult}/P_{section}$

It can be seen that the limit of 82 in AS4100 (SAA 1998), 84.6 in Eurocode 3 (2002) seems suitable for cold-formed CHS but slightly conservative for fabricated tubes. The limit of 100 proposed by Bradford et al. (2001) seems suitable for fabricated tubes, but still very conservative for VHS tubes. According to the element slenderness values of VHS tubes in this Chapter, an element slenderness limit of 258 can be proposed. These different slenderness limits on one hand reflect different residual stresses and geometrical imperfections generated during different manufacturing processes. On the other hand, it is interesting to observe that the ratio of the new limit of 258 for VHS tubes to the current limit of 82 for cold-formed CHS is 3.15, which is similar to the ratio of the yield stress (1350MPa) for VHS tubes to the yield stress (350MPa to 450MPa) for cold-formed CHS, i.e. 3.86 to 3.0. It seems that the yield slenderness limit (λ_{ey}) may be affected by the manufacturing process as well as the yield stress of the tube. The value of λ_{ey} is plotted in Figure 4.6-2 against the yield stress of CHS. More research is needed to either determine λ_{ey} for CHS produced using different manufacturing processes and with yield stress ranging from 450MPa to 1350MPa, or alternatively to keep λ_{ey} as a constant (e.g. 82) and to derive a new expression of element slenderness λ_e which has a new material parameter rather than that (f_y/250) used in Eq.(4.1-1).

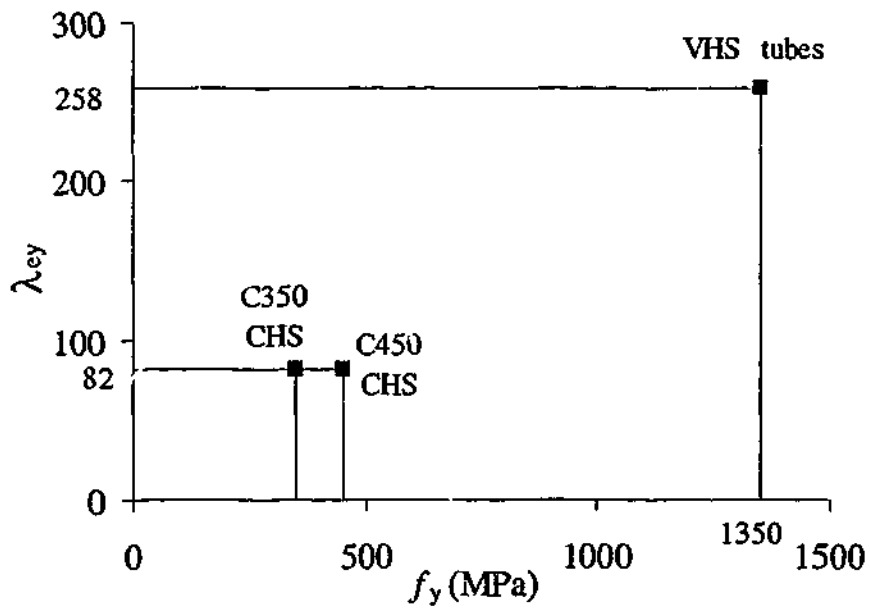

Figure 4.6-2: λ_{ey} versus f_y

As in Figure 4.6-1, the same data are plotted in Figure 4.6-3 against the non-dimensional local buckling parameter α. It should be noted that for thinner tubes, λ_e becomes larger whereas α becomes smaller. The limits of 8.93 in AS/NZS4600 (SAA 1996), 9.46 in Eurocode 3 (2002) and 9.1 in AISI (1996) are found to be suitable for cold-formed tubes but conservative for VHS tubes. A limit for α of 3.1 is obtained for VHS tubes based on the test data.

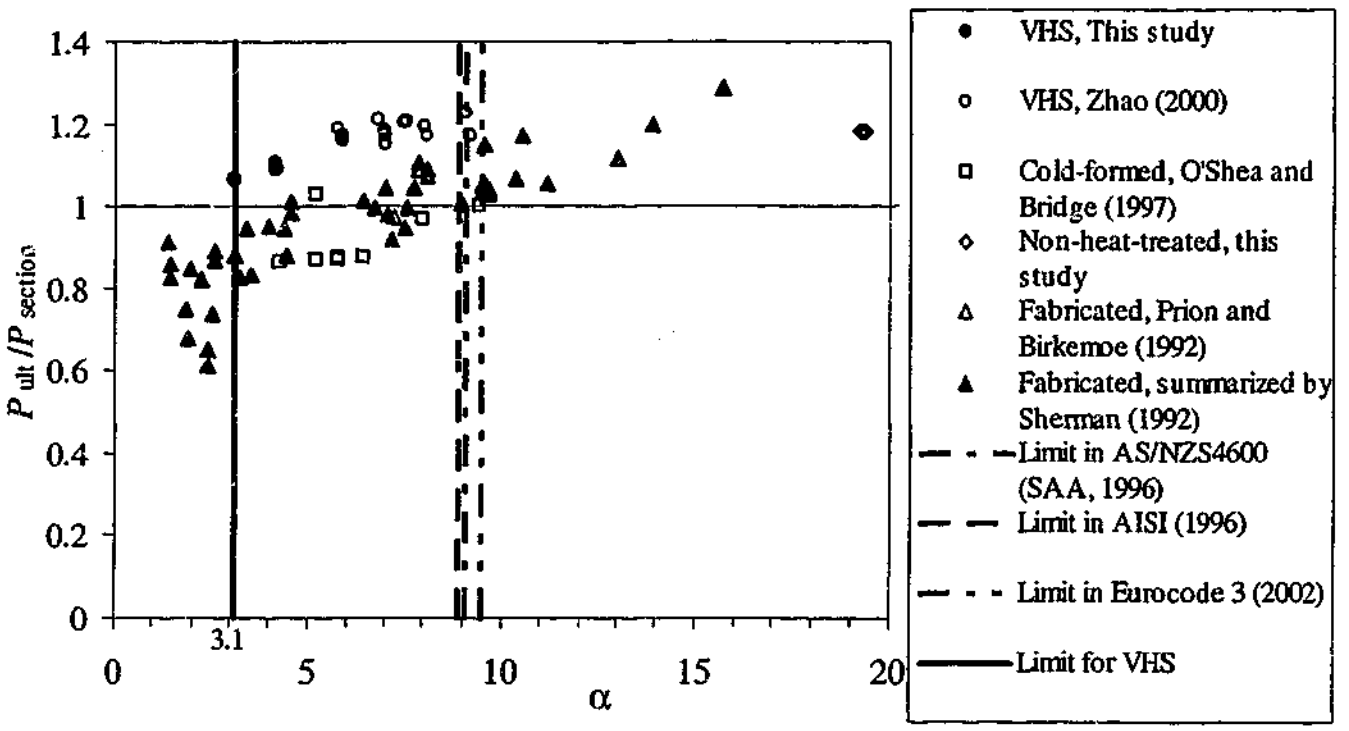

Figure 4.6-3: Non-dimensional local buckling parameter versus $P_{ult}/P_{section}$

4.7 SUMMARY

This chapter has presented the results of an investigation of the initial geometrical imperfections, residual stresses and yield slenderness limit of VHS tubes. The out-of straightness of stub columns was measured with a feeler gauge. The residual stress of VHS tubes was measured by the slicing method. The aim of these measurements was to examine their influence on the buckling and strength of VHS tubes in compression.

The out-of-straightness was found to be about $L/6800$ on average, where L was the length of the stub column. Both VHS tubes and non-heat-treated tubes had a similar level of geometrical imperfections. The measured residual stress was found on average approximately 4% of the yield stress, with the outside surface in compression and the inside surface in tension. The residual stress pattern obtained for non-heat-treated tubes was very different from that of VHS tubes.

Stub columns were tested with the element slenderness ratio ranging from 135 to 258. A new element slenderness limit (λ_{ey}) of 258 and a non-dimensional local buckling parameter limit of 3.1 are proposed for VHS tubes. The very large value of λ_{ey} was obtained partly because of the very large yield stress used in the definition of element slenderness and partly because of the very low residual stress in the section. Stub columns of non-heated-treated tubes were also tested in the same manner. The results were compared with those of the VHS tubes.

Chapter 5

VHS TUBES IN BENDING

5.1 INTRODUCTION

Chapter 2 and Chapter 3 studied the tension and compression behaviour of VHS tubes. The tensile test results showed that the minimum elongation requirements specified in AS/NZS4600 (SAA 1996) was met in terms of the percentage elongation and the ultimate strength to the yield stress ratio. A section slenderness limit of 258 for VHS tubes under compression was proposed. This Chapter focuses on the bending capacity of VHS tubes.

In real life applications of circular steel tubes in bending, the tube section may consist of shear forces and bending moment. In this situation, the steel member may be in a complicated stress-strain state. In this study, only tubes subject to a sole bending moment, i.e. pure bending, was studied. VHS tubes subjected to more complicated load conditions may be studied as future work.

Similar to the failure mode of a CHS under compression, circular steel tubes under a bending moment may yield or lose stability before yielding depending on the section slenderness of the tube. Two kinds of instabilities are associated with the bending of CHS. One is the local buckling in the compression part of the tube. The other is the section ovalisation. The ovalisation may reduce the bending capacity of CHS members.

In current steel design standards, such as AS4100 (SAA 1998), steel tubes are grouped into three categories according to the tube's section slenderness (Hasan and Hancock 1989; Wilkinson and Hancock 1998; Zhao and Hancock 1991), i.e. compact section, non-compact section and slender section. For compact section, the plastic bending

moment can be reached. The section limits of circular steel tubes for plastic design were expressed as follows in some of the current standards:

in AISC (AISC 2000):

$$D/t < 0.0448E/f_y$$

in AS4100 (SAA 1998):

$$\lambda = \frac{D}{t}\frac{f_y}{250} < 50$$

in AISI (2001) and AS/NZS4600 (SAA 1996)

$$D/t \le 0.07E/f_y$$

in Eurocode 3 (2002):

$$D/t \le 50 \cdot \frac{235}{f_y}$$

A limit of 14 on non-dimensional local buckling parameter $\alpha = (\frac{E}{f_y})/(\frac{D}{t})$ was also proposed by Sherman (1992). Table 5.1-1 gives a summary of these limits if applied to VHS tubes with E=200GPa and f_y=1350MPa. A D/t limits between 6 and 10 was obtained. The limit is much lower than those of 36 and 28 for tubes with the yield stress of 350 and 250MPa. Therefore, tests are needed to verify the limit for VHS tubes.

Twelve tests are reported in this Chapter on VHS tubes subject to bending. The diameter to the thickness ratios of tested VHS tubes range from 16 to 48. New section slenderness limits are proposed for VHS tubes in pure bending.

Table 5.1-1: Comparison of slenderness limits for plastic design (compact) of VHS tubes in bending (f_y=1350MPa)

References	D/t limit	λs limit	α limit
AISC (2000)	6.6	36	22.3
AS4100 (1998)	9.3	50	16.0
AISI (2001), AS/NZS4600 (SAA 1996)	10.4	56	14.3
Eurocode 3 (2002)	8.7	47	17.0
Sherman (1992)	10.6	57	14.0

5.2 LITERATURE REVIEW

5.2.1 Bending Tests of Circular Hollow Section (CHS)

Circular hollow section steel beams have a long history and wide application in civil engineering structures. Bending tests were extensively conducted on circular tubes produced with different manufacturing methods. Sherman (1976) tested some hot-formed and electric-resistance welded (ERW) tubes. The tubes' outside diameter was around 270mm with wall thickness between 2.5mm to 15mm. The yield stress of the tested specimens was around 350 MPa. More bending tests on manufactured, hot-rolled and ERW tubes were reported by Sherman (1986). During the tests, the ultimate bending moment, rotation capacity and failure modes were recorded. In addition to these measurements, Jirsa et al (1972) measured the section ovalisation of circular steel tubes in a 4-point-bending test. The *D/t* ratios of the tested tubes were between 30 and 78. The plastic buckling of steel and aluminium cylindrical tubes was experimentally investigated by Reddy (1979). All these tests were performed under a static load. Steel tubes subjected to cyclic loading were studied by Lee et al (2001). Recently, Elchalakani et al (2001a; 2001b; 2002a; 2002b) investigated the bending

capacity, slenderness limits and post buckling behaviour of cold-formed circular steel tubes.

This Chapter deals with the tests of VHS tubes subjected to pure bending. The test results are compared with those obtained from cold-formed, manufactured and hot-rolled steel tubes.

5.2.2 Rotation Capacity Requirements of Steel Beams

It is obvious from a bending test that both the bending moment capacity and the rotation capacity of a circular steel tube are related to *D*/*t* ratio of the tube. For compact section, the plastic bending moment can be reached and a plastic hinge may be formed. However, if the plastic method is used in the structural design, the section rotation capacity of the tube need to meet certain rotation requirement.

In general, the rotation capacity of a plastic hinge is defined from the moment-curvature curve as illustrated in Figure 5.2-1.

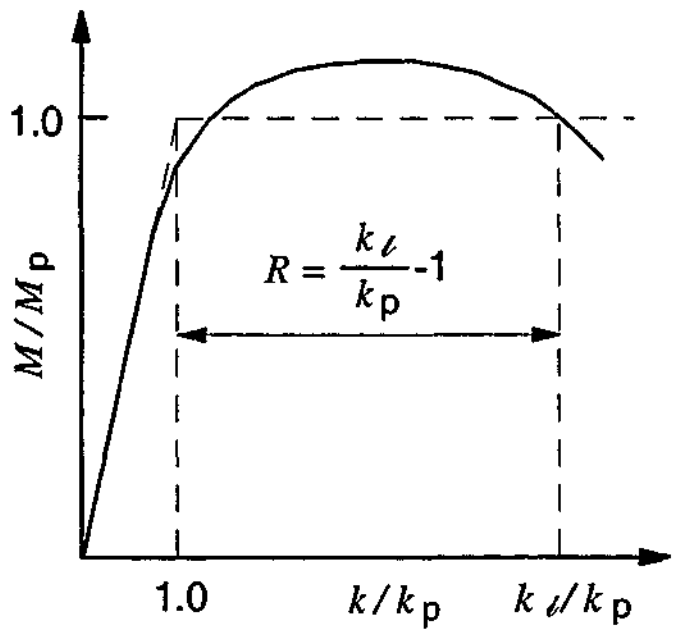

Figure 5.2-1: Illustration of plastic hinge rotation capacity

In Figure 5.2-1, κ is bending curvature; M is the bending moment; M_p is the plastic bending moment; κ_p and κ_l are the curvatures corresponding to the plastic bending

moment at ascending and descending path on the normalized moment-curvature curve. R represents the rotation capacity.

Investigations on the section rotation requirements were performed by many researchers. Korol and Hudoba (1972) studied several structures and proposed a rotation requirement of R=4. Hasan and Hancock (1989), Zhao and Hancock (1991), Wilkinson and Hancock (1998) experimentally investigated rectangular hollow section cold-formed steel beams. They found that a value of R=4 was sufficient for the plastic analysis of rectangular hollow sections. Stranghoener and Sedlacek (1994) studied the rectangular, square and circular hollow section continuous beams by means of experimental and finite element analysis method. They proposed a value of R=3 for continuous beams. In addition to the experimental study, research on the rotation capacity of steel beams was also conducted theoretically. Stranghoener and Sedlacek (1996) studied the buckling of squire hollow section and gave a formula for the descending branch of the moment-curvature curve used for the calculation of rotation capacity. Li et al (1995) presented a method to calculate the necessary rotations for the redistribution of bending moment in a continuous beam.

In this Chapter, both R=3 and R=4 are used in calibrating the plastic slenderness limits of VHS tubes.

5.2.3 Ovalisation of Circular Tubes in Bending

Ovalisation is a unique phenomenon of CHS under bending. It is caused by the stress component (P2) in the transverse direction of the bending stress (P) as shown in Figure 5.2-2.

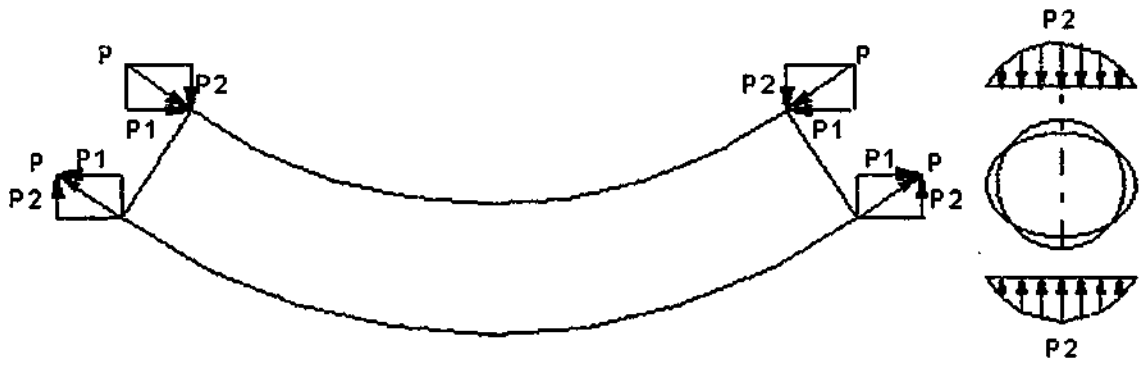

Figure 5.2-2: Illustration of ovalisation of CHS under bending

The ovalisation phenomenon of CHS was also named as Brazier effect, since it was firstly investigated by Brazier (1927). He assumed an infinitely long circular tube under pure bending. Therefore, the end effect was eliminated. The section stress was within the elastic range. By using the principle of minimum strain energy and the calculus of variations, he concluded that a maximum bending moment was reached at a redial deflection of (2/9)r. Here r is the median radius of the undeformed tube. The ovalisation of circular tubes in the non-linear (strain hardening) range was investigated by Ades (1957). He assumed that initially round tubes would become elliptical in shape during pure bending. The same least work principle was used. Ades's theory was extended by Wilhoit and Merwin (1971) to circular tubes subjected to a load combination of bending moment and axial force. Alternatively, Munz and Mattheck (1982) proposed an analytical solution by considering the vertical component of the axial bending stresses. Later, Wierzbicki and Sinmao (1997) used a simplified model to simulate the Brazier effect. In their model, two semi-circular arcs and two flat regions were used to simulate the section flattening instead of the elliptical shape used by Ades (1957).

5.3 BENDING TEST OF VHS TUBES

5.3.1 Test Setup

5.3.1.1 Specimen Preparation

Twelve VHS tubes, with the nominal diameters of 31.8mm, 38mm, 57.5mm and 75mm and nominal thickness of 1.6mm, 1.8mm and 2.0mm, were tested. Eight specimens were tested in a four-point-bending rig (described in Section 5.3.1.2) and the other four were tested in the pure-bending rig used by Elchalakani et al (2001a; 2002a). The length of each specimen was 1500mm. The measured section dimension and section slenderness (ranging from 87 to 264) are listed in Table 5.3-1. The letter B in a label refers to bending tests, followed by the section number S1 to S12.

Table 5.3-1: Specimen dimensions

Specimen Label	D (mm)	t (mm)	D/t	A (mm^2)	λ_s	Test Method
BS1	31.86	1.56	20	148.5	108	4-point-bending
BS2	31.86	1.76	18	166.7	93	4-point-bending
BS3	31.93	1.96	16	184.3	88	4-point-bending
BS4	38.04	1.58	24	181.3	134	4-point-bending
BS5	38.16	1.78	21	203.4	117	4-point-bending
BS6	38.06	1.98	19	224.8	102	4-point-bending
BS7	57.15	1.58	36	275.3	197	4-point-bending
BS8	75.95	1.59	48	370.7	264	4-point-bending
BS9	31.76	1.97	16	184.4	87	Pure bending
BS10	38.10	1.97	19	223.6	103	Pure bending
BS11	57.08	1.56	37	272.1	198	Pure bending
BS12	75.98	1.59	48	370.8	264	Pure bending

5.3.1.2 Test Facilities

Figure 5.3-1 shows the four-point-bending rig used in the test program. A hydraulic jack was attached to the Baldwin machine to increase the travel range. Four pin-connected wheels were used at the loading and supporting points that can rotate freely during tests. Therefore, the friction between tubes and the wheels may be considered as minimal.

The moment M is calculated from the applied load P as follows:

$$M = P'L' \qquad (5.3\text{-}1)$$

$$P' = \frac{P}{2\cos\theta} \tag{5.3-2}$$

$$L' = L_o / \cos\theta - (D + d)\tan\theta \tag{5.3-3}$$

The symbols of L', P', θ, D and d are shown in Figure 5.3-2 with d=70mm and L_o=400mm. The part of the specimen outside the pure bending range is treated as straight element, as observed during tests. A specimen under testing is shown in Figure 5.3-3. It can be seen from Figure 5.3-3 that very large curvature was achieved for some VHS tubes (with $D/t \leq 24$).

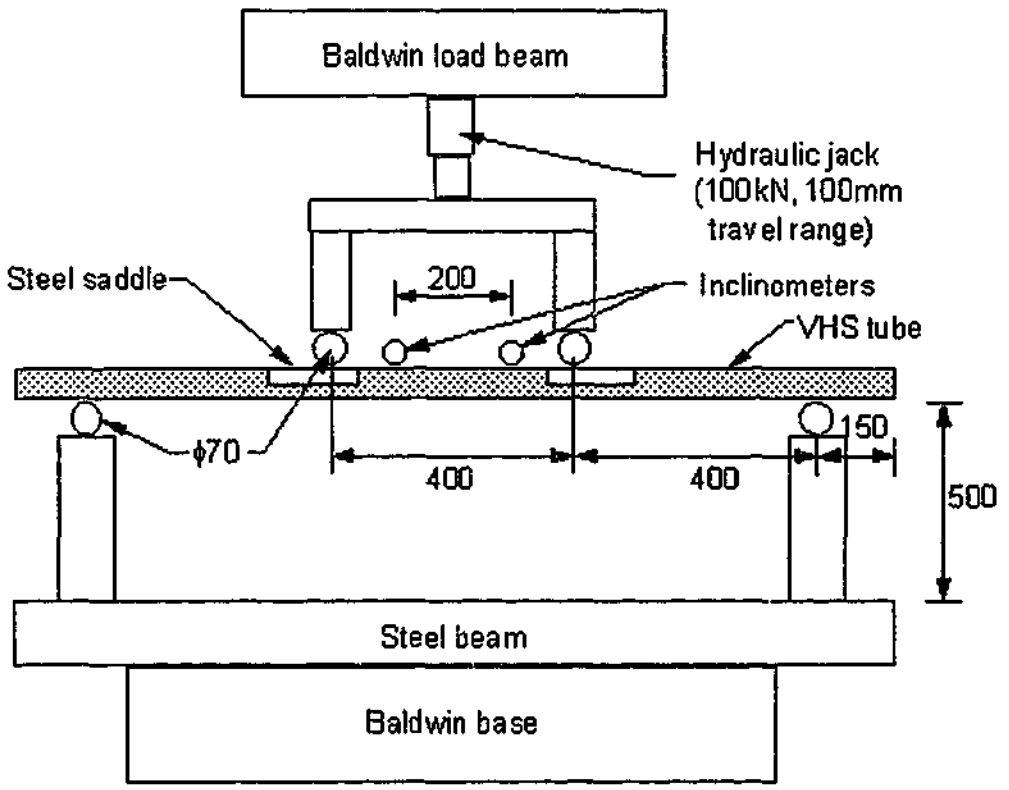

Figure 5.3-1: The setup of the four-point bending rig

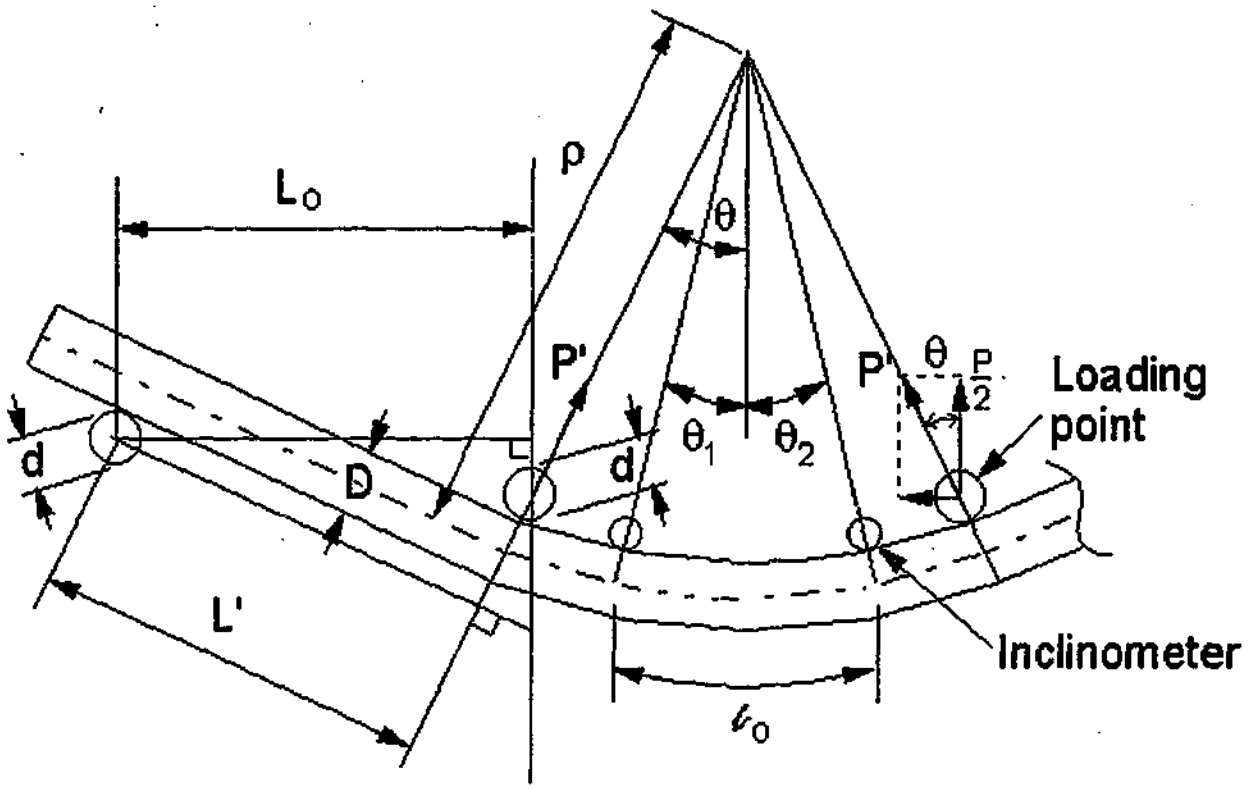

Figure 5.3-2: Measurement of bending moment and tube curvature

In order to spread the concentrated load and to prevent the premature local buckling at the supports, steel saddles were used at the loading points. The free length on each tube was 400mm. To measure the bending curvature, two inclinometers were fixed on each VHS tube with an interval of 200mm. The curvature κ of the beam can be calculated from the measured angles as follows:

$$l_o = \rho(\theta_1 + \theta_2) \tag{5.3-4}$$

$$\kappa = \frac{1}{\rho} = \frac{(\theta_1 + \theta_2)}{l_o} \tag{5.3-5}$$

where l_o, θ_1, θ_2 and ρ are symbols shown in Figure 5.3-2. The inclinometers were calibrated with a divider head. It was found that the inclinometer was not sensitive to the deviation in the plane vertical to the bending direction. This curvature measurement method was similar to the apparatus used in the bending test of circular tubes (Pan et al. 1998; Pan and Hsu 1998; Lee et al. 2001).

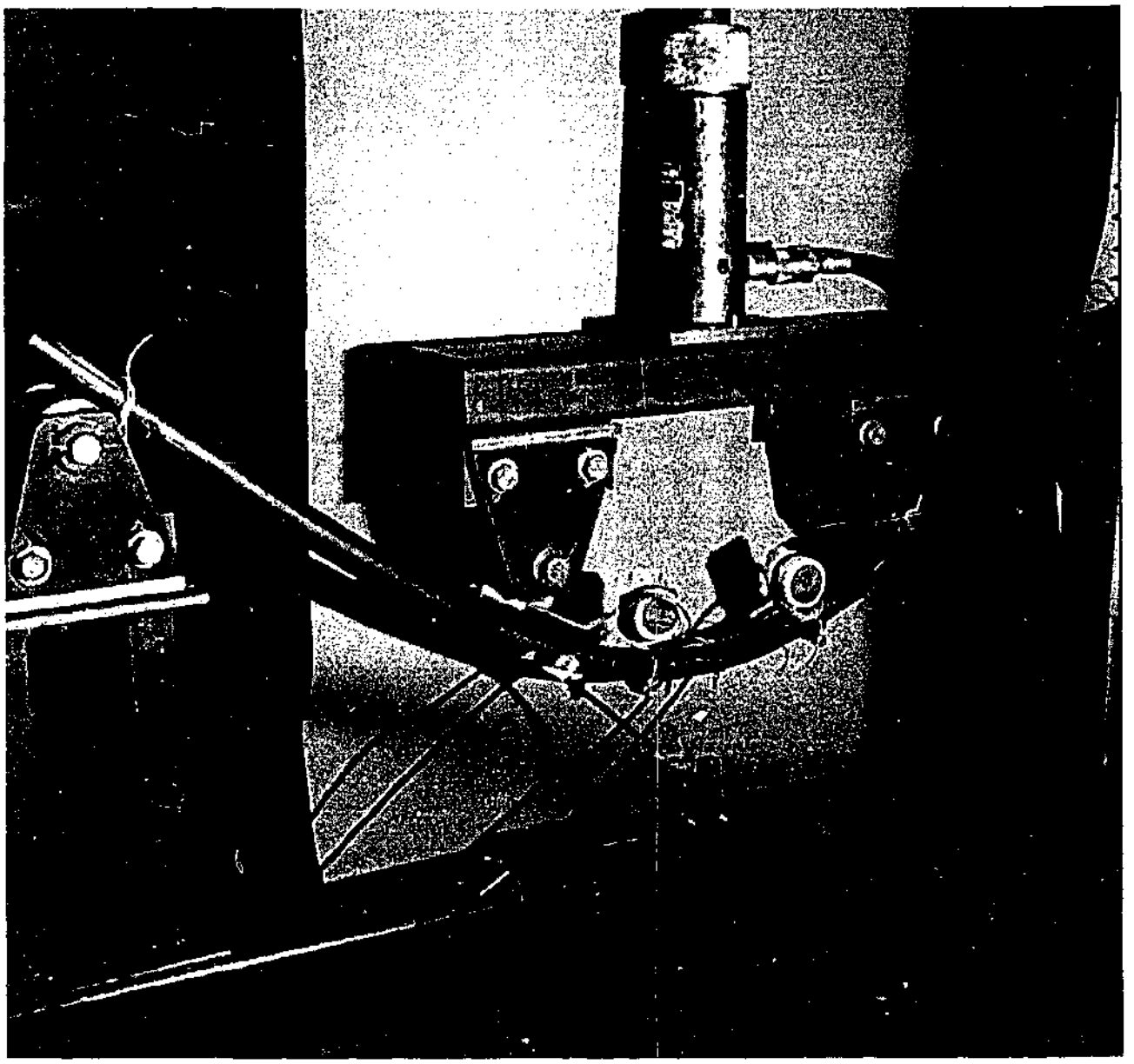

Figure 5.3-3: Specimen (BS6) under Four-point-bending test

The set-up of the pure bending rig was reported in detail by Cimpoeru (1992). It was used by many researchers in the testing of square hollow sections (Zhao and Grzebieta 1999) and circular hollow sections (Elchalakani et al. 2001a; 2002a). Figure 5.3-4 shows one specimen under testing in the pure bending rig.

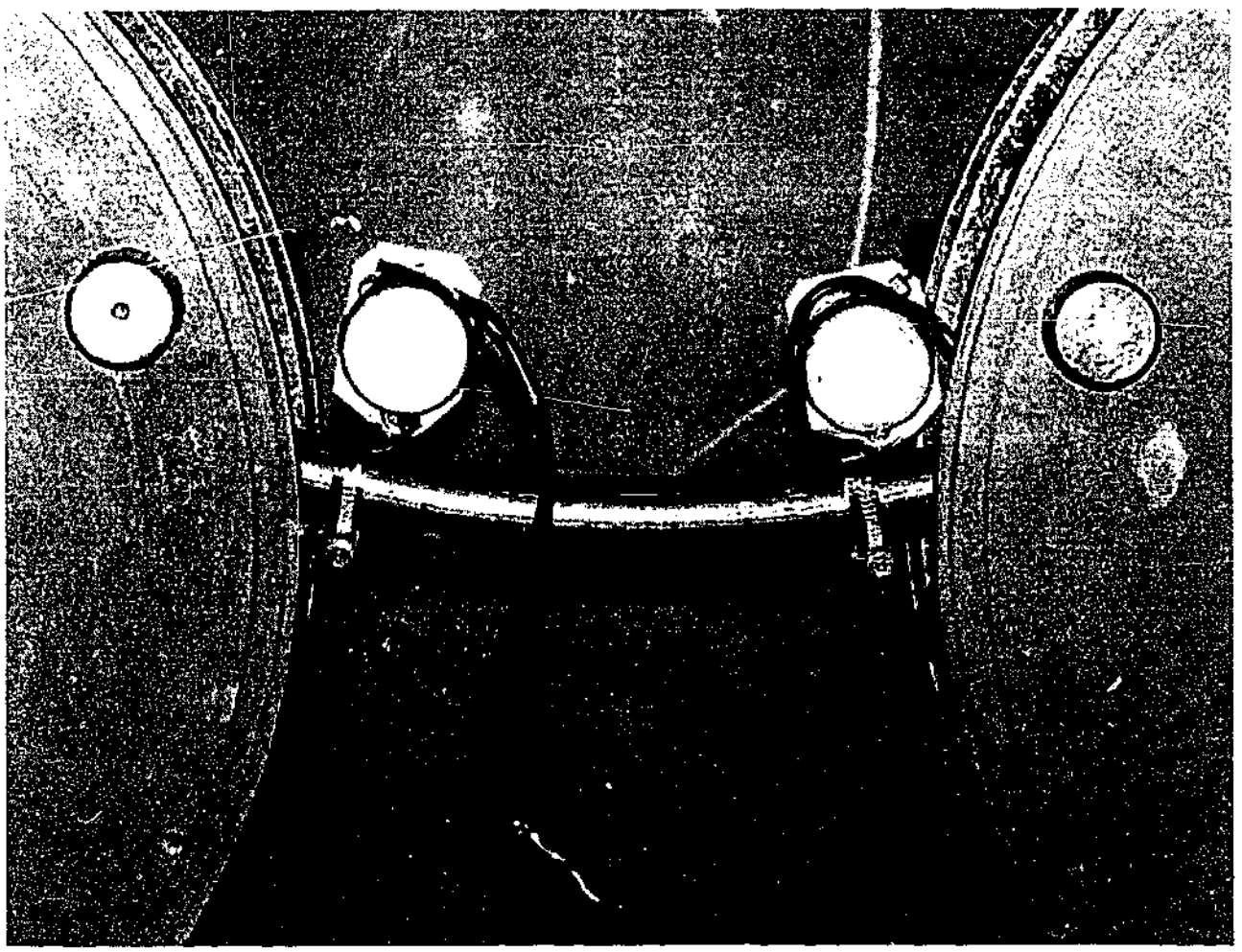

Figure 5.3-4: Specimen (BS9) in the pure bending rig

5.3.2 Failure Mode

The VHS tubes tested on both bending rigs showed a sudden collapse when local buckling happened after a certain deflection. The tested VHS tubes were shown in Figure 5.3-5. The curvature was uniform along the pure bending region before the collapse. The buckle was on the top compression side at one location. The wave-like multiple ripples found on many circular tubes, such as aluminum tubes (Reddy 1979; Kyriakides and Ju 1992) and stainless steel tubes (Calladine 1983), were not found on tested VHS tubes. The local buckling was an inward indentation. The load carrying capacity dropped significantly at the point of collapse. Very large curvatures were observed for tubes with a *D/t* ratio of 24 or less compared with BS7 and BS8 that have a *D/t* ratio of 36 and 48.

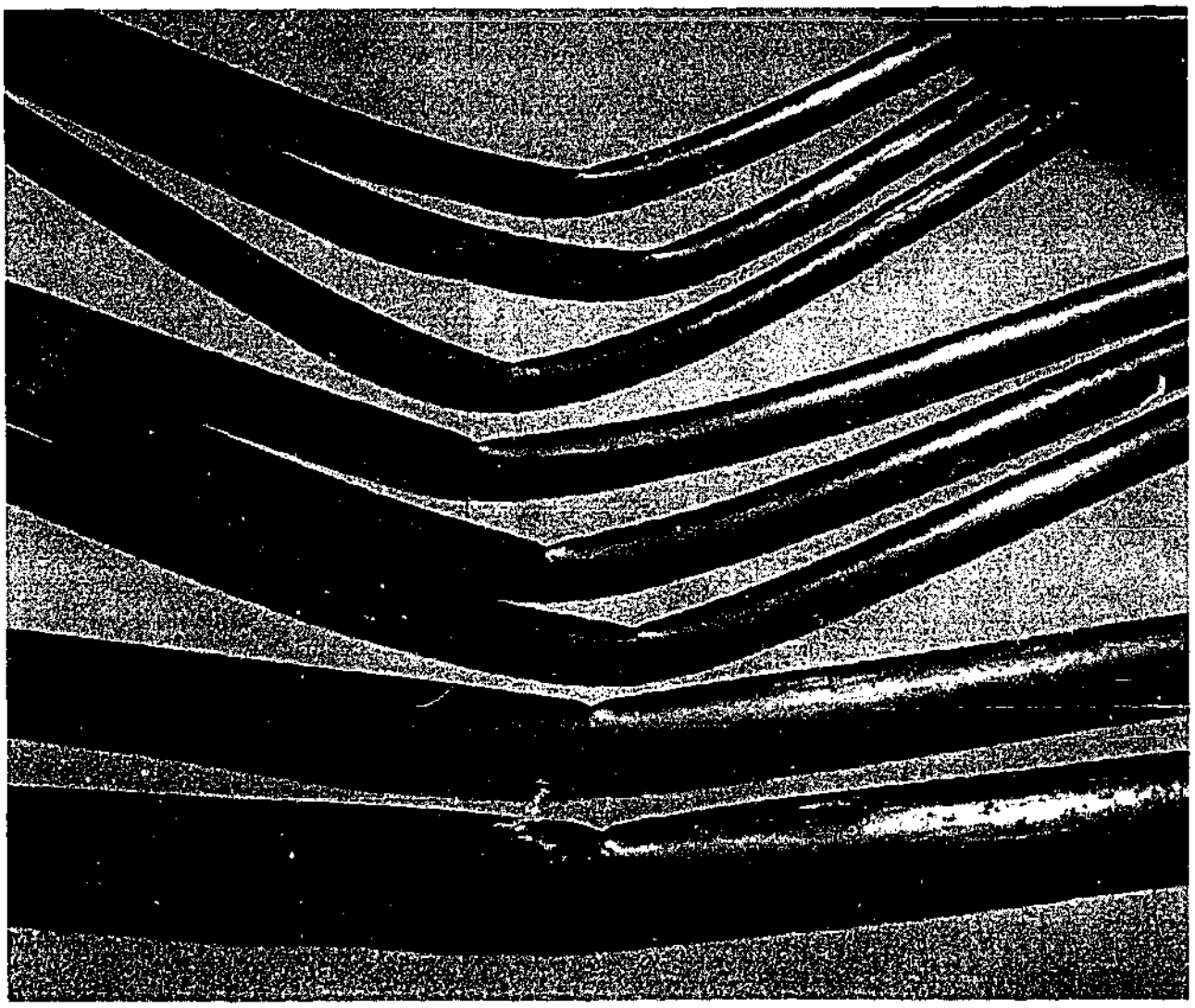

Figure 5.3-5: Tested VHS tubes (from top to bottom: BS1 to BS8)

5.3.3 Section Moment Capacity

The section bending capacity of VHS tubes tested in the four-point-bending rig and the pure bending rig were almost the same for VHS tubes with the same nominal dimensions. The ratios of the ultimate bending moment obtained from the two rigs are shown in Table 5.3-2. The very close results from two different setups provided us with confidence in the current testing program. The maximum moment M_u, the yield moment $M_y = Zf_y$ and the plastic moment $M_p = Sf_y$ are listed in Table 5.3-3. Z and S are the measured elastic and plastic section moduli. f_y is the yield stress obtained from the tensile test in Chapter 3. The shape factor is the ratio of S/Z. It can be seen from Table 5.3-3 that the ultimate moment M_u is larger than the plastic moment M_p for tubes with λ_s less than 198. This is due to the large bending deflection achieved before local buckling happened, making the strains well into the strain-hardening region. This is similar to the fabricated, hot-rolled and electric-resistance-welded cylinders (Sherman 1986) and the cold-formed square and rectangular hollow sections (Zhao and Hancock 1992).

Table 5.3-2: Comparison of bending moment between two bending rigs

Specimen Label (1)	Nominal $D \times t$ (mm) (2)	M_u (kN m)		Ratio of (3) / (4) (5)
		4-point-bending (3)	Pure bending rig (4)	
BS3, BS9	31.8 × 2.0	2.61	2.58	1.01
BS6, BS10	38 × 2.0	3.91	3.94	0.99
BS7, BS11	57.5 × 1.6	7.22	6.90	1.05
BS8, BS12	75 × 1.6	11.68	11.32	1.03
MEAN	-	-	-	1.02
COV	-	-	-	0.020

Table 5.3-3: Test results of moment capacity

Specimen Label	I (10^3mm^4)	Z (10^3mm^3)	S (10^3mm^3)	f_y (MPa)	M_y (kNm)	M_p (kN·m)	M_u (kN·m)	M_u/M_y	M_u/M_p	Shape factor
BS1	17.09	1.07	1.43	1327	1.42	1.90	2.15	1.51	1.13	1.34
BS2	18.94	1.19	1.60	1284	1.53	2.05	2.30	1.51	1.12	1.34
BS3	20.79	1.30	1.76	1350	1.76	2.38	2.61	1.49	1.10	1.35
BS4	30.18	1.59	2.11	1398	2.22	2.94	3.26	1.47	1.11	1.33
BS5	33.73	1.77	2.36	1361	2.41	3.21	3.65	1.52	1.14	1.33
BS6	36.67	1.93	2.58	1330	2.56	3.44	3.91	1.53	1.14	1.34
BS7	106.35	3.72	4.87	1360	5.06	6.62	7.22	1.43	1.09	1.31
BS8	256.31	6.75	8.77	1377	9.29	12.08	11.68	1.26	0.97	1.30
BS9	20.54	1.29	1.75	1350	1.75	2.36	2.58	1.48	1.09	1.35
BS10	36.58	1.92	2.57	1330	2.55	3.42	3.94	1.54	1.15	1.34
BS11	104.92	3.68	4.81	1360	5.00	6.54	6.90	1.38	1.05	1.31
BS12	256.62	6.76	8.78	1377	9.30	12.09	11.32	1.22	0.94	1.30

5.3.4 Section Rotation Capacity

The conventional plastic hinge rotation capacity (R) of a circular tube is defined as:

$$R = \frac{\kappa_l}{\kappa_p} - 1 \tag{5.3-6}$$

here κ_p is the tube curvature when the moment firstly reaches the plastic moment; κ_l is the limit curvature corresponding to the plastic moment at the descending part as shown in Figure 5.3-6 (a). This definition has been used in the study of square and circular hollow sections (Korol and Hudoba 1972; Yura et al. 1978; Kuhlmann 1989; Hasan and Hancock 1989; Zhao and Hancock 1991; Stranghoener et al. 1994; Stranghoener and Sedlacek 1996). In this study, the limit curvature k_l is replaced by the ultimate curvature k_u as shown in Figure 5.3-6 (b), since VHS tubes collapsed before the moment reaches the plastic moment at the descending part of M-k curves, i.e., not enough data points were captured in the unloading curves as shown in Figure

5.3-7. Base on the relationship of Eq.(5.3-5) between the curvature k and the rotation angle $(\theta_1+\theta_2)$, R can be expressed in either of the curvature or the rotation angle as:

$$R = \frac{\kappa_u}{\kappa_p} - 1 = \frac{\theta_u}{\theta_p} - 1 \qquad (5.3\text{-}7)$$

θ_u is the ultimate rotation angle and θ_p is the rotation angle corresponding to the plastic moment. The ultimate curvature κ_u, the plastic curvature κ_p (at M_p, obtained from the moment-curvature curves), κ_p' (calculated from M_p / EI) and their ratios are listed in Table 5.3-4. The values of k_p for BS8 and BS12 are unavailable since M_p is not reached for the two specimens. It can be seen that the rotation capacities obtained from κ_p are larger than that calculated from κ_p'. This may be due to the influence of ovalisation on the tube sections. The normalized M-k curves are plotted in Figure 5.3-7 where the value κ_p' is used.

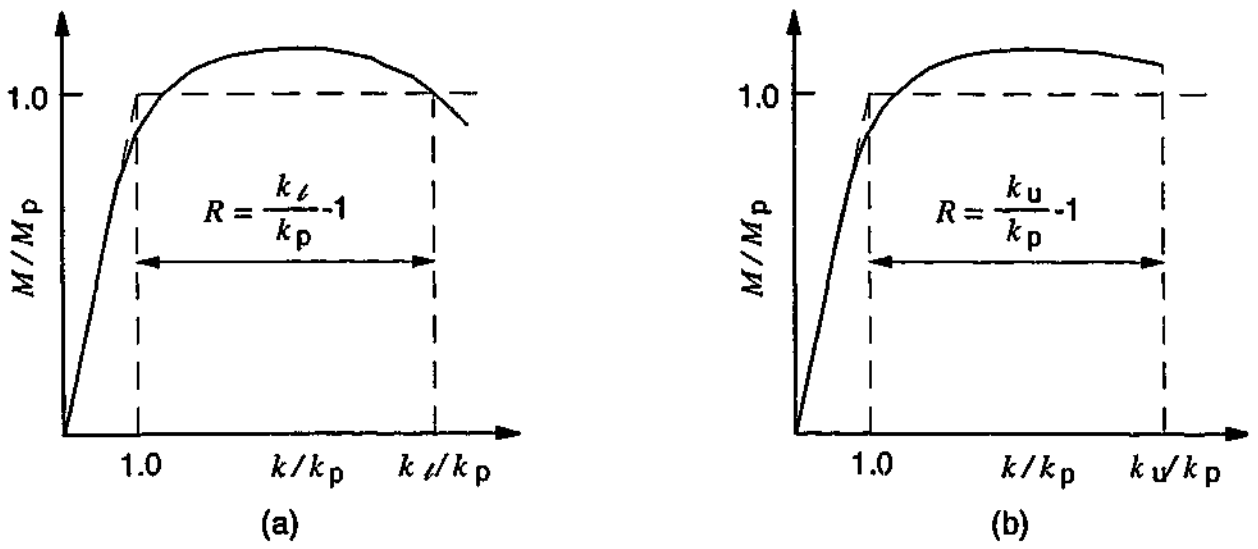

Figure 5.3-6: Measurement of plastic hinge rotation capacity R

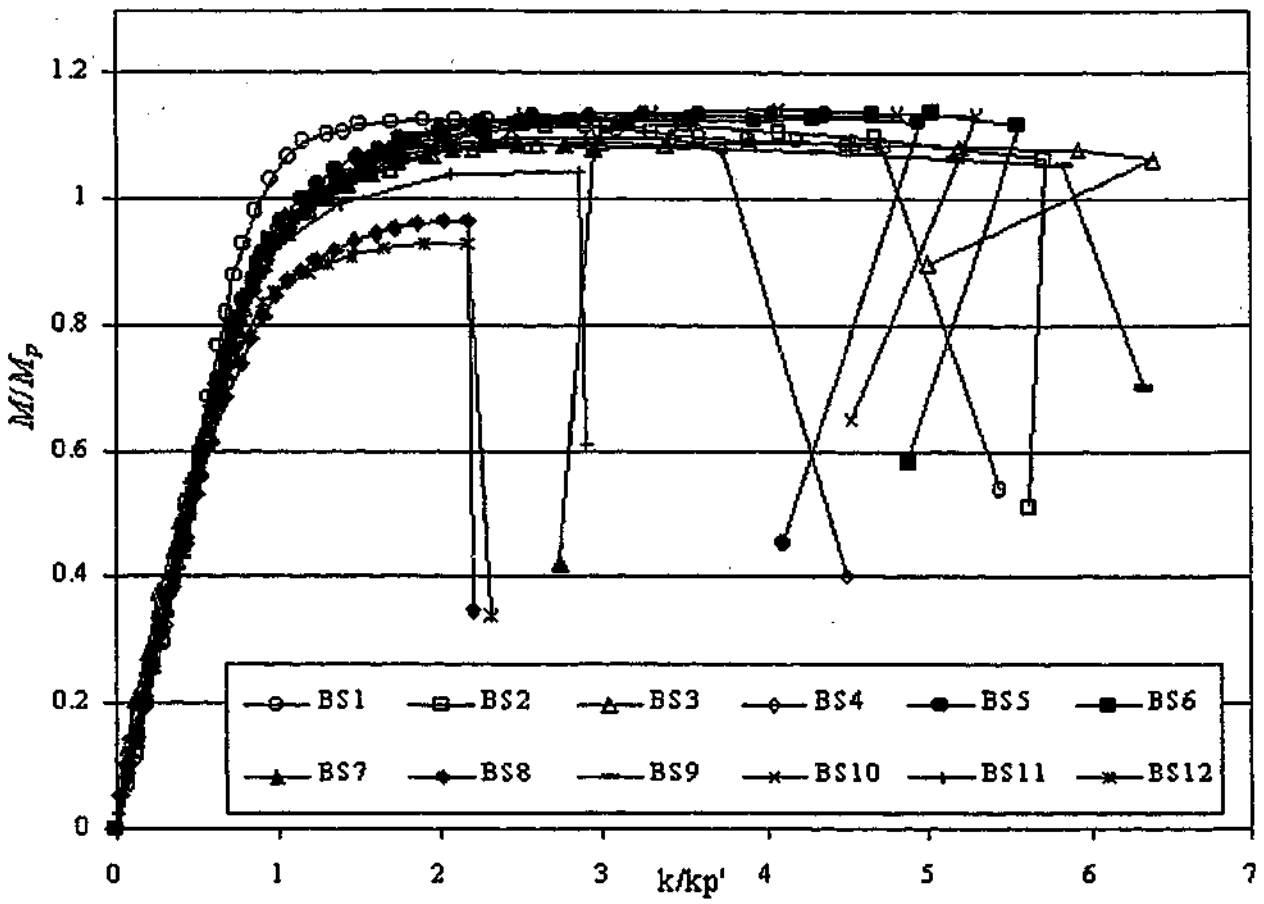

Figure 5.3-7: Curves of the normalized moment versus normalized curvature

Table 5.3-4: Rotation capacities of VHS tubes

Specimen Label	K_p	K_p'	K_u	$K_u/K_p - 1$	$K_u/K_p' - 1$
BS1	0.46	0.56	2.64	4.73	3.74
BS2	0.49	0.54	3.07	5.26	4.65
BS3	0.53	0.57	3.65	5.89	5.38
BS4	0.47	0.49	1.84	2.91	2.77
BS5	0.44	0.48	2.38	4.41	4.00
BS6	0.42	0.47	2.61	5.22	4.58
BS7	0.29	0.31	0.91	2.15	1.93
BS8	-	0.24	0.52	0.00	0.00
BS9	0.53	0.58	3.39	5.40	4.89
BS10	0.41	0.47	2.49	5.07	4.32
BS11	0.27	0.31	0.88	2.26	1.82
BS12	-	0.24	0.52	0.00	0.00

5.4 PLASTIC SLENDERNESS LIMITS

5.4.1 Plastic Rotation Capacity Approach

The plastic slenderness limit of steel tubes can be determined by using the plastic rotation capacity approach. Certain plastic rotation capacity is required in order that the plastic analysis method can be used in the global design of structures. For square or rectangular hollow sections, a value of R=4 was used to determine the plastic slenderness limit (Korol and Hudoba 1972; Zhao and Hancock 1991; Hasan and Hancock 1989; Wilkinson and Hancock 1998), whereas other studies (Yura et al. 1978; Stranghoener et al. 1994) on the continuous beams of square or circular hollow sections proposed that a rotation capacity of R=3 was sufficient for the redistribution of moment in plastic design. In this thesis, both R=3 and R=4 were adopted and two plastic slenderness limits were proposed accordingly for completeness. The rotation capacities (R) from both κ_p and κ_p' versus λ_s of the VHS tubes are plotted in Figure 5.4-1.

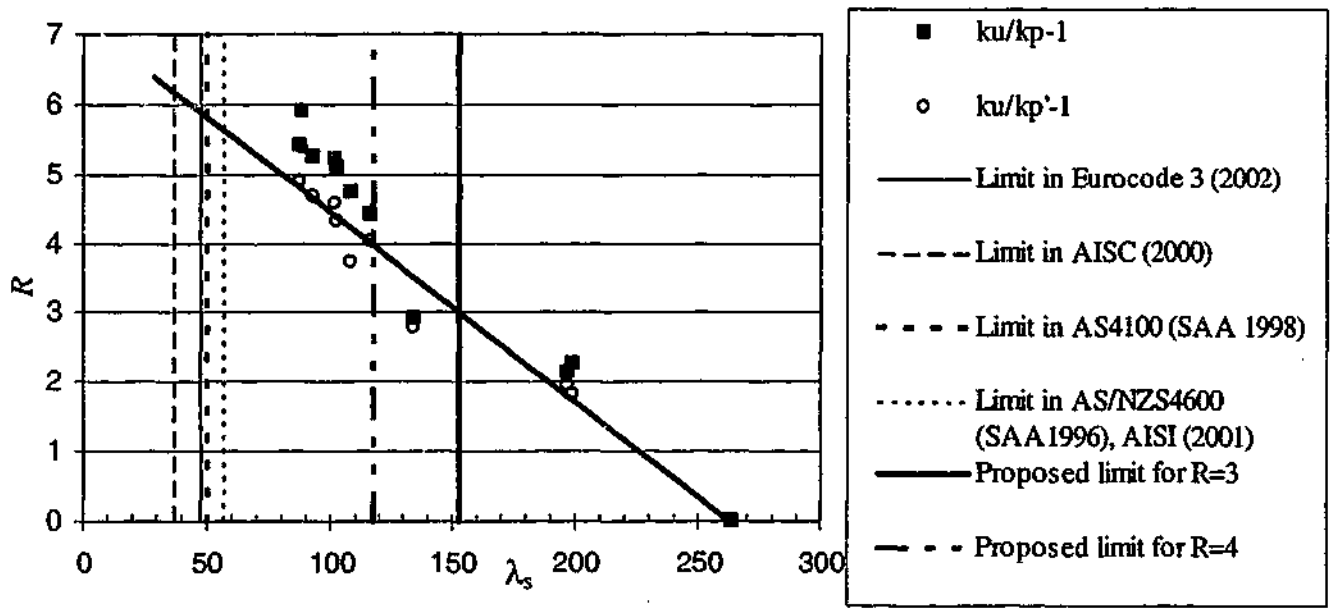

Figure 5.4-1: The rotation capacity R versus λ_s

A regression line was drawn based on the values of R obtained from κ_p' to be on the conservative side. The plastic slenderness limits of 117 and 153 were obtained at R=4 and R=3. It can be seen from Figure 5.4-1 that the new limits are much higher than those specified in AISC (2000), AISI (2001), Eurocode 3 (2002), AS4100 (SAA 1998) and AS/NZS4600 (SAA, 1996). The ratios of these limits to the existing limits of 36 in AISC (2000) and 50 in AS4100 (SAA 1998) are between 2.34 and 4.25. They are similar to the ratios of the yield stress of VHS tubes (1350MPa) to those of the cold-formed tubes (350 and 450MPa for C350 and C450), i.e. 3.0 and 3.86. The values of slenderness limits are plotted in Figure 5.4-2 against the yield stress of CHS.

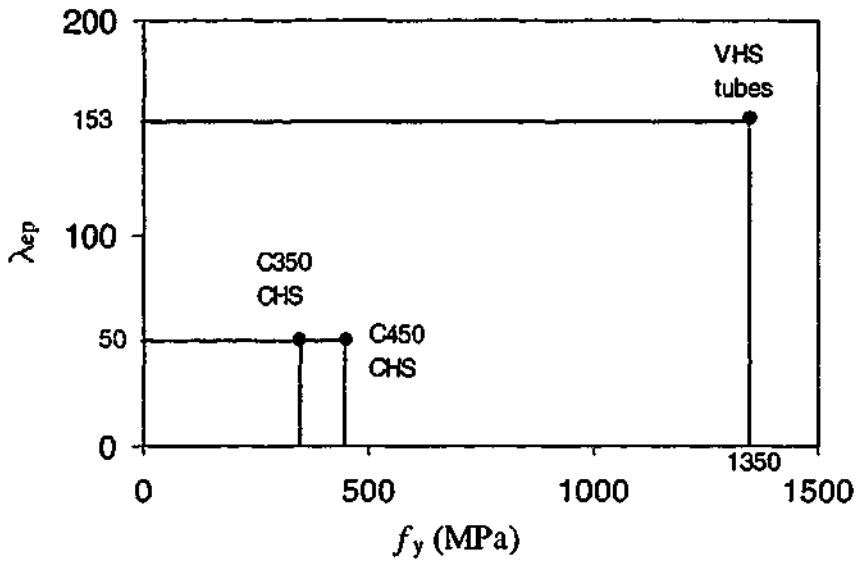

Figure 5.4-2: Plastic slenderness limits λ_{ep} versus f_y for CHS

It seems that the high plastic slenderness limit of VHS tubes may be due to its high yield stress and the use of (f_y/250) in the section slenderness definition:

$$\lambda = \frac{D}{t}\frac{f_y}{250} \tag{5.4-1}$$

Therefore, for the plastic design of VHS tubes, either a higher slenderness limit may be used if keeping the above slenderness expression, or a new slenderness expression may be derived in replacing (f_y/250) to take into account the high strength property of VHS tubes if keeping the current slenderness limit of 50 in AS4100 (SAA 1998). To

further investigate the effect of the yield stress on the plastic slenderness limit, more bending tests may be needed on steel circular hollow sections with the yield stress between 450MPa and 1350MPa.

5.4.2 Rotation Angle Approach

The plastic slenderness limit may also be determined by plotting the ratio of $(\theta_u-\theta_y)/\theta_y$ versus the non-dimensional local buckling parameter α as described by Sherman (1986) and Elchalakani et al (2002a). θ_u and θ_y are the beam rotation angles at buckling and the yield point. The non-dimensional local buckling parameter α is defined as $\alpha = (\frac{E}{f_y})/(\frac{D}{t})$. The limiting value of α corresponds to a sharp transition between tubes with large rotation capacities and those with very limited rotation capacities. The ratio of $(\theta_u-\theta_y)/\theta_y$ is plotted in Figure 5.4-3 against α for VHS tubes and CHS tested in (Sherman 1986; Elchalakani et al. 2001a; 2002a).

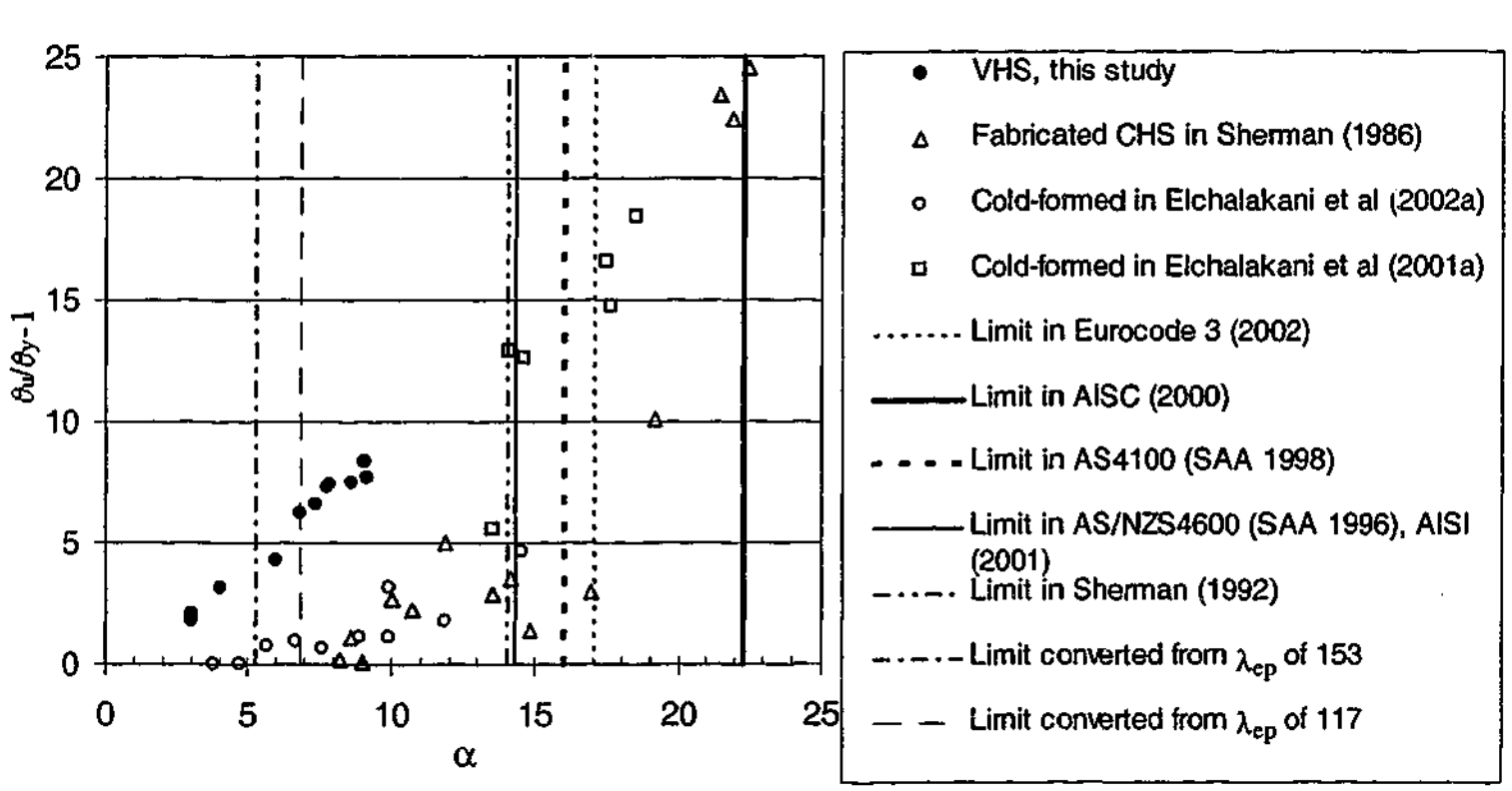

Figure 5.4-3: The ratio of $(\theta_u-\theta_y)/\theta_y$ versus α

The plastic section slenderness limits (λ_{ep}) in existing standards (AISC 2000; AISI 2001; Eurocode 3 2002; SAA 1998; SAA 1996) and the newly proposed limits (117 and 153) for VHS tubes can be converted to limiting α values using:

$$\alpha_{limit} = \frac{E}{250 \cdot \lambda_{ep}} \tag{5.4-2}$$

They are plotted in Figure 5.4-3. The converted limits seem suitable for cold-formed and fabricated CHS.

It can be seen from Figure 5.4-3 that VHS tubes did not show the similar sharp transition in the diagram as for cold-formed and fabricated CHS. Therefore no new limit on α is proposed based on this approach although limiting values of 5.2 and 6.8 can be obtained from Eq. (5.4-2) corresponding to the limits determined using the plastic rotation capacity approach.

5.5 YIELD SLENDERNESS LIMIT

The ratio of M_u/M_y versus λ_s for VHS tubes together with test data from the references (Elchalakani et al. 2001a; 2002a; Stephens et al. 1982; Sherman 1984) are shown in Figure 5.5-1. The yield moment was achieved for all the tested VHS tubes, therefore the yield slenderness limit of VHS tubes can be at least 264, which is slightly larger than the limit in AISC (2000), AS/NZS4600 (SAA 1996) and AISI (2001) when f_y of 1350 MPa is used, but much larger than the limit of 120 specified in AS4100 (SAA 1998) and 85 in Eurocode 3 (2002) for CHS. This proposed limit is slightly higher than the proposed section slenderness limit of 258 for VHS tubes in axial compression. More bending tests of VHS tubes with D/t ratios larger than 48 may be needed in order to determine a higher yield slenderness limit. It is interesting to note that a higher value of yield slenderness limit is specified for bending than for axial compression in AISC (2000), AS4100 (SAA 1998), AS/NZS4600 (SAA 1996) and AISI (2001), although the same value is used in Eurocode 3 (2002). The limit for bending is about 46% higher than that in axial compression in AS4100 (SAA 1998)

while the limit for bending is about 2.7 times that in axial compression in AISC (2000), AS/NZS4600 (SAA 1996) and AISI (2001).

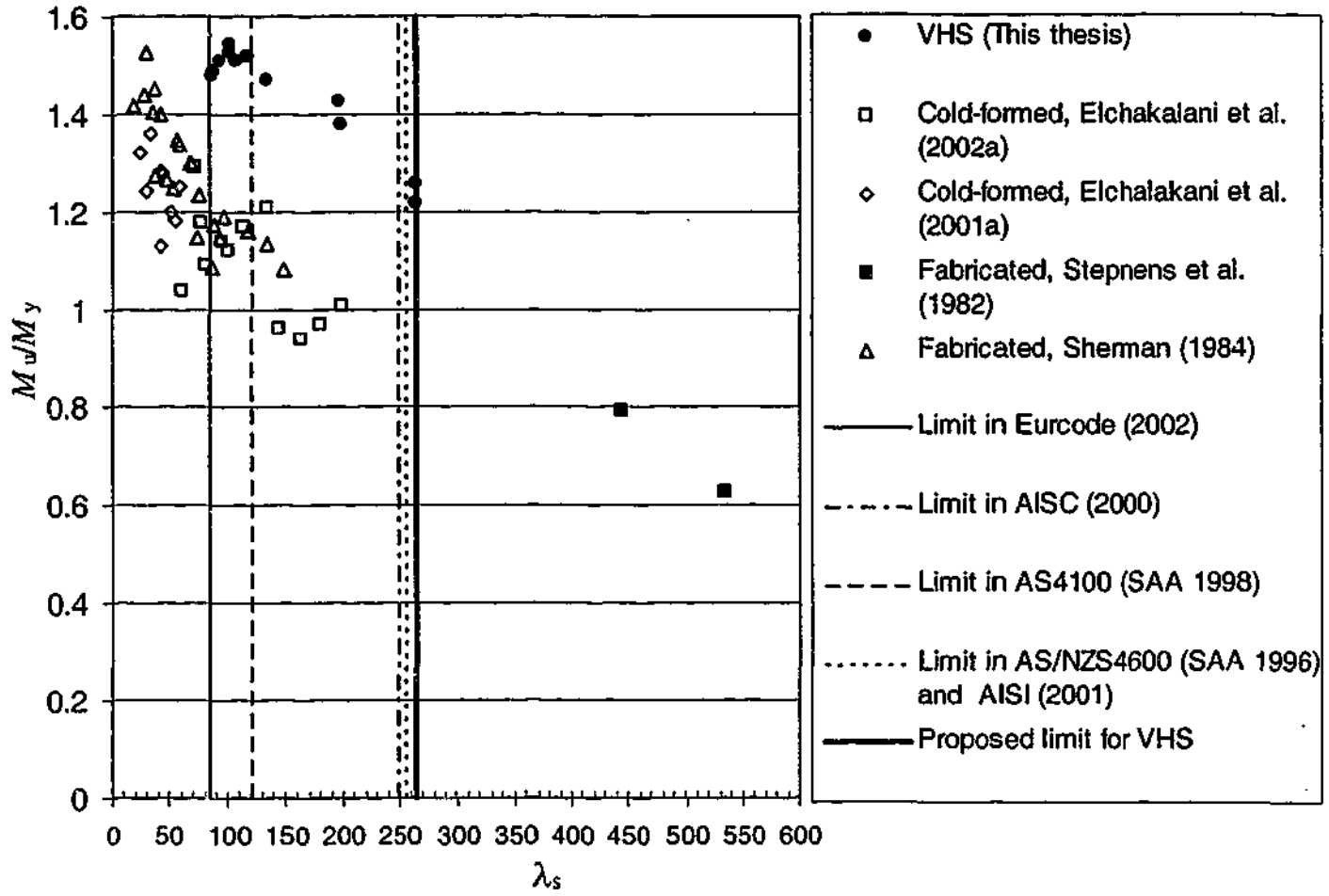

Figure 5.5-1: Ratio of the ultimate moment to the yield moment versus λ_s

5.6 SUMMARY

Bending tests of circular steel tubes were conducted extensively by many researchers. Most of those tested specimens were cold-formed, hot-rolled, manufactured and electric-resistance-welded tubes with the yield stress less than 500 MPa. This Chapter has presented an experimental study on the bending behaviour of very high strength (VHS) circular steel tubes. A total of 12 specimens, with the nominal diameter ranging from 31.8 to 75mm and the tube thickness between 1.6 to 2.0mm, were tested. Large bending deflection was achieved for VHS tubes with the diameter to thickness ratio up to 24. Full plastic moment was reached for tubes with the section slenderness of 197 or less. New plastic slenderness limits of 117 and 153 were proposed based on the beam plastic rotation capacity of 4 and 3. These limits should be viewed with caution due to large rotation angles occurred when VHS tubes reached the limits. The large rotation angle may violate the serviceability requirement for buildings. A yield slenderness limit of 264 was proposed for VHS tubes.

Chapter 6

BUTT-WELDED AND FILLET-WELDED VHS TUBES

6.1 INTRODUCTION

The previous three chapters studied the member capacity of VHS tubes in tension, compression and bending. This Chapter presents an investigation on the tension capacity of VHS circular steel tubes after welding.

Generally, quenched and tempered high strength steels are sensitive to heat generated during fusion welds (Cullison 1995). Strength loss due to the Heat-Affected-Zone (HAZ) softening seems inevitable (Vuceric 1987), whereas the strength reduction were not observed for welded connections in high strength cold-formed steels with wall thickness less than 3mm, such as C350 (Zhao and Hancock 1995a; 1995b) and C450 RHS (Zhao and Hancock 1996; Zhao et al. 1999). For fillet-welded T-connections of these C350 and C450 cold-formed tubes, full section capacity can be achieved if they are welded along the whole perimeter of the tube. Normally, no strength reduction due to HAZ softening is considered for welded connections in most steel design standards, such as AS4100 (SAA 1998), AS/NZS4600 (SAA 1996), AISC (2000) and AISI (2001). Very little information is available on research into the welded connections of very high strength steel tubes. Therefore, it is necessary to study the behaviour of such connections in order to establish a design rule for its engineering application.

In this Chapter, complete penetration butt-welded VHS tubes and fillet-welded T-connections of VHS tubes were tested in tension. The specimen diameters range from 31.8mm to 75mm, with a wall thickness between 1.6mm and 2.0mm. Failure modes

are compared with the connections in other high strength steels. A reduction factor to the base metal strength was proposed to modify the existing design codes for VHS tubes. The reliability indices (β) of the proposed formulae are checked using the first order second moment (FOSM) method.

6.2 MATERIAL PROPERTIES AND WELDING PROCEDURES

6.2.1 Parent (Base) Metal

Twelve complete penetration butt-welded VHS tubes and ten fillet-welded T-connections were tested in tension. The yield stress and ultimate tensile strength of VHS tubes were obtained from tensile coupons and full section tensile tests in Chapter 3. The measured specimen outside diameter (D), wall thickness (t), section area (A), yield stress (f_y) and ultimate tensile strength (f_u) of butt-welded specimens are listed in Table 6.2-1. Similar measurements for transverse fillet-welded specimens are listed in Table 6.2-2. Letters BW in a label refer to butt welded joints and letters FW represent fillet-welded joints, followed by specimen number (S1 to S12).

Table 6.2-1: Measured cross-section dimensions and material properties of VHS tubes used for butt-welded connections

Label (1)	D (mm) (2)	t (mm) (3)	A (mm^2) (4)	f_y (MPa) (5)	f_u (MPa) (6)
BWS1	32.01	1.56	149.23	1326	1470
BWS2	32.00	1.99	187.62	1350	1514
BWS3	38.26	1.55	178.76	1398	1547
BWS4	38.31	1.97	224.91	1329	1487
BWS5	31.95	1.60	152.56	1326	1470
BWS6	31.94	1.82	172.22	1284	1446
BWS7	31.91	2.00	187.93	1350	1514
BWS8	38.25	1.61	185.32	1398	1547
BWS9	38.18	1.80	205.72	1361	1507
BWS10	38.25	2.03	230.99	1329	1487
BWS11	57.34	1.60	280.18	1365	1510
BWS12	75.84	1.60	373.17	1377	1549
MEAN	-	-	-	1349	1504
COV	-	-	-	0.0235	0.0212

Table 6.2-2: Measured cross-section dimensions and material properties of VHS tubes used for transverse fillet welded connections

Label (1)	D (mm) (2)	t (mm) (3)	A (mm^2) (4)	f_y (MPa) (5)	f_u (MPa) (6)
FWS1	38.24	1.55	178.66	1398	1547
FWS2	38.29	1.97	224.78	1329	1487
FWS3	31.77	1.59	150.75	1326	1470
FWS4	32.06	1.80	171.12	1284	1446
FWS5	31.88	1.98	185.99	1350	1514
FWS6	38.07	1.60	183.32	1398	1547
FWS7	38.24	1.80	206.06	1361	1507
FWS8	57.60	1.60	281.49	1365	1510
FWS9	76.13	1.60	374.63	1377	1549
FWS10	75.36	1.65	382.09	1377	1549
MEAN	-	-	-	1357	1513
COV	-	-	-	0.0248	0.0229

6.2.2 Weld Metal

The weld metal used in the connections is classified as AWS A5.28 (AWS 1996) ER110S-G solid wire for welding steels with high tensile strength, which was produced by Metrode Products Ltd., UK. It has a nominal yield stress of 660 MPa and a minimum tensile strength of 760 MPa. It is normally used for welding high strength quenched and tempered steels with good low-temperature toughness.

6.2.3 Welding Procedures

The joint preparation for complete penetration butt-welded VHS tubes and fillet-welded T-connections are illustrated in Figure 6.2-1. The Gas Tungsten Arc Welding (GTAW) method was used for the welding of VHS tubes. The welding procedures were pre-qualified through ETRS Pty. Ltd. (a laboratory accredited by the National Association of Testing Authorities, Australia) in accordance with AS/NZS1554.4

(SAA 1995). The key parameters used in the welding procedures are listed in Table 6.2-3. Radiographic and macro cross-section examination were conducted. The examination results complied with AS2177.1 (SAA 1994). Fillet weld dimensions were measured from specimens for macro cross-section examination. The average measured leg length was 2.4 mm. Vickers hardness survey was also conducted on weld metal, parent metal and HAZ. The average values were 249HV10, 425HV10 and 259HV10 respectively. It can be seen that the hardness of the weld metal is close to that of the HAZ. Both are less than the hardness of the parent metal. This phenomenon is different from that observed for welded C350 and C450 tubes (Mashiri et al. 2001) where the hardness of the weld metal is greater than that of the parent metal with a difference less than 100HV10 as required in (WTIA 1998) for welding structural steel.

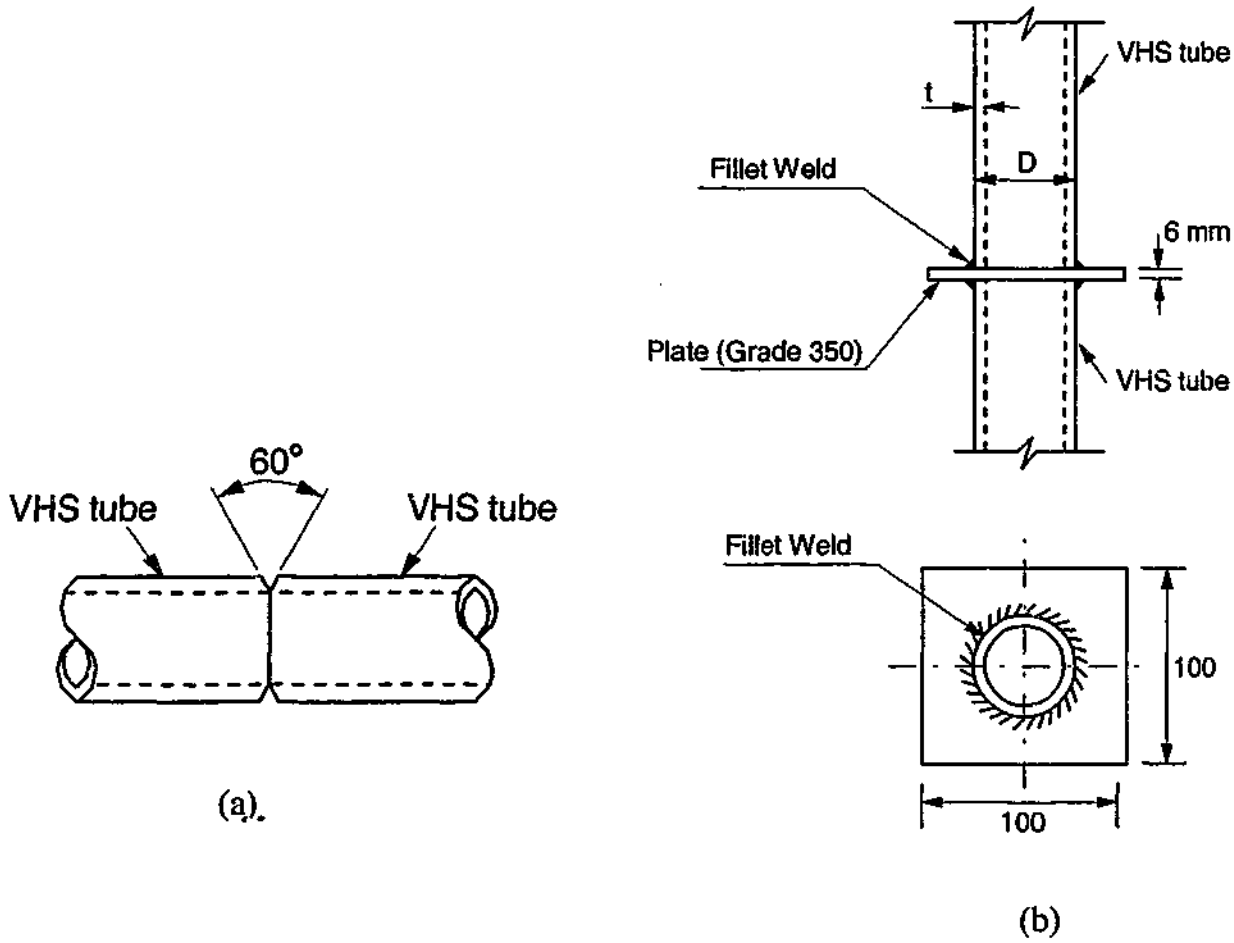

Figure 6.2-1: A schematic view of joint preparation: (a) complete penetration butt-welded VHS tubes (b) VHS tubes fillet-welded to a steel plate along the whole perimeter

Table 6.2-3: Key parameters used in pre-qualified welding procedures

Key Parameters	Description
Wire Material	AWS A5.28
Wire Type	ER 110S-G
Minimum Strength of Wire	760MPa
Welding Machine	Miller Syncrowave
Process	GTAW
Weld Run	One
Current (A) Voltage (V)	46A 13V
Speed Travel	80mm/Min
Heat Input	0.45kj/mm
Ambient Temperature	16°C
Shielding Gas Flow Rate	Pure Argon 9 L/min
Mechanical Tests	Radiographic and Macro Cross-Section Examination

6.3 TESTS OF COMPLETE PENETRATION BUTT-WELDED VHS TUBES

6.3.1 Test Setup

All tests were conducted in a 500kN Baldwin Universal testing machine with a loading rate of 2mm/min. For specimens with diameters of 31.8mm and 38mm, plugs were put in both ends of the specimen to enable the tube to be gripped as shown in Figure 6.3-1(a). The same method of applying tension force was used by Zhao (2000). For specimens with diameters of 57.5mm and 75mm, 20mm thick steel plates were longitudinally welded to both ends of each specimen. This is due to that the tube size was larger than the gripping jaw capacity of the testing machine. The specimens were connected to the testing machine through pin-ended connections. The set-up is shown in Figure 6.3-1(b) which is similar to that used by Zhao and Hancock (1995a), Zhao et al (1999). The tube length (L) was about three times of the tube diameter plus the plug length in Figure 6.3-1(a) or plus the length of the longitudinal fillet weld in Figure 6.2-1(b) so that the end plug or the longitudinal fillet welds have no influence on the strength of the butt joints.

6.3.2 Failure Mode

All the butt-welded specimens failed in the heat-affected-zone (HAZ) of the parent metal. A typical specimen after testing is shown in Figure 6.3-2(a). This failure mode is completely different from the shear failure mode of the parent metal in tension described in Chapter 3 as shown in Figure 6.3-2(b). The failure mode is, however, similar to that of the butt-welded C450 SHS (Zhao and Hancock 1996) as shown in Figure 6.3-2(c) where HAZ failure occurs. It is interesting to observe that no HAZ failure occurred for butt-welded C350 SHS (Zhao et al. 1996) as shown in Figure 6.3-2(d).

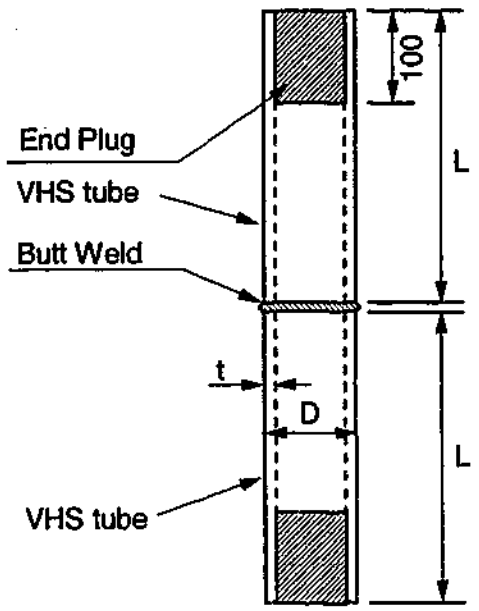

(a)

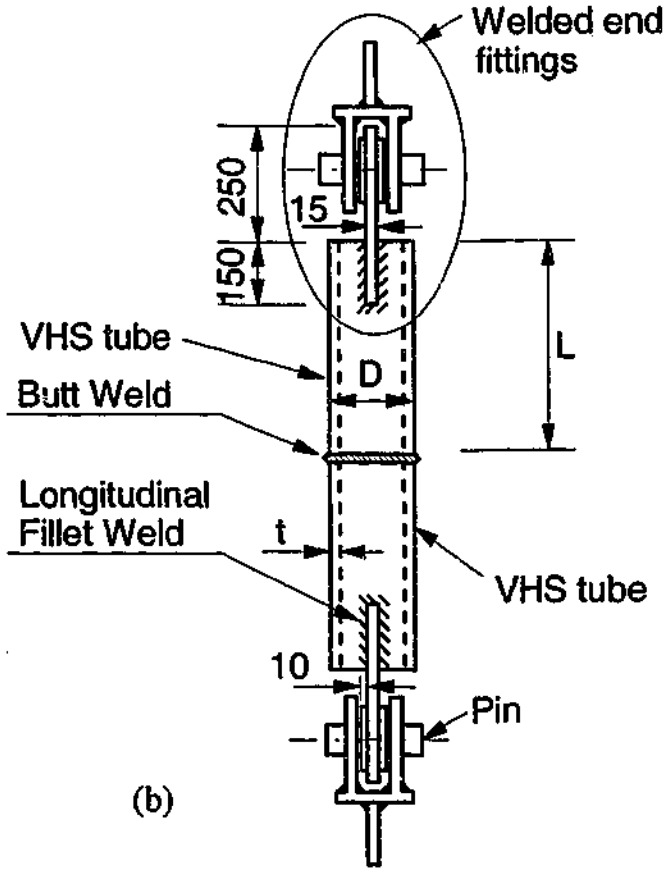

(b)

(c)

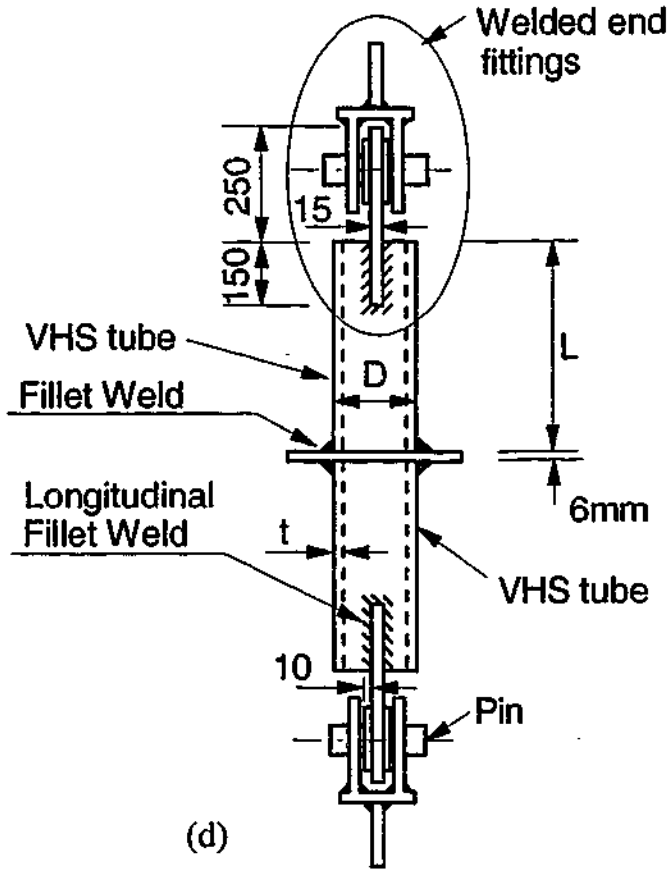

(d)

Figure 6.3-1: Loading arrangement: (a) butt welded connections through end plugs for tube size D≤56mm; (b) butt welded connections through welded end fittings for tube size D>56mm; (c) transverse fillet welded connections through end plugs for tube size D≤56mm; (d) transverse fillet welded connections through welded end fittings for tube size D>56mm

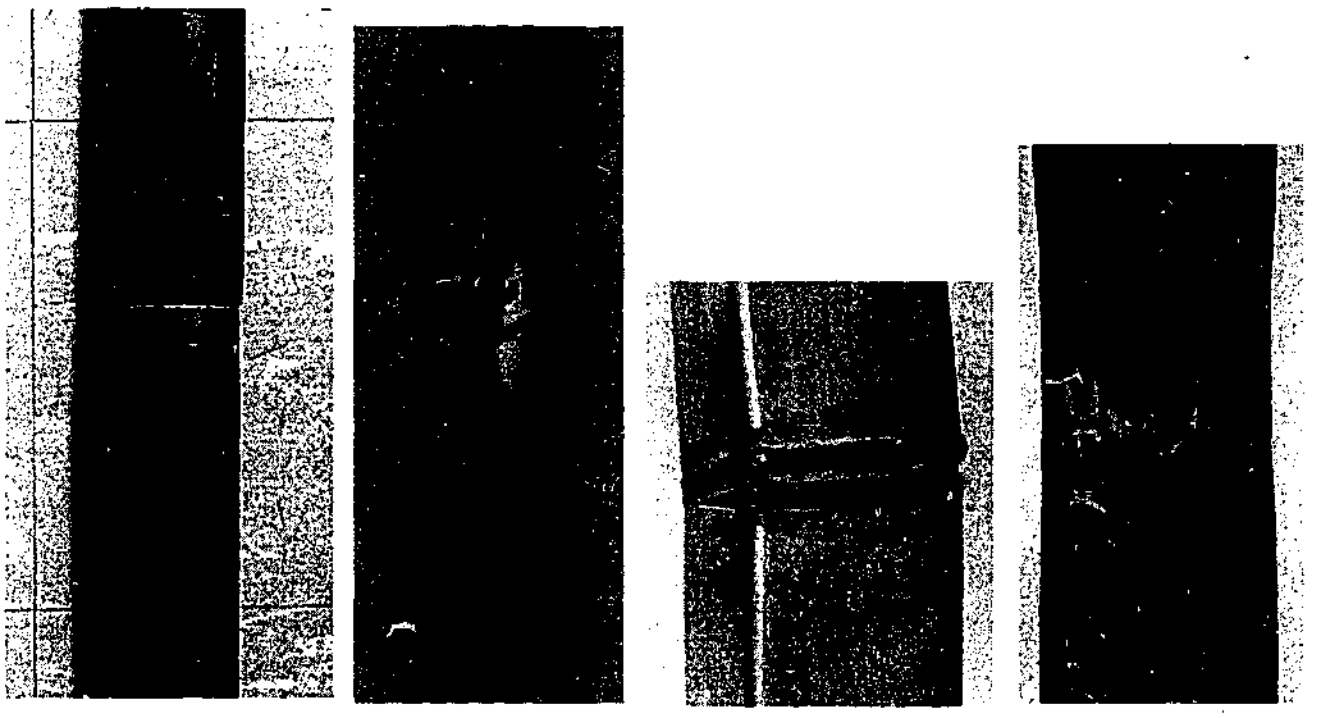

(a) (b) (c) (d)

Figure 6.3-2: Comparison of failure Modes (a) Butt-welded VHS circular tubes; (b) VHS tubes (Chapter 3 of this thesis); (c) Butt-welded C450 (Nominal yield stress of 450 MPa) Square Hollow Sections (Zhao and Hancock 1996); (d) Butt-welded C350 (Nominal yield stress of 350 MPa) Square Hollow Sections (Zhao et al. 1996)

6.3.3 Test Results

The measured maximum load P_{max} for complete penetration butt-welded VHS tubes is listed in Table 6.3-1 where comparisons are given with the predictions from current design codes. The connection strength (P_{max}/A) on average is about 737 MPa. The ratio of the ultimate load to the ultimate capacity of VHS tubes ($P_{max}/f_u A$) is about 0.49. The ratio of the ultimate load to the nominal design capacity ($P_{max}/0.85f_u A$) in AS4100 (SAA 1998) and AS/NZS4600 (SAA 1996) is about 0.58. A reduction factor (ψ) is introduced in the design formula for VHS tubes. The calibration of the reduction factor (ψ) is described later in Section 6.5.3.2.

Table 6.3-1: Tension capacity of complete penetration butt-welded VHS tubes

Label	P_{max} (kN)	P_{max}/A (MPa)	P_{max}/f_yA	P_{max}/f_uA	$P_{max}/0.85f_uA$	$P_{max}/0.85\psi f_uA$ Modified AS4100, AS/NZS4600 (ψ=0.56)	$P_{max}/\psi f_yA$ Modified AISI (2001) (ψ=0.53)	$P_{max}/\psi f_yA$ Modified AISC (2000) (ψ=0.56)	$P_{max}/\psi f_uA$ Modified AISC (2000) (ψ=0.60)
(1)	(2)	(3)	(4)	(5)	(6)	(7)	(8)	(9)	(10)
BWS1	109	730	0.551	0.497	0.585	1.044	1.039	0.984	0.828
BWS2	144	768	0.569	0.507	0.596	1.065	1.073	1.015	0.845
BWS3	135	755	0.540	0.488	0.574	1.026	1.019	0.965	0.814
BWS4	166	738	0.555	0.496	0.584	1.043	1.048	0.992	0.827
BWS5	108	705	0.534	0.482	0.564	1.007	1.003	0.949	0.799
BWS6	128	745	0.579	0.514	0.606	1.082	1.095	1.036	0.859
BWS7	133	709	0.524	0.467	0.551	0.983	0.991	0.938	0.780
BWS8	134	720	0.517	0.467	0.548	0.978	0.972	0.920	0.776
BWS9	155	755	0.554	0.500	0.589	1.052	1.047	0.990	0.835
BWS10	171	741	0.557	0.498	0.586	1.047	1.052	0.996	0.831
BWS11	215	768	0.562	0.508	0.598	1.068	1.061	1.004	0.847
BWS12	267	716	0.520	0.462	0.544	0.971	0.981	0.929	0.770
MEAN	-	737	0.550	0.490	0.580	1.031	1.032	0.976	0.818
COV	-	0.0283	0.0360	0.0350	0.0350	0.0348	0.0357	0.0357	0.0348

6.4 TESTS OF VHS TUBES FILLET-WELDED TO A PLATE

The test setup of fillet-welded T-connections was the same as that of the complete penetration butt-welded VHS tubes except for the connection region as shown in Figure 6.3-1(c) and Figure 6.3-1(d). A 6mm thick plate was used to form the

transverse fillet welded connection. Similar to the failure mode of complete penetration butt-welded VHS tubes, all specimens of the fillet-welded T-connections failed in the HAZ of the parent metal. A typical specimen after testing is shown in Figure 6.4-1(a). This failure mode is different from the two failure modes observed for C350 rectangular hollow section (RHS) fillet-welded to a steel plate along the whole perimeter of the tube (Zhao and Hancock 1993), i.e. dominantly tube failure similar to that shown in Figure 6.3-2(d) and sometimes weld failure initiated in the HAZ of one corner as shown in Figure 6.4-1(b). It should be pointed out that the full yield capacity was achieved for all C350 RHS in such tests. The measured maximum load P_{max} is listed in Table 6.4-1 where comparisons are made with the calculated section capacities from a number of design codes. Similar values are observed for (P_{max}/A), (P_{max}/f_uA) and ($P_{max}/0.85f_uA$) ratios as for butt-welded VHS tubes given in Table 6.3-1.

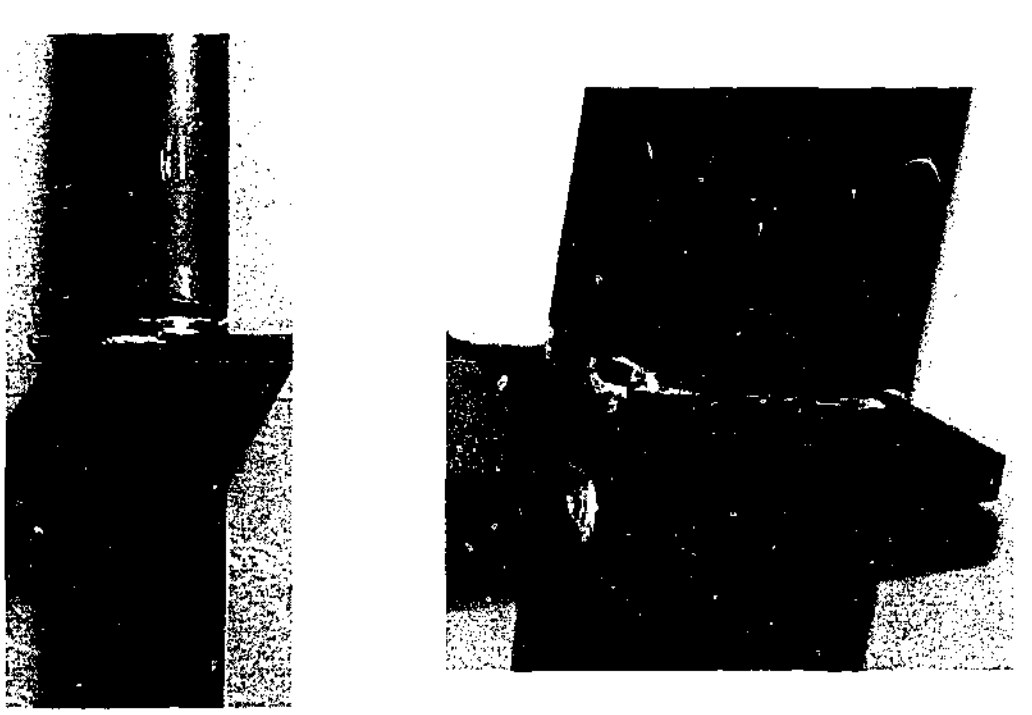

(a) (b)

Figure 6.4-1: Failure mode of transverse fillet welds. (a) VHS tubes, (b) C350 rectangular hollow sections (Zhao and Hancock 1993).

Table 6.4-1: Tension capacity of VHS tubes fillet-welded to a steel plate

Label	P_{max} (kN)	P_{max}/A (MPa)	P_{max}/f_yA	P_{max}/f_uA	$P_{max}/0.85f_uA$	$P_{max}/0.85\psi f_uA$ Modified AS4100, AS/NZS4600 (ψ=0.54)	$P_{max}/\psi f_uA$ Modified AISI (2001) (ψ=0.51)	$P_{max}/\psi f_uA$ Modified AISC (2000) (ψ=0.54)	$P_{max}/\psi f_uA$ Modified AISC (2000) (ψ=0.58)
(1)	(2)	(3)	(4)	(5)	(6)	(7)	(8)	(9)	(10)
FWS1	132	739	0.528	0.478	0.562	1.040	1.036	0.979	0.823
FWS2	167	743	0.559	0.500	0.588	1.089	1.096	1.035	0.861
FWS3	103	685	0.517	0.464	0.548	1.016	1.013	0.957	0.804
FWS4	121	708	0.552	0.490	0.576	1.067	1.082	1.022	0.845
FWS5	129	695	0.515	0.457	0.540	1.000	1.010	0.954	0.792
FWS6	127	694	0.496	0.447	0.528	0.977	0.973	0.919	0.773
FWS7	149	724	0.532	0.479	0.565	1.047	1.043	0.985	0.828
FWS8	214	761	0.557	0.504	0.593	1.097	1.093	1.032	0.868
FWS9	267	712	0.517	0.460	0.541	1.002	1.014	0.958	0.793
FWS10	267	699	0.508	0.451	0.531	0.984	0.996	0.940	0.778
MEAN	-	716	0.528	0.474	0.557	1.032	1.036	0.978	0.817
COV	-	0.0336	0.0389	0.0394	0.0394	0.0394	0.0389	0.0389	0.0394

6.5 DESIGN OF COMPLETE PENETRATION BUTT-WELDED VHS TUBES

6.5.1 Comparison with Existing Design Formulae

In the limit state (LRFD) standards, both AISI (2001) and AISC (2000) specify that the connection strength be calculated based on the yield strength f_y of the parent metal with a capacity factor of 0.90. However if the failure happens in the base metal, a higher capacity factor of ϕ=0.95 is used in AISI (2001). For AISC (2000), the strength of a tension member is determined by the lesser of f_yA with a capacity factor of 0.90 and f_uA with a capacity factor of 0.75. For AS4100 (SAA 1998) and AS/NZS4600 (SAA 1996), the member strength is governed by the lesser of f_yA and $0.85f_uA$ with a

capacity factor of 0.90. It can be seen from Table 6.3-1 that the values of $0.85f_uA$ are less than those of f_yA. The comparisons are given in Columns 4, 5, and 6 in Table 6.3-1. It is obvious that modifications are needed to the existing formulae for design of VHS tubes.

6.5.2 Reliability Analysis Method

The basic reliability analysis method of first order second moment (FOSM) (Ellingwood et al. 1980) has been used in the calibration of many standards. The statistical parameters of this method are defined as:

$$R_m/R_n=M_m\times F_m\times P_m \tag{6.5-1}$$

$$V_R=\sqrt{V_M^2+V_F^2+V_P^2} \tag{6.5-2}$$

in which the mean values (M_m, F_m, P_m) and the corresponding coefficients of variation (V_m, V_F and V_P) represent the uncertainties in "material strength", "fabrication" and "professional model" respectively. The statistical values of M_m, V_M, F_m and V_F were provided by the tube manufacturer. The same values as in Zhao (2000) are used in the analysis. i.e., M_m=1.003, V_M=0.0219, F_m=1.002 and V_F =0.0092. P_m and V_p are the mean & COV (coefficient of variation) given in Column 7 to 10 of Table 6.3-1 for proposed design formulae. The reliability index (β) is expressed by Ellingwood et al. (1980) as:

$$\beta=\frac{\ln(\frac{R_m}{Q_m})}{\sqrt{V_R^2+V_Q^2}} \tag{6.5-3}$$

in which, the ratio of R_m/Q_m and V_Q are given by Ravindra and Galambos (1978):

$$\frac{R_m}{Q_m}=\frac{\gamma_D(\frac{D_n}{L_n})+\gamma_L}{(\frac{D_m}{D_n})(\frac{D_n}{L_n})+(\frac{L_m}{L_n})}(\frac{R_m}{R_n})\frac{1}{\Phi} \tag{6.5-4}$$

$$V_Q = \frac{\sqrt{(\frac{D_m}{D_n})^2 V_D^2 (\frac{D_n}{L_n})^2 + (\frac{L_m}{L_n})^2 V_L^2}}{(\frac{D_m}{D_n})(\frac{D_n}{L_n}) + (\frac{L_m}{L_n})} \qquad (6.5\text{-}5)$$

Here, γ_D and γ_L are the dead load (DL) and live load (LL) factors. The dead load and live load combination (U) is 1.25DL+1.5LL in AS4100 (SAA 1998) and AS/NZS4600 (SAA 1996), whereas it is 1.2DL+1.6LL in AISC (2000) and AISI (2001). D_n is the nominal dead load and L_n is the nominal live load. Φ is the capacity factor in design models. The statistical parameters for load are the same as those given in Table 4 of Zhao and Hancock (1995a), i.e. D_m/D_n=1.05, L_m/L_n=1.0, V_D=0.10 and V_L=0.25. The reliability index (β) versus $D_n/(D_n+L_n)$ curve is used for calibration of a design formula. A load combination $D_n/(D_n+L_n)$ value of 0.25 is adopted (Galambos 1995; Zhao et al. 1999) as a calibration point for comparison with target reliability index.

6.5.3 Proposed Design Formulae

6.5.3.1 General

The VHS steel tubes behave differently from other high strength cold-formed hollow sections (e.g. C350 and C450 tubes) after welding. For C350 and C450 tubes, the butt-welding process did not reduce the tube section capacity (Zhao and Hancock 1995a; 1996). However, for VHS tube, the heat generated during the fusion weld causes the microstructure change in the HAZ of the parent metal. The connection strength is reduced due to the HAZ softening. This can be seen from Column 3 of Table 6.3-1 where the average strength of 737 MPa is significantly less than the average ultimate tensile strength of 1504 MPa listed in Column 6 of Table 6.2-1. To reflect the strength reduction in HAZ for butt-welded VHS tubes, a reduction factor ψ is applied to the existing formulae. The derivation of the reduction factor ψ is based on a reliability analysis shown below.

6.5.3.2 Reliability Analysis

Only tension member rules in design codes such as AISC (2000), AISI (2001), AS4100 (SAA 1998) and AS/NZS4600 (SAA 1996) are calibrated, since no failure happened in the weld metal for the complete penetration butt-welded VHS tubes. The FOSM reliability analysis method is used to calibrate the reduction factor ψ as shown in Figure 6.5-1. The relevant values of P_m and V_p are the MEAN and COV given in Column 7 to Column 10 of Table 6.3-1. The calibrated reliability index values ($\beta_{0.25}$) at $D_n/(D_n+L_n)$ of 0.25 are listed in Table 6.5-1. The reduction factor ψ is so determined that all $\beta_{0.25}$ values are greater than the target reliability index of 2.5 specified in Chapter F of AISI (2001) for cold-formed members.

It can be seen from Figure 6.5-1 that the complete penetration butt-welded VHS tubes may be designed in accordance with the tension member rule in AS4100, AS/NZS4600, AISI (2001) and AISC (2000) with an appropriate reduction factor, ranging from 0.53 to 0.60, on f_u or f_y.

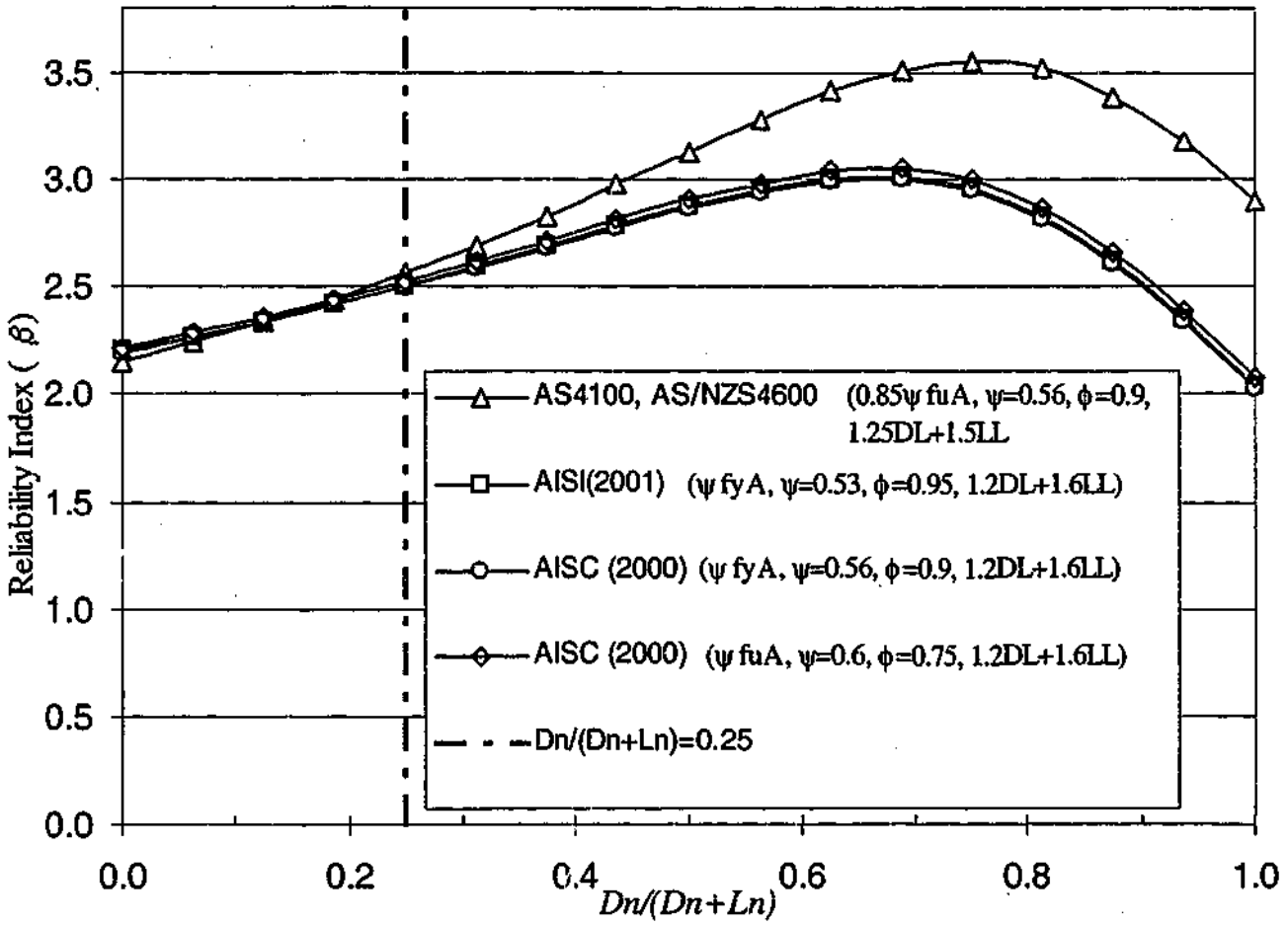

Figure 6.5-1: Reliability analysis of existing design codes for complete penetration butt-welded VHS tubes (FOSM method)

Table 6.5-1: Calibration of reduction factor (ψ) for tensile capacity of VHS tubes after welding

Weld type	Standards	Design Model	ψ	ϕ	$\beta_{0.25}$
Complete penetration butt-weld	AS4100 (1998)	$0.85\psi f_u A$	0.56	0.90	2.56
	AS/NZS4600 (1996)	$0.85\psi f_u A$	0.56	0.90	2.56
	AISI (2001)	$\psi f_y A$	0.53	0.95	2.51
	AISC (2000)	$\psi f_y A$	0.56	0.90	2.50
	AISC (2000)	$\psi f_u A$	0.60	0.75	2.53
Transverse fillet-weld	AS4100 (1998)	$0.85\psi f_u A$	0.54	0.90	2.56
	AS/NZS4600 (1996)	$0.85\psi f_u A$	0.54	0.90	2.56
	AISI (2001)	$\psi f_y A$	0.51	0.95	2.52
	AISC (2000)	$\psi f_y A$	0.54	0.90	2.50
	AISC (2000)	$\psi f_u A$	0.58	0.75	2.51

6.6 DESIGN OF VHS TUBES FILLET-WELDED TO A PLATE ALONG THE WHOLE PERIMETER

6.6.1 Comparison with Existing Design Formulae

As described by Zhao and Hancock (1995a; 1996), the full tension capacity of cold-formed C350 and C450 tubes could be achieved after they were fillet-welded to steel plates along the whole perimeter of the tubes. However, significant strength reduction was observed in HAZ of VHS tubes after they are fillet-welded to a steel plate, as shown in Column 3 of Table 6.4-1 where the average strength of 716 MPa is much less than the average ultimate tensile strength of 1513 MPa for VHS tubes as listed in Column 6 of Table 6.2-2. Similar to complete penetration butt-welded VHS tubes, only tensile member rules in AISC (2000), AISI (2001), AS4100 and AS/NZS4600 are calibrated, since no failure occurred in the weld metal. The comparison given in Column 4, 5 and 6 of Table 6.4-1 indicated the need to modify the existing formulae.

6.6.2 Proposed Design Formulae

To reflect the strength reduction in the HAZ of transverse fillet welded VHS tubes, a reduction factor is used for the design of VHS tubes fillet-welded to a plate. The reliability index (β) versus $D_n/(D_n+L_n)$ curves is plotted in Figure 6.6-1. P_m and V_p are the MEAN and COV given in Column 7 to Column 10 of Table 6.4-1. The calibrated reduction factor (ψ) and the reliability index (β) value at $D_n/(D_n+L_n)$ of 0.25 are listed in Table 6.5-1. The reduction factor (ψ) is so determined that all $\beta_{0.25}$ values are greater than the target reliability index of 2.5 specified in Chapter F of AISI (2001) for cold-formed members. It can be seen from Figure 6.6-1 that VHS tubes fillet-welded to a plate along its whole perimeter can be designed in accordance with the tension member rule in AS4100, AS/NZS4600, AISI (2001) and AISC (2000) with an appropriate reduction factor, ranging from 0.51 to 0.58, on f_u or f_y.

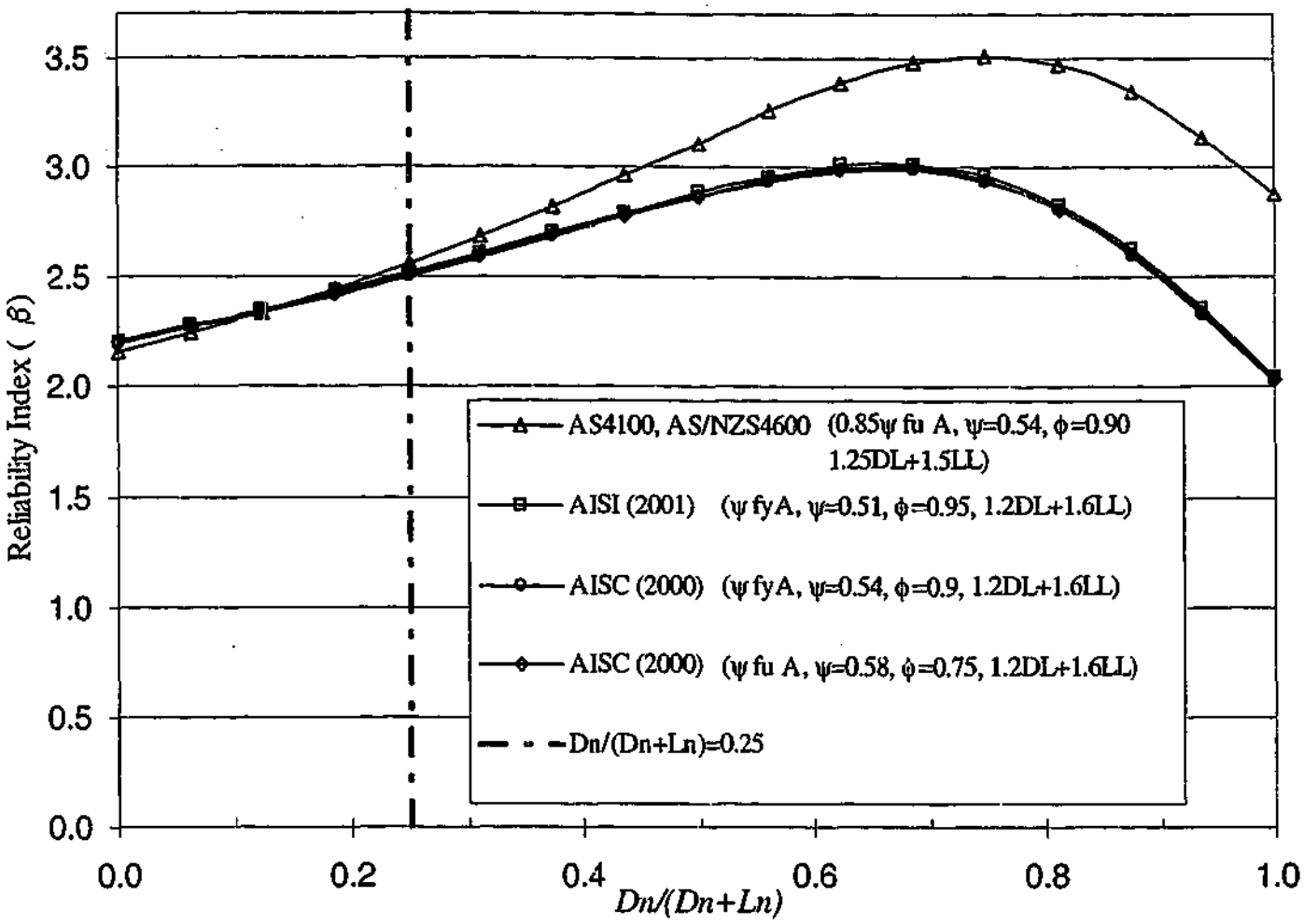

Figure 6.6-1: Reliability analysis of existing design codes for transverse fillet welded VHS tubes (FOSM method)

6.7 MATCHING STRENGTH OF WELD METAL

In some standards, although the connection strength of a welded joint is based on the base metal strength, the weld metal strength is required to match the base metal strength. AISC (1999), for example, specifies that the choice of electrode for use with complete penetration butt-welding shall comply with the matching weld metal requirements in AWS (2002). Generally, matching requires the strength of the weld metal to be equal to or slightly larger than that of the base metal (Funderburk 2001; Kyuba et al. 2001). In AS 4100 (SAA 1998), the welding consumable for complete penetration butt weld is also required to have a minimum strength equal to the base metal strength. However, for high strength steels, such as VHS steel tube, it is difficult to find a consumable with tensile strength equal to or greater than that of the base metal (1500 MPa). The minimum ultimate strength of the weld metal used in this

thesis is 760 MPa. Therefore, the welded joint of VHS tube is always in a state of under-matching according to the matching definition. However, in the butt weld and transverse fillet weld tests, no failure happens in the weld metal based on the weld size and weld consumable used in this study. This may be due to the strength reduction in HAZ. The average strength in the HAZ is 737 MPa and 716 MPa for butt-welded connections and fillet-welded T-connections. Both are smaller than the minimum strength of the weld metal, 760 MPa. Therefore, the welded connection in this study is in a state of matching if the weld metal strength is compared with that in HAZ. The strength in HAZ is about 50% of the base metal ultimate tensile strength f_u. It seems that when selecting weld metal for VHS tubes, the strength of the weld metal should match or exceed the reduced strength of the base metal, i.e., about 0.5 f_u.

6.8 SUMMARY

This chapter studies the tension capacity of welded VHS tubes. Two types of welded connections are used in the study: (1) complete penetration butt-welded VHS tubes, (2) VHS tubes fillet welded to a steel plate along the whole perimeter of VHS tubes. Both butt welded connections and transverse fillet welded connections failed in the heat-affected-zone (HAZ). The failure modes are compared with those of welded cold-formed C350 and C450 square hollow sections. Significant strength reduction was observed in the HAZ compared with the strength of the VHS tubes. A strength reduction factor is proposed to modify the existing design rules in Australian standards and American specifications for VHS tubes. The FOSM (First Order Second Moment) reliability analysis method is used to calibrate the reduction factor. The issue of matching between the base metal and weld metal is also discussed.

Chapter 7

CFRP STRENGTHENED BUTT-WELDED VHS TUBES

7.1 INTRODUCTION

Chapter 6 studied the connection strength of butt-welded and fillet-welded T-connections of VHS tubes. The tested specimens failed in the HAZ of the parent metal. The load carrying capacity of welded connections reduced about 50% compared to that of VHS members. Therefore it is necessary to develop a method to strengthen the welded connection of VHS tubes. This Chapter describes the application of CFRP-epoxy strengthening system on butt-welded VHS tubes, aiming to recover the strength loss due to HAZ softening.

CFRP material has been widely used to strengthen concrete structures (Teng et al. 2002). The application of CFRP material in strengthening metallic structures has been increasing rapidly in recent years due to its advantages over traditional strengthening materials, including high strength to weight ratio, resistance to corrosion and environmental degradation, and ease and speed of handling during construction (Tumialan et al. 2002; Cederquist 1999; Moy 2001). Some examples of these applications includes the strengthening of cast iron beams of underground structures (Moriarty and Barnes 1998), retrofitting of steel bridge beams or steel bridge piers (Sen et al. 2001; Miller et al. 2001; Tavakkolizadeh and Saadatmanesh 2003a; 2003b; Tani et al. 2000) and repair of fatigue damage for riveted connections (Bassetti et al. 1998). However no studies on the strengthening of HAZ softening in welded high strength steels are found.

In this Chapter, CFRP with a Young's modulus of 230 GPa and three types of epoxies were chosen in the strengthening of butt-welded VHS tubes. Tests were conducted to determine the lap shear strength between CFRP and VHS tubes. A total of 21 butt-welded specimens with different CFRP layers and bonding length were tested in axial tension. The suitable epoxy for this strengthening purpose was recommended. The effective bond length and the minimum number of CFRP layers were determined. A formula for predicting the connection capacity was proposed.

7.2 LITERATURE REVIEW

The application of fibre-reinforced polymers (FRP) in civil engineering structures has progressed rapidly during the last decades. There are three types of fibre in general use, i.e., aramid, glass and carbon fibre. In these three types, carbon fibre (CFRP) has been the most extensively used in strengthening civil engineering structures due to its high strength and high Young's modulus.

CFRP material was firstly attempted in retrofitting reinforced concrete structures in the mid-1980s (Leeming and Hollaway 1999). Since then, many literatures can be found in CFRP strengthened concrete columns and concrete beams. Many analytical and design models were summarized by Teng et al (2002).

In recent years, there is also an increasing interest in the use of externally bonded CFRP laminates or plates in strengthening steel structures. Application of CFRP on metallic structures was first found in mechanical engineering, where the high cost of fibres was not a significant drawback. For instance, CFRP laminates were used for repairing damaged aluminum and steel aircraft structures (Karbhari and Shulley 1995).

In civil engineering, the application of CFRP on steel structures is also increasing. It was reported by Moriarty and Barnes (1998) that the rehabilitation of London underground steel infrastructures involved the application of CFRP. The significant increase in ultimate strength showed that it is feasible to strengthen steel composite bridge members using CFRP laminates (Sen et al. 2001). It was found that the bonding of pretensioned strips of CFRP on cracked bridge elements is more efficient than the replacement of rivets with prestressed bolts (Bassetti et al. 1998; Bassetti et al. 2000). CFRP plates can also be used to restore loss of stiffness and strength in deteriorated bridge girders. An increase of 10-37% in stiffness was achieved for the corrosion damaged bridge girders (Miller et al. 2001). An average of 60% strength increase in CFRP retrofitted steel beams was reported by Mertz and Gillespie (1996). Fatigue life of CFRP bonded steel beams can be improved up to 3.4 times (Tavakkolizadeh and Saadatmanesh 2003b). A design guide on life extension and strengthening of metallic structures using FRP was proposed by Moy (2001).

Many of these research has been focused in strengthening of iron or unweldable steel girders (Barnes et al. 1999), rehabilitation of corroded steel girders (Tavakkolizadeh and Saadatmanesh 2001b) and repair of fatigue damage for riveted connections (Bassetti et al. 2000). However few studies can be found on the strengthening of HAZ softening in welded high strength steels. In this study, the butt-welded VHS tubes were strengthened by using CFRP-epoxy strengthening system.

7.3 MATERIAL PROPERTIES

7.3.1 VHS Steel Tube

The VHS steel tubes used in this Chapter were the same as those tested in previous Chapters. Therefore the average yield stress of 1349 MPa (The average of f_y from Table 3.3-2 and Table 3.4-2 for coupon and full section VHS tubes) and the average ultimate tensile strength of 1505 MPa (The average of f_u from Table 3.3-2 and Table 3.4-2 for coupon and full section VHS tubes) obtained from the tensile tests in Chapter 3 were adopted. The average ultimate tensile strength in the HAZ of butt-welded VHS tubes (737 MPa, see Table 6.3-1) obtained from the test results in Chapter 6 was used in this Chapter.

7.3.2 CFRP Material

The CFRP composite fabric used in this study was the SikaWrap® Hex-230C. It was fabricated by Sika Australia Pty. Ltd. According to the manufacturer's data sheet, the fabric had a typical unidirectional tensile strength of 3500 MPa and Young's modulus of 230 GPa with an ultimate strain of 1.5%. The thickness of one layer is 0.13 mm. The material is available in the width of 610mm and a length of over 40m. It was flexible and can be easily applied on circular shaped specimens.

7.3.3 Adhesives

Three types of epoxy resins were used in this study. They are Sikadur-330 (Fabricated by Sika Australia Pty. Ltd), Araldite® 420 and Araldite® Kit K138 (Produced by Vantico Pty. Ltd. Australia). All of them are two components epoxy based adhesives.

Araldite 420 is a high strength adhesive. It is suitable for bonding of metal, FRP and aerospace structures. Features include very high shear strength and good moisture resistance. The main feature of Araldite kit K138 is heat resistance. It can sustain up to 120°C without significant loss of bond strength. Sikadue-330 has been mainly used in strengthening concrete structures.

7.4 LAP SHEAR STRENGTH BETWEEN CFRP AND VHS TUBES

The lap shear strength between CFRP and the steel substrate is an important factor in the bonding. Therefore tests were conducted in this study to obtain the shear strength between the CFRP and the VHS steel tube. A standard test method was provided by ASTM (2001e). The specimens specified in this standard are flat coupons. However the shear strength value may be affected by the specimen geometry and material properties (ASTM 1999b). Therefore in this thesis, CFRP was bonded on two full-section VHS tubes (no welding is applied) as illustrated in Figure 7.4-1. To avoid fibre break failure in the joints, five layers of CFRP were applied on each specimen. Three specimens were prepared and tested initially for each of the three epoxies. Eight more specimens were tested with Araldite 420 that showed the best shear performance. The specimen dimensions (D, t, l_1, l_2) are listed in Table 7.4-1. The CFRP bond length at one side (l_1) was made shorter than the bond length (l_2) at the other side, expecting failure to happen at the side with a shorter CFRP bond length. The tested specimens bonded with Araldite 420 are shown in Figure 7.4-2. The lap shear strength (V) is simply defined as an average lap shear strength over the whole contact area between CFRP and VHS steel tube although some CFRP strips were found left on the bond surface. The definition can be written as:

$$V = \frac{P_{ult}}{\pi D l_1} \tag{7.4-1}$$

in which, P_{ult} is the ultimate load obtained in bond tests; D is the outside diameter of VHS tubes; l_1 is the bond length shown in Figure 7.4-1.

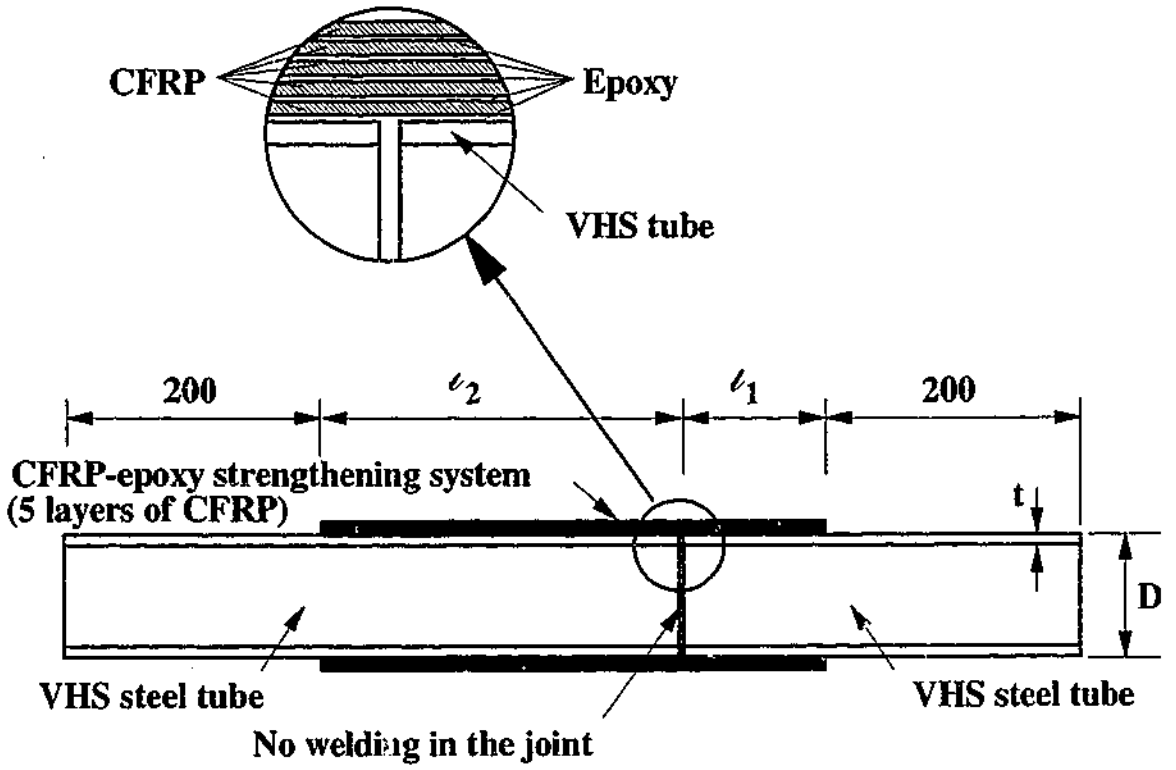

Figure 7.4-1: Specimen illustration for the lap shear strength test

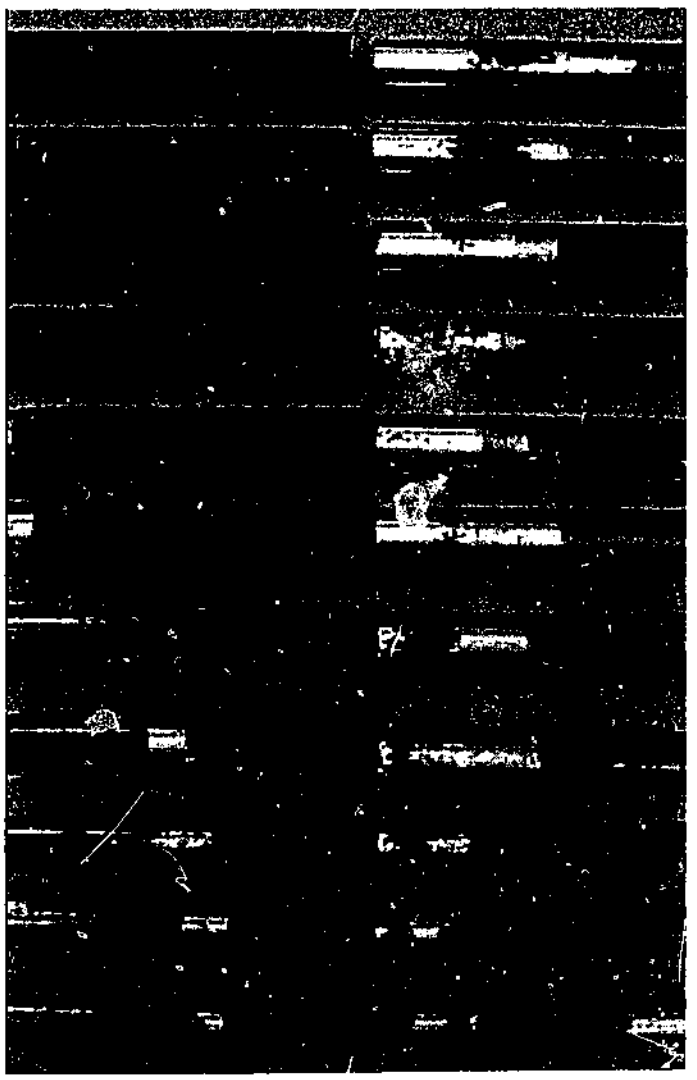

Figure 7.4-2: Tested specimens for the lap shear strength bonded with Araldite 420 (From bottom to top: A1 to A11)

Table 7.4-1: Shear strength between CFRP and VHS tubes

Label	D (mm)	t (mm)	l_1 (mm)	l_2 (mm)	P_{ult} (kN)	$V=P_{ult}/(\pi D l_1)$ (MPa)	Epoxy
A1	31.82	1.61	23.0	57.0	65.8	28.6	Araldite 420
A2	31.84	1.60	31.5	48.5	90.1	28.6	
A3	31.80	1.60	24.0	56.0	67.3	28.1	
A4	38.22	1.59	24.5	74.5	83.5	28.4	
A5	38.27	1.60	50.0	100.0	119.4	19.9	
A6	38.25	1.59	62.0	112.0	104.4	14.0	
A7	38.18	1.60	65.0	150.0	103.1	13.2	
A8	38.22	1.60	75.0	150.0	121.4	13.5	
A9	38.15	1.60	85.0	150.0	123.5	12.1	
A10	38.25	1.60	101.0	151.0	136.9	11.3	
A11	38.26	1.60	126.0	176.0	133.9	8.8	
S1	31.81	1.62	31.5	48.5	67.8	21.5	Sikadue-330
S2	31.82	1.61	33.0	47.0	75.0	22.7	
S3	31.81	1.60	32.0	48.0	69.6	21.8	
AK1	31.80	1.61	30.0	50.0	41.4	13.8	Araldite K138
AK2	31.83	1.61	36.5	44.0	45.6	12.5	
AK3	31.81	1.60	33.0	47.0	50.3	15.3	

The lap shear strength (V) obtained from Eq.(7.4-1) is plotted in Figure 7.4-3 against the CFRP bond length l_1. It can be seen from Figure 7.4-3 that V reduces as l_1 increases especially when l_1 is less than 75 mm. The ultimate load (P_{ult}) is plotted in Figure 7.4-4 against l_1. It seems that the ultimate load increases as l_1 increases. The load increase is not significant when l_1 reaches about 75 mm. A similar phenomenon is observed later in testing welded connections strengthened with CFRP.

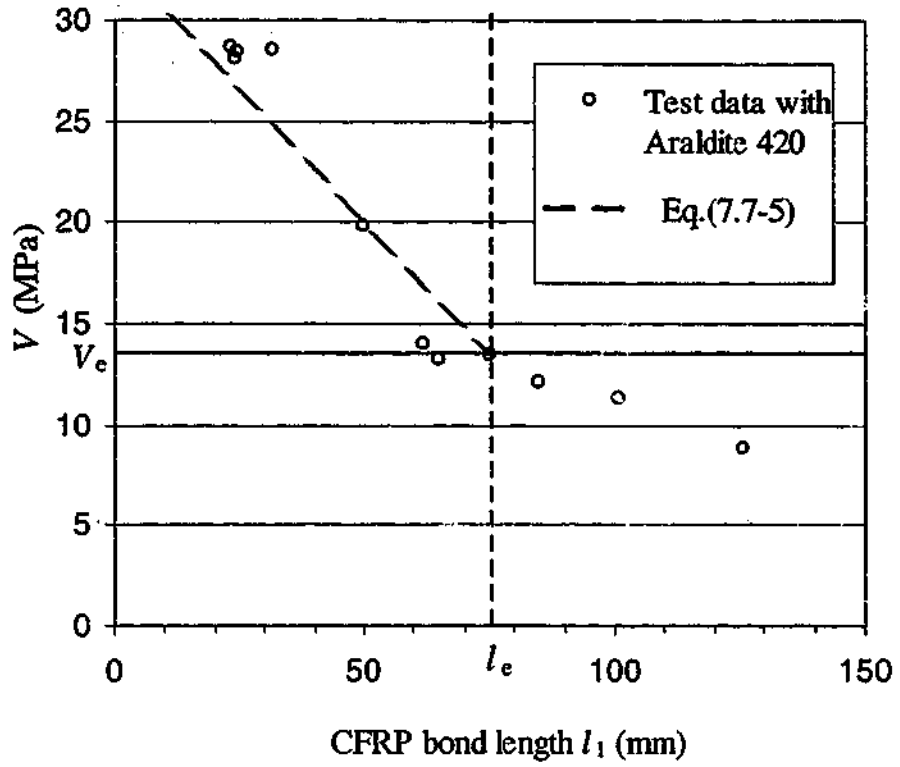

Figure 7.4-3: The lap shear strength (V) versus l_1

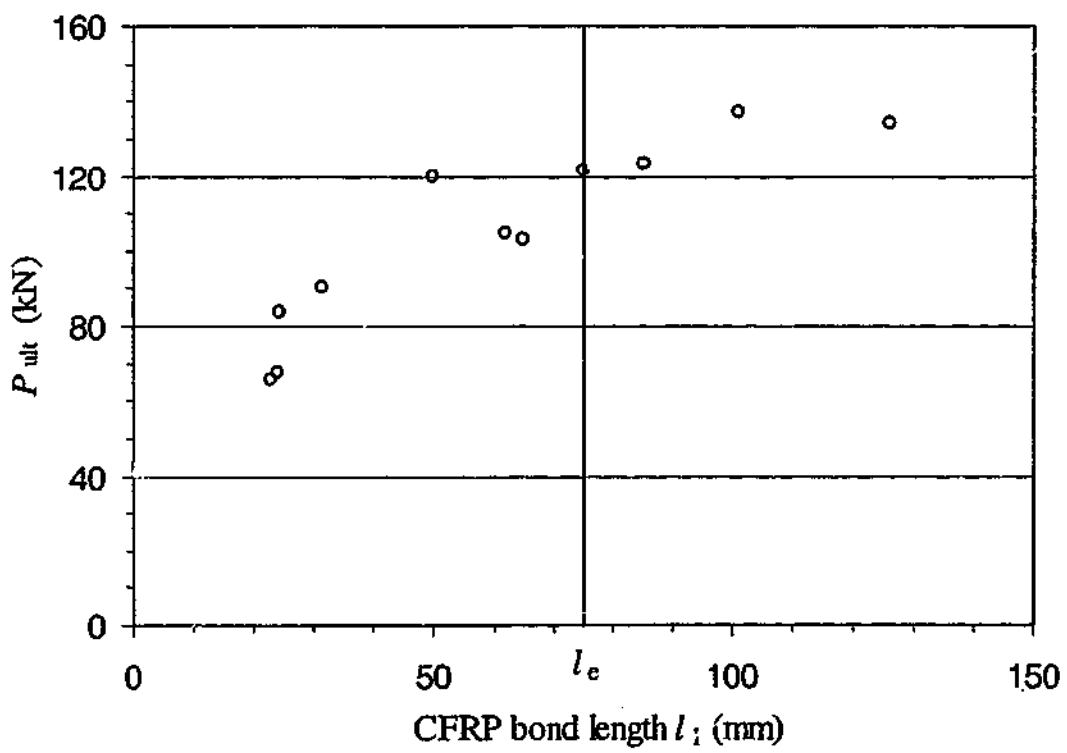

Figure 7.4-4: The ultimate load (P_{ult}) versus l_1

7.5 SPECIMEN PREPARATION AND TEST SETUP OF BUTT-WELDED VHS TUBES

7.5.1 Specimen Preparation

A total of 21 specimens (CFS1 to CFS21) were prepared, where CFRP and three kinds of epoxies were used. The specimen and CFRP applied are symmetric about the butt weld. The section dimensions, bond length (l_o), specimen overall length (L), the type of epoxy and number of CFRP layers (n) are listed in Table 7.5-1. The bond length (l_o) was measured from one end of bonded CFRP to the center of the weld in the longitudinal direction of each tube. First of all, VHS tubes were butt-welded using the same welding procedures and techniques as in Chapter 6. The welding procedures were pre-qualified through ETRS Pty. Ltd. (a laboratory accredited by the National Association of Testing Authorities, Australia) in accordance with AS1554.5 (SAA 1995). In order to make a smooth CFRP bonding on the welds, the bulged edge of the welds was milled flat. To improve the adhesive bonding, slightly abraded surfaces were recommended instead of highly polished ones (Ciba Adhesives 2000). Therefore the bonding area on the VHS tubes was ground with emery cloth. The loose steel particles and grease were removed with acetone. Finally the fully mixed epoxy resin was uniformly spread on both VHS tube and CFRP fabric. After the CFRP fabric was applied on VHS tube, the tube was rolled on a hard surface to force the excessive epoxy out. This process was repeated until the desired layers of CFRP were applied. Figure 7.5-1 shows some of the CFRP strengthened VHS tubes. All specimens were cured for at least one week before testing.

7.5.2 Test Setup

Axial tensile tests were conducted in a 500 kN capacity Baldwin universal testing machine with a loading rate of 2 mm/min. Steel plugs were put in both ends of each specimens to enable the tubes to be gripped. The same technique was used by Zhao (2000) and Ling et al. (2002) to apply tension force.

Table 7.5-1: Specimen dimensions

Specimen label	D_o (mm)	t (mm)	A_s (mm^2)	n	r_o (mm)	L (mm)	Epoxy type	Failure mode: In butt-welded VHS steel	Failure mode: In CFRP-Epoxy system
CFS1	38.11	1.59	182.42	3	15	600	Araldite 420	HAZ fracture failure for all (CFS1 to CFS21)	A
CFS2	38.12	1.58	181.37	3	30	600	Araldite 420		M
CFS3	38.17	1.60	184.92	4	50	600	Araldite 420		M
CFS4	38.15	1.58	185.37	4	75	600	Araldite 420		M
CFS5	38.08	1.59	182.27	4	100	600	Araldite 420		M
CFS6	38.28	1.80	206.29	4	50	600	Araldite 420		M
CFS7	38.17	1.79	204.58	4	75	600	Araldite 420		M
CFS8	38.22	1.80	205.95	4	100	600	Araldite 420		M
CFS9	38.09	1.58	181.23	5	125	700	Araldite 420		M
CFS10	38.14	1.59	182.57	5	150	700	Araldite 420		M
CFS11	38.05	1.60	183.22	6	100	600	Araldite 420		M
CFS12	38.07	1.80	205.10	6	100	600	Araldite 420		A
CFS13	38.10	1.59	182.37	3	50	600	Sikadue-330		A
CFS14	38.29	1.80	206.35	3	50	600	Sikadue-330		A
CFS15	38.30	1.79	205.31	4	50	600	Sikadue-330		A
CFS16	38.21	1.80	205.89	4	75	600	Sikadue-330		A
CFS17	38.22	1.79	204.86	4	100	600	Sikadue-330		A
CFS18	38.40	1.62	187.19	6	90	600	Sikadue-330		A
CFS19	38.20	1.81	206.92	6	105	600	Sikadue-330		A
CFS20	38.10	2.00	226.82	6	85	600	Sikadue-330		A
CFS21	38.28	1.80	206.29	3	50	600	Araldite K138		FT

Figure 7.5-1: Some CFRP strengthened butt-welded VHS tubes before testing. From top to bottom: CFS8 and CFS6 (With Araldite 420); CFS17 and CFS15 (With Sikadue-330); and CFS21 (with Araldite K138)

7.6 FAILURE MODES

7.6.1 Failure Mode in CFRP Strengthened Butt-Welded VHS Tubes

Failure was found to occur in the HAZ of the strengthened welded connections, i.e., HAZ fracture failure. This is the same failure mode as that observed in Chapter 6 for butt-welded VHS tubes without CFRP strengthening.

7.6.2 Failure Mode in CFRP-Epoxy System

For adhesively bonded FRP-FRP lap joints, seven classes of failure modes were classified in ASTM standard (ASTM 1999c). Three of the seven classes are related to adhesives. According to the failed position in the adhesive, they are called adhesive

failure (at the adhesive-substrate interface), cohesive failure (within the adhesive) and thin layer cohesive failure (within the adhesive and close to the adhesive-substrate interface). Another three failure modes are related to CFRP. They are fibre-tear failure (within FRP matrix), light fibre-tear failure (within FRP but close to the FRP-adhesive interface) and stock-break failure (break of FRP outside the adhesively bonded area). Any combination of two or more of these six classes of failure modes is called mix failure. For CFRP strengthened VHS tubes tested in this study, only two out of the above classified seven failure modes were observed, i.e., adhesive failure and fibre-tear failure. Another failure mode that does not exist for adhesively bonded FRP-FRP lap joints was observed for CFRP strengthened VHS tubes, i.e. a mixed failure of fibre break and adhesive failure. The failure mode for each specimen is listed in Table 7.5-1 and explained below.

7.6.2.1 Adhesive Failure (A)

All specimens strengthened with Sikadue-330 showed an adhesive failure mode. The rupture happened at the adhesive-steel interface shown in Figure 7.6-1. The CFRP on the failed specimens formed a tube-shape except for specimens CFS14 and CFS15 that split into two parts. Two specimens strengthened with Araldite 420 (CFS1 and CFS12) also showed this failure mode. CFS1 had a very short bond length and only 3 layers of CFRP were applied. The failure is most likely due to the low adhesive capacity caused by the very short bond length. CFS12 had a long bond length and 6 layers of CFRP. The adhesive failure is most likely due to the fact that the applied CFRP is strong enough to sustain the load.

7.6.2.2 Fibre-Tear Failure (FT)

Figure 7.6-2 shows the fibre-tear failure mode of the specimen CFS21 that was bonded with Araldite K138. This epoxy has relatively higher viscosity value (opposite to flow) than Araldite 420 and Sikadue-330. The carbon fibre within a layer cannot be fully soaked by the epoxy resin to form a composite system. Failure happened within the CFRP fabric. The fibre-tear prevented the joint from achieving its expected capacity. Therefore apart from CFS21, no further tests were conducted using Araldite K138.

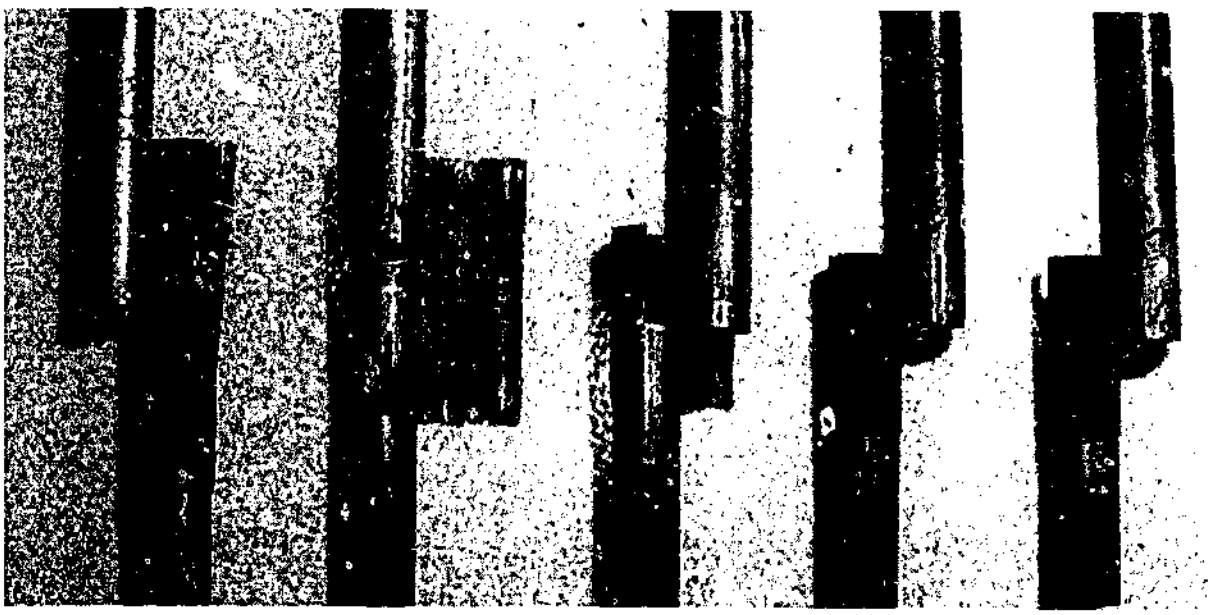

Figure 7.6-1: Failure mode of tubes bonded with Sikadue-330 (From right to left: CFS13-CFS17)

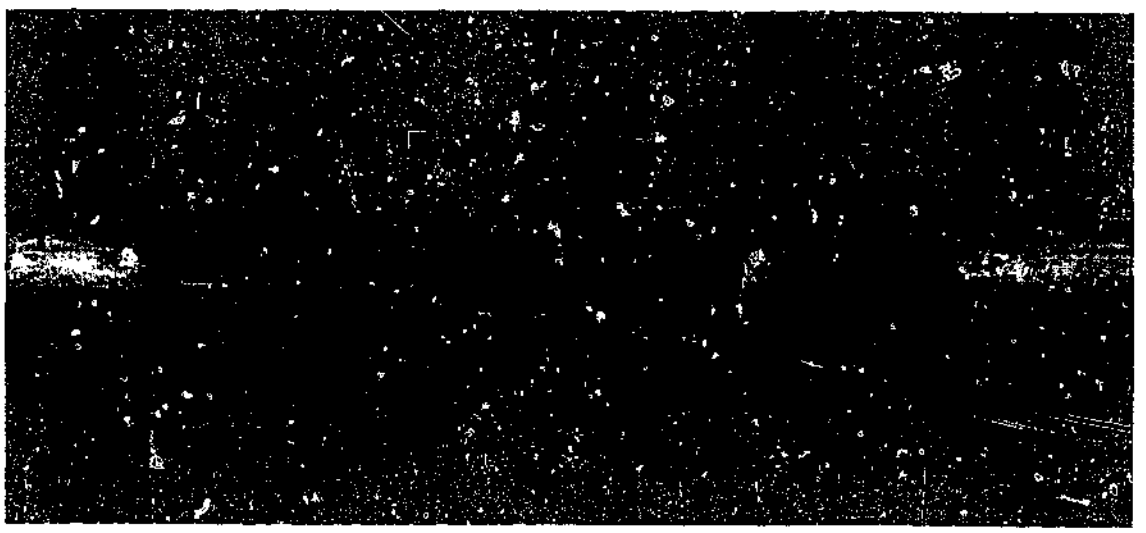

Figure 7.6-2: CFRP-tear failure mode (CFS21)

7.6.2.3 Mixed Failure (M)

Most specimens strengthened with Araldite 420 showed a combination of adhesive failure and fibre-break failure mode. A few tested specimens are shown in Figure 7.6-3. The mixed failure seems to be the preferred failure mode, since the strengthened connections with this failure mode almost reached the original VHS tube strength as shown later in this Chapter.

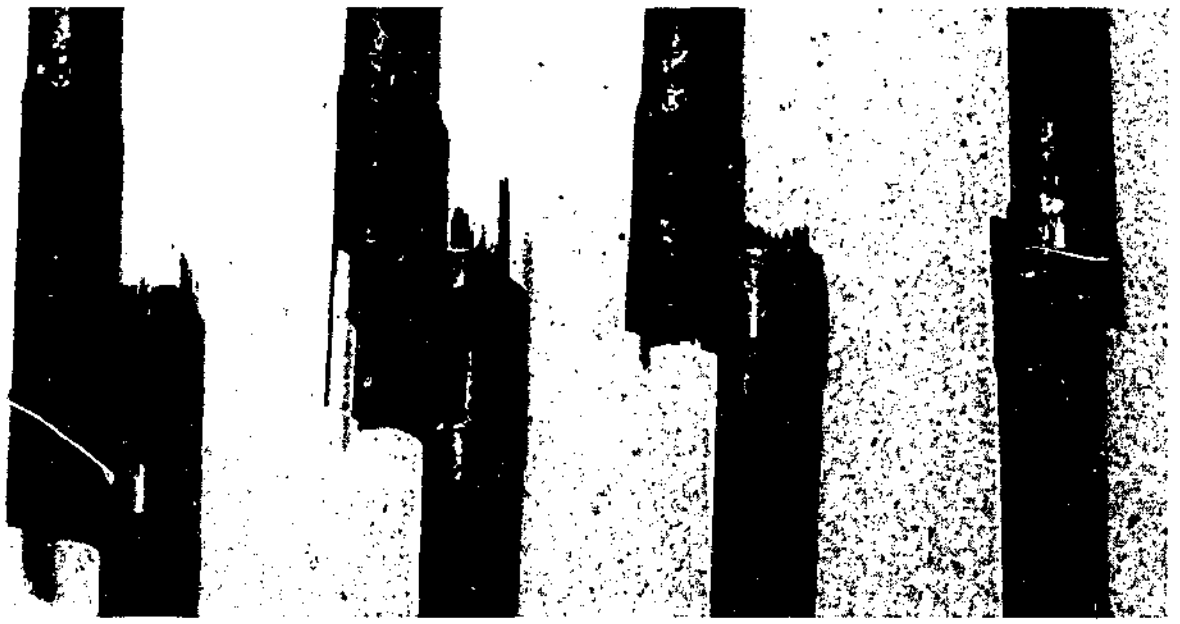

Figure 7.6-3: Mixed failure mode of CFRP-break failure and adhesive failure (From left to right: CFS2-CFS5)

7.7 CONNECTION STRENGTH

7.7.1 Load Carrying Capacity

The measured ultimate load P_{max}, the VHS tube's capacities at yielding ($P_{VHS\text{-}y}=f_yA_s$), at ultimate load ($P_{VHS\text{-}u}=f_uA_s$), nominal design capacity ($P_{VHS\text{-}d}=0.85f_uA_s$) and the load carrying capacity in the HAZ ($P_{HAZ}=f_{HAZ}A_s$) are compared in Table 7.7-1. Here, f_y and f_u are the average yield stress and ultimate tensile strength of VHS tubes tested in Chapter 3, i.e. f_y=1349 MPa and f_u=1505 MPa; f_{HAZ} is the tube connection strength in the HAZ tested in Chapter 6, i.e. f_{HAZ}=737 MPa; A_s is the cross-section area of VHS tubes. It can be seen from Table 7.7-1 that a more consistent strength increase was obtained for specimens using Araldite 420. Therefore, Araldite 420 seems suitable for strengthening butt-welded VHS tubes. Only ratios for specimens with Araldite 420 are discussed further in this thesis.

The ratios of P_{max}/P_{VHS} and P_{max}/P_{HAZ} versus l_o for specimens bonded with the epoxy of Araldite 420 are plotted in Figure 7.7-1 and Figure 7.7-2. It can be seen from Figure 7.7-1 that the load carrying capacity of CFRP-strengthened butt-welded VHS tubes increases with the increase of the CFRP bond length. When the bond length reaches around 75mm with four layers of CFRP, the load carrying capacity of CFRP-strengthened connection approaches that of VHS steel tubes. The ratio of P_{max}/P_{HAZ} reaches a plateau after the bond length exceeds 75 mm. This length of 75 mm is defined in this thesis as the effective bond length (l_e). A similar phenomenon was found in Teng et al. (2002) that any increase in bond length beyond effective bond length cannot increase the bond strength between CFRP and concrete. The concept of effective bond length was also used by Teng et al (2002). In addition to CFRP bond length, a minimum number of CFRP layers is also required. From Table 7.5-1 and Table 7.7-1 it can be seen that the yield capacity of VHS tubes can be recovered when four layers of CFRP are applied. Therefore a minimum of four layers of CFRP is recommended.

Table 7.7-1: Experimental load carrying capacity

Label (1)	P_{max} (kN) (2)	P_{VHS-y} (f_yA_s) (kN) (3)	P_{VHS-u} (f_uA_s) (kN) (4)	P_{VHS-d} ($0.85f_uA_s$) (kN) (5)	P_{HAZ} ($f_{HAZ}A_s$) (kN) (6)	(2)/(3) (7)	(2)/(4) (8)	(2)/(5) (9)	(2)/(6) (10)	Epoxy type (11)
CFS1	147.8	246.1	274.5	233.4	134.4	0.601	0.538	0.633	1.099	Araldite 420
CFS2	191.8	244.7	273.0	232.0	133.7	0.784	0.703	0.827	1.435	Araldite 420
CFS3	240.4	249.5	278.3	236.6	136.3	0.964	0.864	1.016	1.764	Araldite 420
CFS4	255.3	250.1	279.0	237.1	136.6	1.021	0.915	1.077	1.869	Araldite 420
CFS5	263.5	245.9	274.3	233.2	134.3	1.072	0.961	1.130	1.962	Araldite 420
CFS6	256.5	278.3	310.5	263.9	152.0	0.922	0.826	0.972	1.687	Araldite 420
CFS7	296.0	276.0	307.9	261.7	150.8	1.073	0.961	1.131	1.963	Araldite 420
CFS8	297.1	277.8	310.0	263.5	151.8	1.069	0.959	1.128	1.957	Araldite 420
CFS9	257.9	244.5	272.7	231.8	133.6	1.055	0.946	1.112	1.931	Araldite 420
CFS10	272.7	246.3	274.8	233.6	134.6	1.107	0.992	1.168	2.027	Araldite 420
CFS11	267.5	247.2	275.7	234.4	135.0	1.082	0.970	1.141	1.981	Araldite 420
CFS12	290.2	276.7	308.7	262.4	151.2	1.049	0.940	1.106	1.920	Araldite 420
CFS13	196.3	246.0	274.5	233.3	134.4	0.798	0.715	0.841	1.460	Sikadue-330
CFS14	183.5	278.4	310.6	264.0	152.1	0.659	0.591	0.695	1.207	Sikadue-330
CFS15	243.9	277.0	309.0	262.6	151.3	0.881	0.789	0.929	1.612	Sikadue-330
CFS16	289.3	277.8	309.9	263.4	151.7	1.042	0.934	1.098	1.907	Sikadue-330
CFS17	219.5	276.4	308.3	262.1	151.0	0.794	0.712	0.838	1.454	Sikadue-330
CFS18	236.6	252.5	281.7	239.5	138.0	0.937	0.840	0.988	1.715	Sikadue-330
CFS19	210.7	279.1	311.4	264.7	152.5	0.755	0.677	0.796	1.382	Sikadue-330
CFS20	269.0	306.0	341.4	290.2	167.2	0.879	0.788	0.927	1.609	Sikadue-330
CFS21	183.1	278.3	310.5	263.9	152.0	0.658	0.590	0.694	1.204	Araldite K138

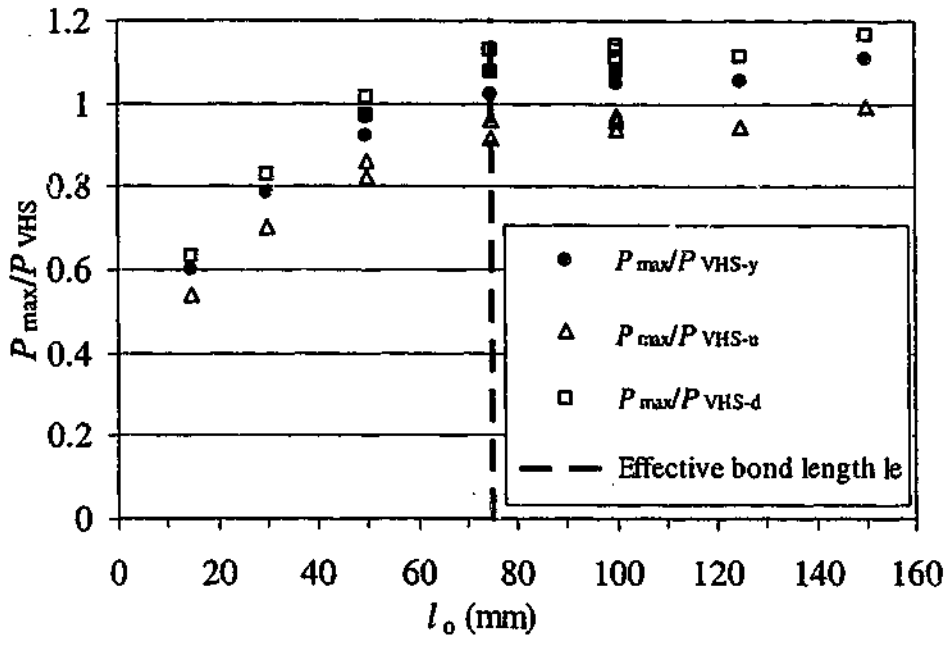

Figure 7.7-1: P_{max}/P_{VHS} versus l_o for specimens bonded with Araldite 420

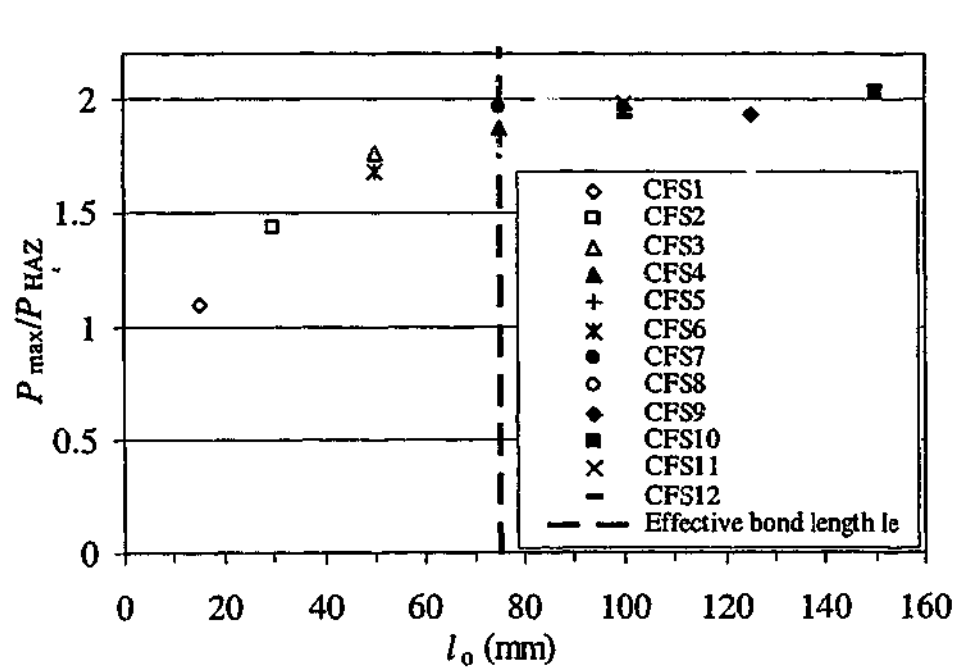

Figure 7.7-2: P_{max}/P_{HAZ} versus l_o for specimens bonded with Araldite 420

7.7.2 Prediction of Load Carrying Capacity

It can be seen from Figure 7.7-1 and Figure 7.7-2 that the steel strength in the HAZ was enhanced by the CFRP-epoxy system. The load carrying capacity of the CFRP-bonded joint can be calculated as:

$$P_{\text{CFRP-bonded}} = P_{\text{HAZ}} + P_{\text{CFRP}} \tag{7.7-1}$$

in which, P_{HAZ} is the load carrying capacity of HAZ in the connection; P_{CFRP} is the load carrying capacity of CFRP composite system.

$$P_{\text{HAZ}} = A_s f_{\text{HAZ}} \tag{7.7-2}$$

$$P_{\text{CFRP}} = \pi D\, l_o\, V \qquad \text{if } l_o \le l_e \tag{7.7-3}$$

$$P_{\text{CFRP}} = \pi D\, l_e\, V_e \qquad \text{if } l_o > l_e \tag{7.7-4}$$

where V can be derived from a regression analysis in Figure 7.4-3 for l_1<75mm, and expressed in terms of l_o:

$$V = -0.256 l_o + 32.7 \tag{7.7-5}$$

V_e is the value of V when $l_o = l_e$, i.e. V_e=13.5MPa; l_e is the effective CFRP bond length; f_{HAZ} is the ultimate strength in the HAZ; A_s is the cross section area of VHS tube; D is the outside diameter of VHS tube. The calculated load carrying capacity for the full section VHS tubes strengthened with Araldite 420 is listed in Table 7.7-2 together with the ultimate load obtained in the tests. Specimens CFS1 and CFS2 are not included in Table 7.7-2 since less than four layers of CFRP were applied. By comparing the load carried by the CFRP-epoxy system (P_{CFRP}) and the total load ($P_{\text{CFRP-bonded}}$), it can be seen that about 46% of the total load was carried by the CFRP and Araldite 420 epoxy system. The ratios of the calculated load ($P_{\text{CFRP-bonded}}$) to the measured ultimate load (P_{max}) are plotted in Figure 7.7-3. An average $P_{\text{CFRP-bonded}}/P_{\text{max}}$ value of 0.976 is obtained with a standard deviation of 0.052.

Table 7.7-2: Comparison with predicted load carrying capacity

Specimen Label (1)	l_o (mm) (2)	V_w (MPa) (3)	P_{CFRP} (kN) (4)	$P_{CFRP\text{-}bonded}$ (kN) (5)	P_{max} (kN) (6)	$P_{CFRP\text{-}bonded}/P_{max}$ (7)	$P_{CFRP}/P_{CFRP\text{-}bonded}$ (8)
CFS3	50	19.9	119.3	255.6	240.4	1.063	0.467
CFS4	80	13.5	121.4	258.0	255.3	1.010	0.470
CFS5	100	13.5	121.1	255.5	263.5	0.969	0.474
CFS6	50	19.9	119.7	271.7	256.5	1.059	0.440
CFS7	75	13.5	121.4	272.2	296.0	0.920	0.446
CFS8	100	13.5	121.6	273.4	297.1	0.920	0.445
CFS9	125	13.5	121.2	254.7	257.9	0.988	0.476
CFS10	150	13.5	121.3	255.9	272.7	0.938	0.474
CFS11	100	13.5	121.0	256.1	267.5	0.957	0.473
CFS12	100	13.5	121.1	272.3	290.2	0.938	0.445
MEAN						0.976	0.461
COV						0.052	0.031

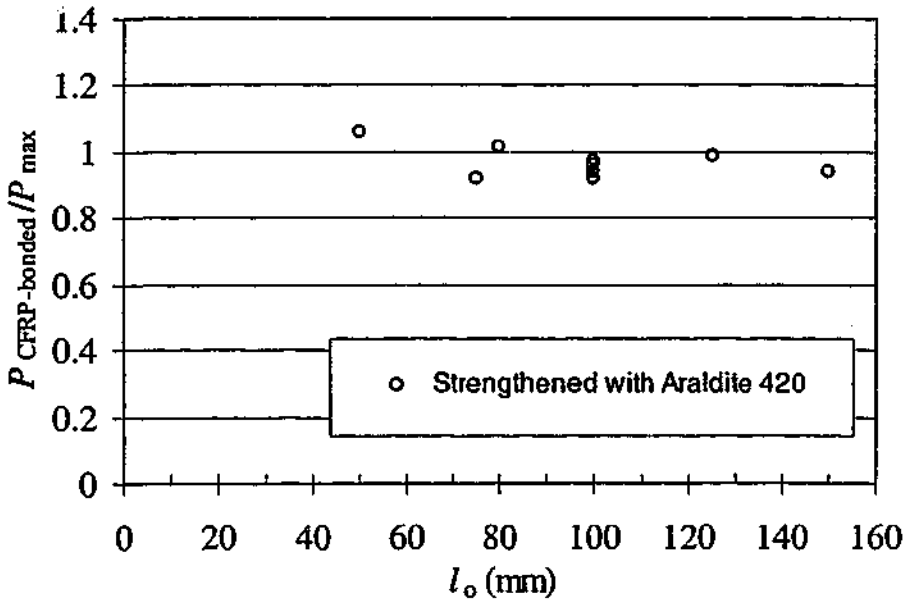

Figure 7.7-3: Ratios of $P_{CFRP\text{-}bonded}/P_{max}$ versus bond length l_o

7.8 SUMMARY

This chapter investigates the behaviour of CFRP (Carbon Fibre Reinforced Plastics) strengthened butt-welded VHS tubes. Some applications of CFRP materials on metallic structures were reviewed. Experimental studies were conducted on strengthening butt-welded VHS tubes.

Three types of epoxy resins with different lap shear strength were used. Tests were conducted to determine the lap shear strength between CFRP and VHS steel tube. Among the tested epoxies, Araldite 420 was recommended for the strengthening purpose in this study due to the highest lap shear strength.

A total of twenty-one butt-welded VHS tubes strengthened with CFRP were tested in axial tension. Three kinds of failure modes, i.e. adhesive failure, fibre tear and mixed failure of CFRP break and adhesive failure were observed. Among them, the mixed failed mode was the dominating mode for specimens with Araldite 420. It was found that the load carrying capacity of CFRP strengthened butt-welded VHS tubes increases with the increase of the CFRP bond length until an effective bond length of 75mm was reached. Any increase in bond length beyond this effective bond length does not significantly increase the bond strength between CFRP and VHS tubes. The yield capacity of VHS tubes was recovered by using this CFRP-epoxy strengthening system when the minimum four layers of CFRP with effective bond length were applied. A theoretical model was developed to estimate the load carrying capacity of butt-welded VHS tubes strengthened using CFRP.

Future research in this area is identified in next Chapter.

Chapter 8

FUTURE WORK

8.1 INTRODUCTION

The previous five chapters (from Chapter 3 to Chapter 7) deal with the behaviour of VHS members and welded connections. The material ductility, residual stresses, section slenderness limits, strength in VHS member and in HAZ, and CFRP strengthening techniques of butt-welded VHS tubes were investigated. Design rules were also proposed. Since the tensile strength of VHS members is about three times higher than that of most structural steel members being used today, in order for VHS tubes to be used as a structural steel hollow section, more research work may need to be conducted in the future.

This Chapter identified a number of future research topics. They include the shear band formation of VHS tubes during axial tension; finite element analysis of VHS tubes in compression and in bending; ovalisation simulation of VHS tubes; post-weld-heat-treatment of welded VHS tubes and the load transfer mechanism of CFRP strengthened VHS tubes. Preliminary work are presented first followed by suggestions for further investigation.

8.2 SHEAR BAND FORMATION OF VHS TUBES IN TENSION

8.2.1 Introduction

The shear band orientation of VHS tubes in tension was discussed in Chapter 3. Comparison on the shear band angle was made with other thin-walled circular or sheet steels. Possible factors that may affect the shear band formation were roughly explained. However, the question that why 62.5° rather than 45° was formed between the shear band and the loading direction for VHS tubes still remains unanswered. To solve this problem, more work may be needed using the analysis of plastic instability of solids.

According to the theory of solid mechanics, instabilities of solids under a static load occur at a bifurcation point or at a limit point. The shear band instability is due to the plastic flow localization. A general theory for the analysis of the plastic flow for deformed solids was given by Hill (1958; 1998), Hill and Hutchinson (1975). The shear band formation is a material response rather than a consequence of boundary conditions. A model was proposed by Tvergaard (1999) to study the effect of different constitutive laws on the onset of shear band. In his model the localized shearing was assumed to occur in a thin slice of material, whereas strains outside the shear band were assumed uniform throughout the deformation history. A specific case of shear band formation in a plane strain tensile test was studied by Tvergaard et al. (1981). The dynamic shear band formation of a 3D solid model was numerically studied by Zbib and Jubran (1992). The analytical or numerical analysis of the shear band formation of VHS tubes may be conducted using these theoretical models.

8.2.2 Measurement of Maximum Shear Stress Orientation

An experimental test was conducted attempting to measure the shear band development process of VHS tubes in tension. Details of this test are explained as follows.

Two specimens of full section VHS tubes with nominal diameter of 38mm and thickness of 1.8mm were tested under axial tension. A 45° strain rosette (Figure 8.2-1)

was mounted on the surface of each specimen. The tests were conducted in a 500 kN Baldwin universal testing machine with a strain rate of 1×10^{-4}/s.

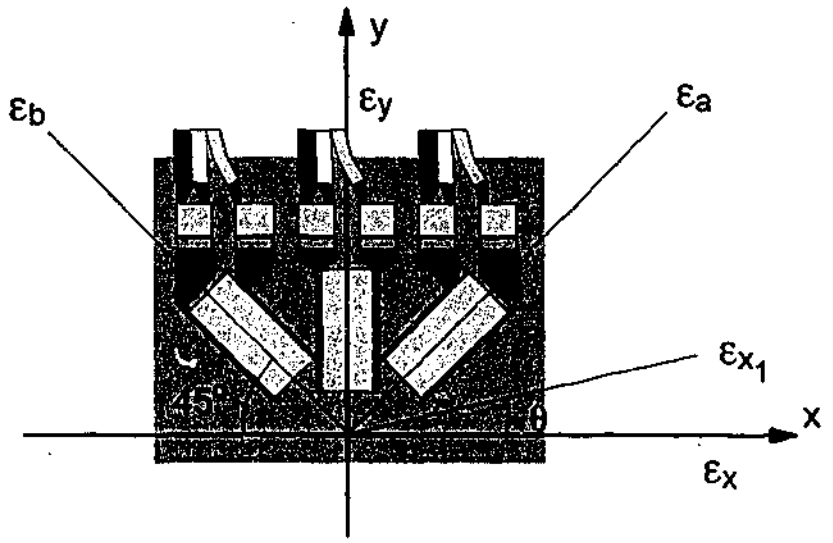

Figure 8.2-1: Strain rosette mounted on VHS tubes (y axis is the loading direction)

Since VHS tubes are thin-walled hollow sections, when an infinitesimal area is selected, the stress status can be treated as plane stress. The transformation equations derived from plane strain can be used for the strains in plane stress (Gere and Timoshenko 1999). The transformation equation for strains at any direction is expressed as:

$$\varepsilon_{x1} = \frac{\varepsilon_x + \varepsilon_y}{2} + \frac{\varepsilon_x - \varepsilon_y}{2}\cos 2\theta + \frac{\gamma_{xy}}{2}\sin 2\theta \qquad (8.2\text{-}1)$$

where ε_{x1} is the normal strain in x_1 direction; θ is the angle between x axis and x_1 direction. According to Eq.(8.2-1), the shear strain γ_{xy} and normal strain ε_x based on the measured strain elements in the strain rosette of Figure 8.2-1 can be expressed as:

$$\gamma_{xy} = \varepsilon_a - \varepsilon_b \qquad (8.2\text{-}2)$$

$$\varepsilon_x = \varepsilon_a + \varepsilon_b - \varepsilon_y \qquad (8.2\text{-}3)$$

The measured strains from the strain rosette are shown in Figure 8.2-2. γ_{xy} was calculated using Eq.(8.2-2).

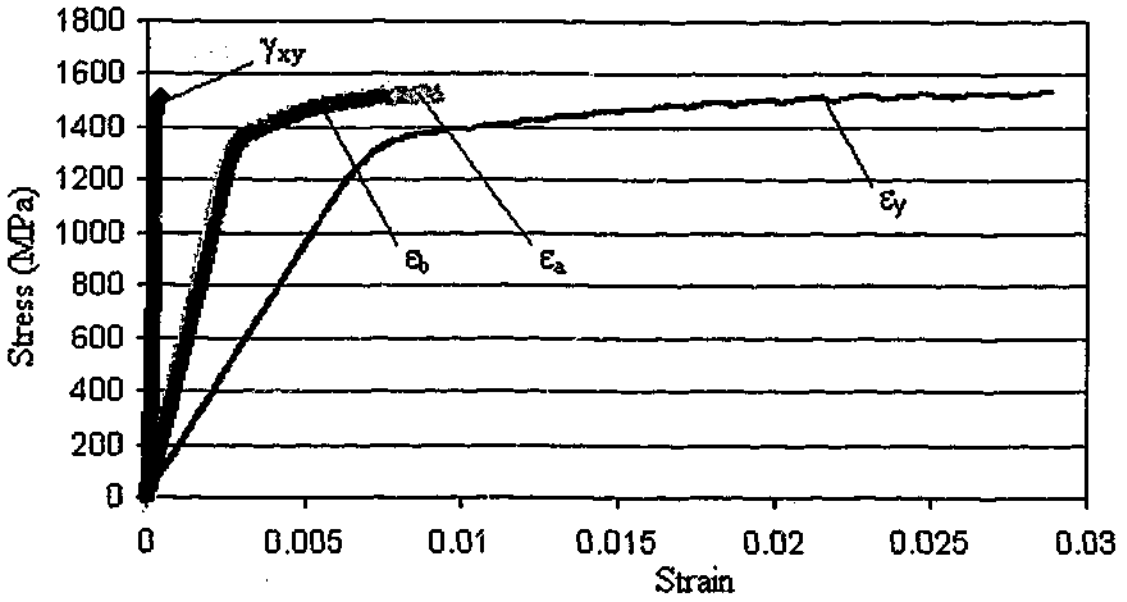

Figure 8.2-2: The measured strain elements

It can be seen from Figure 8.2-2 that there is no shear strain (γ_{xy}=0) in the loading direction even when VHS steel entered into the non-linear part of the stress-strain curves, i.e., ε_x and ε_y are principle strains. The maximum shear stress orientation is 45° towards the loading direction.

Before shear bands appeared on the tested specimens, the strain rosette peeled off or became useless due to that the plastic strain was beyond the measurement limit of the strain rosette. Therefore the shear band development process cannot be measured by this experimental method.

8.2.3 Summary and Suggested Future Work

An attempt was made to measure the shear band formation of VHS tubes in a tension test by means of strain rosette. However this test method was unsuccessful due to the measurement limitation of strain rosettes. Therefore future research on this topic may be focused on the numerical simulation of the shear band formation by means of finite element analysis method using the plastic flow and bifurcation theory in solid mechanics.

8.3 FINITE ELEMENT ANALYSIS OF VHS TUBES IN COMPRESSION

8.3.1 Introduction

An initial work on the simulation of VHS tubes in compression was conducted by means of finite element (FE) analysis method. The elephant's foot failure mode was obtained from the FE model. However the diamond-shaped local buckling that was observed on VHS tubes (with *D/t* ratio of 47) during experimental test was not shown on the analytical model. The ratio of the calculated ultimate load to that obtained from experiments was about 0.93. More work is needed to refine the FE model.

8.3.2 Analytical Model

The Strand7 finite element analysis system was used. The system is a general-purpose finite element analysis system developed by G+D computing Pty. Ltd., Australia (G+D Computing 2002). It can be used to solve linear and non-linear static, dynamic and buckling problems. This system supports non-linear geometry, material (including plasticity and large strain) and boundary non-linearity.

An elastic-plastic model of VHS tubes was established. The stress-strain property of VHS tubes obtained from tensile test in Chapter 3 was used. Since the measured initial imperfection and residual stress of VHS tubes described in Chapter 4 were negligible, they are not considered in the analysis process. Two separate loading steps, i.e. the elastic step and the plastic step, were adopted in the analysis process.

8.3.3 Element Type

The three-dimensional plate shell element type was selected in this study. It is the most general type of shell element. It can be used for the analysis of general three-dimensional shells. In Strand7, Shells can be classified as either thick or thin depending on the wall thickness of the shell compared to the overall dimensions of the specimen. In general, the shell is considered thick when the thickness is greater than about 1/10 of a nominal dimension of the shell. For circular hollow sections, if the wall thickness is greater than about 1/10 of the radius, it is usually considered thick.

Since the wall thickness of all the VHS tubes in this analysis are ranging between 1/12 and 1/23 of the tube radius, the thin shell element type was used through out this analysis. This 4-node element type can provide efficient analysis for thin-walled structures with certain accuracy. The element size was 2 mm for all columns in the analysis. The geometric non-linearity was also considered.

8.3.4 Loading and Boundary Conditions

The effect of geometrical imperfections and boundary conditions on the buckling strength of thin-walled shells was investigated by Calladine (1995). He reported that not only the initial geometrical imperfections were important to the buckling behaviour of thin shells, but the fixed boundary conditions may also have their contributions. Since VHS tubes are axisymmetric structures, only a quarter of the tube needs to be selected for analysis. However, in order to simulate the elephant's foot failure mode, the whole cross section was selected. Only the top half of the VHS tube was chosen for modeling. The boundary conditions are simplified for VHS tubes in compression as shown in Figure 8.3-1. To model the restriction of both ends of the VHS tube, the top edge of the tube is constrained in the lateral direction. The bottom of the tube is simply supported to reflect the symmetry. A displacement (-U2) was given on top end of the tube. Therefore the analysis was in displacement control.

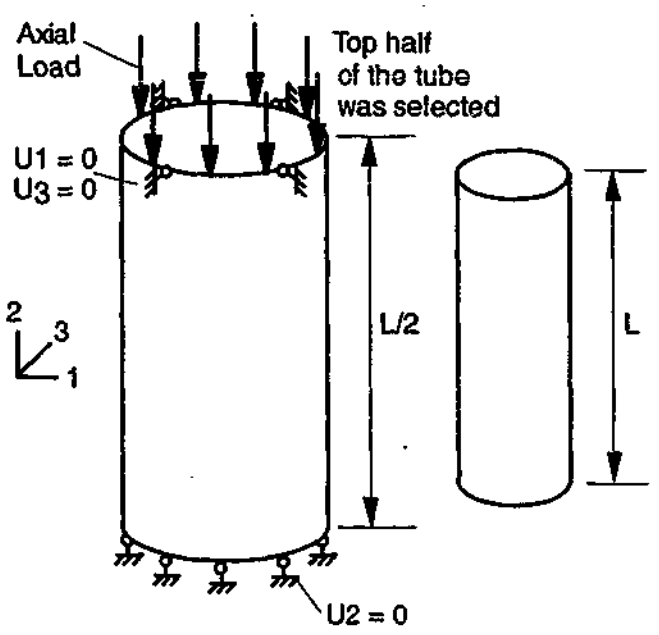

Figure 8.3-1: Load and boundary conditions of VHS tube

8.3.5 Comparison Between the Analytical and Experimental Results

8.3.5.1 Failure Mode

The deformed shape of the VHS tube is shown in Figure 8.3-2. The same elephant's foot failure mode as observed during compression tests was obtained for all tubes. The comparison of tested specimens and their simulations from the finite element analysis are shown in Figure 8.3-3. The finite element model did not show the diamond shape buckling (for CS7A) that occurred after the formation of elephant's foot mode in the test.

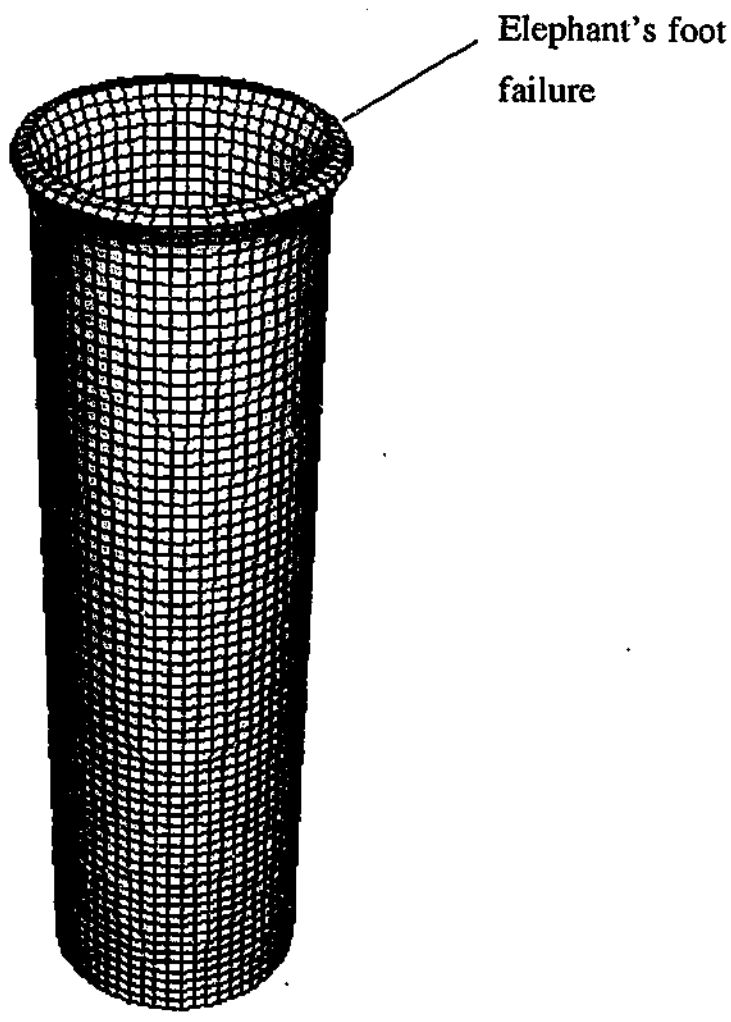

Figure 8.3-2: Deformed VHS tube

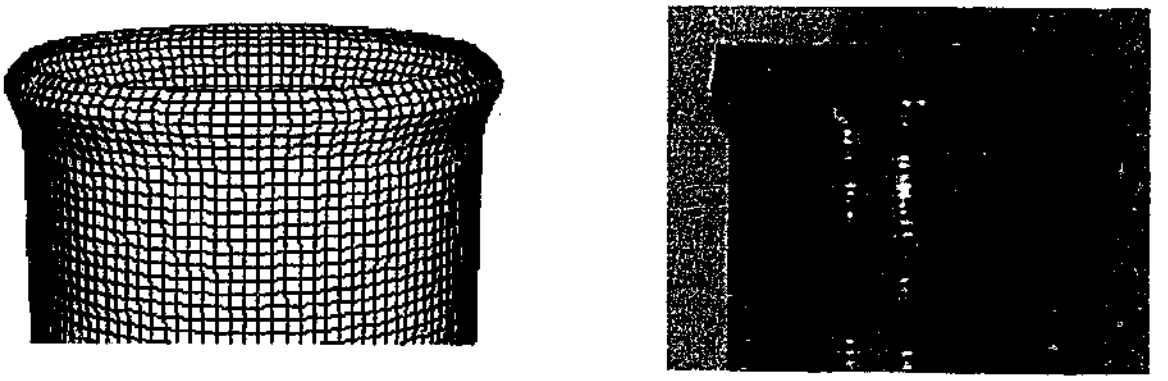

(a) CS7A

(b) CS8A

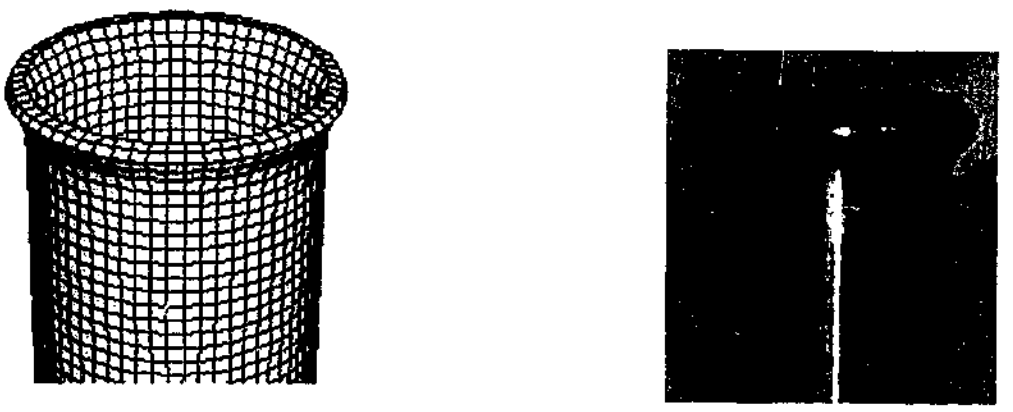

(c) CS9A

Figure 8.3-3: Comparison of failure mode between the numerical analysis and experimental results

8.3.5.2 Comparison of Load Carrying Capacity

The load-displacement curves obtained from testing and finite element method for specimen CS7A, CS8A and CS9A were shown in Figure 8.3-4. It can be seen from Figure 8.3-4 that the ultimate load from the finite element model is slightly smaller than that obtained from the test data. This may be due to the simplification of fixed-end boundary conditions on the top edge of the VHS tube. The ultimate loads are listed in Table 8.3-1. The ratio of the ultimate loads between the finite element (FE) model and the test is about 0.93.

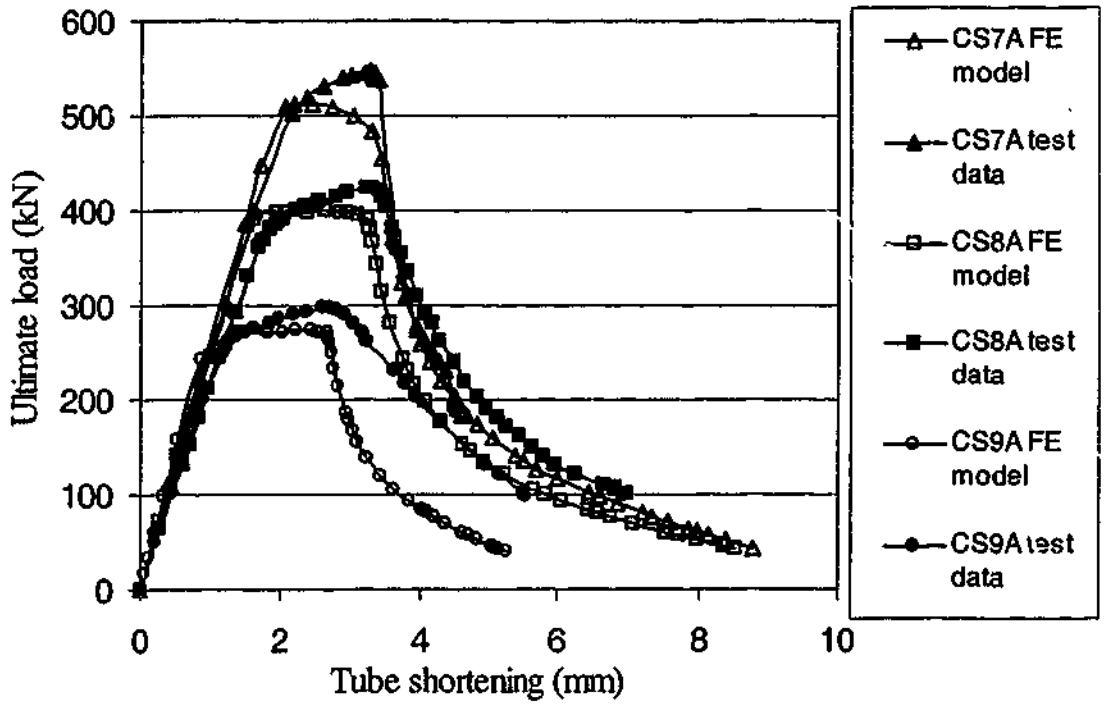

Figure 8.3-4: Load-displacement curves from finite element model and test data

Table 8.3-1: Comparison of ultimate load

Label (1)	Ultimate load (kN)		(3)/(2)
	Test data (2)	FE model (3)	(4)
CS7A	547	513	0.94
CS8A	425	399	0.94
CS9A	298	273	0.92
Mean			0.93
COV			0.0122

8.3.6 Summary and Suggested Future Work

A preliminary FE analysis of VHS tubes in compression was conducted. The elephant's foot failure mode was obtained for the analytical model, although the diamond shape local buckling did not show on the FE model. To improve the analytical model, the following factors may be considered:

- To add a steel block on top of the VHS tube to more accurately simulate the test condition;
- To take into account the effects of residual stress and initial geometric imperfection.

8.4 FINITE ELEMENT ANALYSIS OF VHS TUBES IN BENDING

8.4.1 Initial Work

An analysis of VHS tubes in 4-point-bending was initially conducted using FE method. The same shell element type as adopted in Section 8.3.3 was used. Steel saddles that were put at the loading points and supports during experiments were extruded from the tube elements. The stress-strain curves obtained from tensile tests in Chapter 3 were used for material properties of VHS steel. The load and the boundary conditions are shown in Figure 8.4-1. A displacement was given at two loading points to control the calculation.

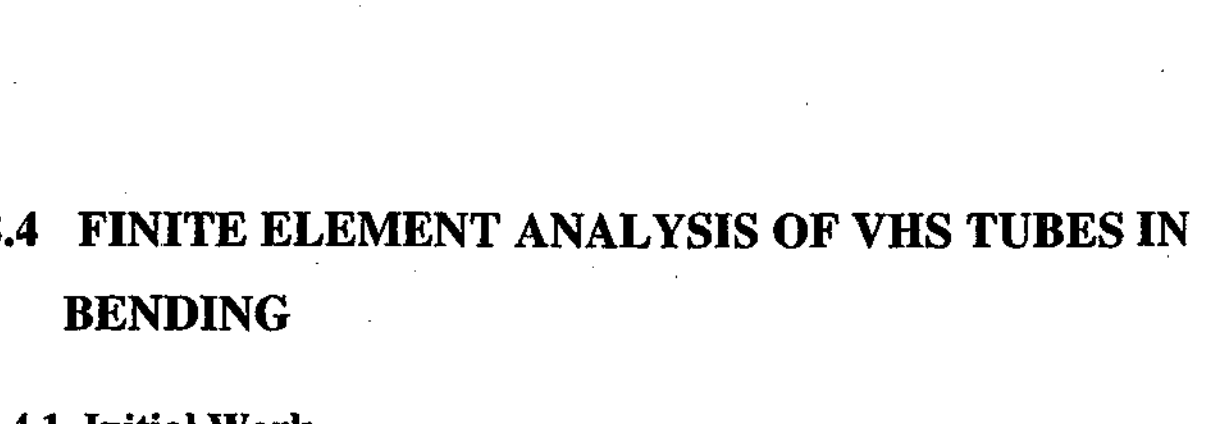

Figure 8.4-1: Load and boundary conditions of a VHS tube in 4-point-bending

The model was firstly calculated by considering the geometric non-linearity. The deformed VHS tube for specimen BS8 is shown in Figure 8.4-2. It can be seen from Figure 8.4-2 that local buckling appeared next to the loading point between the two steel saddles, whereas the experimental local buckling occurred in the middle of the two steel saddles as shown in Figure 8.4-3. The calculated ultimate bending moment (M_u') is 9.77 kNm. The ratio of M_u'/M_u is about 0.84 (M_u is the ultimate bending

moment obtained from experiments, M_u=11.68 kNm for specimen BS8). Since the failure mode and the ultimate bending moment from this model did not match the experimental results, the FE model was revised that the geometric non-linearity was turned off during the analysis. The deformed tube calculated from the revised FE model is shown in Figure 8.4-4.

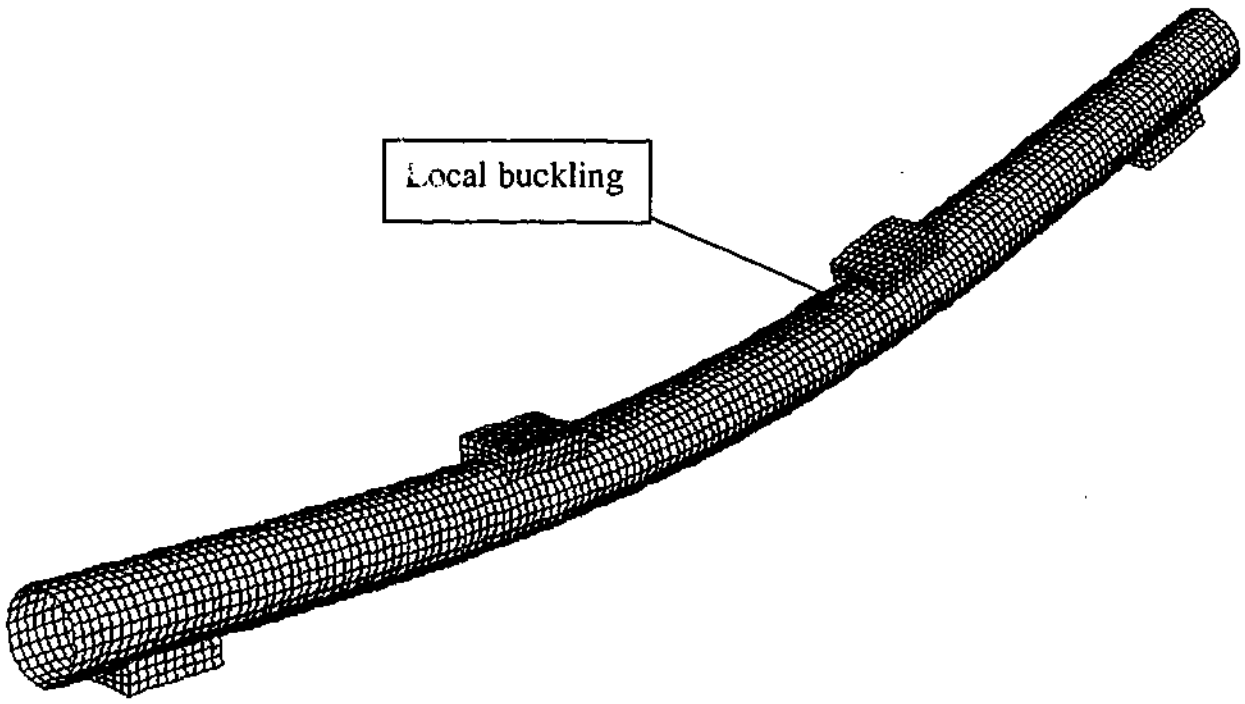

Figure 8.4-2: Deformed VHS tube (BS8) with geometric non-linearity

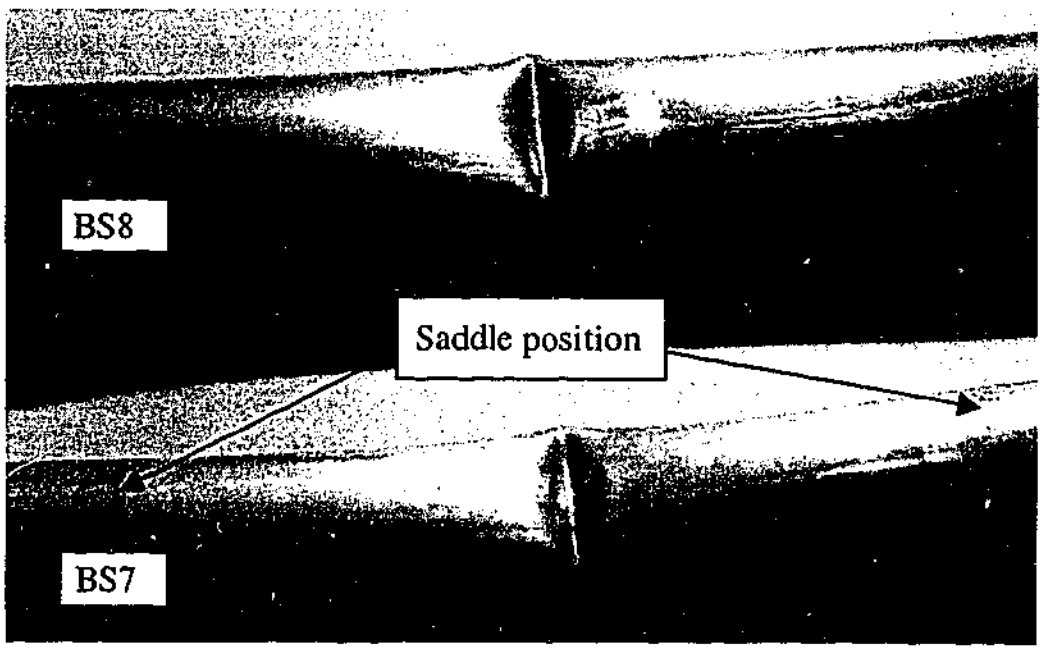

Figure 8.4-3: Experimental local buckling of VHS tubes (BS7 and BS8)

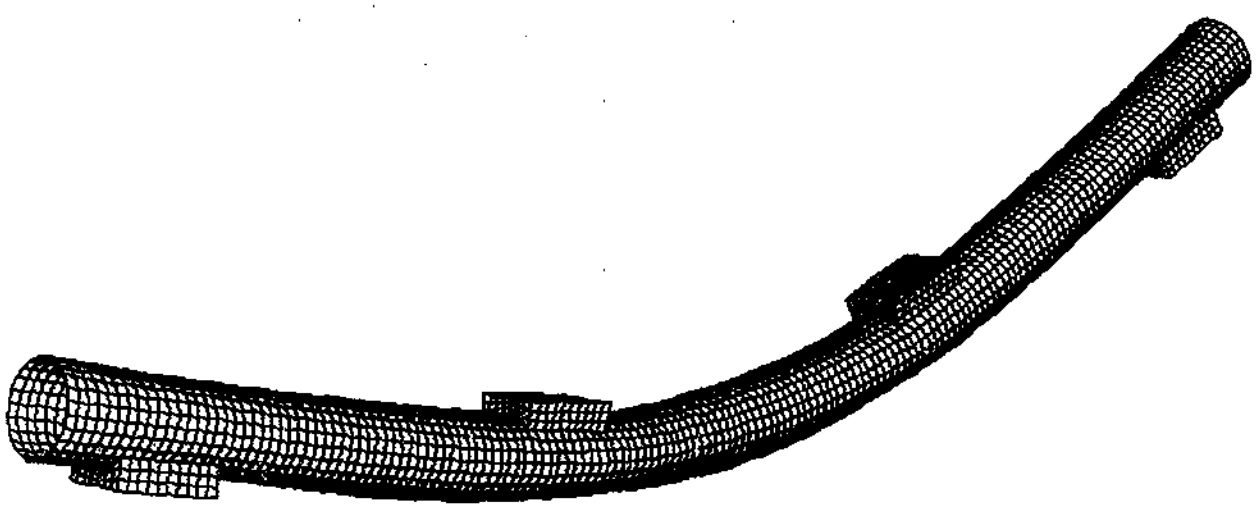

Figure 8.4-4: Deformed VHS tube (BS8) without geometric non-linearity

It can be seen from Figure 8.4-4 that there is no buckling on the tube. An ultimate bending moment of 12.1 kNm is obtained, which is slightly larger than the experimental result of 11.68 kNm. The Moment-curvature curves from the calculated models and from the experimental result for specimen BS8 are compared in Figure 8.4-5.

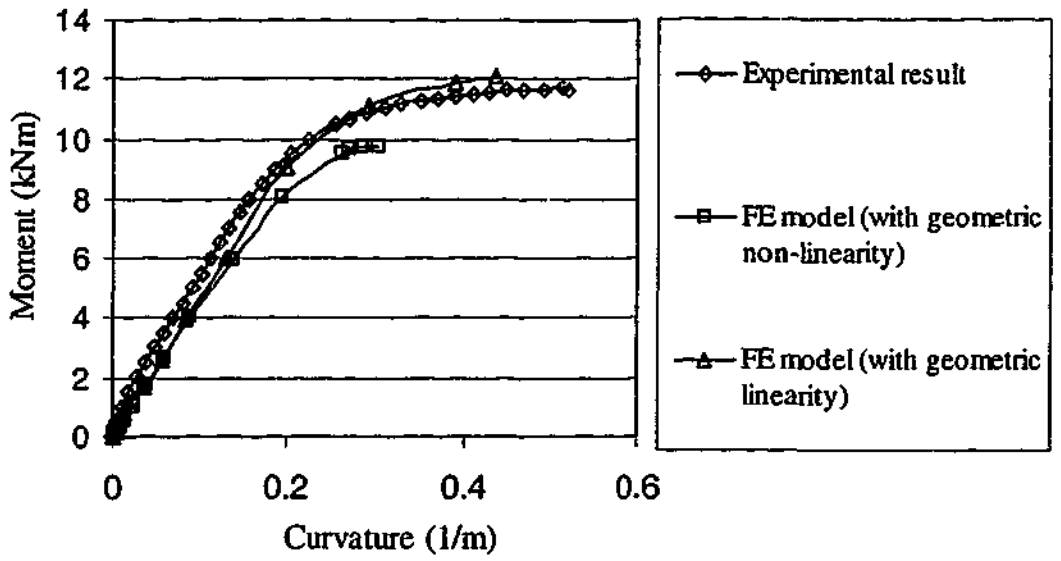

Figure 8.4-5: Comparison of Moment-curvature curves for specimen (BS8)

8.4.2 Summary and Suggested Future Work

VHS tubes subjected to 4-point-bending were initially analyzed using finite analysis method. The established FE model did not perfectly simulate the bending capacity and failure mode observed in the experimental test. The model may be improved in the future by considering the following points:

- To replace the extruded steel saddles with separate steel saddle elements;
- To define contact properties between steel saddles and VHS tubes;
- To take into account the initial geometric imperfection of VHS tubes.

8.5 OVALISATION OF VHS TUBES IN BENDING

It has been stated in Chapter 5 that ovalisation is a unique phenomenon for circular tubes in bending. The ovalisation of some VHS tubes was measured with a vernier during 4-point-bending tests. The measured values are listed in Table 8.5-1. M is the bending moment; κ is the tube curvature corresponding to the bending moment; κ_u is the curvature at the ultimate bending moment; D_l and D_s is the diameter of deformed tube shown in Figure 8.5-1. The ovalisation is defined as $\Delta D/D$. D is the diameter of undeformed tube. ΔD equals to D_l-D_s.

Table 8.5-1: The measured ovalisation of VHS tubes

Specimen Label	M (kN m)	κ (1/m)	κ/κ_u	D_l (mm)	D_s (mm)	$\Delta D/D$ (%)
BS5	3.39	0.68	0.286	38.65	37.65	2.62
	3.63	1.62	0.681	39.63	36.23	8.91
	3.63	1.82	0.765	39.90	35.98	10.27
	3.65	2.00	0.840	40.03	35.85	10.95
BS6	2.94	0.38	0.146	38.25	37.82	1.13
	3.46	0.58	0.222	38.49	37.72	2.02
	3.69	0.80	0.307	38.58	37.58	2.63
	3.78	0.98	0.375	38.67	37.39	3.36
	3.83	1.15	0.441	38.78	37.19	4.18
	3.87	1.64	0.628	39.37	36.5	7.54
	3.88	2.00	0.766	39.94	35.76	10.98
	9.91	2.28	0.874	40.53	34.86	14.90
BS7	6.24	0.31	0.341	58.38	56.00	4.16
	6.86	0.46	0.505	59.23	55.04	7.33
	7.06	0.57	0.626	59.78	54.42	9.38
	7.20	0.73	0.802	60.77	53.15	13.33
BS8	2.10	0.03	0.058	76.04	75.73	0.41
	6.84	0.13	0.250	76.12	74.34	2.34
	8.56	0.17	0.327	76.53	73.63	3.82
	11.07	0.32	0.615	78.37	72.00	8.39

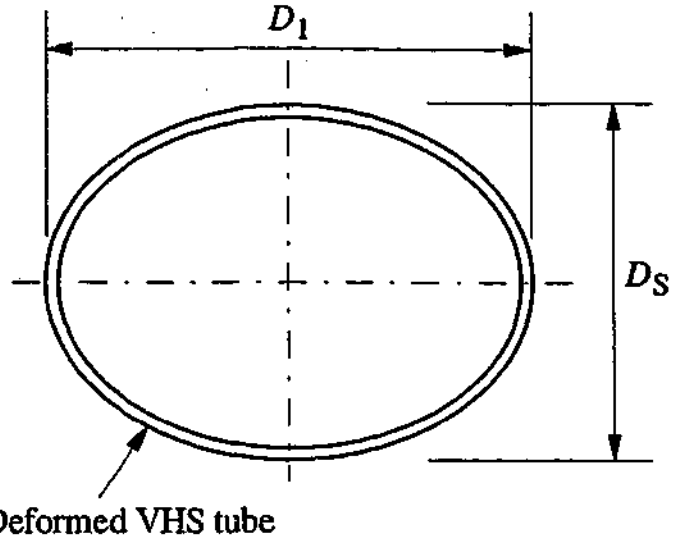

Figure 8.5-1: Measurement of ovalisation of VHS tube

A numerical analysis was conducted using Ades's plastic ovalisation theory to predict the ovalisation of VHS tubes. Three assumptions were made by Ades (1957). They are:

- The ovalled shape was assumed to be elliptical;
- The circumference remained the same for the ellipse and the initial circular cross section;
- The material is isotropic with the same stress-strain curves in tension and compression.

Detailed formulae of Ades's theory and a computer program written by the candidate in Java language to perform the analysis can be found in Appendix E of this thesis. A comparison between the experimental results and the analytical results is shown in Figure 8.5-2.

It can be seen from Figure 8.5-2 that the ovalisation calculated from the analytical model does not reflect VHS tube's actual ovalisation when κ/κ_u is greater than 0.3. This may be due to the elliptical assumption in Ades' ovalisation theory is not suitable for VHS tubes. In order to simulate the ovalisation of VHS tubes in bending tests, a new model needs to be developed.

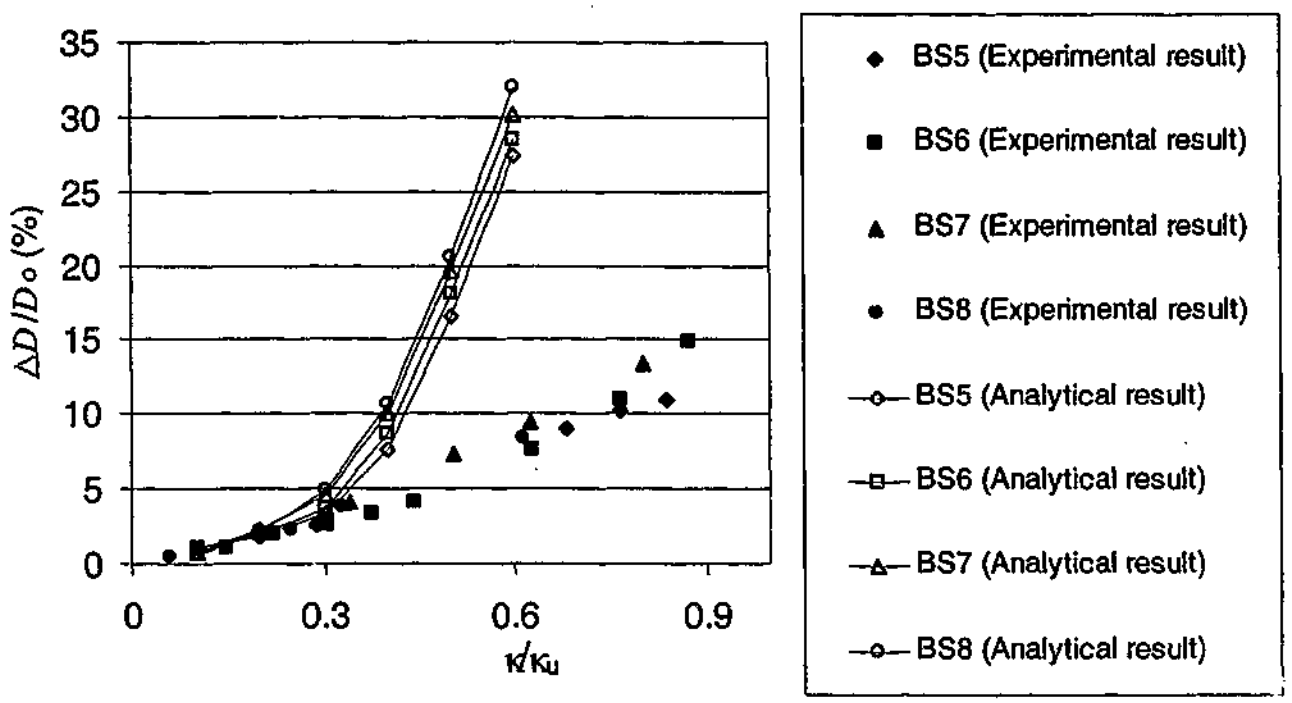

Figure 8.5-2: Comparison of ovalisation between experimental and analytical results

8.6 POST WELD HEAT TREATMENT OF VHS TUBES

8.6.1 General

It has been described in Chapter 6 that the strength loss in HAZ of welded VHS tubes is due to the microstructure change of the steel during fusion weld. Olabi and Hashmi (1995) studied the influence of post-weld-heat-treatment (PWHT) on steel properties. They found that PWHT could improve steel toughness by about 15%. The residual stress was also reduced by about 70% for welded box-sections. The microstructure of the steel changes again during PWHT process (Olabi and Hashmi 1996). Therefore, it might be possible to improve the connection strength by applying PWHT on welded VHS tubes.

8.6.2 Initial Work

A trial test was conducted on two butt-welded VHS tubes. Two soaking temperatures, 650°C and 950°C were chosen for the PWHT. The temperature of 950°C is the same as that used in manufacturing VHS tubes. The temperature of 650°C was chosen to see what would happen if a lower soaking temperature was used. During PWHT, the whole specimens were put in an oven. Firstly, the temperature in the oven was elevated to the soaking degree and keep for 10 minutes. Then the tubes were put in cold water for quenching. In the tempering process, the temperature of the tubes was elevated to 230°C and kept for 15 minutes, then let them cool down in room temperature.

Tensile tests of butt-welded VHS tubes with PWHT were conducted in a Baldwin testing machine. Two LVDTs were used to measure the displacement between the welds. The specimen dimensions and test results are shown in Table 8.6-1. The letter (P) in a label refers to PWHT, followed by specimen number (S1 to S11). Steel plugs were put in both ends of each tube to enable the tube to be gripped. The symbols D, t, and A are the diameter, wall thickness and cross-section area of specimens; P_{max} is the ultimate load; f_{up} refers to the tensile strength of VHS tubes after PWHT; f_u is the tensile strength of VHS tubes; f_y is the yield stress of VHS tubes. A value of 1505MPa and 1349MPa is used for f_u and f_y in Table 8.6-1.

Table 8.6-1: Test results of VHS tubes with PWHT

Label	D (mm)	t (mm)	A (mm^2)	P_{max} (kN)	f_{up} (MPa)	f_{up}/f_u	f_{up}/f_y	Soaking temperature (°C)	Weld Type
PS1	38.10	1.61	184.57	82.8	449	0.30	0.33	650	Butt weld
PS2	38.20	1.63	187.01	246.9	1320	0.88	0.98	950	Butt weld

Different failure modes were observed for butt-welded VHS tubes with different PWHT soaking temperatures as shown in Figure 8.6-1.

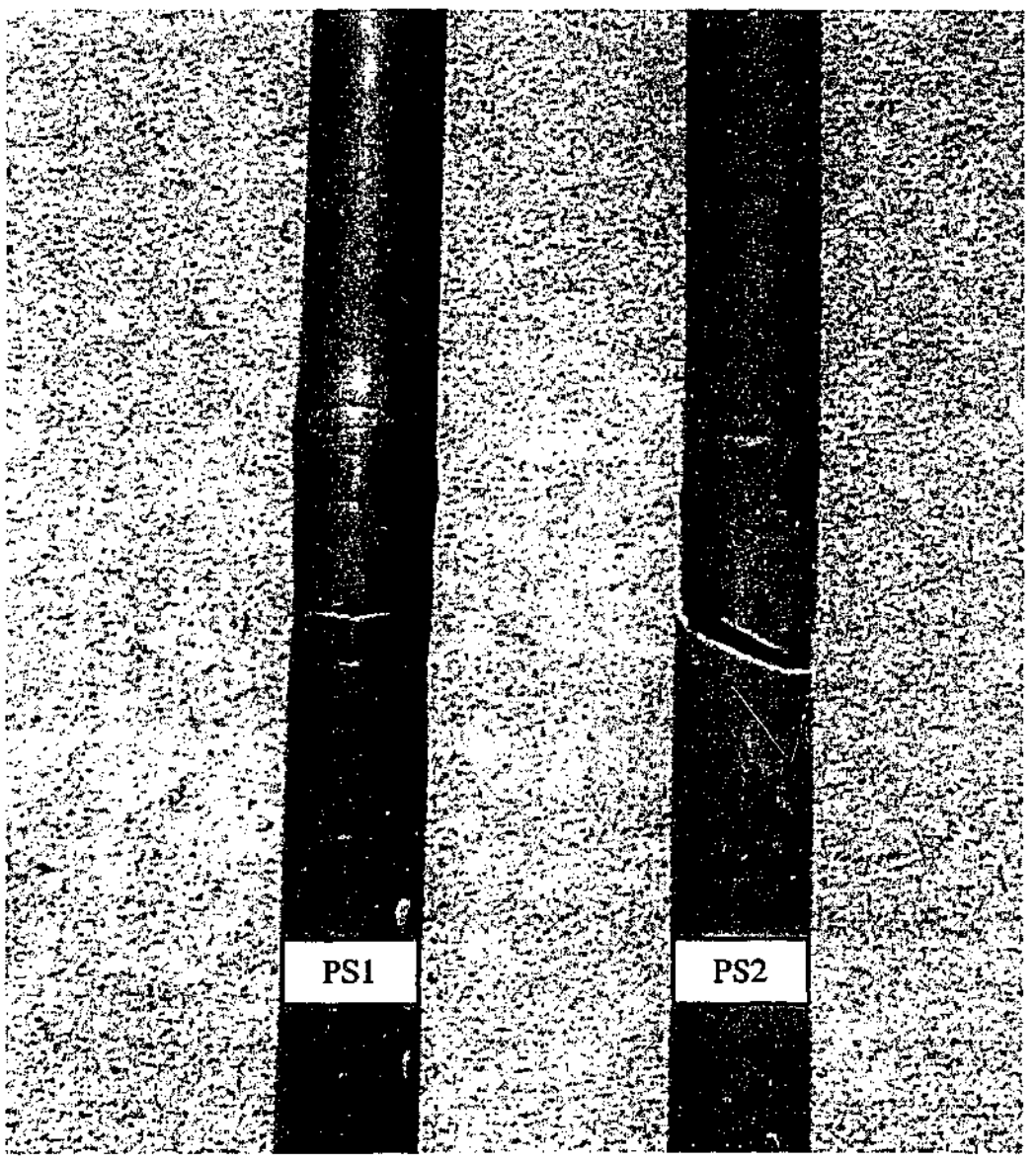

Figure 8.6-1: Failure mode of butt-welded VHS tubes with PWHT

Unlike the failure mode of butt-welded VHS tubes that failed in HAZ, both specimens failed in the section away from HAZ. Specimen PS1, that was heat treated with the soaking temperature of 650°C, failed similar to the non-heat-treated tubes described in Chapter 3. Multiple necking and cracks appeared on the seam weld. A tensile strength of 449MPa was obtained. However specimen PS2, that was heat treated with the soaking temperature of 950°C, failed similar to VHS members. Shear band failure mode was observed. An ultimate tensile strength of 1320MPa was obtained for specimen PS2, which is much higher than the strength of 737MPa in HAZ obtained in Chapter 6. It seems that the full yielding of VHS tubes can be recovered by using PWHT technique.

8.6.3 Summary and Suggested Future Work

An attempt was made to use the PWHT method to strengthen the load carrying capacity of butt-welded VHS tubes. Two soaking temperatures of 650°C and 950°C were chosen in the PWHT process. Different failure modes were observed for tubes heat treated with different soaking temperatures. The connection strength of butt-welded VHS tubes was significantly increased by PWHT with the soaking temperature of 950°C.

The increase in strength may accompany the loss in ductility. Therefore it is necessary to study the material ductility of VHS tubes after PWHT. Expressions need to be established between the soaking temperature used in PWHT and material ductility.

It should be noted that the PWHT method described above was a kind of complete treatment, i.e. the whole specimen was put in an oven for PWHT. This kind of PWHT method is not suitable for large-scale engineering structures. It is necessary to study a partial PWHT method, i.e. instead of heat-treating the whole specimen, applying PWHT to HAZ areas only.

8.7 SHEAR STRESS DISTRIBUTION IN CFRP STRENGTHENED BUTT-WELDED VHS TUBES

8.7.1 Initial Experimental Work

It was demonstrated in Chapter 7 that CFRP-epoxy system could be used in strengthening butt-welded VHS tubes. The yield capacity of VHS tubes was recovered when four layers of CFRP were applied with the effective bond length. The definition of effective bond length was established based on the experimental results. To further study the phenomenon of effective bond length, more research may be needed on the load transfer mechanism between CFRP and VHS tubes.

Miller et al. (2001) studied CFRP strengthened steel bridge girders. Strain gauges were mounted on top of the CFRP plates. They found that about 98% of the total force transfer occurred within the first 100mm from the end of the CFRP plate.

A trial test was conducted in this study to measure the shear stress distribution on CFRP strengthened VHS tubes. A notch with the length of 120mm and the width of 25mm was cut at the end of one tube before welding. Then the tube was butt-welded by the same welding procedures described in Chapter 6. Five strain gauges were mounted on the inside surface of a VHS tube, with four strain gauges in the CFRP bond area and one mounted outside the bonding area where there was no effect of epoxy shear strain. The specimen is illustrated in Figure 8.7-1. All strain gauges were mounted after two tubes were butt-welded and CFRP strengthened. The failed specimen was shown in Figure 8.7-2. By comparing the strains measured from the two positions (within and outside the bond area), the epoxy lap shear strain (γ) can be calculated as:

$$\gamma = \varepsilon_s - \varepsilon_c \tag{8.7-1}$$

here, ε_c is the strain on VHS tube within the CFRP bonding area and ε_s is the strain on VHS tubes outside CFRP bonding as shown in Figure 8.7-2. The strains of ε_c and ε_s are measured at the same load level. The shear strains calculated from Eq. (8.7-1) from the position of HAZ to the end of bonded CFRP are shown in Figure 8.7-3. It

can be seen that γ is not uniform in the bond area. The shear stress increases from the end of CFRP to the direction of the HAZ. The value of γ becomes larger with the increase of the section stress level. The stress was calculated from the measured load and the cross-sectional area of tube A in notched area. The shear strain at the HAZ is complicated and cannot be calculated by Eq. (8.7-1).

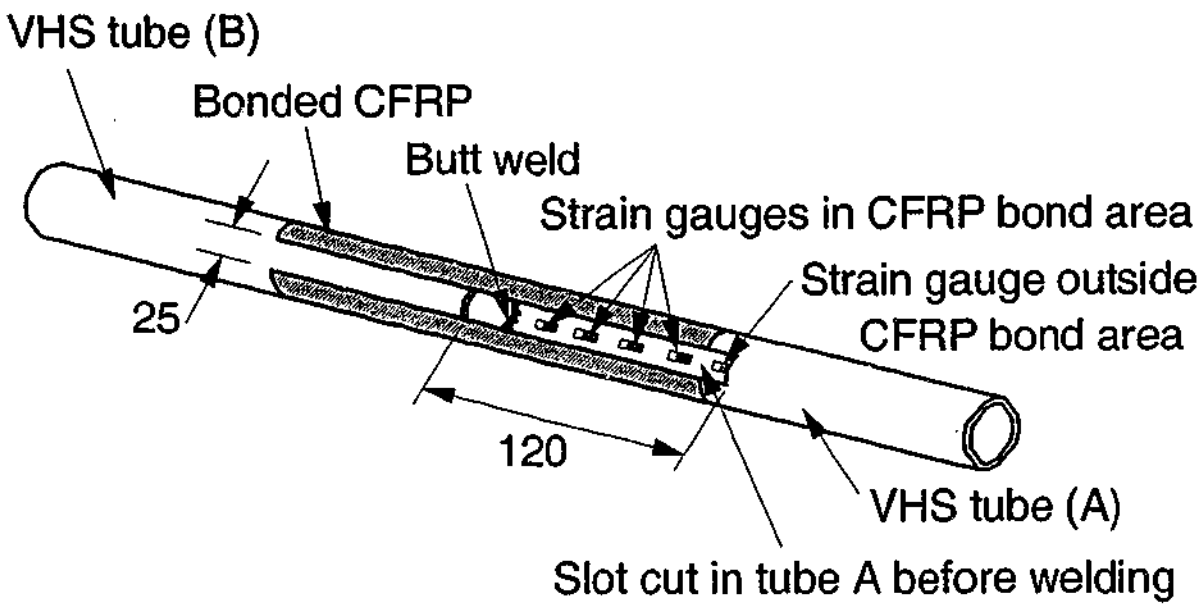

Figure 8.7-1: Strain gauges were mounted on the inside surface of VHS tube

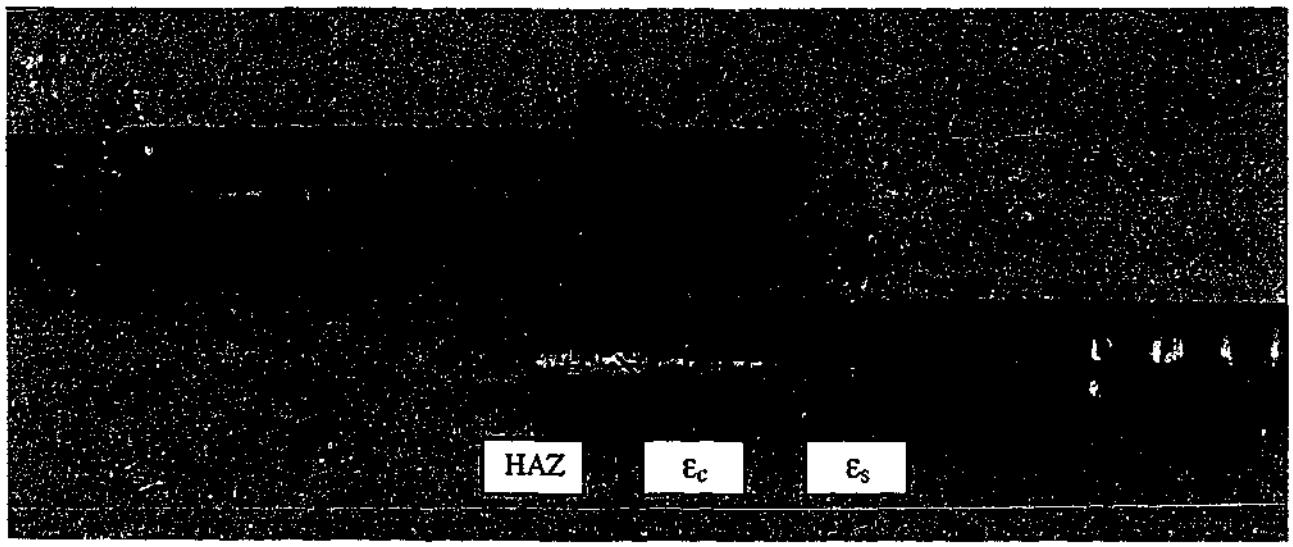

Figure 8.7-2: The failed specimen for the measurement of the shear strain

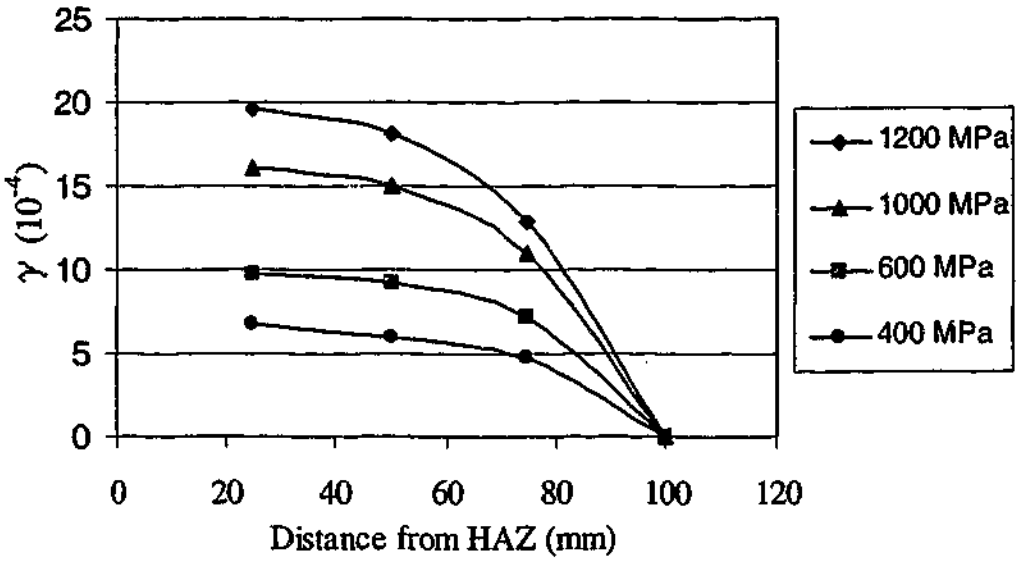

Figure 8.7-3: Lap shear strain distribution

8.7.2 Suggested Future Work

The effective CFRP bonding length and the optimal number of CFRP layers applied on VHS tubes are not fully investigated in this thesis. The effective bond length of 75mm described in Chapter 7 needs to be verified when different types of CFRP and epoxy are used, especially for high modulus CFRP (with Young's modulus over 600 MPa). More tests are needed for tubes with large diameter. More analytical work needs to be conducted on the load transfer mechanism within the CFRP bond area. The analytical model may include the material properties of VHS steel, HAZ, epoxy and CFRP.

In addition to the effect of materials, the preparation techniques may also affect the load carrying capacity of CFRP strengthened VHS tubes. The CFRP applying method used in this research and in some other studies (Tavakkolizadeh and Saadatmanesh 2003a; 2003b) was hand lay-up, i.e. steel specimens were coated with epoxy resin, then CFRP was laid onto the resin and pressed to force the air out. This process is repeated until desired number of plies of CFRP is added. This method may leave large amount of voids between CFRP and VHS tubes. As a result, the overall specimen

quality may not be in good consistency. Especially when the specimen surface is not flat, it may be impossible to use a roller to drive off the air. Some methods may be considered to improve the quality of applying technique. For instance, a vacuum bag may be used to compress the uncured composite, forcing out entrapped air and excessive resin (Moy 2001). The steel surface preparation and pretreatment is also important. It was pointed out that different effectiveness might be achieved if treating the steel surface by degreasing, degreasing and abrading, or degreasing and chemically pre-treating (Ciba Adhesives 2000).

The test results reported in Chapter 7 did not reflect the long-term effect – durability of CFRP strengthened steel structures. The galvanic corrosion between CFRP and steel may jeopardize the bonding strength. Studies showed that this problem existed when there was a direct contact between a CFRP laminate and steel substrate. The galvanic rate was related to the epoxy coating thickness (Tavakkolizadeh and Saadatmanesh 2001a). The influence of environmental effects, such as exposure to high moisture, humidity and high chloride content, or high temperature in a fire, may change the performance of CFRP bonded steel structures. These environmental factors may have detrimental effects on the bonding strength for some epoxy resins (Malvar et al. 2003). Therefore studies on the durability of CFRP strengthened VHS tubes may be carried out in the future.

8.8 SUMMARY

This Chapter reported some preliminary work on a number of issues that need to be further studied about VHS tubes. These issues include the shear band formation during tensile tests, finite element analysis of VHS tubes subjected to compression and bending, ovalisation of VHS tubes in bending, PWHT technique and some topics related to CFRP strengthening of welded VHS tubes. Suggestions were outlined at the end of each sub-section.

quality may not be in good consistency. Especially when the specimen surface is not flat, it may be impossible to use a roller to drive off the air. Some methods may be considered to improve the quality of applying technique. For instance, a vacuum bag may be used to compress the uncured composite, forcing out entrapped air and excessive resin (Moy 2001). The steel surface preparation and pretreatment is also important. It was pointed out that different effectiveness might be achieved if treating the steel surface by degreasing, degreasing and abrading, or degreasing and chemically pre-treating (Ciba Adhesives 2000).

The test results reported in Chapter 7 did not reflect the long-term effect – durability of CFRP strengthened steel structures. The galvanic corrosion between CFRP and steel may jeopardize the bonding strength. Studies showed that this problem existed when there was a direct contact between a CFRP laminate and steel substrate. The galvanic rate was related to the epoxy coating thickness (Tavakkolizadeh and Saadatmanesh 2001a). The influence of environmental effects, such as exposure to high moisture, humidity and high chloride content, or high temperature in a fire, may change the performance of CFRP bonded steel structures. These environmental factors may have detrimental effects on the bonding strength for some epoxy resins (Malvar et al. 2003). Therefore studies on the durability of CFRP strengthened VHS tubes may be carried out in the future.

8.8 SUMMARY

This Chapter reported some preliminary work on a number of issues that need to be further studied about VHS tubes. These issues include the shear band formation during tensile tests, finite element analysis of VHS tubes subjected to compression and bending, ovalisation of VHS tubes in bending, PWHT technique and some topics related to CFRP strengthening of welded VHS tubes. Suggestions were outlined at the end of each sub-section.

Chapter 9

CONCLUSIONS

9.1 GENERAL

This thesis has presented an investigation on strength, ductility, slenderness limit, residual stress and weldability of very high strength (VHS) circular steel tubes.

Currently, VHS tubes are not included in Australian steel design standards, since the strength of VHS tubes is about three times higher than most structural steel members. There is a concern about the material ductility of VHS tubes, since it is generally believed that the higher the strength the lower the ductility. The main aim of this project was to study the behaviour of VHS members and welded connections in order to assess the suitability and potential of VHS tubes to be used as structural steel hollow section members in buildings or temporary structures for emergency or military purpose.

Extensive experiments were conducted on VHS members, including tension, compression and bending tests. Investigations on butt-welded and transverse fillet welded VHS tubes were also carried out. The CFRP strengthening techniques were used to recover the strength loss in HAZ of butt-welded VHS tubes. Preliminary finite element analysis was conducted for VHS tubes in compression and in bending. A summary of the experimental work is outlined as follows.

- Seventeen coupons and seventeen full section VHS and NHT tubes were tested in tension. The material ductility was measured in terms of percentage elongation and the ultimate strength to yield strength ratio.
- Compression tests on ten stub columns were performed. The out of straightness of these specimens was measured. The residual stresses in longitudinal and

transverse directions of VHS and NHT tubes were investigated by the slicing method.

- Bending tests on twelve VHS tubes were carried out in a 4-point-bending and a pure bending rig. New slenderness limits were proposed.
- Tension tests on 12 butt-welded and 10 transverse fillet welded VHS tubes were performed. Strength reduction factors on HAZ were proposed based on the design rules in Australian and American standards.
- Seventeen CFRP bonded un-welded VHS specimens and twenty-one CFRP strengthened butt-welded VHS tubes were tested in tension, in order to recover the strength loss in HAZ.

The main conclusions of this thesis are:

- VHS tubes satisfy the ductility requirements specified in AS/NZS4600 for thin-walled hollow sections in terms of percentage elongation and the ultimate strength to yield stress ratio.
- VHS tubes have prospective potential to be used as structural steel hollow section members. Different slenderness limits from those specified in current design codes need to be applied for VHS tubes subjected to compression and bending.
- VHS tubes can be connected by welding method. However a strength reduction factor needs to be applied when using the design rules in current steel design standards.

Detailed observations and conclusions obtained from each individual Chapter are summarized in the following sub-sections.

9.2 DEVELOPMENT OF HIGH STRENGTH STEELS

The development history and application of high strength steels were briefly reviewed. The strength of plain carbon steels can be increased up to around 500 MPa. Further increase in strength for carbon steel is limited by the low ductility caused by high carbon content. Adding small addition of alloy elements can increases the strength of steel. However, heat treating steel elements is a common practice to raise the strength of steels with optimum ductility.

About the application of high strength steels, the following conclusions were obtained from the literature review:

- There is an increasing need to use high strength steels in the automotive industry and in other engineering applications around the world.
- Some problems may exist in the application of high strength steels, including low material ductility and HAZ softening in welded connections.
- Some strengthening techniques, such as CFRP strengthening system, could be used to recover the strength loss in HAZ.
- Currently, no steel design standard is applicable for design of structural elements with a yield stress over 800 MPa. The very high strength (VHS) circular steel tubes have a yield stress about 1350 MPa and an ultimate tensile strength about 1500 MPa. Therefore VHS steel tubes need to be studied thoroughly in order to examine if they could be used as structural elements.

9.3 VHS TUBES IN TENSION

Material ductility of VHS tubes was investigated through coupon and full section tensile tests. The ductility of VHS tubes was expressed in terms of percentage elongation and the ultimate strength to yield stress ratio, since these two parameters has been well established during the last century and adopted as ductility parameters by many steel design standards. The main observation and conclusions obtained from the tension tests are:

- An oblique shear band was observed on VHS coupons, whereas multiple shear bands appeared on full section VHS tubes. The same shear band angle was obtained in both tests.
- For cold-formed steel hollow sections and sheet steels, the ultimate strength to yield stress ratios decreases as the yield stress increases. The ratio approaches 1.0 when the yield stress reaches around 550 MPa. However, the heat-treated steels including VHS tubes do not follow the trend. Ratios of 1.113 and 1.119 were obtained for VHS coupons and full section tubes. Both ratios are larger than the requirement of 1.08 specified in AS/NZS4600. The NHT tubes also satisfied this requirement with ratios being 1.16 and 1.09 for coupons and full section tubes.
- The average elongation on 50mm gauge length for VHS coupons is 7.32% which is slightly lower than the minimum requirement of 10% in AS/NZS4600. However, the average elongation on 50mm gauge length for VHS full section tubes is 10.96% which satisfies this requirement. The NHT tubes also satisfied this requirement with e_{50} being 26.9% for coupons and 13% to 27% for full sections.
- The very low P_f/P_{max} ratio for NHT tubes seems to match their failure mode of necking gradually, whereas the very high P_f/P_{max} ratio for VHS tubes seems to match their failure mode of oblique shear band occurred suddenly.
- The ultimate to yield strain ratio for VHS tubes is much smaller than that for NHT tubes, although the ultimate strength to yield stress ratio is very much the same for the two kinds of tubes.

9.4 VHS TUBES IN COMPRESSION

The section capacity of VHS tubes in compression was investigated through stub column tests. The column behaviour that may consist of overall buckling for long columns is not studied in this thesis. The conclusions obtained from the compression tests are:

- The ratio of the maximum measured wall imperfection to the gauge length specified in ECCS (1988), (μ/L_t), is about 10 times less than the tolerance of 0.01 specified in ECCS (1988). This is expected since the *D/t* ratios of VHS tubes are relatively small (ranging from 24 to 47).
- The residual stress of VHS tubes is about 4% of the yield stress with the outside surface in compression and the inside surface in tension. This is true for both longitudinal and transverse directions.
- The residual stress of NHT tubes is about 50% of the yield stress along the longitudinal direction and 20% of the yield stress along the transverse direction. The residual stress is always compressive on the inside surface and tensile on the outside surface.
- The failure mode of VHS stub columns is a ring-like bulge (elephant's foot), followed by a diamond shape buckling for *D/t* reaching 47.
- A yield slenderness limit of 258 and non-dimensional local buckling parameter limit of 3.1 for VHS tubes are proposed based on the test results in Chapter 4 and the test results provided by Zhao (2000). It seems that the yield slenderness limit may be affected by the manufacturing process as well as by the yield stress of the tube.
- More research is needed to determine λ_{ey} for CHS produced using different manufacturing process and with yield stress ranging from 450MPa to 1350MPa, or alternatively to keep λ_{ey} as a constant (e.g. 82) but derive a new expression of element slenderness λ_e which has a new material parameter rather than that (f_y/250) used in Eq. (4.1-1).

9.5 VHS TUBES IN BENDING

VHS tubes did not show the wave-like multiple ripples that were found on may circular tubes in pure bending. Only one inward indentation was observed when a VHS tube loses stability in bending. Other conclusions for VHS tubes in bending are:

- Full plastic moment capacity M_p can be reached for VHS tubes with the section slenderness up to 198.
- New plastic slenderness limits of 117 and 153 are proposed based on a rotation capacities requirement of R=4 and R=3. Large deflection was observed when reaching these limits. The deflection may exceed the Serviceability Limit State Specification in building design standards. However, such deflection may be allowed in temporary structures for the purpose of emergency or in military applications. More tests are needed on CHS with yield stress between 450MPa and 1350MPa to investigate the effect of yield stress on the plastic slenderness limit of high strength CHS.
- A yield slenderness limit of 264 was proposed for VHS tubes in bending. A higher value of yield slenderness is found for CHS in bending than for axial compression in most standards.

9.6 BUTT-WELDED AND FILLET WELDED VHS TUBES

The connection strength of butt-welded and transverse fillet welded VHS tubes was investigated. GTAW welding method (GAS Tungsten Arc Welding) was used in welding VHS tubes. The following conclusions show that VHS tubes can be welded by fusion welding method, although strength reduction is found in HAZ.

- Under tension, the complete penetration butt-welded VHS tubes failed in the HAZ of the base metal. The same failure was observed for VHS tubes fillet-welded to a plate along its whole perimeter. There is a significant strength reduction in HAZ. The strength in HAZ is about half of the strength in VHS base metal.
- The complete penetration butt-welded VHS tubes may be designed in accordance with the tension member rule in AS4100 (SAA 1998), AS/NZS4600 (SAA 1996), AISI specification (AISI 2001) and AISC specification (AISC 2000) with an appropriate reduction factor ranging from 0.53 to 0.60 on f_u or f_y.
- VHS tubes fillet-welded to a steel plate along the whole perimeter of the VHS tubes may be designed in accordance with the tension member rule in AS4100 (SAA 1998), AS/NZS4600 (SAA 1996), AISI specification (AISI 2001) and AISC specification (AISC 2000) with an appropriate reduction factor ranging from 0.51 to 0.58 on f_u or f_y.
- For simplicity, a single reduction factor of 0.5 might be adopted conservatively for all standards mentioned above.
- It is suggested that the strength of the weld metal (f_{uw}) match the reduced strength of the based metal, i.e., f_{uw} should be equal to or greater than $0.5 f_u$.

9.7 CFRP STRENGTHENED BUTT-WELDED VHS TUBES

Unlike CFRP strengthened concrete structures that failure happened in concrete, CFRP strengthened VHS tubes failed either in the interface between CFRP and steel or in CFRP. The load carrying capacity is affected by the material properties of CFRP and epoxy resin. Based on the tests conducted in Chapter 7, the following conclusions were obtained:

- Significant strength increase was obtained for CFRP strengthened butt-welded VHS tubes. The connection strength was increased up to 200% with the CFRP-Araldite 420 strengthening system. The full yield capacity of VHS steel tubes was recovered.
- Different failure modes and connection strength were observed for tubes bonded with different epoxies. A suitable epoxy needs to be selected in order to avoid the fibre-tear failure mode. Araldite 420 was found suitable for the purpose of strengthening butt-welded VHS tubes.
- An effective bond length of 75mm for the Araldite 420 bonded CFRP system was found. No significant strength increase was observed when bond length exceeds 75mm.
- A minimum number of four layers of CFRP is recommended when strengthening butt-welded VHS tubes with Araldite 420.
- Future work is needed to investigate the effective bond length in terms of the tube diameter and the shear stress distribution within the bond region.

9.8 RECOMMENDED FUTURE WORK

The following research topics were recommended for further study of VHS tubes:

- Numerical simulation of the shear band formation using the plastic flow and bifurcation theory in solid mechanics.
- Finite element analysis of VHS tubes in compression and bending with the consideration of the residual stress and initial geometric imperfection.
- Numerical simulation of the ovalisation of VHS tubes in bending.
- Post-weld-heat-treatment of welded VHS tubes.
- The effective bond length of CFRP strengthened VHS tubes

REFERENCES

Ades, C. S. (1957) "Bending strength of tubing in the plastic range", *Journal of Aeronautical Sciences*, August: 605-610.

AISC (1999) "Load and resistance factor design specification for structural steel buildings", December 27, 1999, American Institute of Steel Construction, Chicago, Illinois, USA.

AISC (2000) "Load and resistance factor design specification for steel hollow structural sections", November 10, 2000, American Institute of Steel Construction, Chicago, Illinois, USA.

AISI (1996) "Specification for the design of cold-formed steel structural members", American Iron and Steel Institute, Washington, D.C., U.S.A.

AISI (2001) "North American specification for the design of cold-formed steel structural members", November 9, 2001, American Iron and Steel Institute, Washington, D.C., U.S.A.

Akselsen, O. M., Rorvik, G., Onsoien, M. I. and Grong, O. (1989) "Assessment and predictions of HAZ tensile properties of high-strength steels", *Welding Journal*, 68(9): 356s-362s.

Alikhail, M., Zhao, X. L., Koss, L., Grundy, P., Dagg, H. and Shield, A. (1998) "High strength steel RHS domestic flooring system". in *Tubular Structures VIII: Proceedings of the Eighth International Symposium on Tubular Structures*, Choo and Vegte (eds.), 625-634.

Allen, R., Bluff, K. and Oppenheim, B. (2000) "Software development 1", Swinburne University of Technology, Melbourne, Australia.

Anand, L. and Spitzig, W. A. (1980) "Initiation of localized Shear Bands in Plain Strain", *Journal of the Mechanics and Physics of Solids*, 28: 113-128.

Armitage, B. and Young, J. F. (1983). "High strength automotive tubing". *High Strength Steel for Automotive Use*: 93-101.

ASTM (1998) "Standard terminology relating to methods of mechanical testing", *ASTM Designation E6*: 17-27.

ASTM (1999a) "Standard test methods for tensile testing of metallic materials", *ASTM Designation: E8M-99*: 78-98.

ASTM (1999b) "Standard guide for use of adhesive-bonded single lap-joint specimen test results", *ASTM Designation D 4896-01*: 424-429.

ASTM (1999c) "Standard practice for classifying failure modes in fibre-reinforced plastic (FRP) joints", *ASTM Designation D 5573*: 476-478.

ASTM (2000a) "Standard specification for electric-resistance-welded carbon and alloy steel mechanical tubing", *ASTM Designation A513-00*: 370-385.

ASTM (2000b) "Standard specification for high-yield-strength, quenched and tempered alloy steel plate, suitable for welding", *ASTM Designation A514/a514M-00a*: 253-255.

ASTM (2001a) "Standard specification for carbon structural steel", *ASTM Designation A 36/A 36M-01*: 108-110.

ASTM (2001b) "Standard specification for carbon and high-strength low-alloy structural steel shapes, plates, and bars and quenched-and-tempered alloy structural steel plates for bridges", *ASTM Designation A709/A709M-01a*: 344-351.

ASTM (2001c) "Standard specification for steel, sheet, cold-rolled, carbon, structural, high-strength low-alloy and high-strength low-alloy with improved formability", *ASTM Designation A1008/A1008M-01a*: 538-544.

ASTM (2001d) "Standard specification for steel, sheet and strip, hot-rolled, carbon, structural, high-strength low-alloy and high-strength low-alloy with improved formability", *ASTM Designation A1011/A1011M-01a*: 547-552.

ASTM (2001e) "Standard test method for lap shear adhesion for fibre reinforced plastic (FRP) bonding", *ASTM Designation D 5868-01*: 518-519.

AWS (1996) "Low alloy steel electrodes for gas shielded metal arc welding, AWS A5.28", American Welding Society, Miami, Fla., USA.

AWS (2002) "Structural welding code--steel, AWS D1.1", American Welding Society, Miami, Fla., USA.

Barnes, F. J., Murai, T. and Nakagoshi, A. (1999) "The development and validation of composite structures for rail infrastructure rehabilitation". in *Railway Engineering Conference,* Commonwealth Institute, London, U. K.

Bassetti, A., Liechti, P. and Nussbaumer, A. (1998) "Fatigue resistance and repairs of riveted bridge members". in *Fatigue Design '98*, Espoo, Finland. 535-546.

Bassetti, A., Nussbaumer, A. and Hirt, M. A. (2000) "Crack repair and fatigue life extension of riveted bridge members using composite materials". in *Bridge Engineering Conference, ESE-IABSE-FBI*, Sharm El Sheikh, Egypt. 227-238.

Benham, P. P., Crawford, R. J. and Armstrong, C. G. (1996) "Mechanics of engineering materials", 2nd edition, Harlow, Longman.

BHP Steel (2002) "BHP steel - a strategic element of the automotive future", Submission to the Productivity Commission Review of Post-2005 Assistance Arrangements for the Australian Automotive Industry, BHP Steel Limited, Melbourne, Australia.

Bisalloy steels Pty. Ltd (2003). "Quenched and tempered steel plate". *Bisalloy Steel Catalogue*, Sydney, Australia.

Bradford, M. A., Loh, H. Y. and Uy, B. (2001) "Slenderness limits for CHS sections". in *Tubular Structures IX*, Puthli and Herion (eds.), 377-381.

Brazier, L. G. (1927) "On the flexure of thin cylindrical shells and other thin sections", *Proceedings of the Royal Society of London (serial A)*, 116(773): 104-114.

Brockenbrough, R. L. (1973) "Design trends for high-strength low-alloy steels". in *Processing and Properties of Low Carbon Steel*, Metallurgical society of AIME. 389-397.

BSI (2000) "Structural use of steelwork in building, Part 1", *British Standard BS5950*, London, U.K.

Calladine, C. R. (1983) "Plastic buckling of tubes in pure bending". in *Collapse: The Buckling of Structures in Theory and Practice*, London, Cambridge Univ Press, Cambridge, UK.

Calladine, C. R. (1995) "Understanding imperfection-sensitivity in the buckling of thin-walled shells", *Thin-Walled Structures*, 23(1-4): 215-235.

Cederquist, S. C. (1999) "Repairing America's deteriorating bridges", *Materials Performance*, 38(5): 20-25.

Chen, W. F. and Ross, D. A. (1977) "The axial strength and behaviour of cylindrical columns", *Journal of Petroleum Technology*,(March): 239-241.

Ciba Adhesives (2000) "Surface preparation and pretreatment of structural adhesives", Section III of Manuals-Surface Preparation and Pretreatments, Working Directions for Optimum Adhesion Between Structural Materials with Araldite Adhesives: 136-146.

Cimpoeru, S. J. (1992) "The modelling of the collapse during roll-over of bus frames consisting of square thin-walled tubes", *PhD Thesis*, Monash University, Melbourne, Australia.

Cullison, A. (1995) "Know your high-strength steel before welding", *Welding Journal*, 74(March): 20.

Dennis, W. E. (1983) "High strength sheet steels - applications, problems and potential". in *International Conference on Technology and Applications of HSLA Steels*, Philadelphia, USA.

Dhalla, A. K. and Winter, G. (1974a) "Suggested Steel Ductility Requirements", *Journal of The Structural Division, ASCE,* 100(ST2): 445-462.

Dhalla, A. K. and Winter, G. (1974b) "Steel Ductility Measurements", *Journal of the Structural Division, ASCE* 100(ST2): 427-444.

Dieter, G. E. and Bacon, D. J. (1988) "Mechanical metallurgy", SI metric /, *McGraw-Hill Series in Materials Science and Engineering*, London ; Singapore, McGraw-Hill.

Donnell, L. H. and Wan, C. C. (1950) "Effect of imperfections on buckling of thin cylinders and columns under axial compression", *Journal of Applied Mechanics*, 17(1): 73-79.

Dowling, P. J., Harding, J. E. and Bjorhovde, R. (1992) "Constructional steel design : an international guide", London, New York, Elsevier Applied Science.

ECCS (1988) "Buckling of steel shells: European recommendations, 4th edition." *European Convention for Constructional Steelwork,* Brusels.

Elchalakani, M., Zhao, X. L. and Grzebieta, R. H. (2001a) "Plastic slenderness limits for cold-formed circular hollow sections", *Australian Journal of Structural Engineering*, 3(3): 127-141.

Elchalakani, M., Zhao, X. L. and Grzebieta, R. H. (2001b) "Concrete-filled circular steel tubes subjected to pure bending", *Journal of Constructional Steel Research*, 57(11): 1141-1168.

Elchalakani, M., Zhao, X. L. and Grzebieta, R. H. (2002a) "Bending tests to determine slenderness limits for cold-formed circular hollow sections", *Journal of Constructional Steel Research*, 58(11): 1407-1430.

Elchalakani, M., Zhao, X. L. and Grzebieta, R. H. (2002b) "Plastic mechanism analysis of circular tubes under pure bending", *International Journal of Mechanical Sciences*, 44(6): 1117-1143.

Ellingwood, B. and et al. (1980). "Development of a probability based load criterion for American National Standards A58". *National Code Requirements for Minimum Design Loads in Building and Other Structures*. NBS Spec. Pub. No. 577, National Bureau of Standards, Washington, DC, USA.

Eurocode 3 (2002) "Design of steel structures-Part 1.1: General rules, prEN 1993-1-1: 1 May 2002", London, UK.

Fletcher, E. E. (1979) "High-strength, low-alloy steels : status, selection, and physical metallurgy", Metals and Ceramics Information Center (U.S.), Columbus, Ohio, USA, Battelle Press.

Funderburk, R. (2001) "Selecting filler metals: matching strength criteria", Research, Education, Technical Support & Information. Welding Technology Institute of Australia, Sydney, Australia.

G+D Computing (2002) "Using strand7: Introduction to the Strand7 finite element analysis system", Sydney, Australia.

Galambos, T. V. (1995) "Public safety - is it compromised by new LRFD design standards?" *Journal of Structural Engineering, ASCE*, 121(1): 142-144.

Gellert, W., Kustner, H., Hellwich, M. and Kastner, H. (1977) "The VNR concise encyclopedia of mathematics", New York, Van Nostrand Reinhold Co.

Gere, J. M. and Timoshenko, S. (1999) "Mechanics of materials", 4th SI Edition, Cheltenham, Stanley Thornes.

Gillett, H. W. (1940) "The limited significance of the ductility features of the tension test". in *Symposium on Significance of the Tension Test*, Atlantic, N. J., American Society for Testing Materials. 551-578.

Hasan, S. W. and Hancock, G. J. (1989) "Plastic bending tests of cold-formed rectangular hollow sections", *Journal of the Australian Institute of Steel Construction*, 23(4): 2-19.

Hatherly, M. and Malin, A. S. (1984) "Shear bands in deformed metals", *Scripta Metallurgica*, 18: 449-454.

High Strength Steel Task Force (1994) "The right time for the right material", An Update on Cost - Effective Weight Reduction Opportunities Bulletin, Auto/Steel Partnership, 10.

High Strength Steel Task Force (1995) "High strength steel usage reaches new heights on the wings of Ford Windstar", *An Update On Cost - Effective Weight Reduction Opportunities Bulletin, Auto/Steel Partnership*, 11.

Hill, R. (1958) "A general theory of uniqueness and stability in elastic-plastic solids", *Journal of the Mechanics and Physics of Solids*, 6: 236-249.

Hill, R. (1998) "The mathematical theory of plasticity", *Oxford Engineering Science*, Oxford, New York.

Hill, R. and Hutchinson, J. W. (1975) "Bifurcation Phenomena in the Plane tension test", *Journal of the Mechanics and Physics of Solids*, 23: 239-264.

Honeycombe, R. W. K. and Bhadeshia, H. K. D. H. (1995) "Steels: microstructure and properties", 2nd Edition, *Metallurgy and Materials Science*, London ; New York, Edward Arnold.

Huber, A. W. and Beedle, L. S. (1954) "Residual stress and the compressive strength of steel", *Welding Journal Research Supplement*, 33(12): 589-614.

ISO (1984) "ISO 2566/2 Steel-conversion of elongation values", *International Organization for Standardization.*

Jackson, K. J. (1962) "Low alloy ultra high strength steels : a review", Department of Supply Aeronautical Research Laboratories, Melbourne, Australia.

Jirsa, J. O., Fook-Hoy, L., Wilhoit, J. C. and Merwin, J. E. (1972) "Ovaling of pipelines under pure bending". in *Offshore Technology Conference*, Dallas, Texas, USA. 573-579.

Karbhari, V. M. and Shulley, S. B. (1995) "Use of composites for rehabilitation of steel structures - determination of bond durability", *Journal of Materials in Civil Engineering*, November: 239-245.

Kashima, T., Tanaka, Y., Watanabe, K., Shirasawa, H., Miyahara, M. and Sawaki, S. (1992) "Development of door beam ERW tubing made of 1470N/mm^2 cold rolled high strength steel sheet", *SAE Technical Paper Series*,(920785): 1-6.

Kennedy, B. (1996) "Effect of holes on the ductility of Condeck HP and Bondek II", 4th Year Student Project, Department of Civil Engineering, Monash University, Melbourne, Australia.

Key, P. W. and Hancock, G. J. (1985) "An experimental investigation of the column behaviour of cold formed square hollow sections", Research Report - R493, School of Civil and Mining Engineering, University of Sydney, Sydney, Australia.

Korchynsky, M. (1984) "High strength low alloy steels", *SEAISI Quarterly*, January: 63-69.

Korol, R. M. and Hudoba, J. (1972) "Plastic behaviour of hollow structural sections", *Journal of the Structural Division, ASCE*, 98(5): 1007-1023.

Kuhlmann, U. (1989) "Definition of flange slenderness limits on the basis of rotation capacity values", *Journal of Constructional Steel Research*, 14(1): 21-40.

Kusnierz, J. (1994) "State of stress and strain in cold-rolled metal and the localization of strain in shear bands", *Scripta Metallurgica et Materialia*, 30(4): 405-410.

Kyriakides, S. and Ju, G. T. (1992) "Bifurcation and localization instabilities in cylindrical shells under bending. I. Experiments", *International Journal of Solids & Structures*, 29(9): 1117-1142.

Kyuba, H., Fukuda, Y. and Miki, C. (2001) "Strength matching of butt-welded joint under cyclic loading". in *First International Conference on Steel & Composite Structures*, Pusan, Korea. 261-266.

Lankford, W. T., Samways, N. L., Craven, R. F. and Mcgannon, H. E. (1985) "The making, shaping, and treating of steel", 10th Edition, Association of Iron and Steel Engineers, Pittsburgh, Pennsylvania, USA,.

Lee, K. L., Pan, W. F. and Kuo, J. N. (2001) "The influence of the diameter-to-thickness ratio on the stability of circular tubes under cyclic bending", *International Journal of Solids & Structures*, 38(14): 2401-2413.

Leeming, M. B. and Hollaway, L. (1999) "Strengthening of reinforced concrete structures: using externally-bonded FRP composites in structural and civil engineering", Cambridge, UK., Boca Raton, Calif., USA., Woodhead Pub.

Li, T. Q., Choo, B. S. and Nethercot, D. A. (1995) "Determination of rotation capacity requirements for steel and composite beams", *Journal of Constructional Steel Research*, 32(3): 303-332.

Ling, T. W., Zhao, X. L. and Al-Mahaidi, R. (2002) "Test and design of longitudinal fillet welds in very high strength (VHS) steel circular tubes". in *Advances in Steel Structures*, S. L. Chan, J. G. Teng and K. F. e. Chung (eds.), Elsevier, Oxford. 245-252.

Maddin, R. (1992). "A history of martensite: some thoughts on the early hardening of iron". *Martensite*, G. B. Olson and W. S. Owen (eds.): 11-19.

Malvar, L. J., Joshi, N. R., Beran, J. A. and Novinson, T. (2003) "Environmental effects on the short-term bond of carbon fibre-reinforced polymer (CFRP) composites", *Journal of Composites for construction*, 7(1): 58-63.

Mamalis, A. G. and Johnson, W. (1983) "Quasi-static crumpling of thin-walled circular cylinders and frusta under axial compression", *International Journal of Mechanical Sciences*, 25(9-10): 713-732.

Martukanitz, R., Wilson, A. L. and Howell, P. R. (2000) "Loss of strength within the heat affected zone of Al-Cu and Al-Cu-Li alloys", *Materials Science Forum*, 331(II): 1291-1296.

Mashiri, F. R., Zhao, X. L., Grundy, P. and Tong, L. W. (2001) "Fatigue of welded connections in high strength cold-formed SHS (t<4 mm), CIDECT Project Final Report No. 7T-8/01", Department of Civil Engineering, Monash University, Melbourne, Australia.

Mathew, M. D., Mannan, S. L. and Rodriguez, P. (1985) "Influence of gage dimensions on elongation values for type 316 stainless steel", *Journal of Testing and Evaluation*, 13(3): 191-195.

Matsuoka, T., Takahashi, M., Nozaki, N. and Okada, Y. (1979). "Development of quenched and tempered 760 MPa grade steel sheets with superior bendability". *Formable HSLA and Dual-Phase Steels: Proceedings of a Symposium,* A. T. Davenport (ed.), Metallurgical Society of AIME, Ferrous Metallurgy Committee., New York: 229-244.

Mazhar, A. A., Khokhar, E. A. and Khan, A. Q. (1988) "Effect of strain rate on tensile deformation and fracture behaviour of 18%Ni 300 maraging steel sheet", *Materials Science and Technology*, 4(6): 535-9.

Mertz, D. and Gillespie, J. (1996) "Rehabilitation of steel bridge girders through the application of advanced composite material", *Report No. NCHRP 931-1D11,* Transportation Research Board, Washington, DC, USA: 1-20.

Miller, T. C., Chajes, M. J., Mertz, D. R. and Hastings, J. N. (2001) "Strengthening of a steel bridge girder using CFRP plates", *Journal of Bridge Engineering, ASCE*, 6(6): 514-522.

Moriarty, J. and Barnes, F. (1998) "The use of carbon fibre composites in the London underground limited civil infrastructure rehabilitation program", *SAMPE Journal*, 34(2): 23-28.

Moy, S. S. J. (2001) "FRP composites: life extension and strengthening of metallic structures", *ICE Design and Practice Guides*, London, Thomas Telford.

Munz, D. and Mattheck, C. (1982) "Cross-sectional flattening of pipes subjected to bending", *International Journal of Pressure Vessels and Piping*, 10(6): 421-429.

Nagata, M. (2001) "Latest steel products for building construction", *Steel Today and Tomorrow, News of Japanese Steel*, November(156): 5-9.

Needleman, A. and Tvergaard, V. (1992) "Analyses of plastic flow localization in metals", *Applied Mechanics Reviews*, 45(3): S3-S15.

Okazawa, S. and Usami, T. (2000) "Plastic instability simulation of steel in tension". in *Structural Failure and Plasticity (IMPLAST 2000)*, X. L. Zhao and R. H. Grzebieta (eds.), Melbourne, Australia, Elsevier Science Ltd. 775-780.

Olabi, A. G. and Hashmi, M. S. J. (1995) "Effect of post-weld heat-treatment on mechanical properties and residual-stresses mapping in welded structural steel", *Journal of Materials Processing Technology*, 55(2): 117-122.

Olabi, A. G. and Hashmi, M. S. J. (1996) "The microstructure and mechanical properties of low carbon steel welded components after the application of PWHTS", *Journal of Materials Processing Technology*, 56(1-4): 88-97.

Oliver, D. A. (1928) "proposed new criteria of ductility from a new law connecting the percentage elongation with size of test piece", *Inst. of Mech. Engrs., Proc.*, 4: 827-864.

Ooyen, K. V. (2002) "HPS success", Modern Steel Construction, American Iron and Steel Construction, September, USA.

Osgood, W. R. (1951) "The efffect of residual stress in column strength", U.S. National Congress of Applied Mechnics, 1: 415.

O'Shea, M. D. and Bridge, R. Q. (1997) "Local buckling of thin-walled circular steel sections with or without internal restraint", *Journal of Constructional Steel Research*, 41(2-3): 137-157.

Pan, W. F. and Hsu, C. M. (1998) "An experimental study of viscoplasticity-creep interaction of thin-walled tubes under pure bending". in *Thin-Walled Structures: Research and Development: Second International Conference on Thin-Walled Structures,* N. E. Shanmugam, J. Y. R. Liew and V. e. Thevendran (eds.), Elsevier. 689-696.

Pan, W. F., Wang, T. R. and Hsu, C. M. (1998) "A curvature-ovalization measurement apparatus for circular tubes under cyclic bending", *Experimental Mechanics*, 38(2): 99-102.

Pearce, R. and Painter, M. J. (1977). "The future of high strength steel sheet". *Low Carbon Structural Steels for the Eighties, Spring Residential Conference; Series 3, No. 6*, Institution of Metallurgists, London: IV15-17.

Prion, H. G. L. and Birkemoe, P. C. (1992) "Beam-column behaviour of fabricated steel tubular members", *Journal of Structural Engineering, ASCE*, 118(5): 1213-1232.

Ramberg, W. and Osgood, W. R. (1943) "Description of stress strain curves by three parameters", *Nat. Advisory Com. for Aeronautics, Tech. Note No. 902,* Washington, DC., USA.

Rasmussen, K. J. R. and Hancock, G. J. (1992) "Plate slenderness limits for high strength steel section", *Journal of Constructional Steel Research*, 23: 73-96.

Ravindra, M. K. and Galambos, T. V. (1978) "Load and resistance factor design for steel", *Journal of the Structural Division, ASCE*, 104(9): 1337-53.

Ray, S. K., Bhaduri, A. k. and Rodriguez, P. (1994) "New ductility parameters from the tensile test", *International Journal of Pressure Vessels & Piping*, 57(3): 331-333.

Reddy, B. D. (1979) "An experimental study of the plastic buckling of circular cylinders in pure bending", *International Journal of Solids & Structures*, 15: 669-683.

Rogers, C. A. and Hancock, G. J. (1997) "Ductility of G550 sheet steels in tension", *Journal of Structural Engineering, ASCE*, 123(12): 1586-1594.

Rogers, C. A. and Hancock, G. J. (2001) "Fracture toughness of G550 sheet steels subjected to tension", *Journal of Constructional Steel Research*, 57(1): 71-89.

Rotter, J. M. (1985) "Buckling of ground-supported cyclindrical steel bins under vertical compressive wall loads", *Metal Structures Conference,* Melbourne, Australia: 112-127.

Rotter, J. M. (1998a) "Development of proposed European design rules for buckling of axial compressed cylinders", *Advances in Structural Engineering-An International Journal*, 1(4): 273-286.

Rotter, J. M. (1998b) "Shell structures: The new European standard and current research needs", *Thin-Walled Structures*, 31(1-3): 3-23.

Runble, S. J. and Sparrow, J. G. (1985) "Review of ultrasonic velocity methods of determining residual stress", *Structural Technical Memorandum 416, DSTO,* Aeronautical Research Laboratories, Australia.

SAA (1991a) "Methods for tensile testing of metals", *Australian Standard AS1391*, Sydney, Australia.

SAA (1991b) "Structural steel hollow sections". *Australian Standard AS 1163.* Sydney, Australia.

SAA (1993a) "Structural and pressure vessel steel-Quenched and tempered plate", *Australian Standard AS 3597*, Sydney, Australia.

SAA (1993b) "Steel sheet and strip - Hot-dipped zinc-coated or aluminium/zinc-coated", *Australian Standard AS 1397*, Sydney, Australia.

SAA (1994) "Non-destructive testing, radiography of welded butt joints in metal", *Australian Standard AS2177.1*, Sydney, Australia.

SAA (1995) "Structural steel welding Part 4: welding of high strength quenched and temped steels", *Australian/New Zealand Standard AS/NZS1554.4*, Sydney, Australia.

SAA (1996) "Cold-formed steel structures", *Australian/New Zealand Standard AS/NZS4600*, Sydney, Australia.

SAA (1998) "Steel Structures", *Australian Standard AS 4100*, Sydney, Australia.

Schilling, C. G. (1965) "Buckling strength of circular tubes", *Journal of the Structural Division, ASCE*, 91(ST5): 325-348.

Sen, R., Liby, L. and Mullins, G. (2001) "Strengthening steel bridge sections using CFRP laminates", *Composites Part B: Engineering*, 32(4): 309-322.

Shah Khan, M. Z., Alkemade, S. J. and Weston, G. M. (1998) "Fracture studies on high hardness BISALLOY 500 steel", *Research Report; DSTO-RR-0130*, DSTO Aeronautical and Maritime Research Laboratory. Melbourne, Australia.

Sherman, D. R. (1969) "Residual stress measurement in tubular members", *Journal of the Structural Division, ASCE*, 95(ST4): 635-647.

Sherman, D. R. (1976) "Tests of circular steel tubes in bending", *Journal of the Structural Division, ASCE*, 102: 2181-2195.

Sherman, D. R. (1984) "Supplemental tests for bending capacity of fabricated pipes", Report, Dept. Civ.Eng. Uni. Wisconsini Milwaukee, USA.

Sherman, D. R. (1986). "Inelastic flexural buckling of cylinders". *Steel Structures: Recent Research Advances and Their Applications to Design*, M. e. Pavlovic (ed.): 339-357.

Sherman, D. R. (1992). "Tubular members". *Constructional Steel Design: An International Guide* P. J. Dowling, J. E. Harding and R. Bjorhovde (eds.), Elsevier Applied Science, London ; New York: 91-104.

Singer, J. and Abramovich, H. (1995) "Development of shell imperfection measurement techniques", *Thin-Walled Structures*, 23(1-4): 379-398.

Sivakumaran, K. S. and Yuan, B. (1998) "Slenderness limits and ductility of high strength steel sections", *Journal of Constructional Steel Research*, 46(1-3): 149-151.

Sperle, J. O. and Nilsson, T. (1992) "The application of high strength steels for fatigue loaded structures". in *HSLA Steels: Processing, Properties and Applications*, Tither, G. and Zhang, S. H. (eds.)., Beijing, China. 353-364.

Stephens, M., J., Kulak, G. L. and Montgomery, C. J. (1982) "Local buckling of thin-walled tubular steel members", *Structural Engineering Report*, Dept. Civ. Eng., Uni. of Alberta, 103.

Stranghoener, N. and Sedlacek, G. (1996) "Modelling of the rotation capacity of cold- and hot-formed SHS beams by a plastic collapse mechanism". in *Proceedings of the 6th International Offshore and Polar Engineering Conference*, Part 4 (of 4), Golden, CO, USA. 101-104.

Stranghoener, N., Sedlacek, G. and Boeraeve, P. (1994). "Rotation requirement and rotation capacity of rectangular, square and circular hollow section beams". *Tubular structures VI: Proceedings Sixth International Symposium on Tubular Structures*, P. Grundy, A. Holgate and B. Wong (eds.): 143-150.

Tanabe, H., Anai, I., Miyasaka, A. and Tanioka, S. (1995) "HAZ softening-resistant high-strength steel tubes for automobile propeller shafts", *Nippon Steel Technical Report*, 64: 62-68.

Tanabe, H., Miyasaka, A., Yamazaki, K., Iwasaki, T. and Akada, H. (1995) "High-strength steel tubes for automobile door impact beams", *Nippon Steel Technical Report*, 64: 55-61.

Tani, K., Matsumura, M., Kitada, T. and Hayashi, H. (2000) "Experimental study on seismic retrofitting method of steel bridge piers by using carbon fibre sheets". in *6th Korea-Japan Joint Seminar on Steel Bridges*, Tokyo, Japan. 437-445.

Tavakkolizadeh, M. and Saadatmanesh, H. (2001a) "Galvanic corrosion of carbon and steel in aggressive environments", *Journal of Composites for Construction*, 5(3): 200-210.

Tavakkolizadeh, M. and Saadatmanesh, H. (2001b) "Repair of cracked steel girder using CFRP sheet". *Proceedings of Creative Systems in Structural and Construction Engineering*. Honolulu, Hawaii, USA: 461-466.

Tavakkolizadeh, M. and Saadatmanesh, H. (2003a) "Strengthening of steel-concrete composite girders using carbon fibre reinforced polymers sheets", *Journal of Structural Engineering, ASCE*, 129(1): 30-40.

Tavakkolizadeh, M. and Saadatmanesh, H. (2003b) "Fatigue strength of steel girders strengthened with carbon fibre reinforced polymer patch", *Journal of Structural Engineering, ASCE*, 129(2): 186-196.

Tebedge, N., Alpsten, G. and Tall, L. (1973) "Residual-stress measurement by the sectioning method", *Experimental Mechanics*, 13(2): 88-96.

Teng, J. G., Chen, J. F., Smith, S. T. and Lam, L. (2002) "FRP strengthened RC structures", New York, Wiley.

Teoh, L. L. (1983) "Advances in low carbon high strength low alloy steels", *SEAISI Quarterly*, January: 71-81.

Tomita, Y. (1994) "Simulations of plastic instabilities in solid mechanics", *Applied Mechanics Reviews.*, 47(6): 171-205.

Tumialan, G., Nanni, A., Ibell, T. and Fukuyama, H. (2002) "FRP composites for strengthening civil infrastructure around the world", *SAMPE Journal*, 38(5): 9-15.

Tvergaard, V. (1999) "Studies of elastic-plastic instabilities", *Journal of Applied Mechanics*, 66(1): 3-9.

Tvergaard, V., Needleman, A. and Lo, K. K. (1981) "Flow localization in the plane strain tensile test", *Journal of the Mechanics and Physics of Solids*, 29(2): 115-142.

Unwin, W. C. (1903) "Influence of gauge length and section of test bar on the percentage of elongation", *Engineering Committee Report*, London, U.K., Crosby Lockwood and Son.

Unwin, W. C. (1910) "Testing of materials of construction", London, Longmans Green and Co.

Uwer, D. and Dibelmeyer, H. (1986) "New sights into the processing of high-strength water-quenched and tempered structural steel StE 890", *Schweissen und Schneiden*, 38(9): e138-e142.

Vuceric, M. (1987) "Some aspects of welding and weldability of QT-steel", *Zavarivanje (Zagreb)*, 30(3): 147-154.

Wierzbicki, T. and Sinmao, M. V. (1997) "A simplified model of Brazier effect in plastic bending of cylindrical tubes", *International Journal of Pressure Vessels and Piping*, 71(1): 19-28.

Wilhoit, J. C. and Merwin, J. E. (1971) "The effect of axial tension on moment carriing capacity of line pipe stressed beyond the elastic limit". in *3rd Offshore Technology Conference*, Houston. 293-296.

Wilkinson, T. and Hancock, G. J. (1998) "Tests to examine compact web slenderness of cold-formed RHS", *Journal of Structural Engineering, ASCE*, 124(10): 1166-1174.

WTIA (1996) "Welding & fabrication of quenched and tempered steel", *WTIA Technical Note; No. 15*, Welding Technology Institute of Australia, NSW, Australia.

WTIA (1998) "Commentary on the structural steel welding standard AS/NZS1554, TN11-98", Published Jointly by the Welding Technology of Australia and the Australian Institute of steel Construction, NSW, Australia.

Yang, D. and Hancock, G. J. (2002a) "Compression tests of cold-reduced high strength steel stub columns", *Research Report - R815*, School of Civil and Mining Engineering, University of Sydney, Sydney, Australia.

Yang, D. and Hancock, G. J. (2002b) "Compression tests of cold-reduced high strength steel long columns", *Research Report - R816*, School of Civil and Mining Engineering, University of Sydney, Sydney, Australia.

Yura, J. A., Galambos, T. V. and Ravindra, M. K. (1978) "The bending resistance of steel beams", *Journal of the Structural Division, ASCE*, 104(9): 1355-1370.

Zbib, H. M. and Jubran, J. S. (1992) "Dynamic shear banding: A three-dimensional analysis", *International Journal of Plasticity*, 8(6): 619-641.

Zhao, X. L. (2000) "Section capacity of very high strength (VHS) circular tubes under compression", *Thin-Walled Structures*, 37(3): 223-240.

Zhao, X. L., Al-Mahaidi, R. and Kiew, K.-P. (1999) "Longitudinal fillet welds in thin-walled C450 RHS members", *Journal of Structural Engineering, ASCE*, 125(8): 821-828.

Zhao, X. L. and Grzebieta, R. H. (1999) "Void-filled SHS subject to large deformation cyclic bending", *Journal of Structural Engineering, ASCE*, 25(9): 1020-1027.

Zhao, X. L. and Hancock, G. J. (1991) "Tests to determine plate slenderness limits for cold-formed rectangular hollow sections of grade C450", *Steel Construction*, 25(4): 2-16.

Zhao, X. L. and Hancock, G. J. (1992) "Square and rectangular hollow sections subject to combined actions", *Journal of Structural Engineering, ASCE*, 118(3): 648-668.

Zhao, X. L. and Hancock, G. J. (1993). "Test and design of butt welds and transverse fillet welds in thin cold-formed RHS members". *Research Report-R681,* School of Civil and Mining Engineering, University of Sydney, Sydney, Australia.

Zhao, X. L. and Hancock, G. J. (1995a) "Butt welds and transverse fillet welds in thin cold-formed RHS members", *Journal of Structural Engineering, ASCE*, 121(11): 1674-1682.

Zhao, X. L. and Hancock, G. J. (1995b) "Longitudinal fillet welds in thin cold-formed RHS members", *Journal of Structural Engineering, ASCE*, 121(11): 1683-1690.

Zhao, X. L. and Hancock, G. J. (1996) "Tests and design of butt welds and fillet welds in Duragal RHS members". in *Connections in Steel Structures III: Behaviour, Strength, and Design,* R. Bjorhovde, A. Colson and R. Zandonini (eds.), Oxford, Elsevier Science Ltd. 89-98.

Zhao, X. L., Hancock, G. J. and Sully, R. M. (1996) "Design of tubular members and connections using amendment number 3 to AS 4100", *Steel Construction,* Australian Institute of Steel Construction, 30(4): 2-15.

Zhao, X. L. and Mahendran, M. (1998) "Recent innovations in cold-formed tubular sections", *Journal of Constructional Steel Research*, 46(1-3): 472-473.

APPENDIX A

A.1 STRESS-STRAIN CURVES OF TENSILE COUPONS

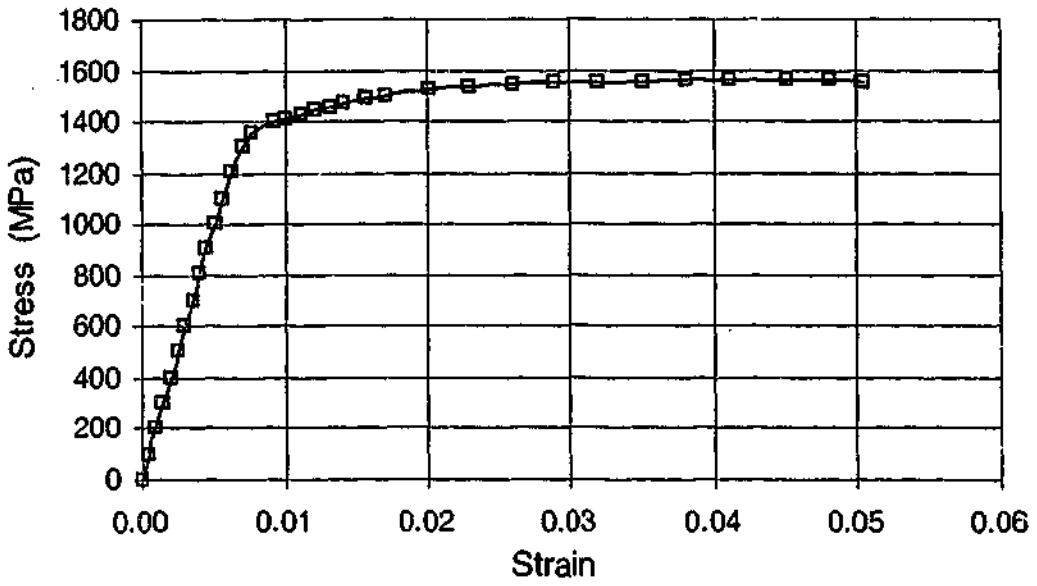

Figure A.1-1: Stress-strain curve of specimen TS1A (VHS)

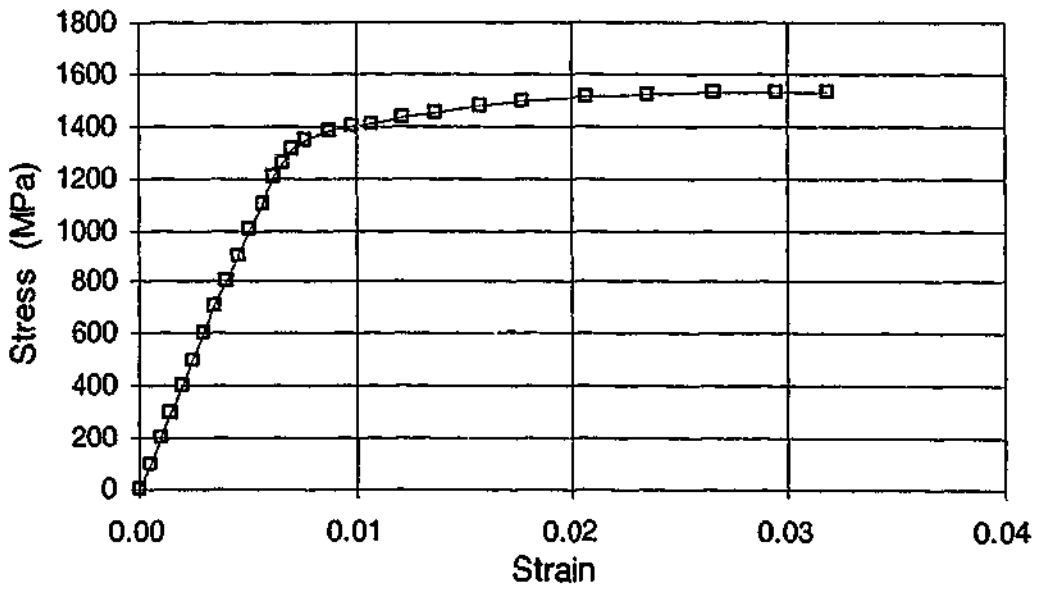

Figure A.1-2: Stress-strain curve of specimen TS1B (VHS)

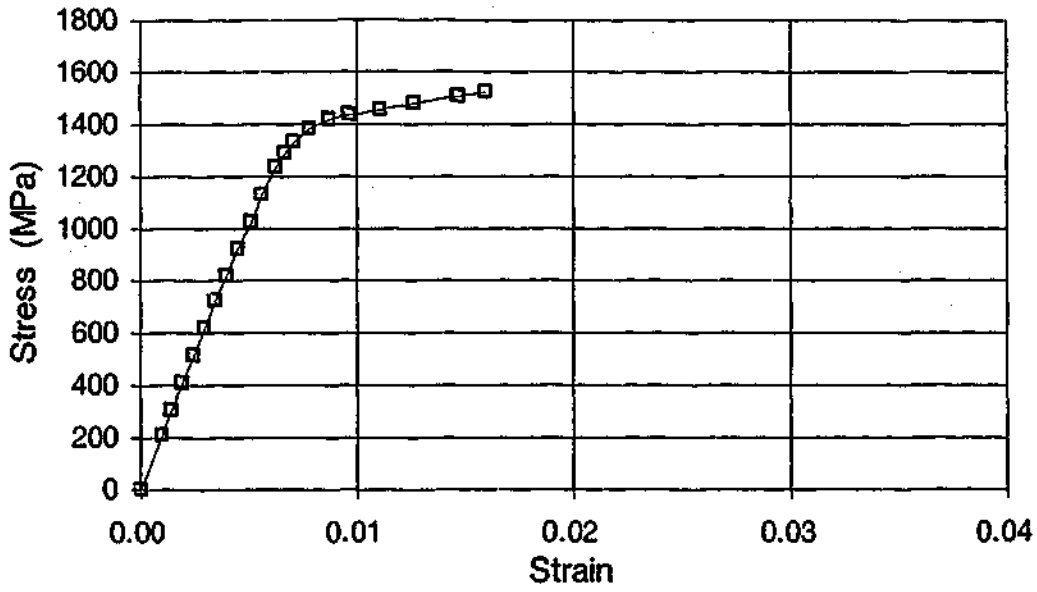

Figure A.1-3: Stress-strain curve of specimen TS1C (VHS)

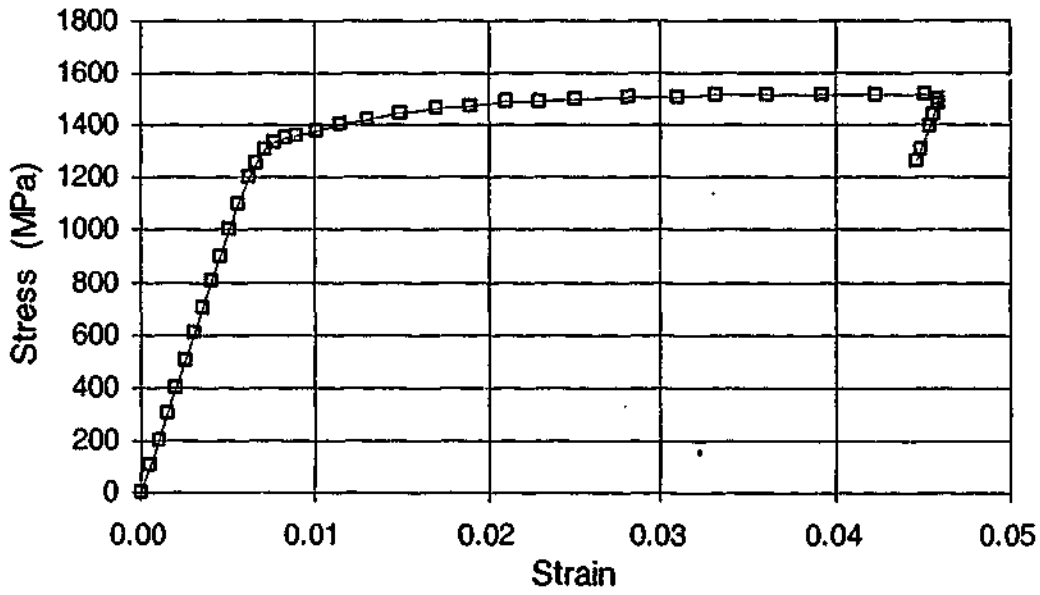

Figure A.1-4: Stress-strain curve of specimen TS2A (VHS)

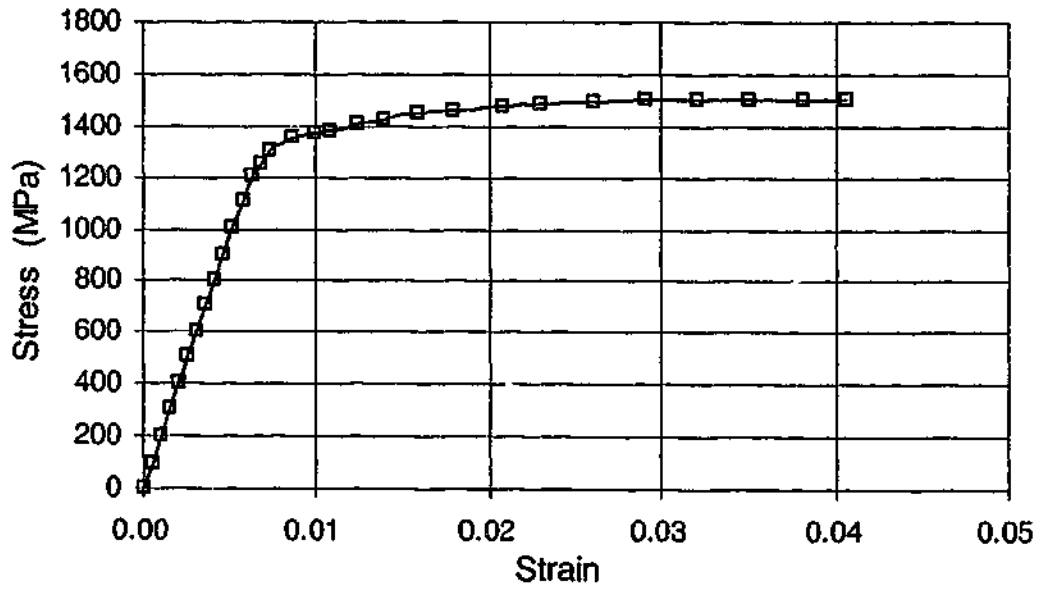

Figure A.1-5: Stress-strain curves of specimen TS2B (VHS)

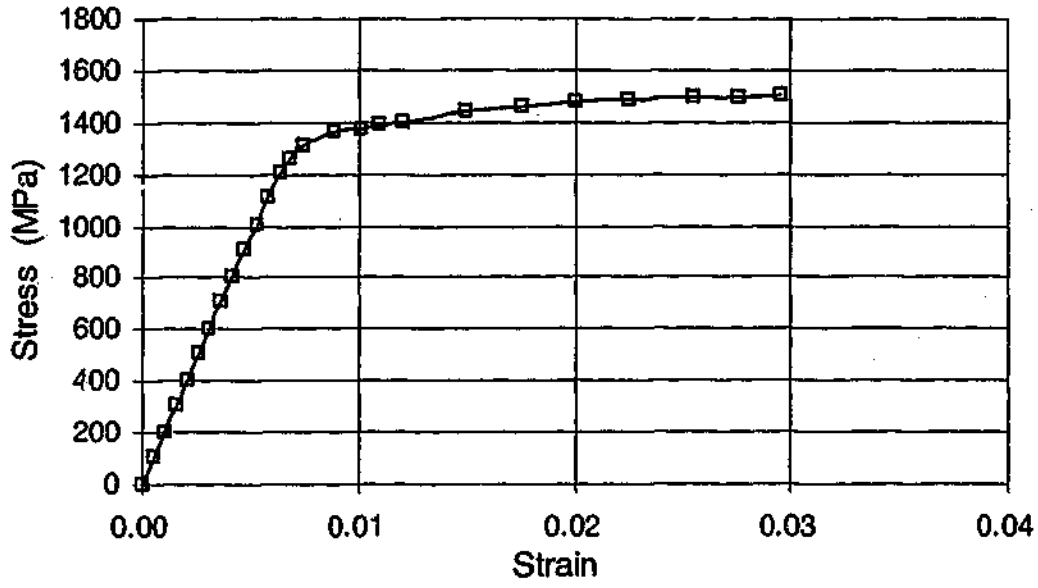

Figure A.1-6: Stress-strain curve of specimen TS2C (VHS)

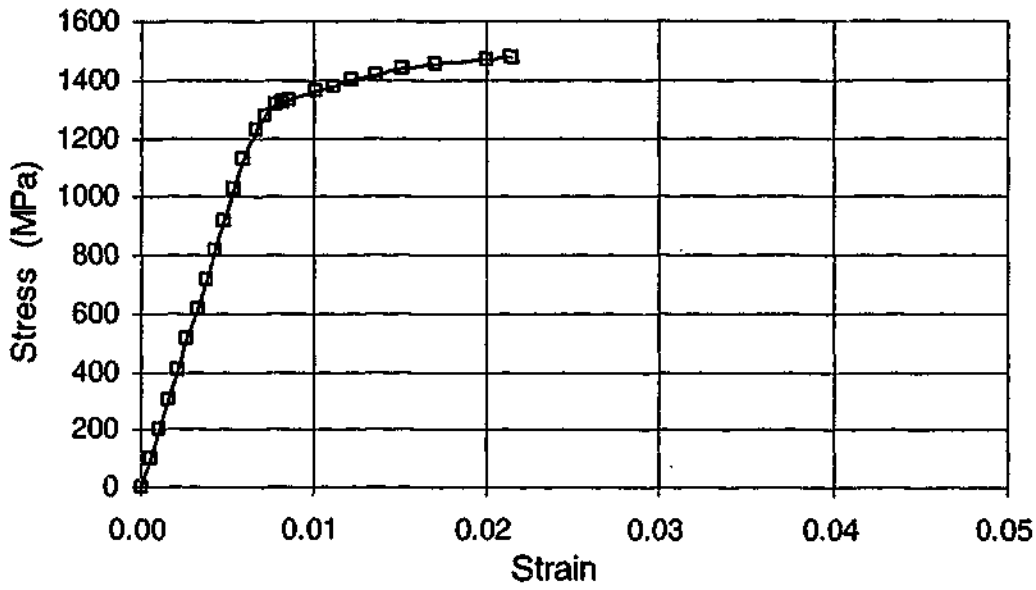

Figure A.1-7: Stress-strain curve of specimen TS3A (VHS)

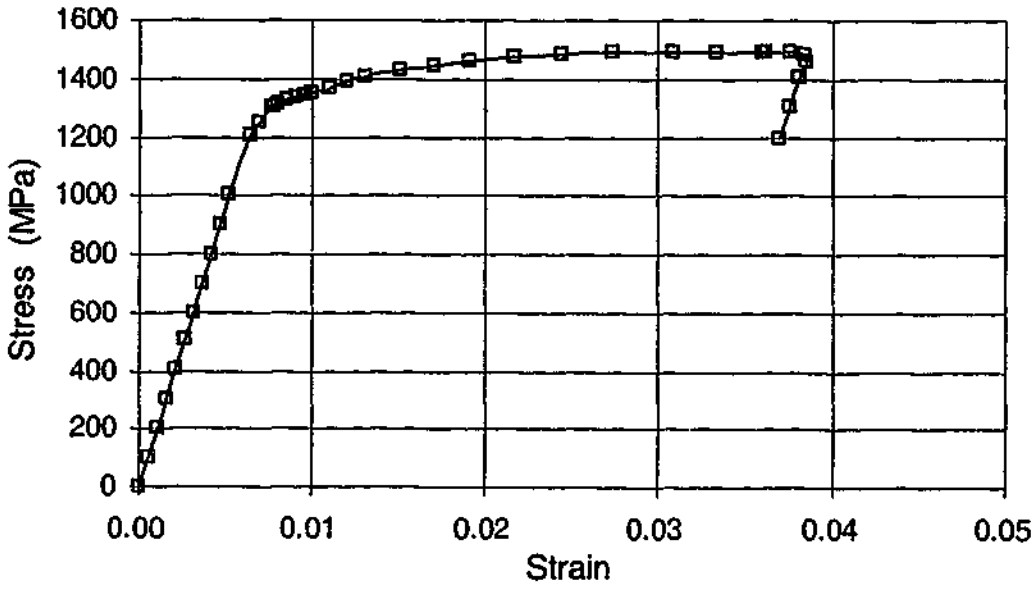

Figure A.1-8: Stress-strain curve of specimen TS3B (VHS)

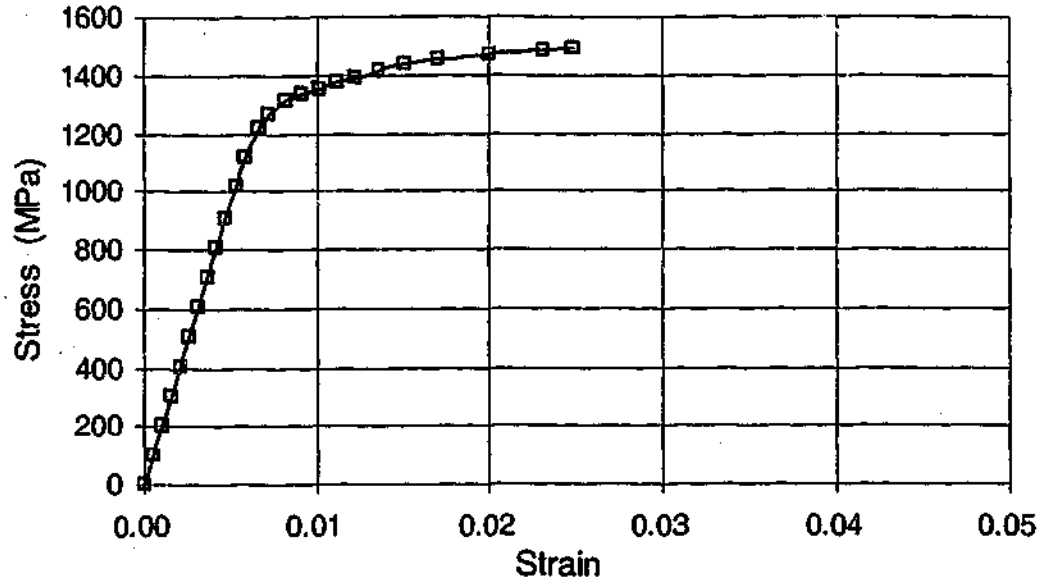

Figure A.1-9: Stress-strain curve of specimen TS3C (VHS)

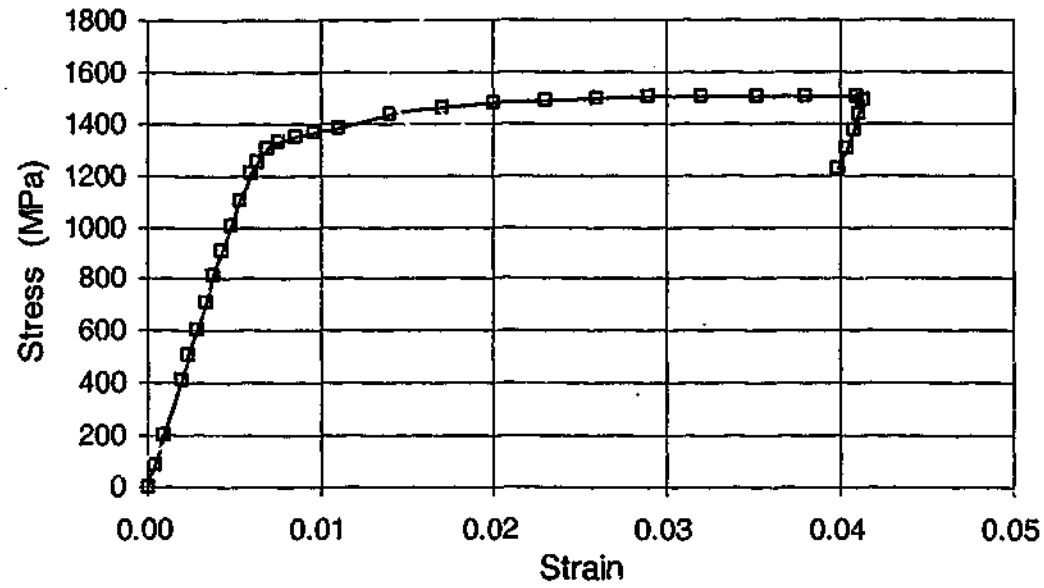

Figure A.1-10: Stress-strain curve of specimen TS4A (VHS)

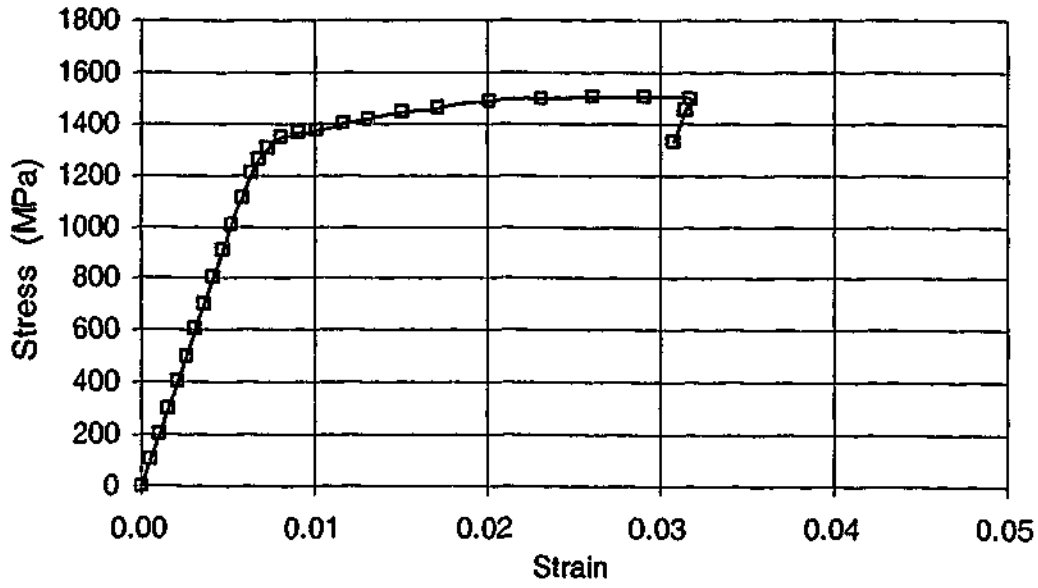

Figure A.1-11: Stress-strain curve of specimen TS4B (VHS)

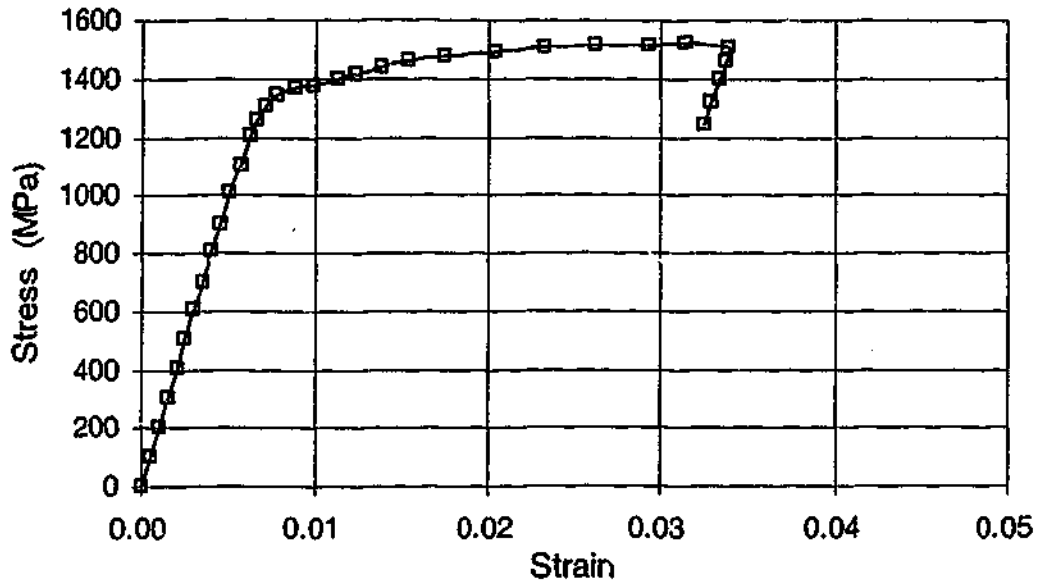

Figure A.1-12: Stress-strain curve of specimen TS4C (VHS)

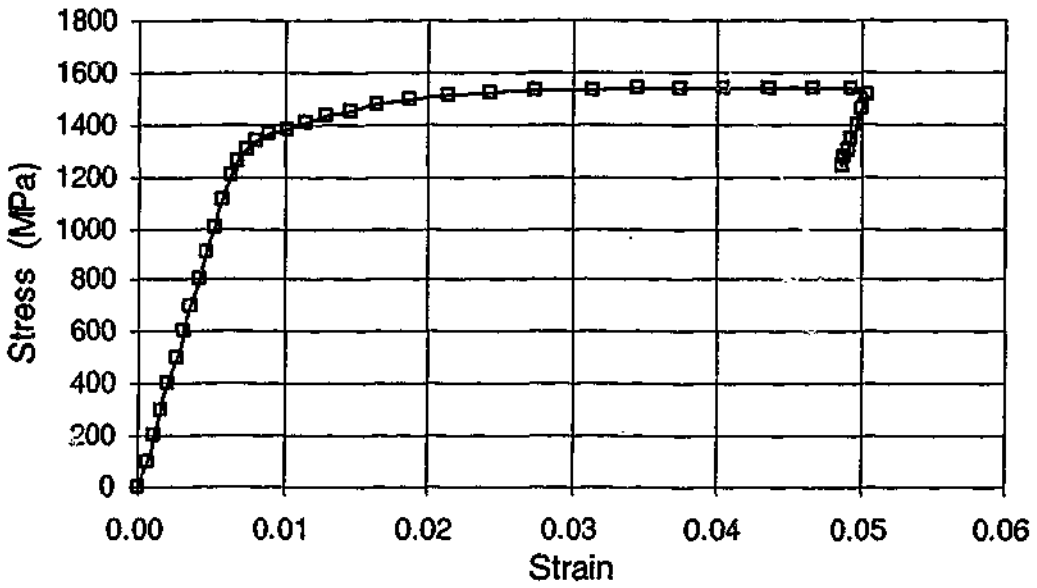

Figure A.1-13: Stress-strain curve of specimen TS5A (VHS)

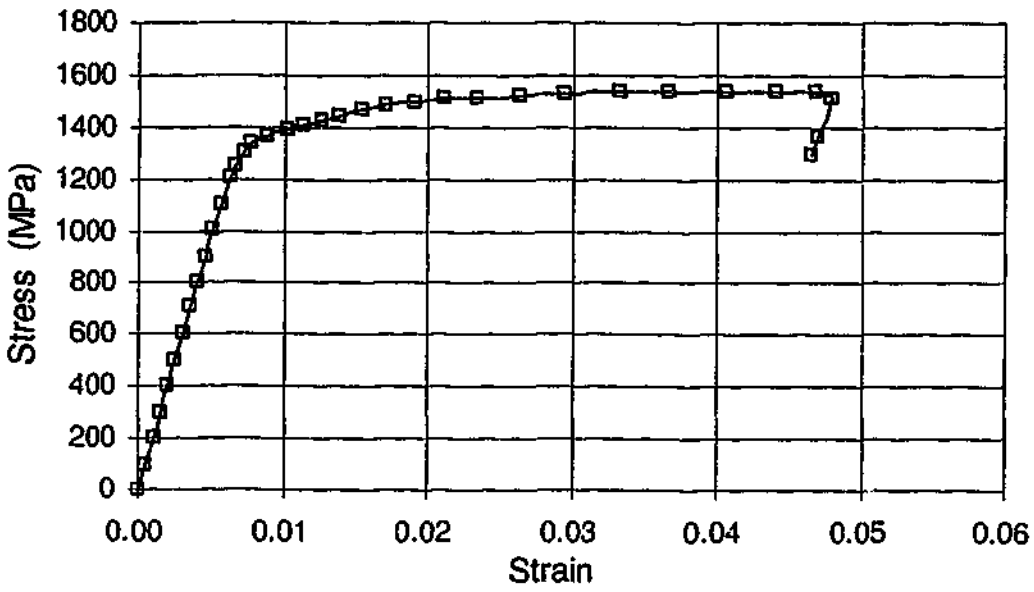

Figure A.1-14: Stress-strain curve of specimen TS5B (VHS)

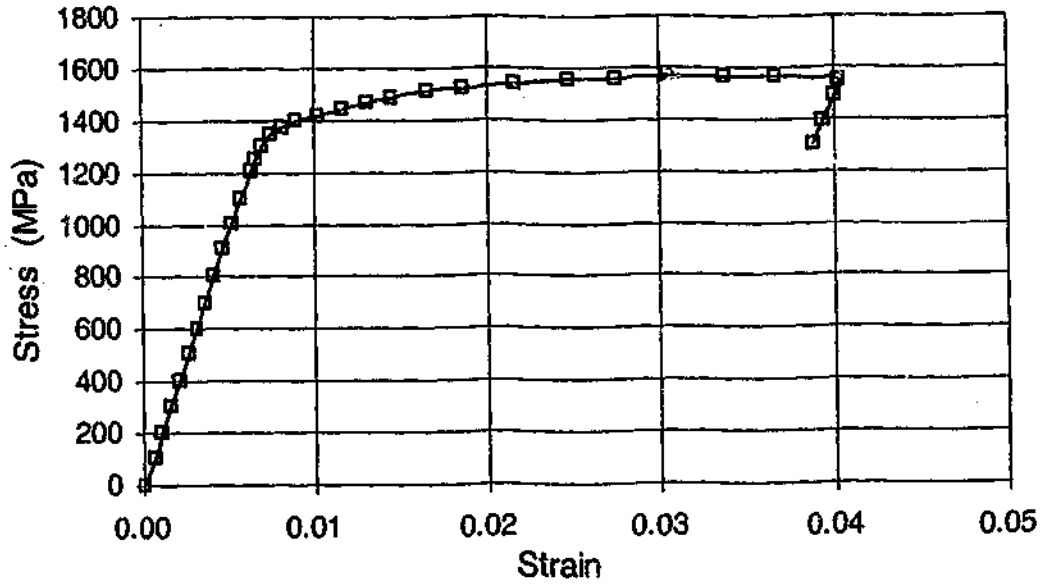

Figure A.1-15: Stress-strain curve of specimen TS5C (VHS)

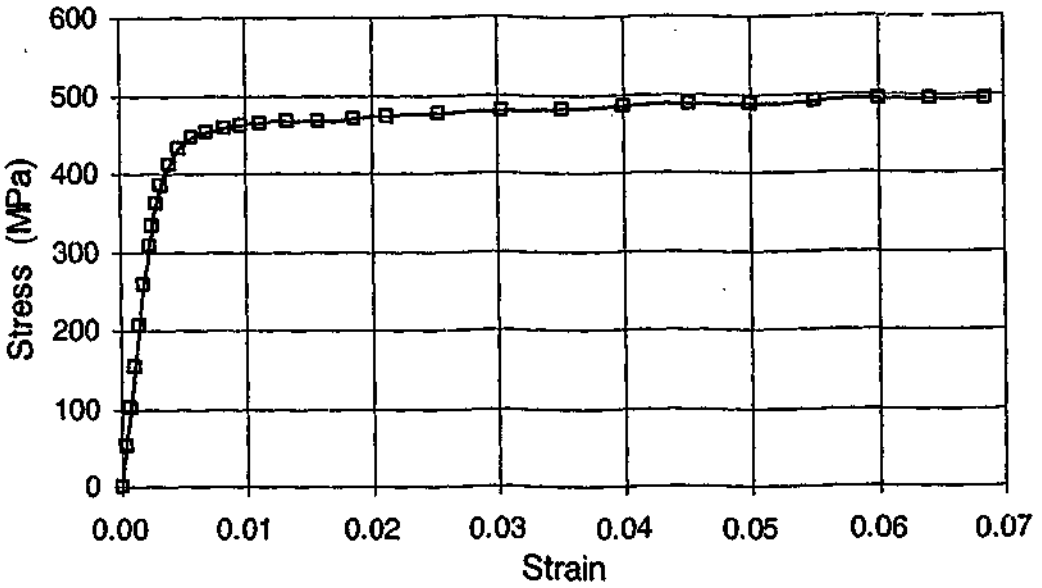

Figure A.1-16: Stress-strain curve of specimen TS6A (NHT)

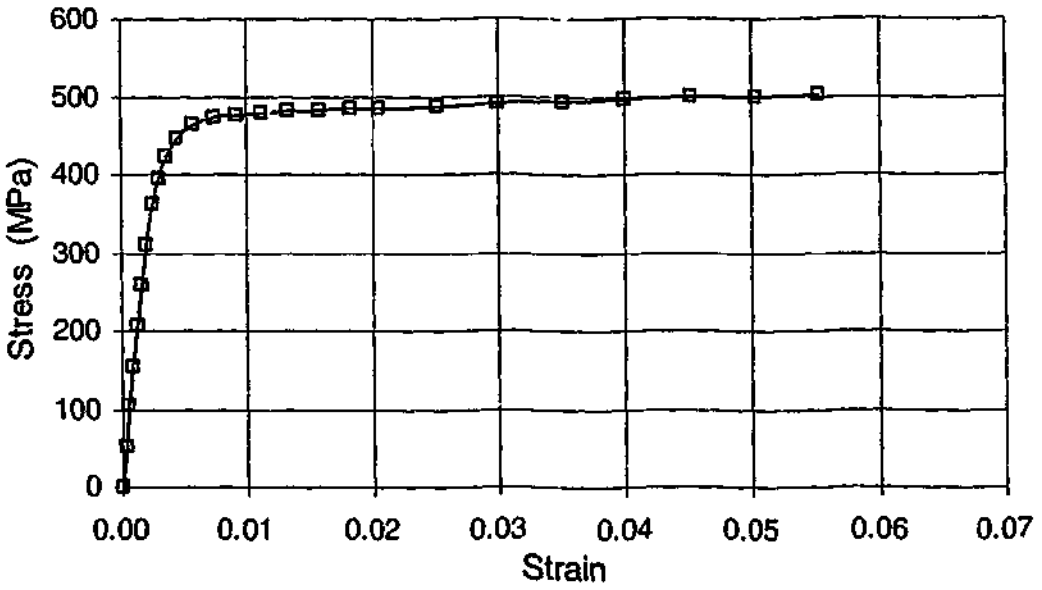

Figure A.1-17: Stress-strain curve of specimen TS6B (NHT)

A.2 STRESS-STRAIN CURVES OF VHS AND NHT FULL SECTION TUBES IN TENSION

Note: No stress-strain data was recorded for Specimen FTS1A due to the damaged strain gauge.

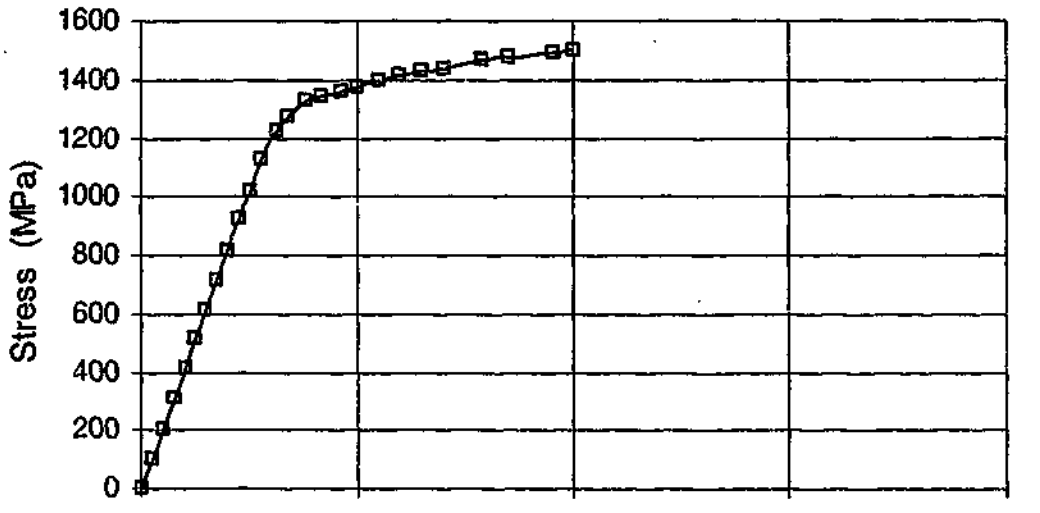

Figure A.2-1: Stress-strain curve of specimen FTS1B (VHS)

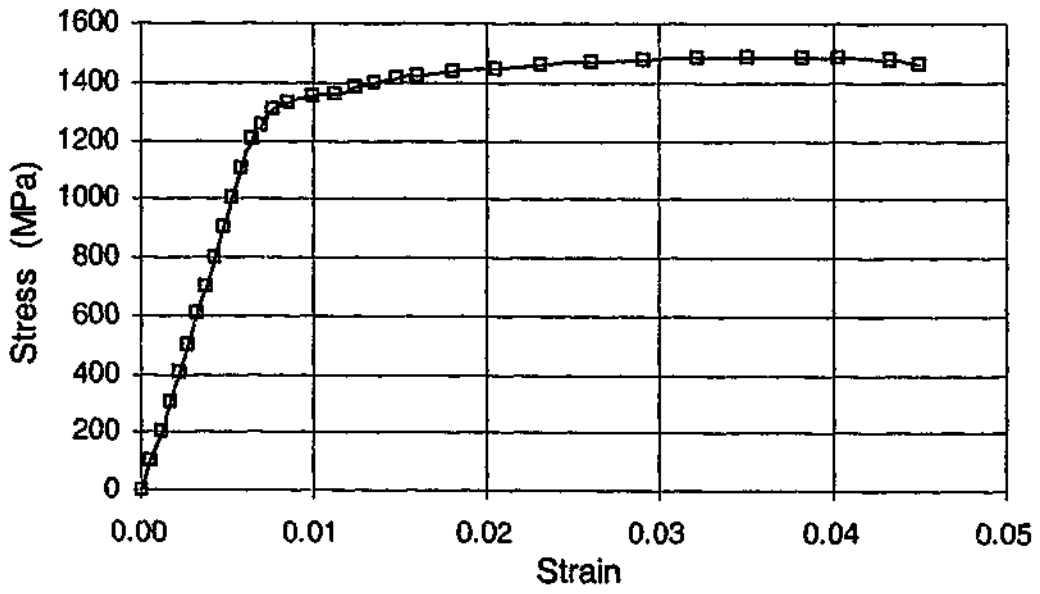

Figure A.2-2: Stress-strain curve of specimen FTS2A (VHS)

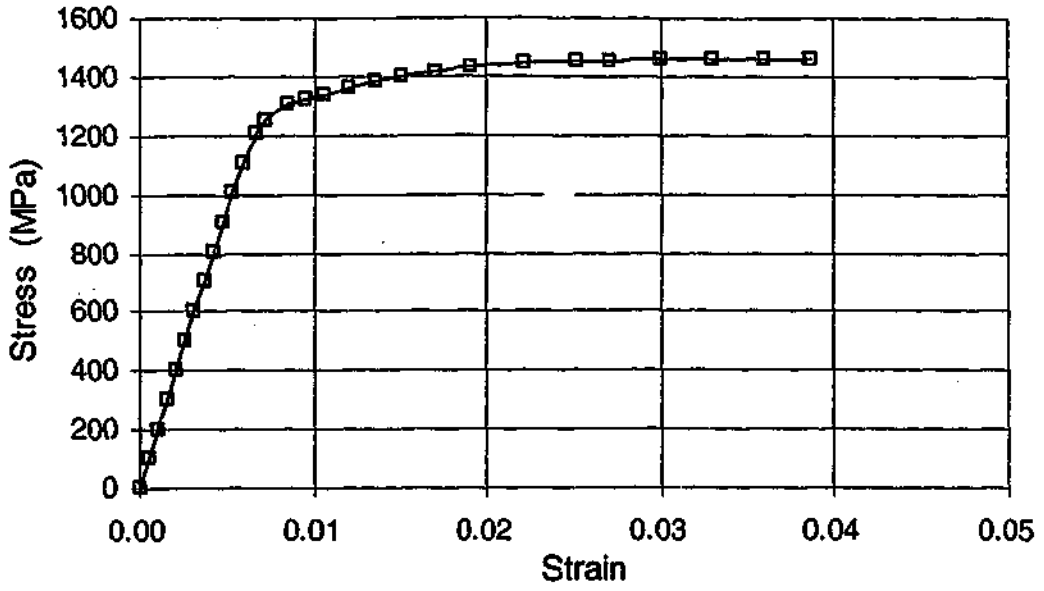

Figure A.2-3: Stress-strain curve of specimen FTS2B (VHS)

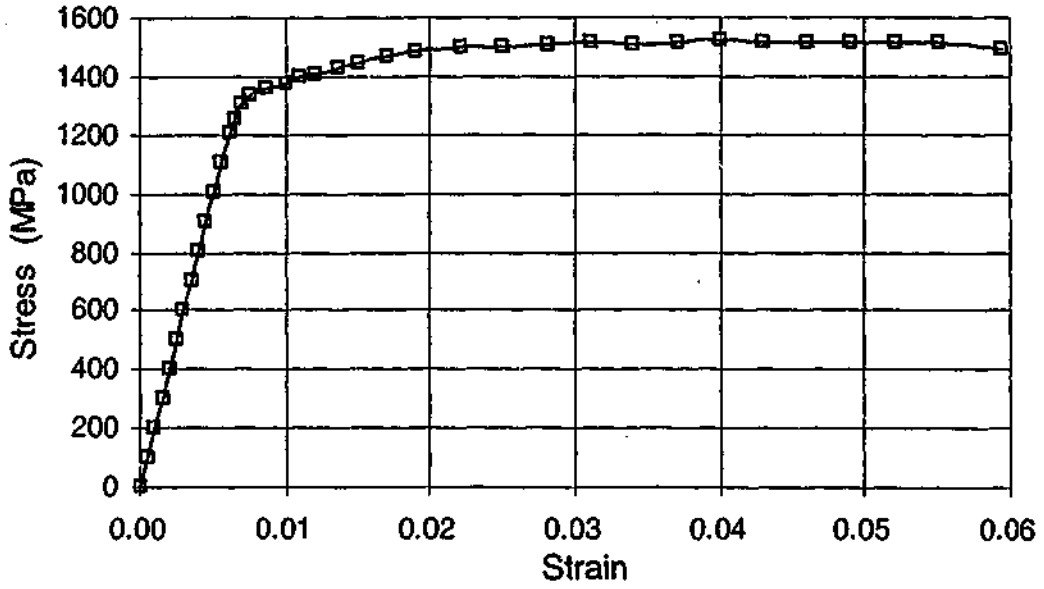

Figure A.2-4: Stress-strain curve of specimen FTS3A (VHS)

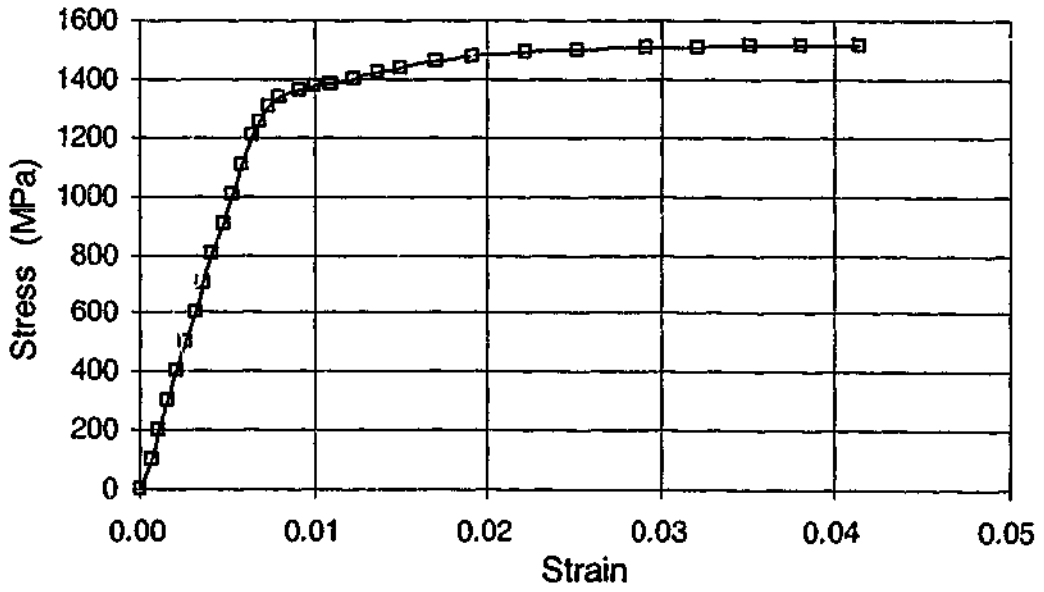

Figure A.2-5: Stress-strain curve of specimen FTS3B (VHS)

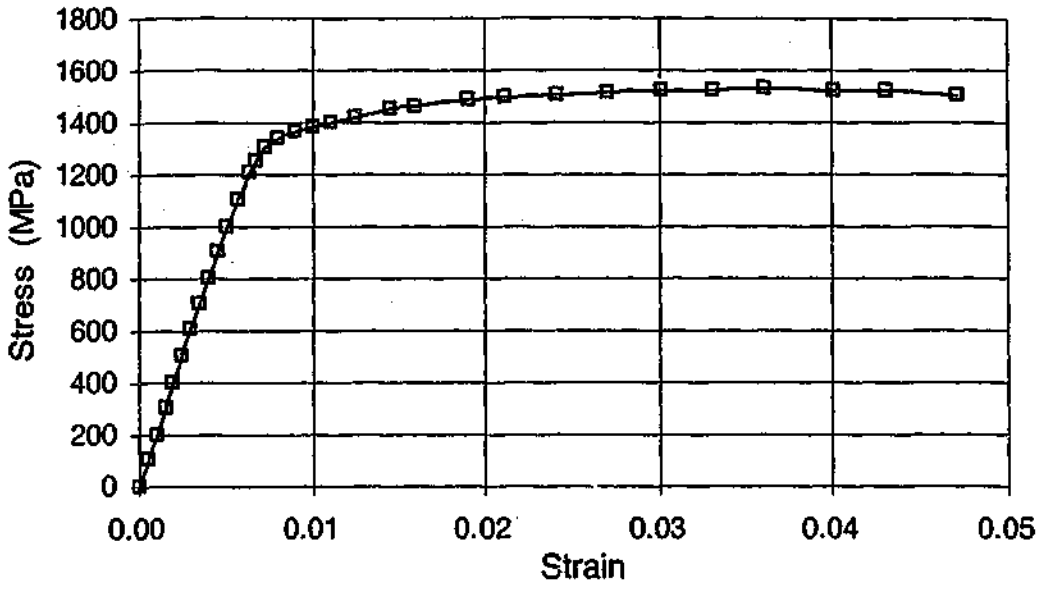

Figure A.2-6: Stress-strain curve of specimen FTS4A (VHS)

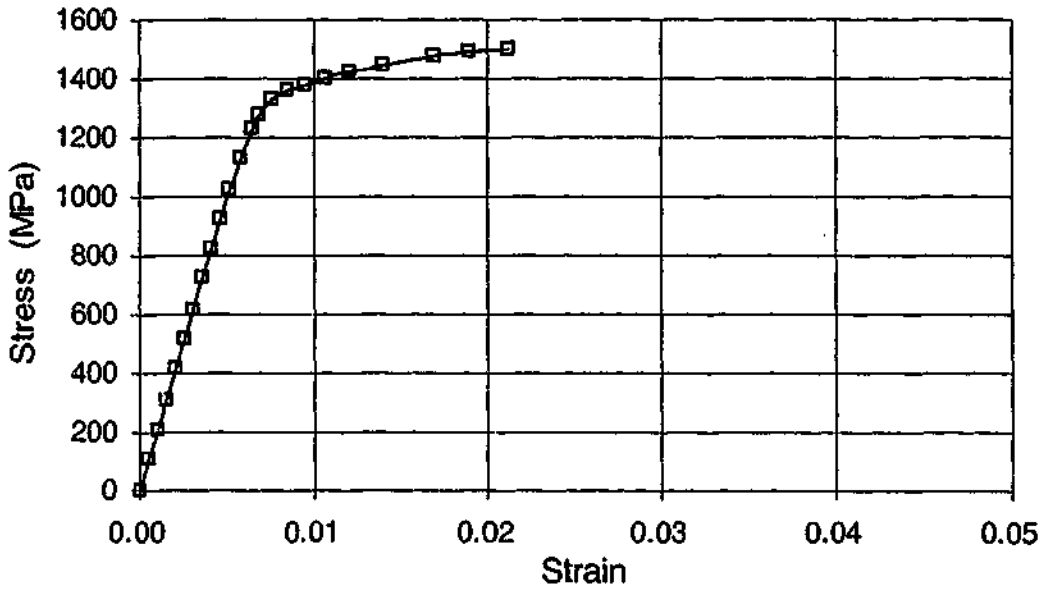

Figure A.2-7: Stress-strain curve of specimen FTS4B (VHS)

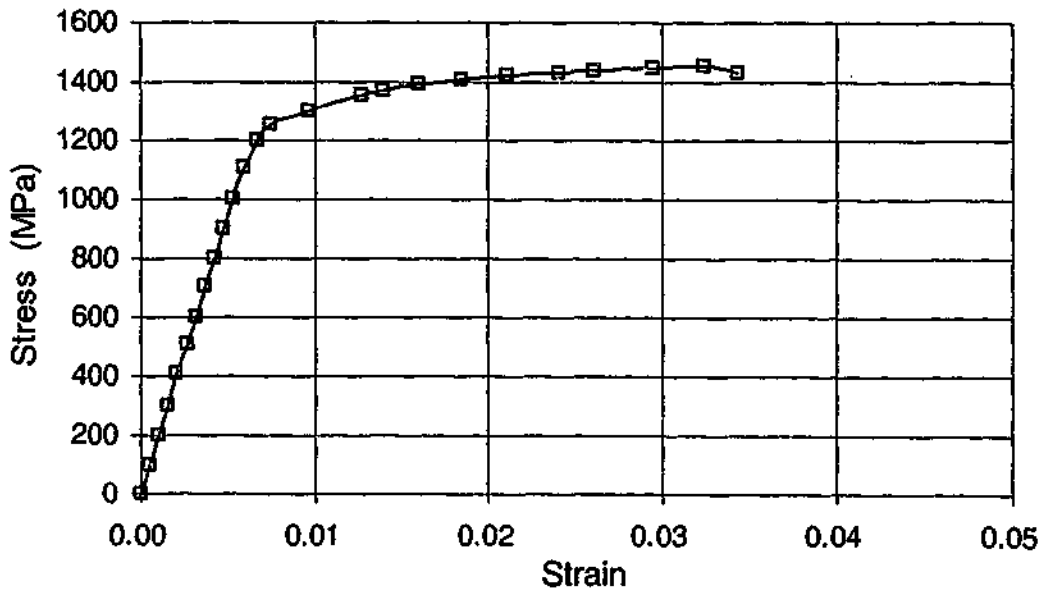

Figure A.2-8: Stress-strain curve of specimen FTS5A (VHS)

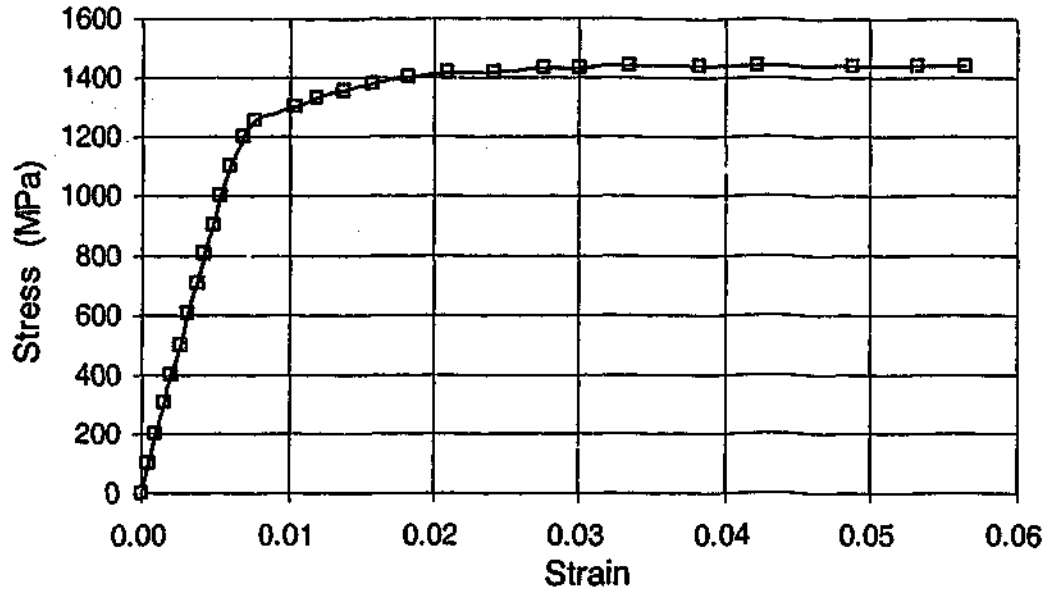

Figure A.2-9: Stress-strain curve of specimen FTS5B (VHS)

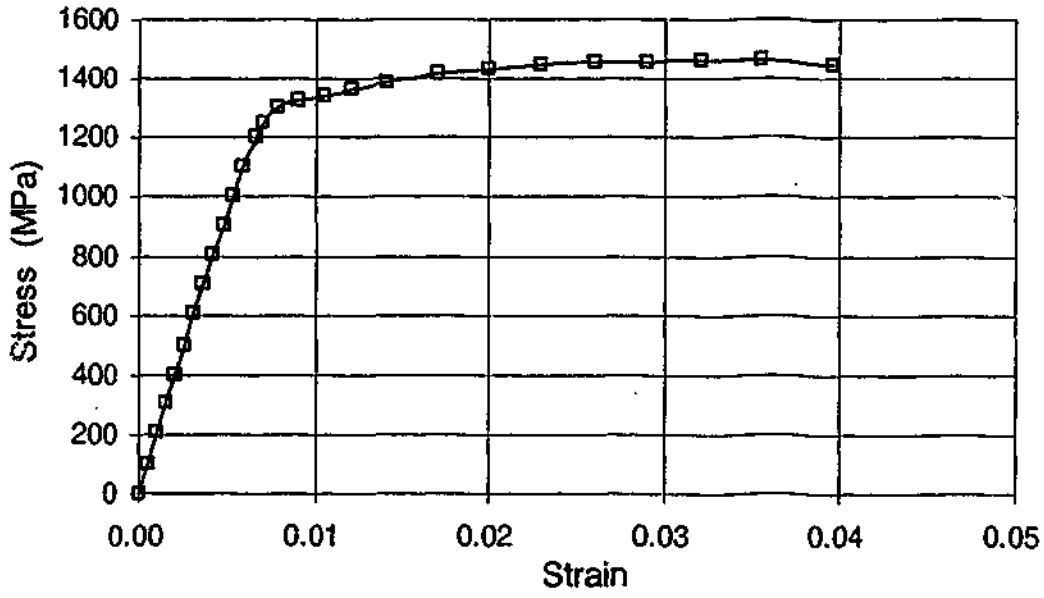

Figure A.2-10: Stress-strain curve of specimen FTS6A (VHS)

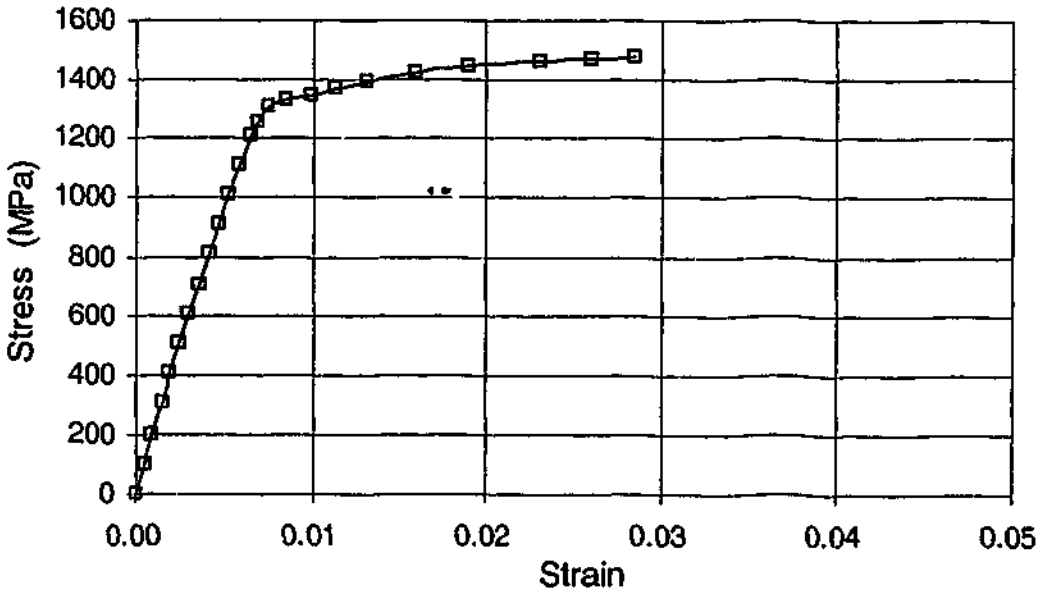

Figure A.2-11: Stress-strain curve of specimen FTS6B (VHS)

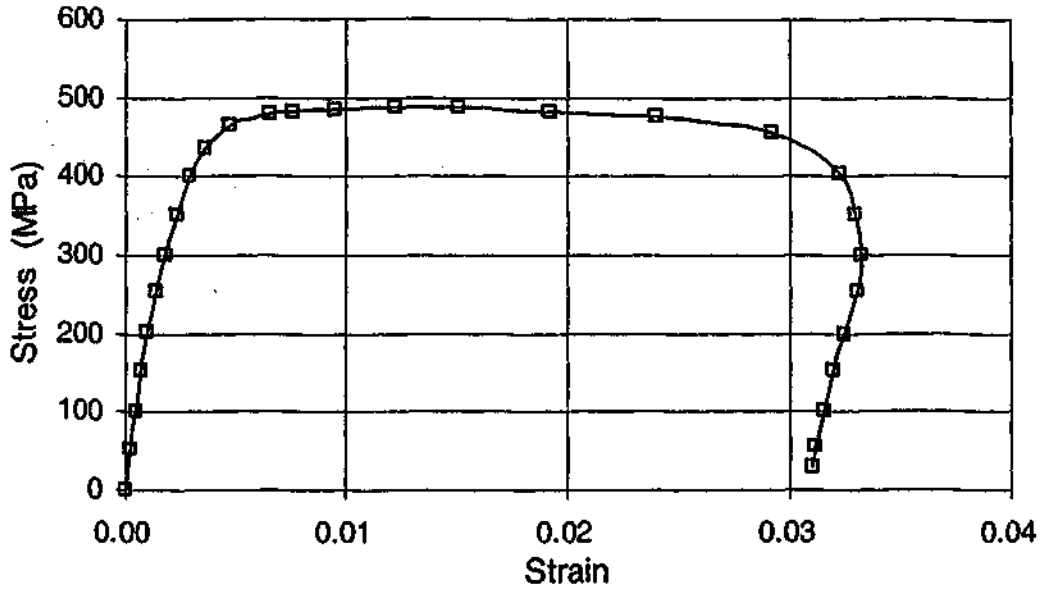

Figure A.2-12: Stress-strain curve of specimen FTS1NA (NHT)

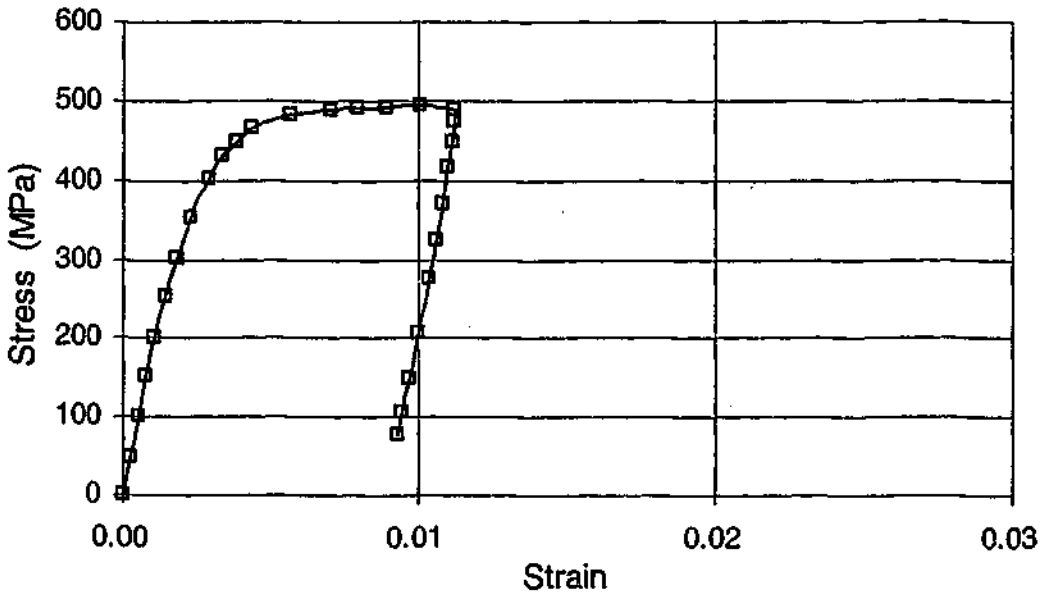

Figure A.2-13: Stress-strain curve of specimen FTS1NB (NHT)

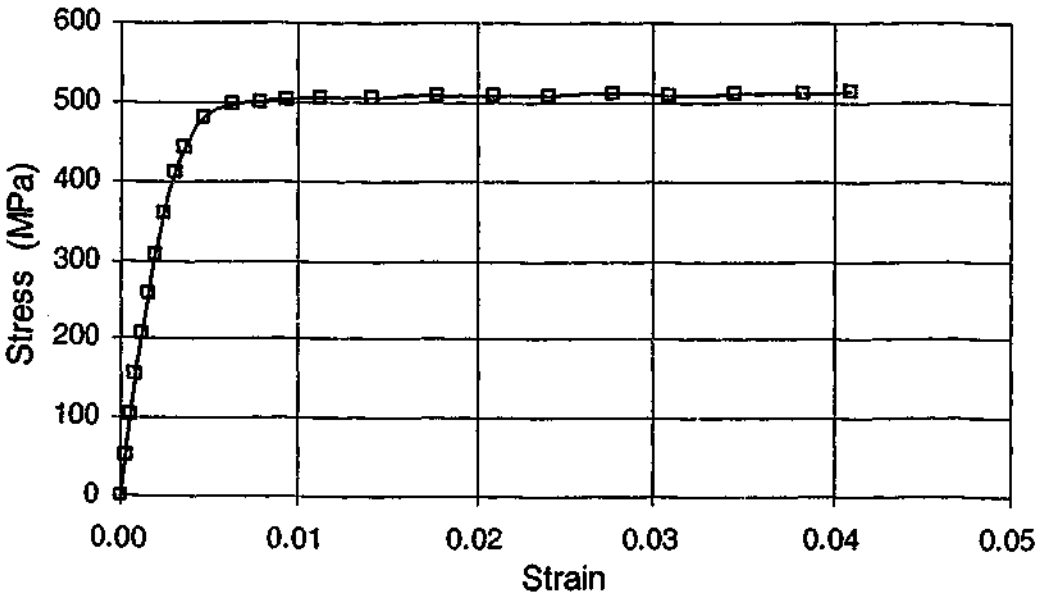

Figure A.2-14: Stress-strain curve of specimen FTS2NA (NHT)

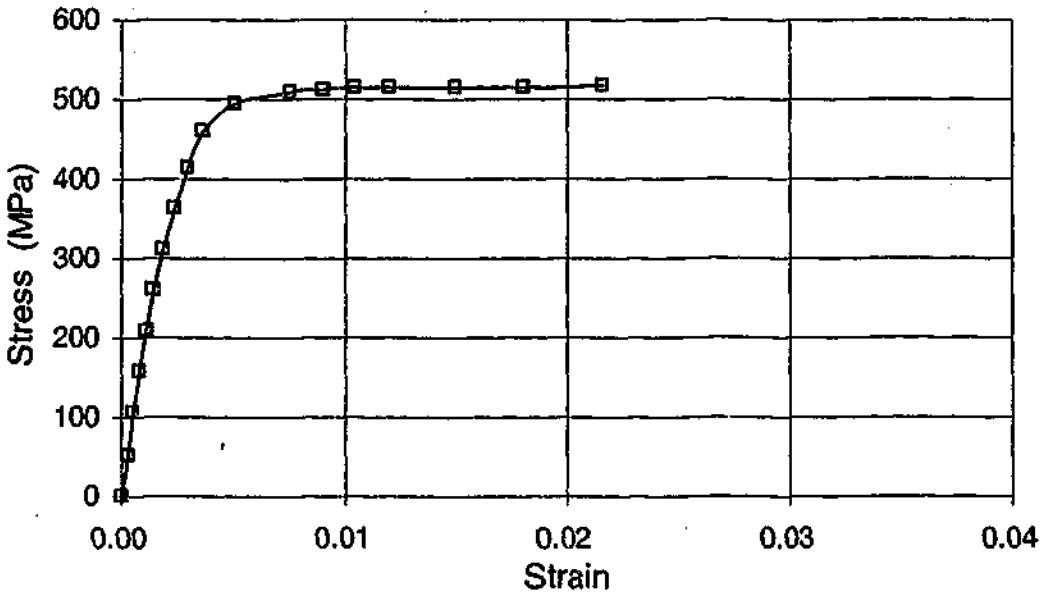

Figure A.2-15: Stress-strain curve of specimen FTS2NB (NHT)

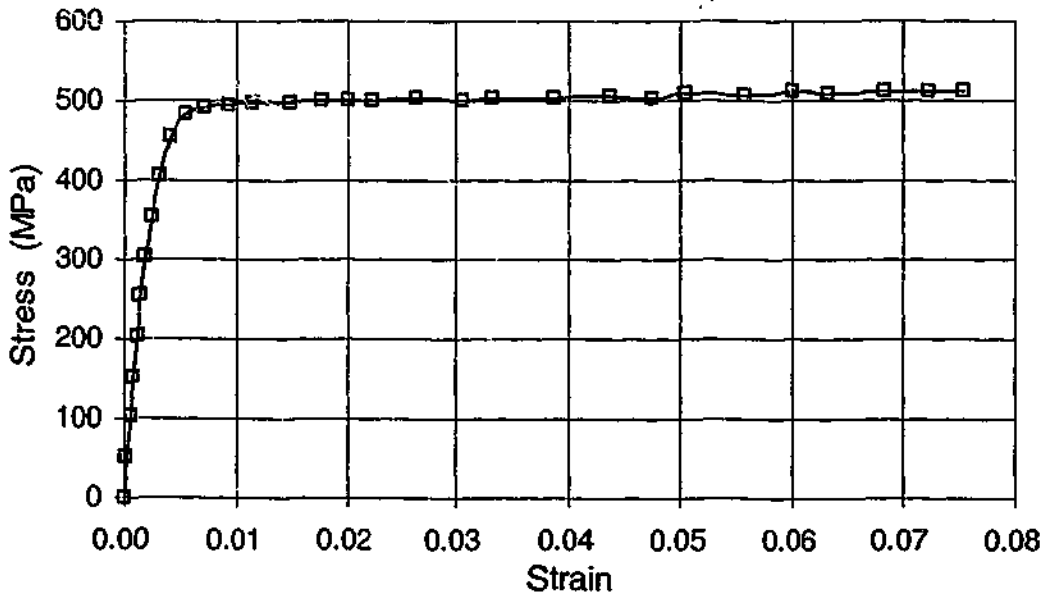

Figure A.2-16: Stress-strain curve of specimen FTS3NA (NHT)

A.3 STRESS-STRAIN CURVES OF VHS AND NHT STUB COLUMNS IN COMPRESSION

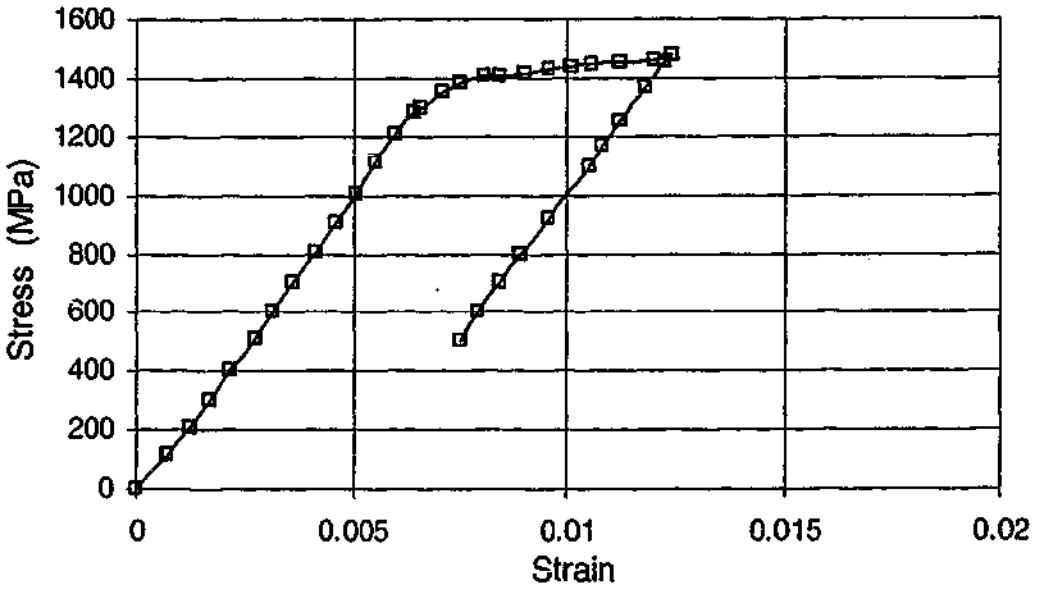

Figure A.3-1: Stress-strain curve of specimen CS7A (VHS)

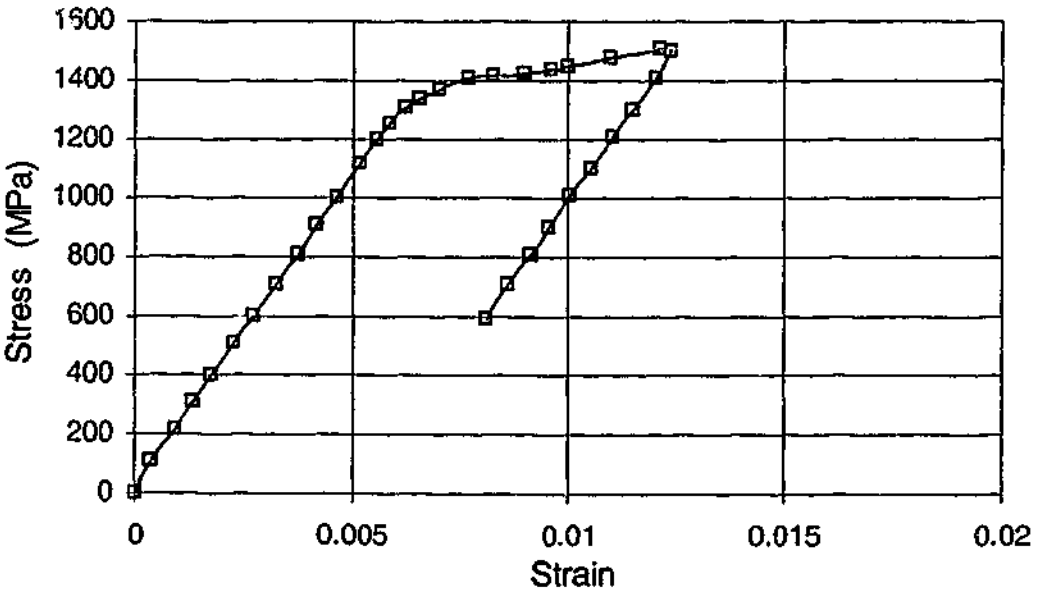

Figure A.3-2: Stress-strain curve of specimen CS7B (VHS)

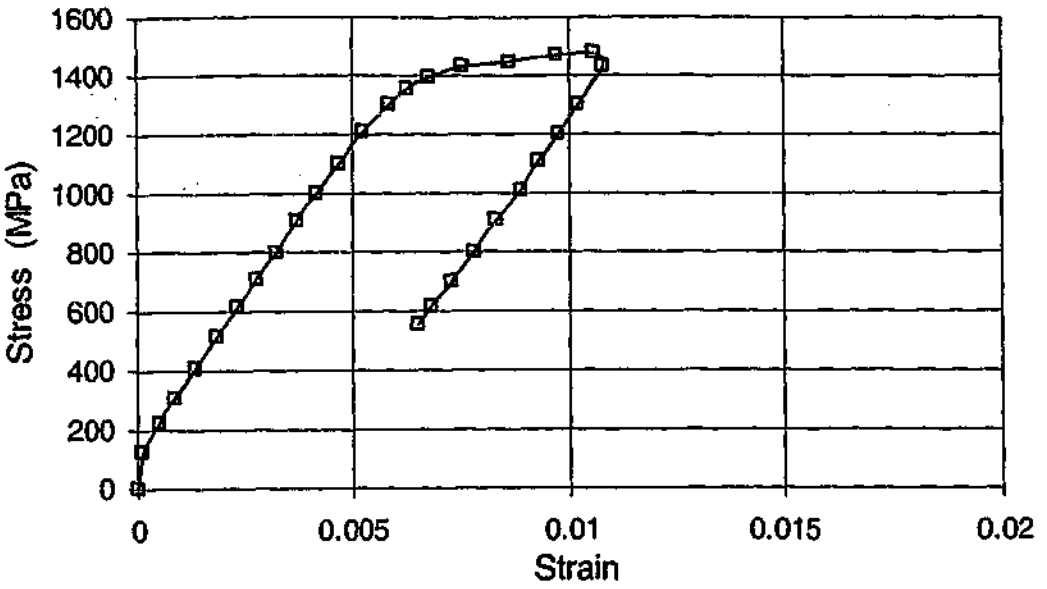

Figure A.3-3: Stress-strain curve of specimen CS7C (VHS)

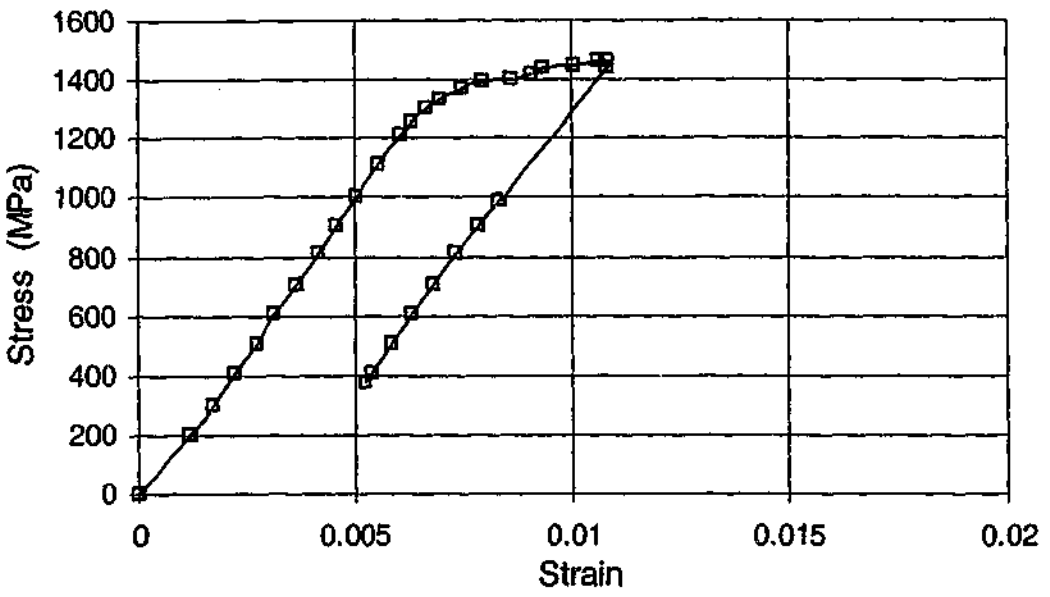

Figure A.3-4: Stress-strain curve of specimen CS8A (VHS)

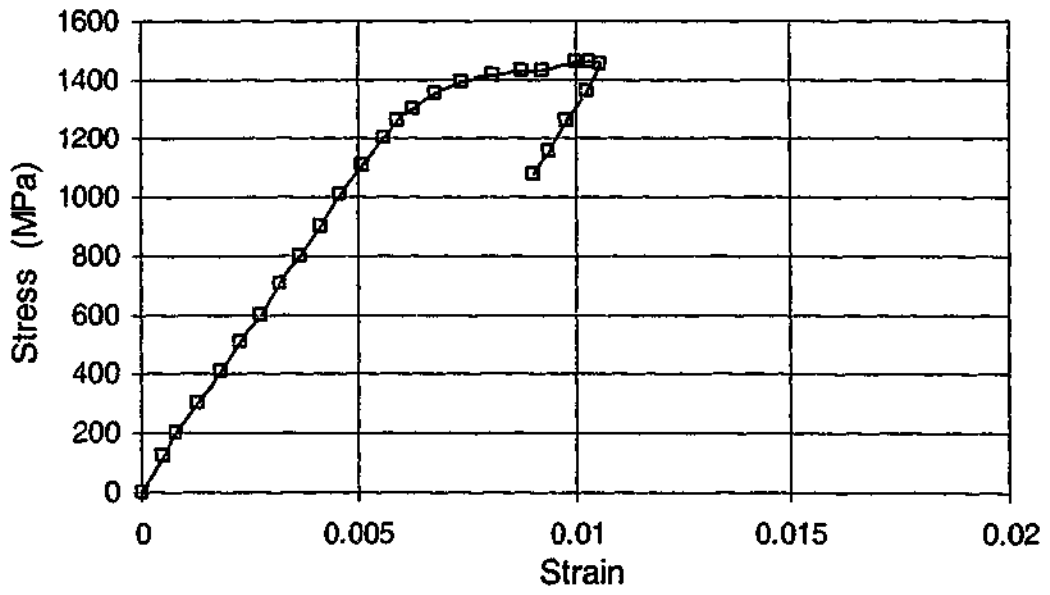

Figure A.3-5: Stress-strain curve of specimen CS8B (VHS)

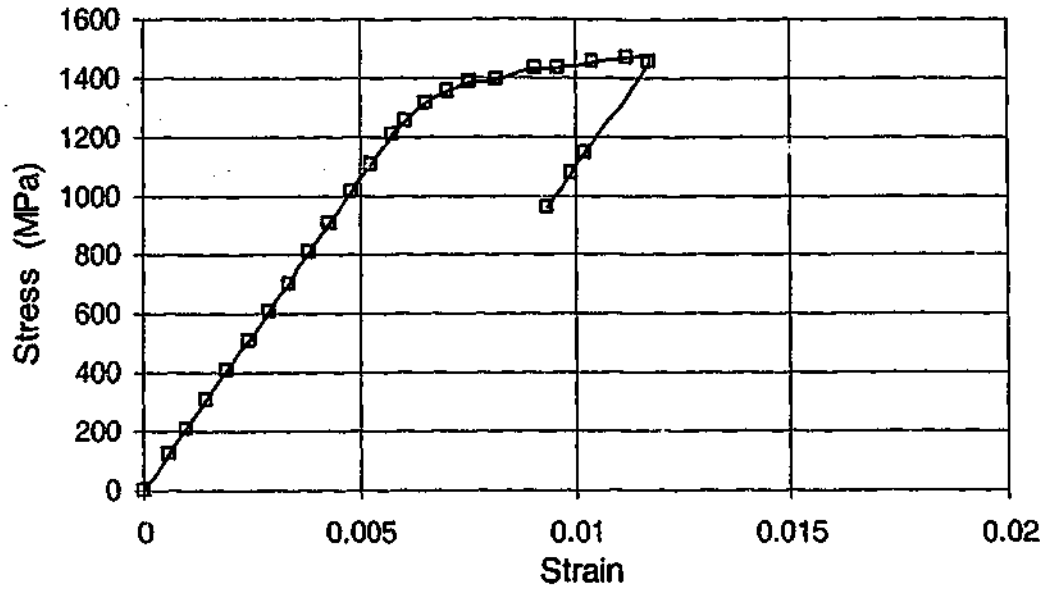

Figure A.3-6: Stress-strain curve of specimen CS8C (VHS)

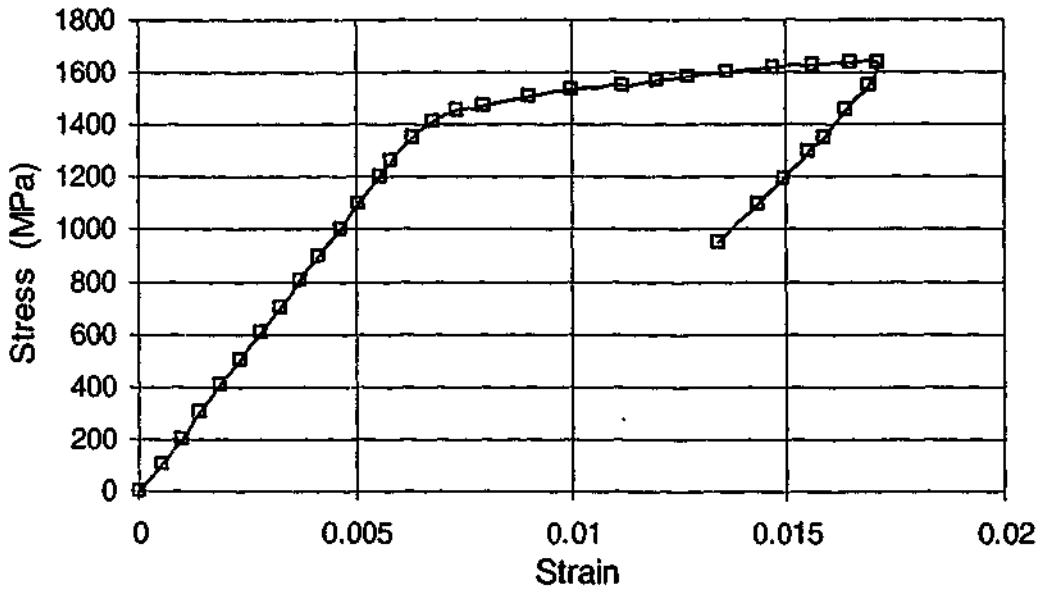

Figure A.3-7: Stress-strain curve of specimen CS9A (VHS)

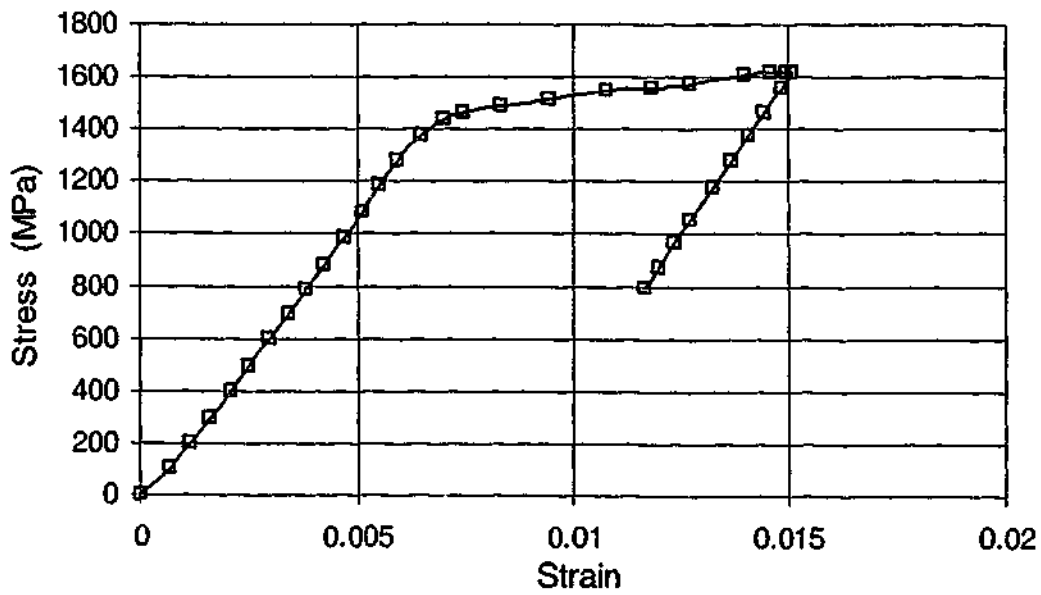

Figure A.3-8: Stress-strain curve of specimen CS9B (VHS)

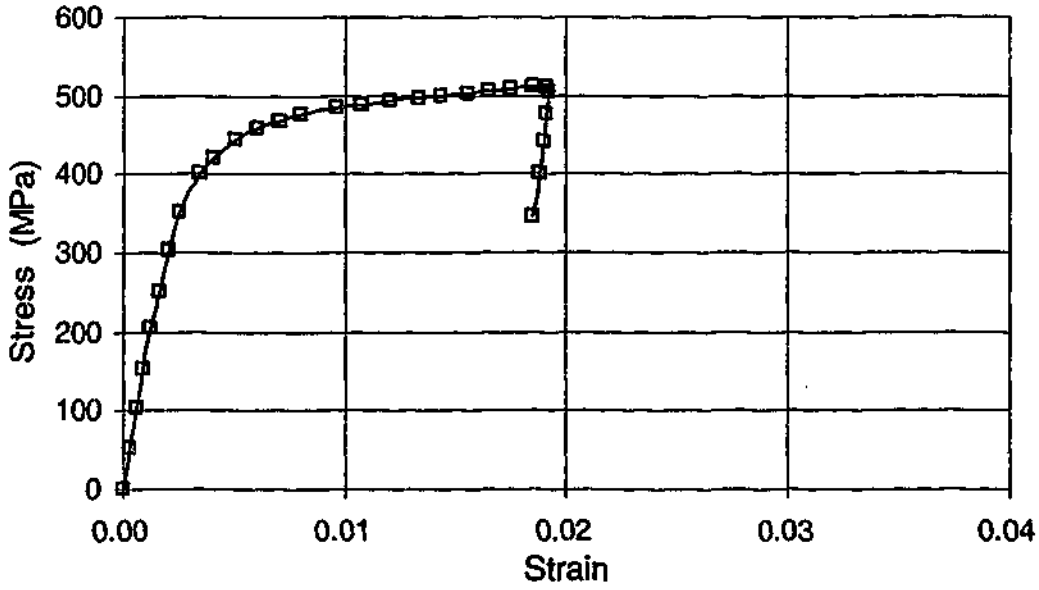

Figure A.3-9: Stress-strain curve of specimen CSNA (NHT)

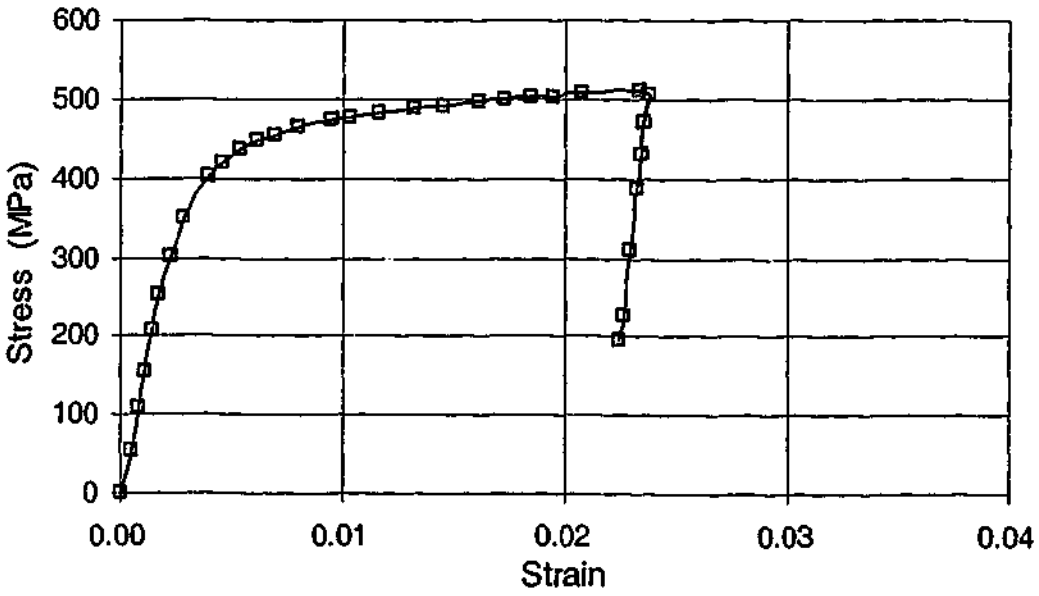

Figure A.3-10: Stress-strain curve of specimen CSNB (NHT)

APPENDIX B

B.1 MOMENT-CURVATURE CURVES OF VHS TUBES IN 4-POINT-BENDING

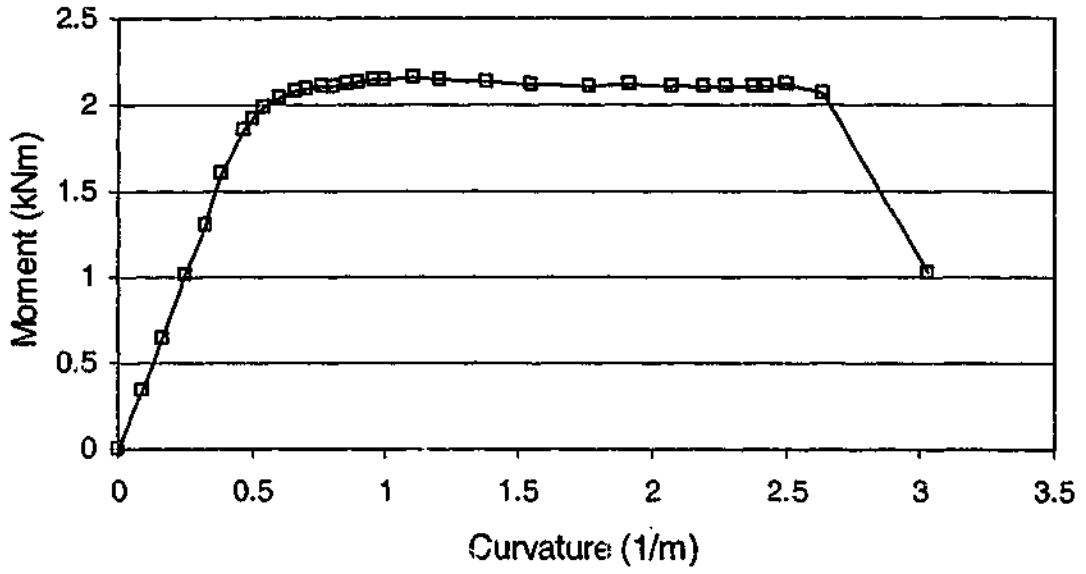

Figure B.1-1: Moment-curvature curve of specimen BS1

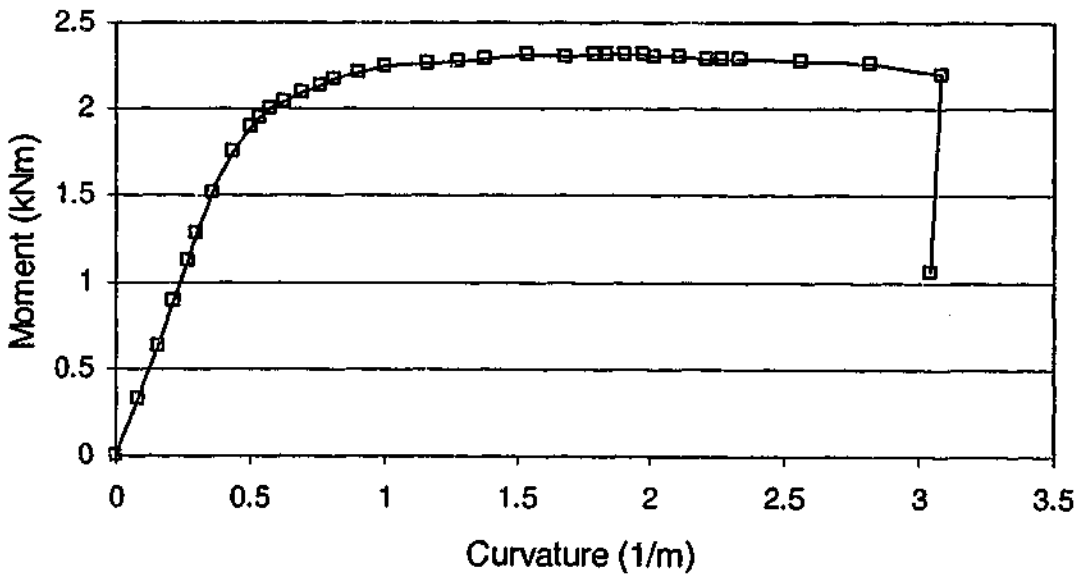

Figure B.1-2: Moment-curvature curve of specimen BS2

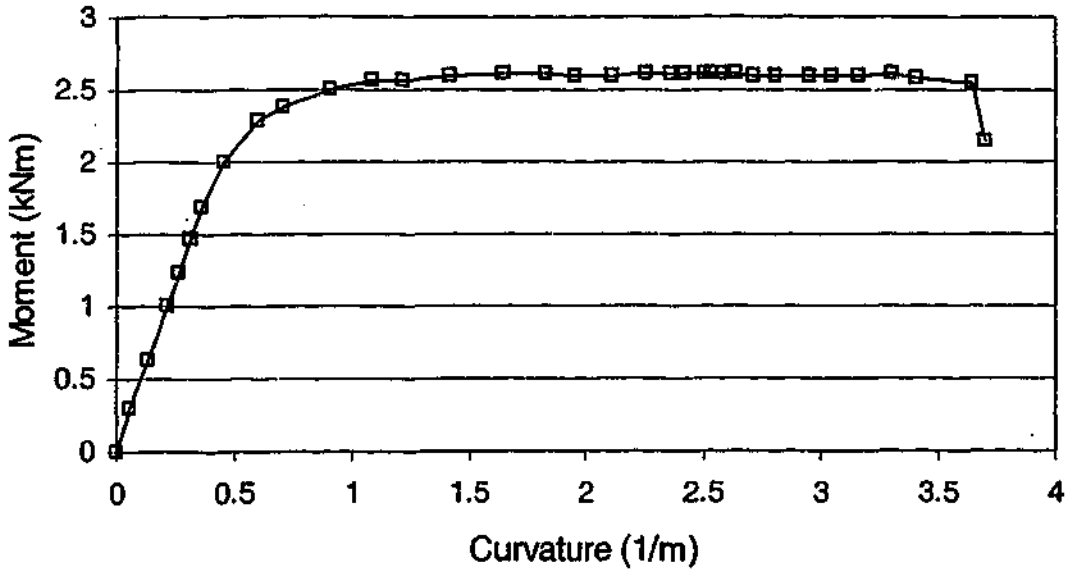

Figure B.1-3: Moment-curvature curve of specimen BS3

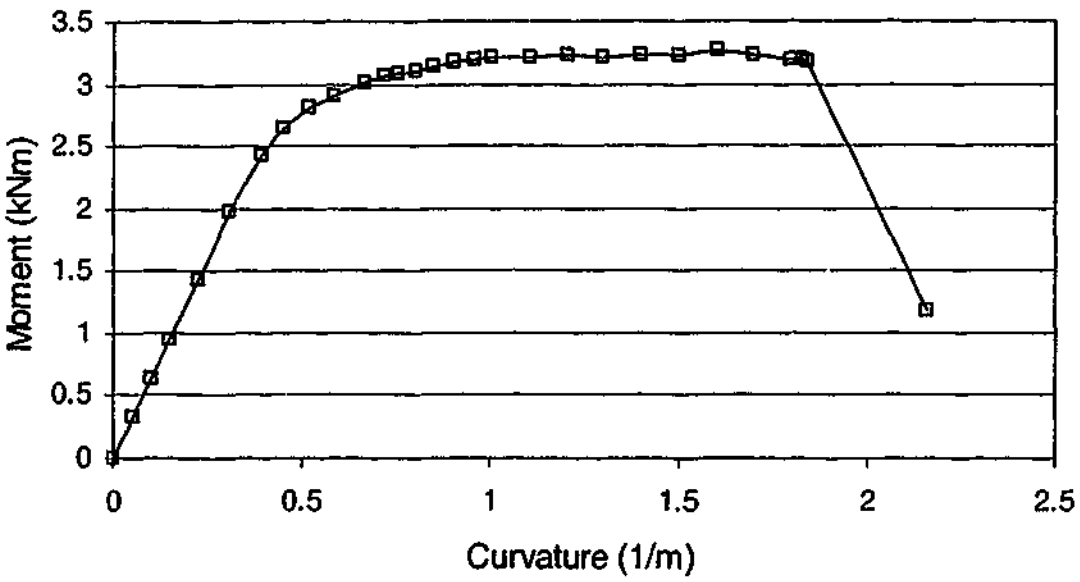

Figure B.1-4: Moment-curvature curve of specimen BS4

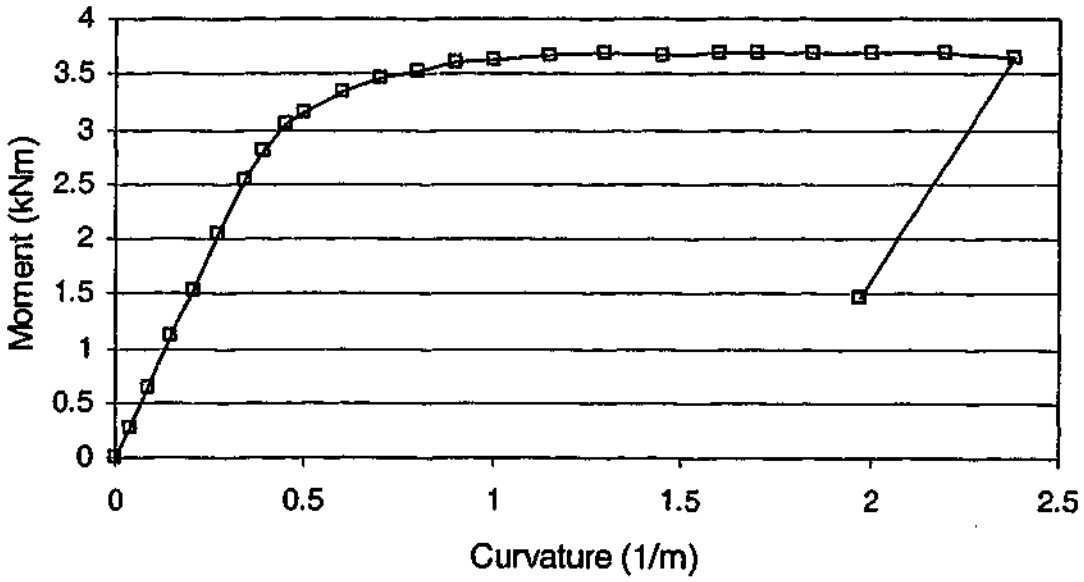

Figure B.1-5: Moment-curvature curve of specimen BS5

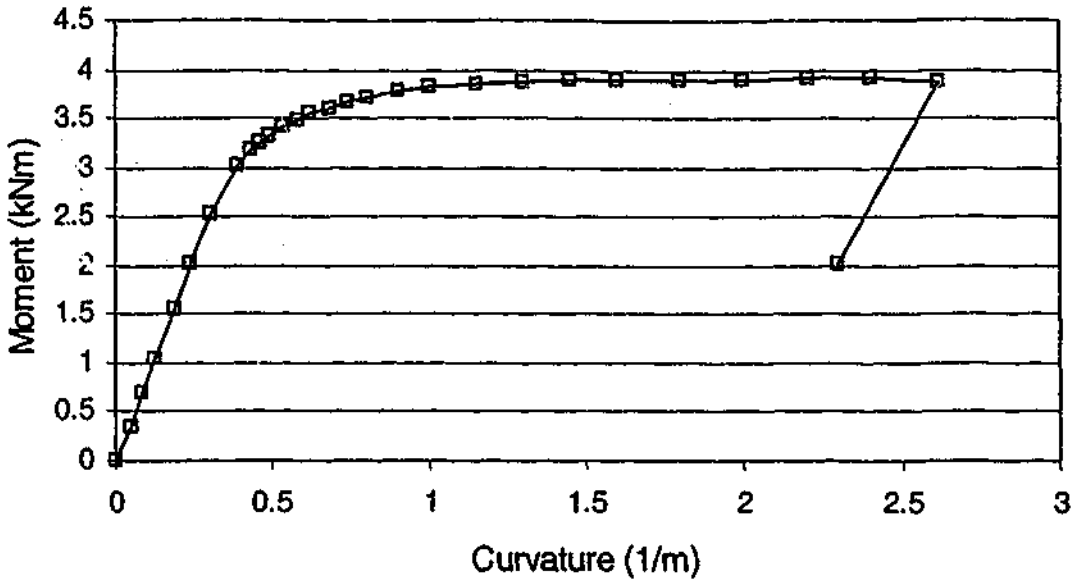

Figure B.1-6: Moment-curvature curve of specimen BS6

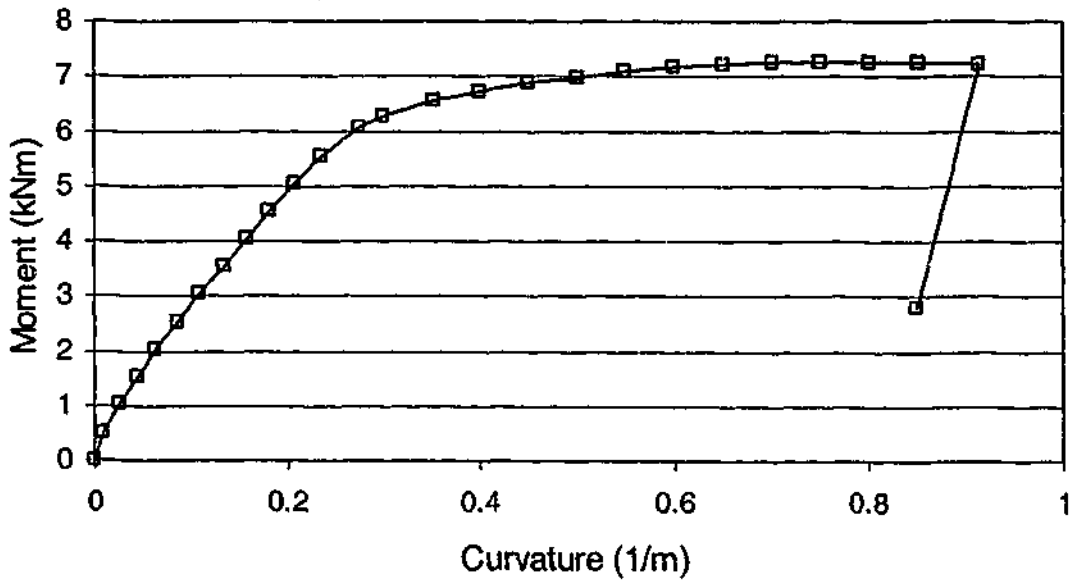

Figure B.1-7: Moment-curvature curve of specimen BS7

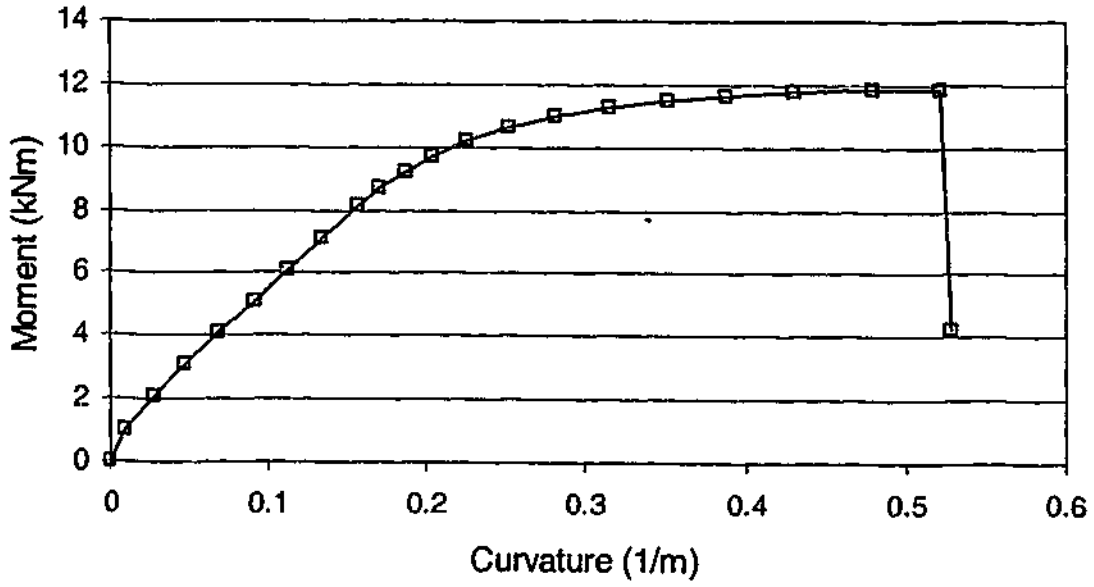

Figure B.1-8: Moment-curvature curve of specimen BS8

B.2 MOMENT-CURVATURE CURVES OF VHS TUBES IN PURE BENDING

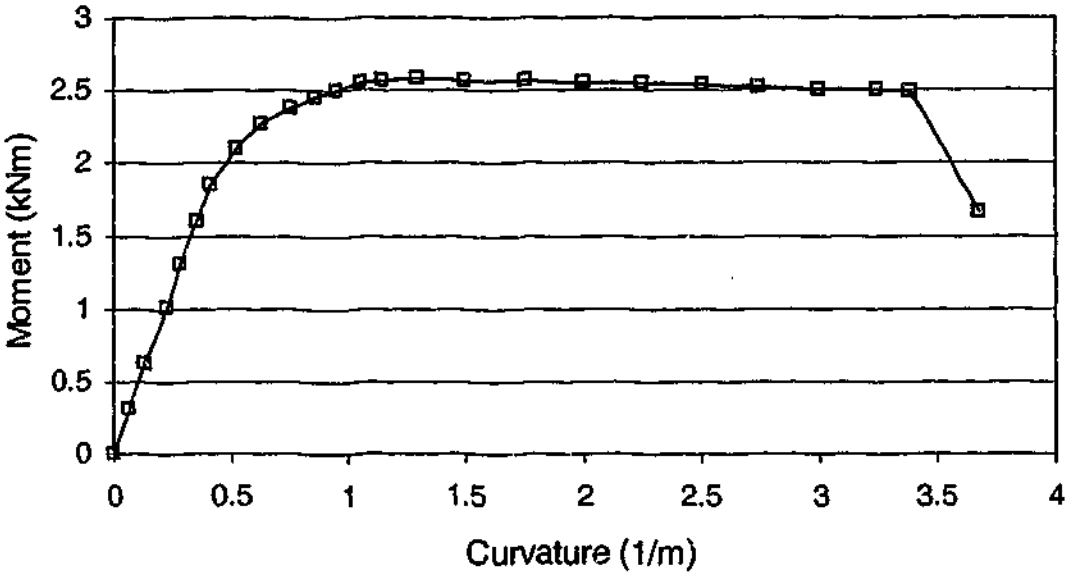

Figure B.2-1: Moment-curvature curve of specimen BS9

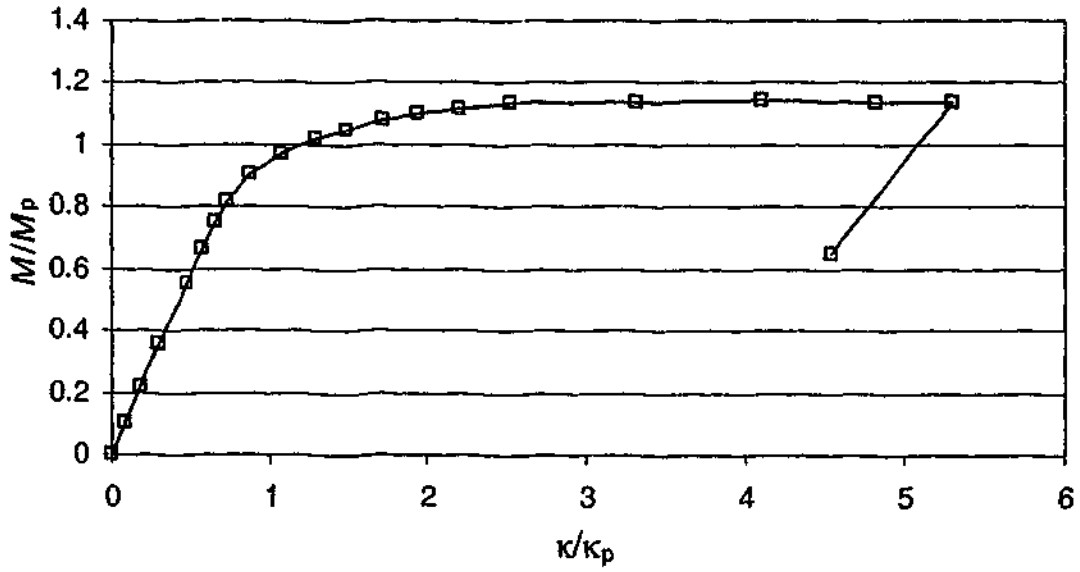

Figure B.2-2: Moment-curvature curve of specimen BS10

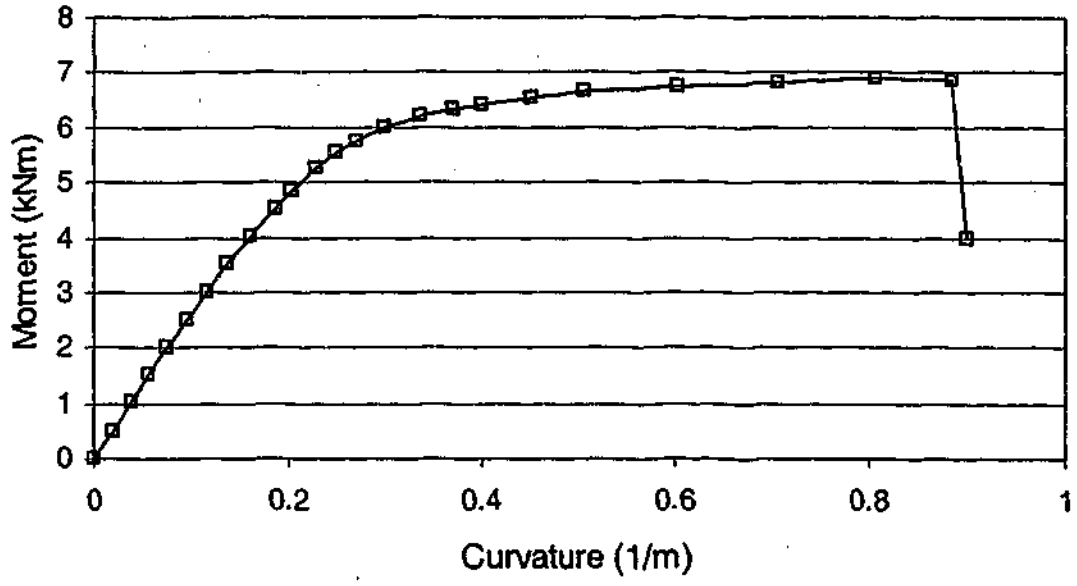

Figure B.2-3: Moment-curvature curve of specimen BS11

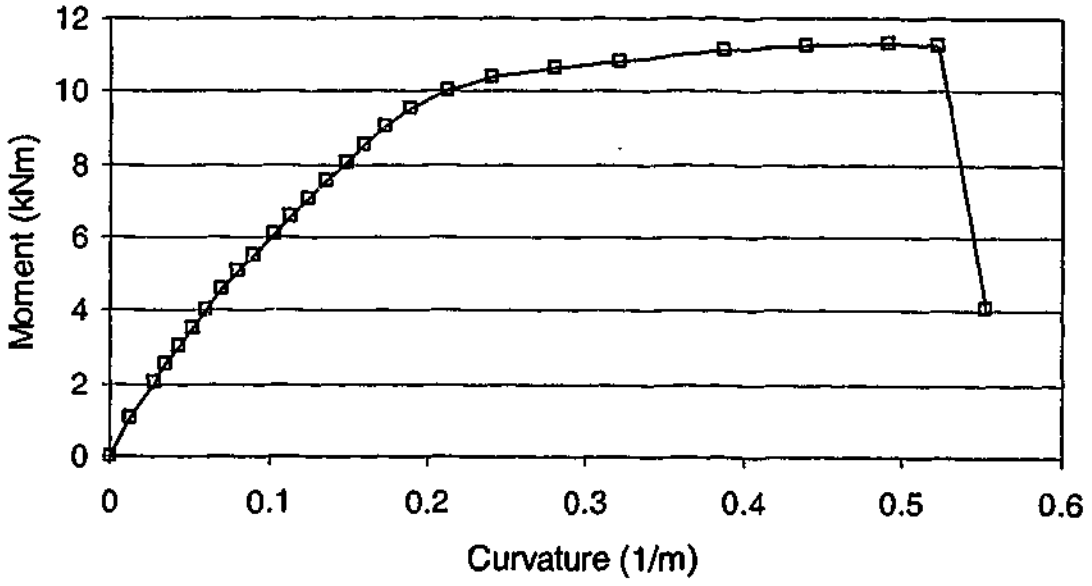

Figure B.2-4: Moment-curvature curve of specimen BS12

B.3 NORMALIZED MOMENT-CURVATURE CURVES OF VHS TUBES IN 4-POINT-BENDING

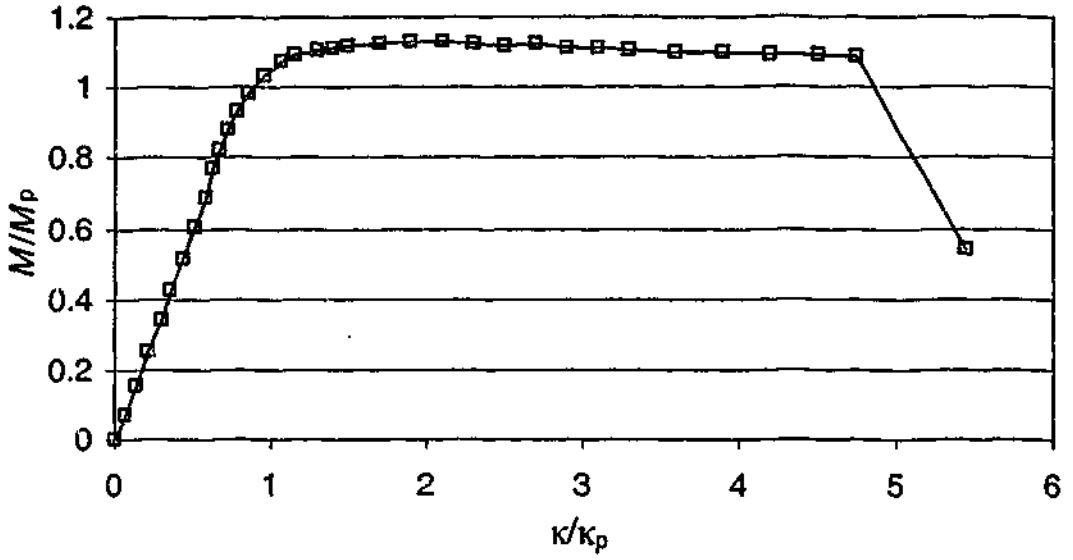

Figure B.3-1: Normalized moment-curvature curve of specimen BS1

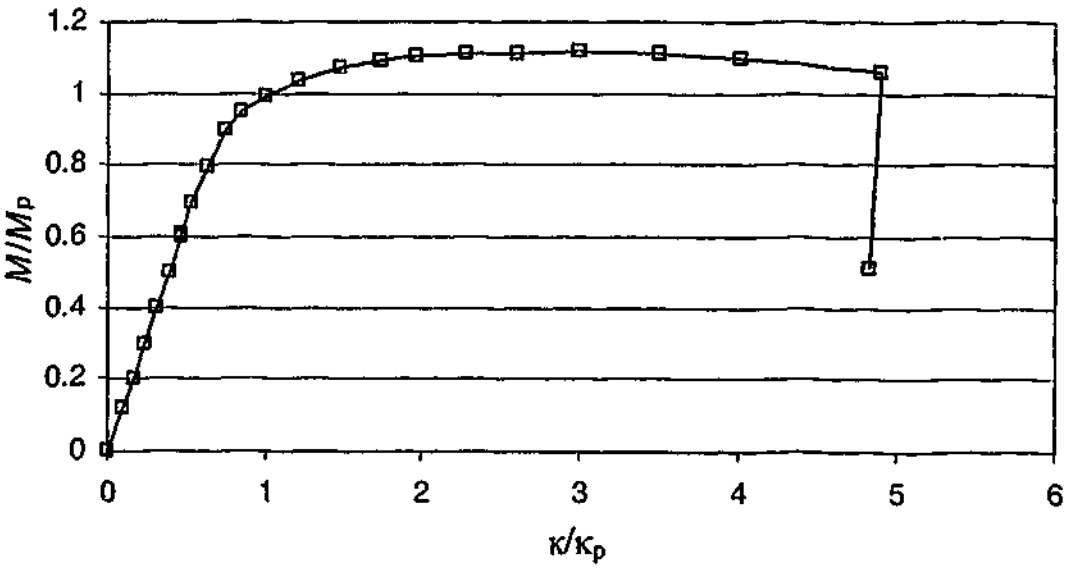

Figure B.3-2: Normalized moment-curvature curve of specimen BS2

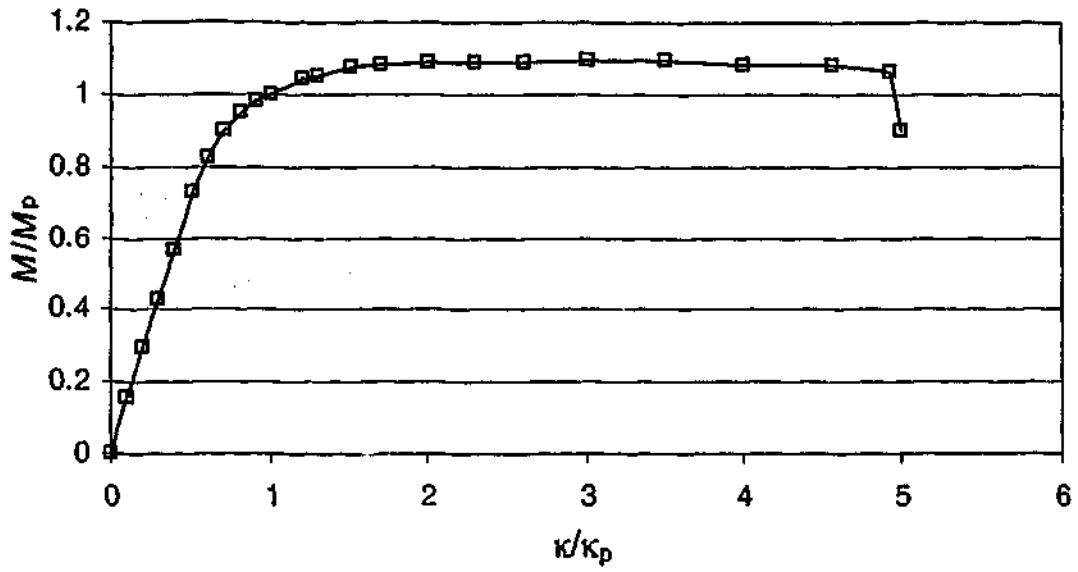

Figure B.3-3: Normalized moment-curvature curve of specimen BS3

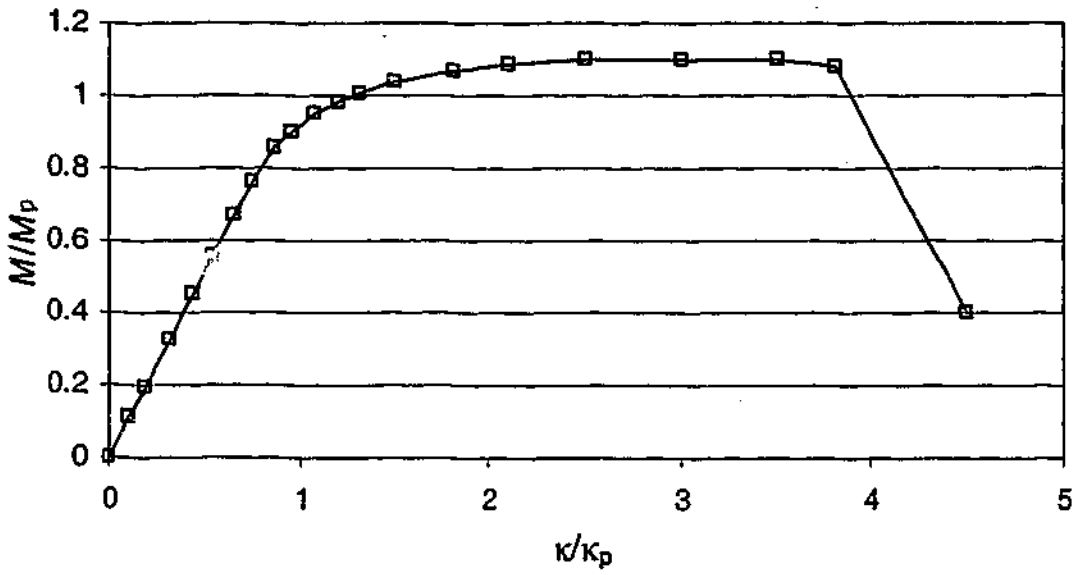

Figure B.3-4: Normalized moment-curvature curve of specimen BS4

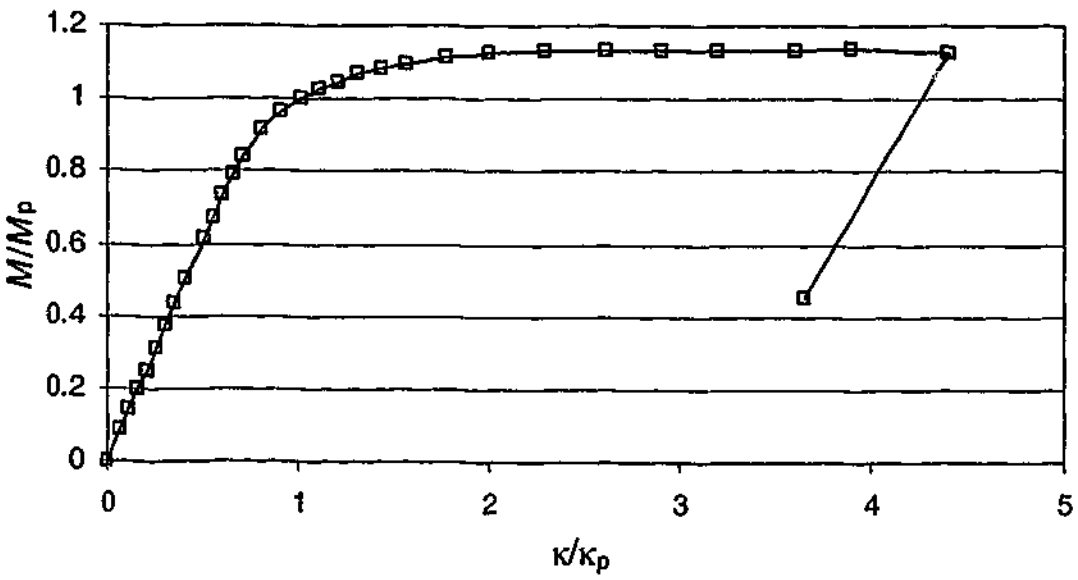

Figure B.3-5: Normalized moment-curvature curve of specimen BS5

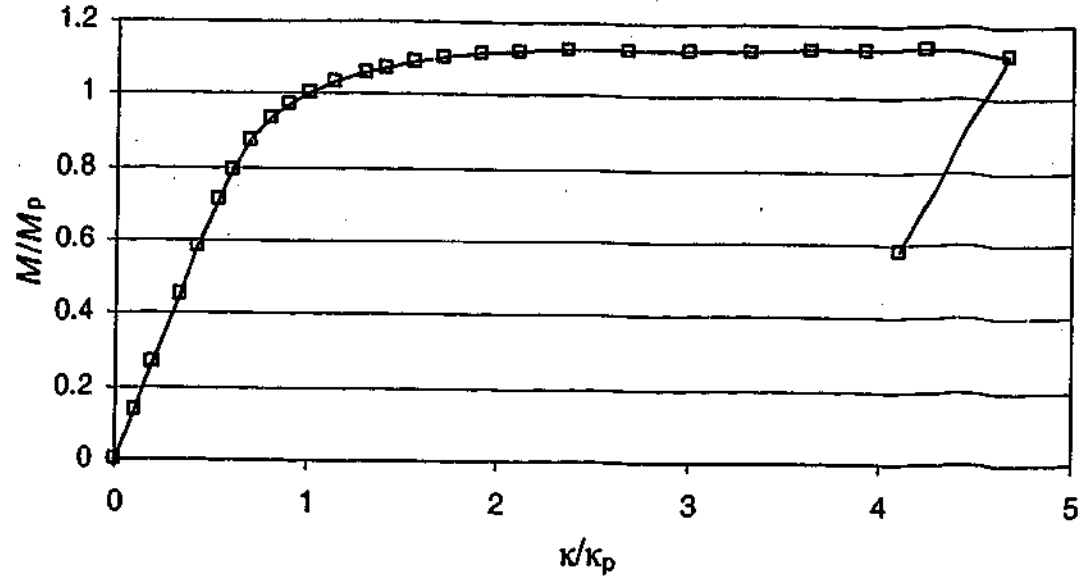

Figure B.3-6: Normalized moment-curvature curve of specimen BS6

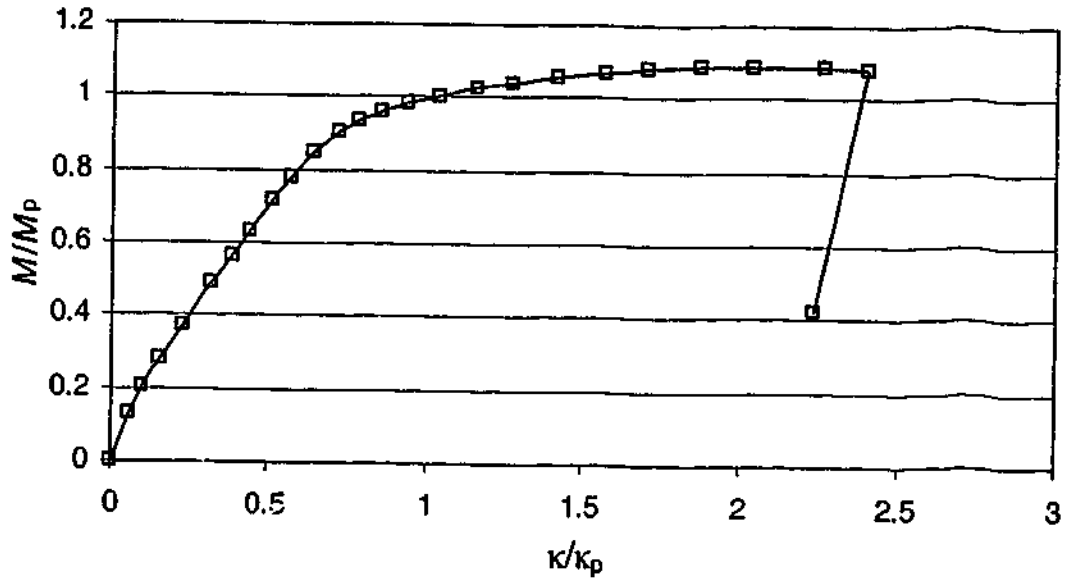

Figure B.3-7: Normalized moment-curvature curve of specimen BS7

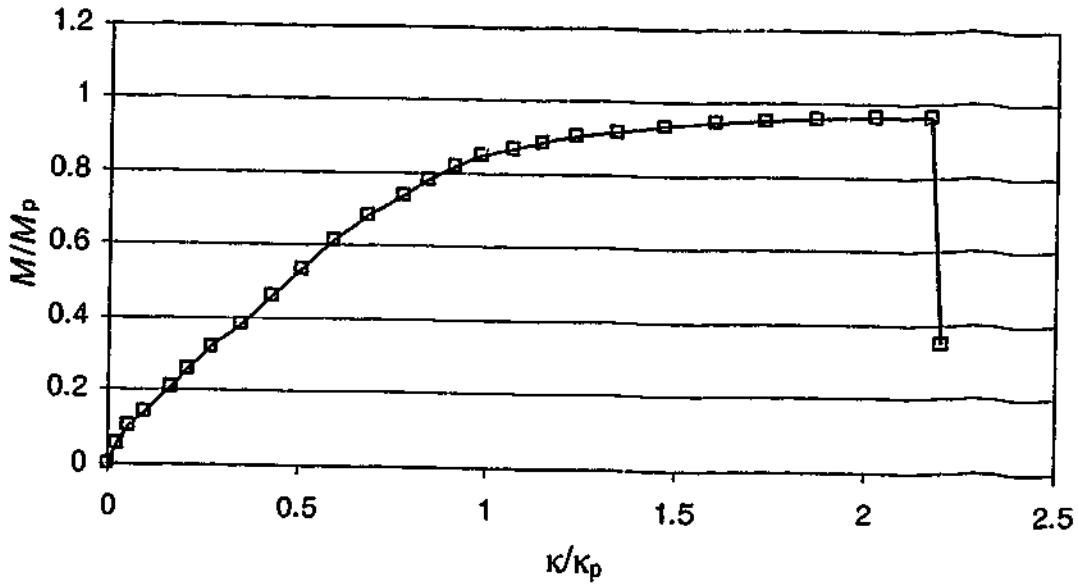

Figure B.3-8: Normalized moment-curvature curve of specimen BS8

B.4 NORMALIZED MOMENT-CURVATURE CURVES OF VHS TUBES IN PURE BENDING

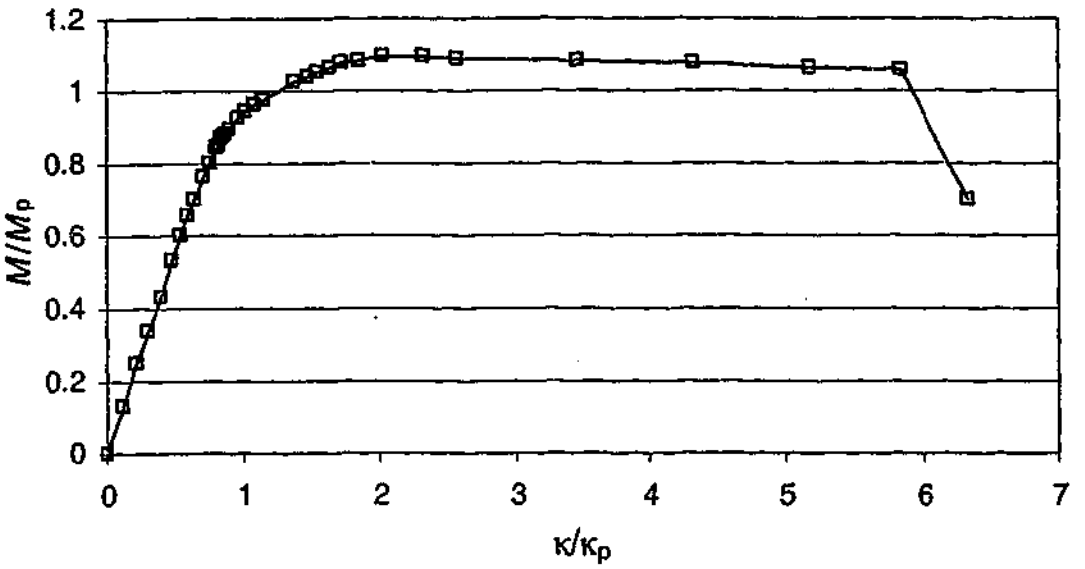

Figure B.4-1: Normalized moment-curvature curve of specimen BS9

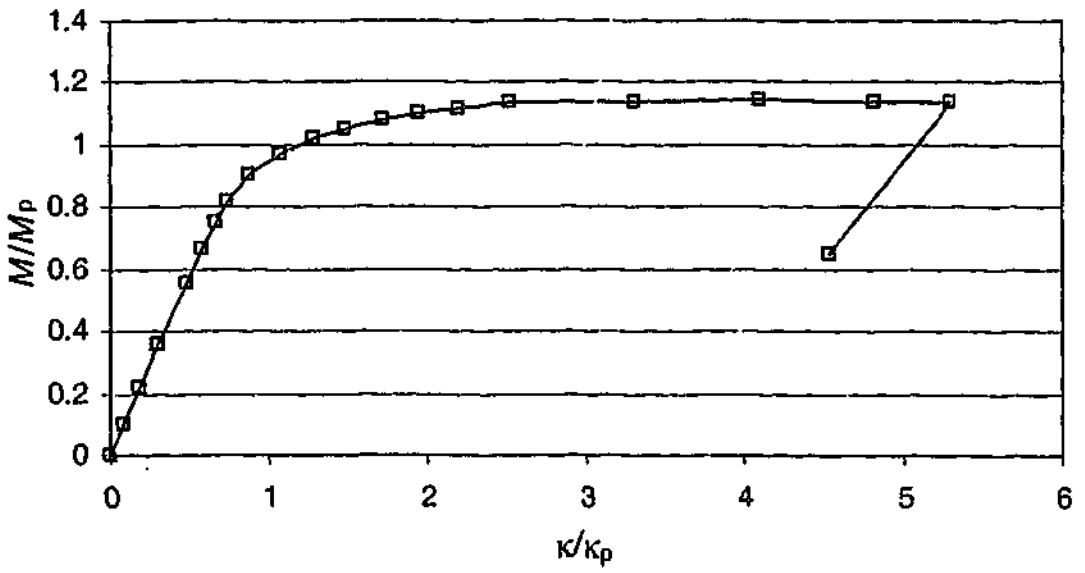

Figure B.4-2: Normalized moment-curvature curve of specimen BS10

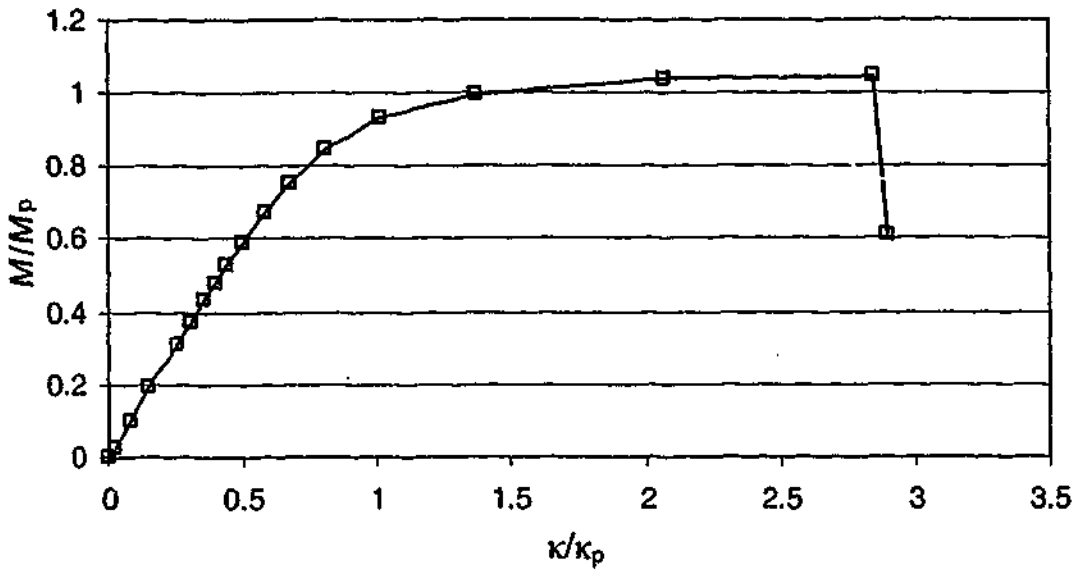

Figure B.4-3: Normalized moment-curvature curve of specimen BS11

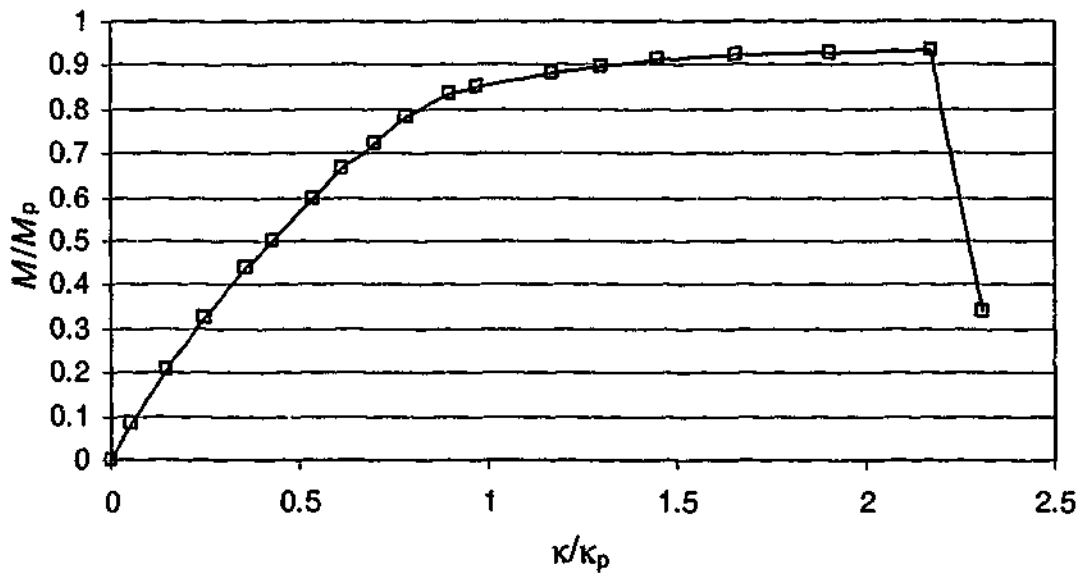

Figure B.4-4: Normalized moment-curvature curve of specimen BS12

APPENDIX C

C.1 STRESS-STRAIN CURVES OF BUTT-WELDED VHS TUBES IN TENSION

The strains on butt-welded and transverse fillet welded VHS tubes were average strains that were calculated from the displacement measured using two strain pots that were fixed on specimens shown in Figure F.2-4 of Appendix F. Strains on specimens of BWS1 to BWS4 and FWS1 to FWS2 were not measured by this method, therefore, stress-strain curves of these specimens are not listed here.

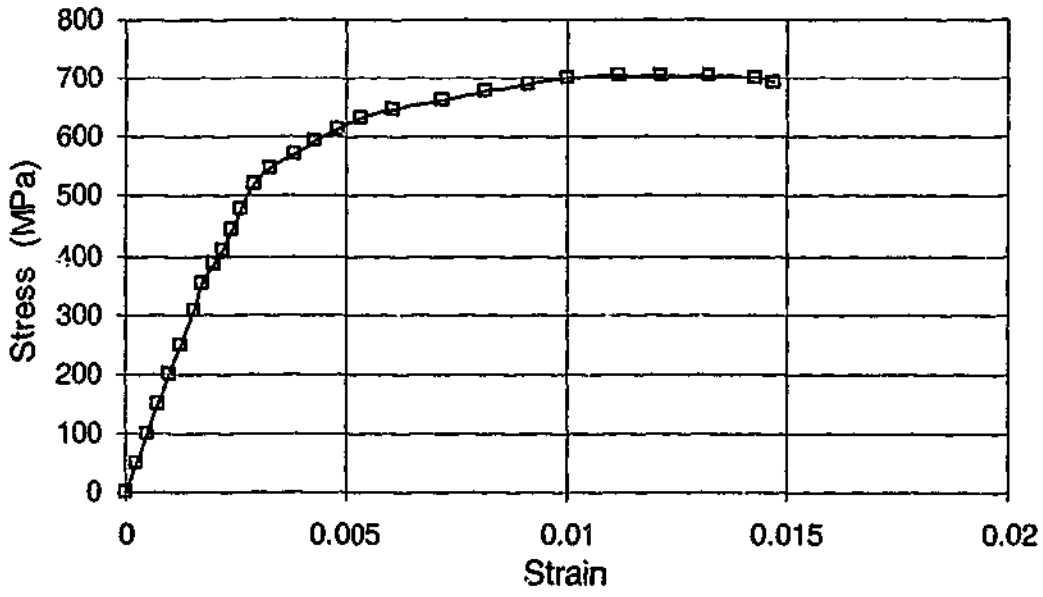

Figure C.1-1: Stress-strain curves of specimen BWS5

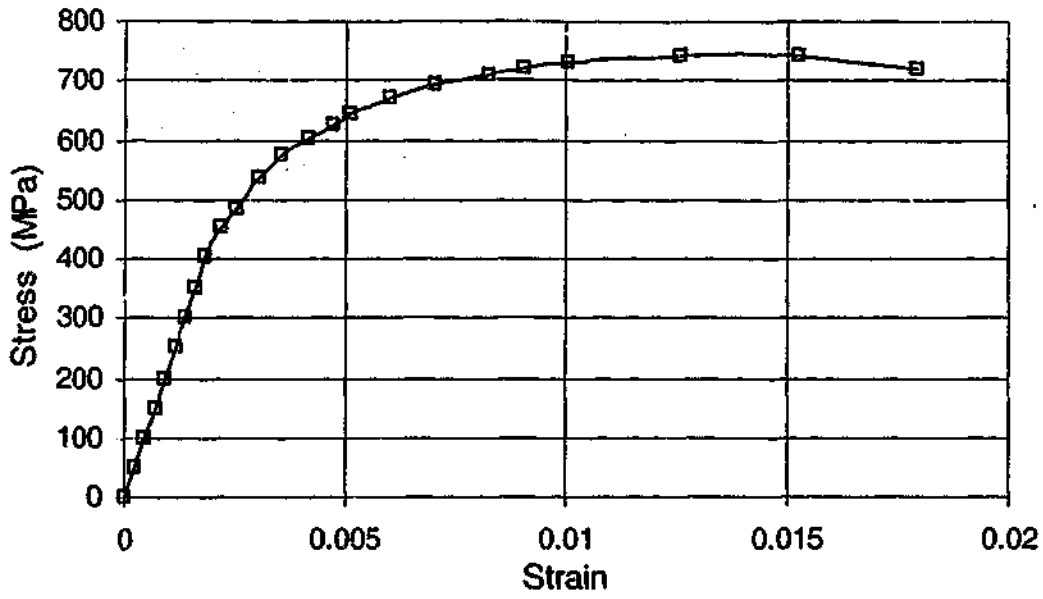

Figure C.1-2: Stress-strain curves of specimen BWS6

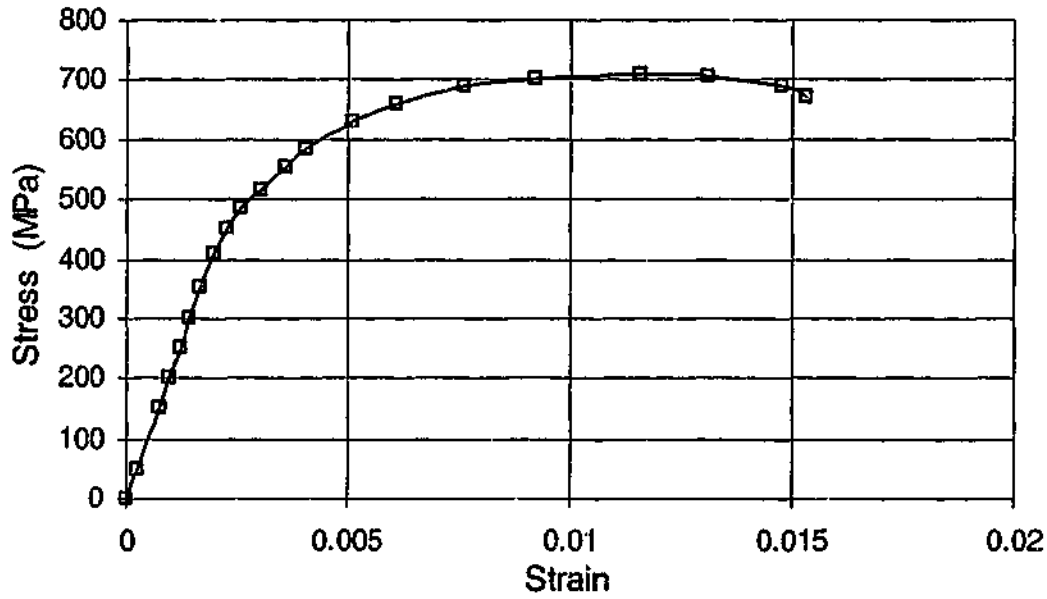

Figure C.1-3: Stress-strain curves of specimen BWS7

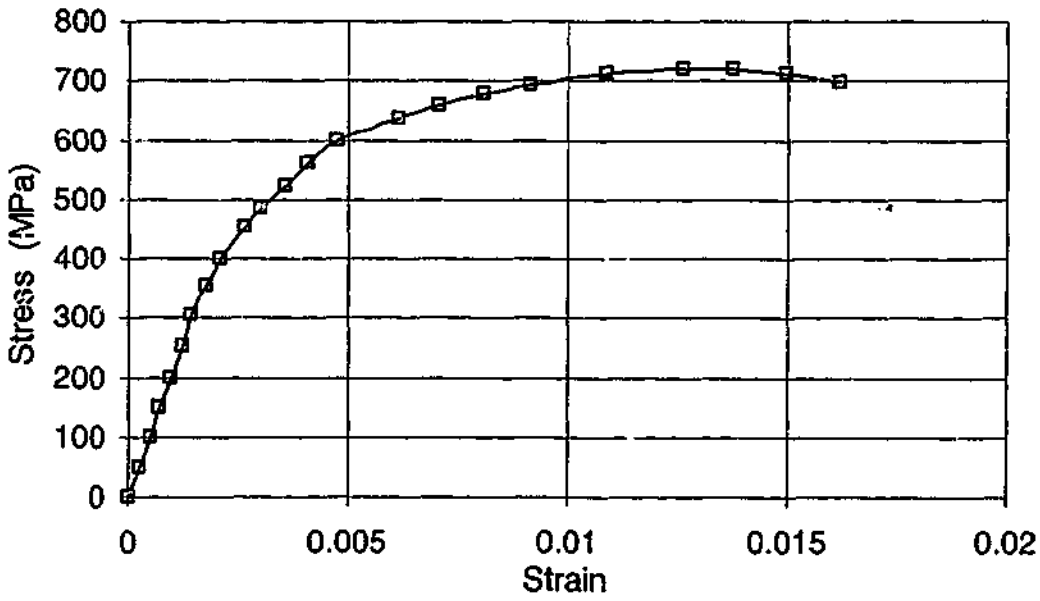

Figure C.1-4: Stress-strain curves of specimen BWS8

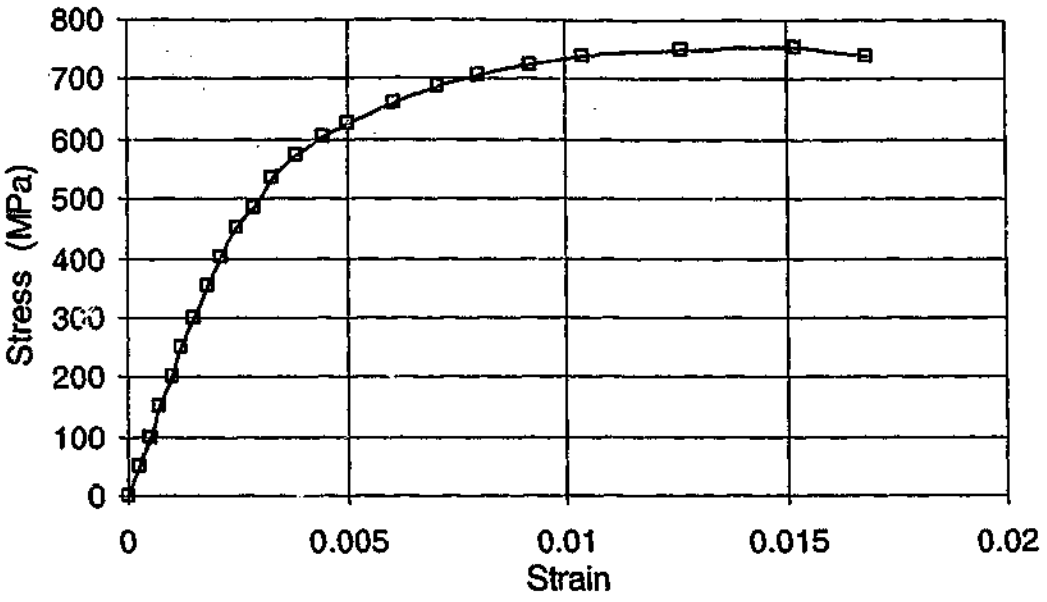

Figure C.1-5: Stress-strain curves of specimen BWS9

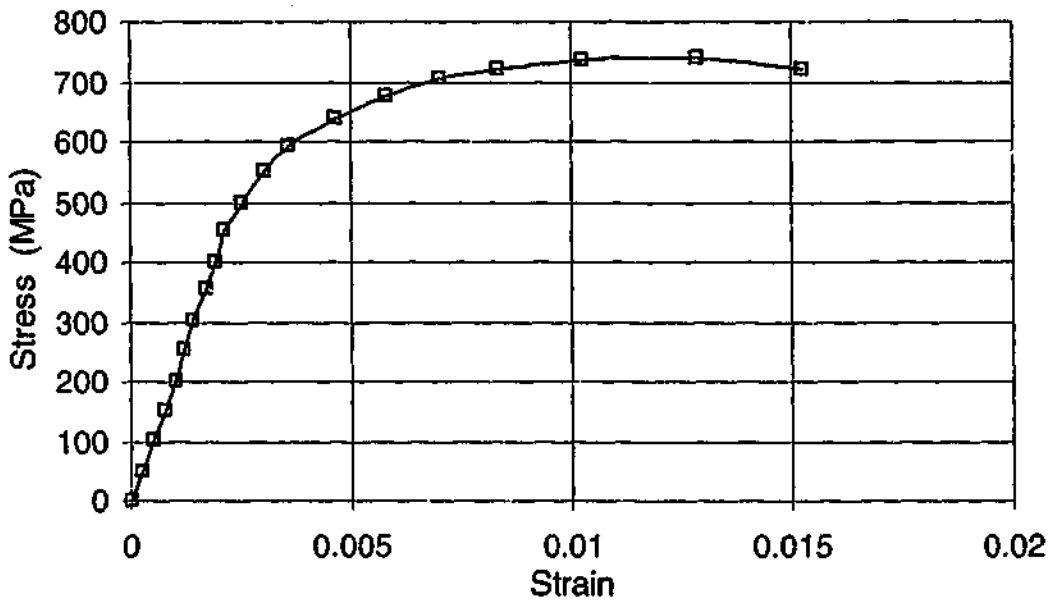

Figure C.1-6: Stress-strain curves of specimen BWS10

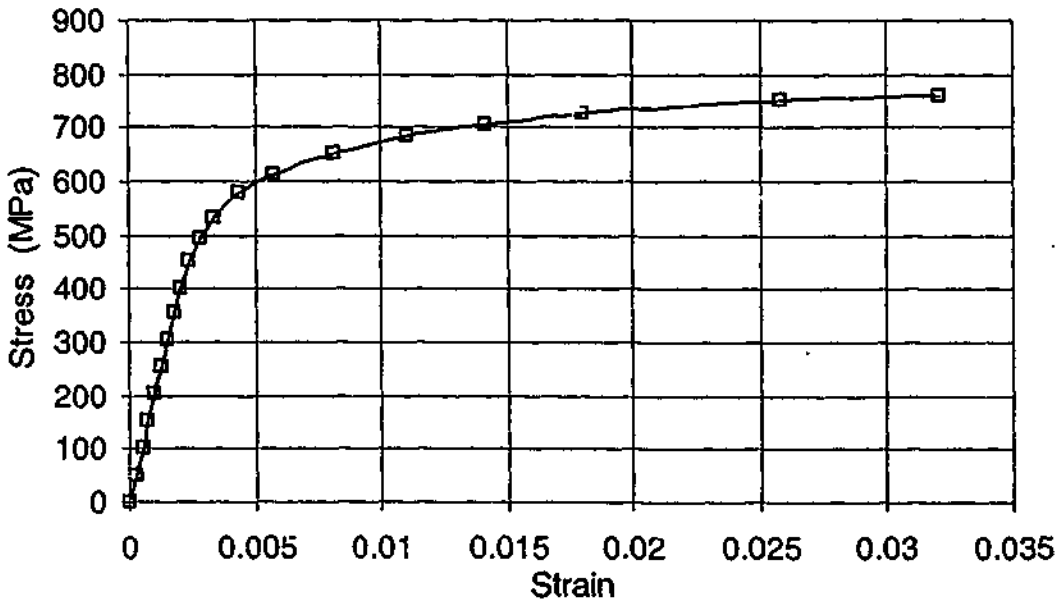

Figure C.1-7: Stress-strain curves of specimen BWS11

C.2 STRESS-STRAIN CURVES OF TRANSVERSE FILLET WELDED VHS TUBES IN TENSION

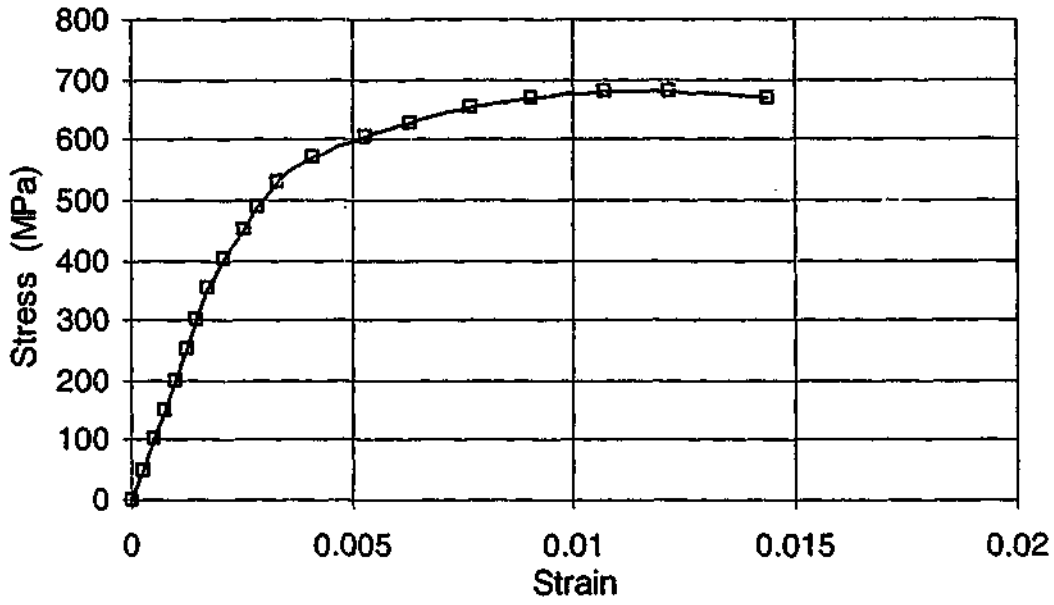

Figure C.2-1: Stress-strain curves of specimen FWS3

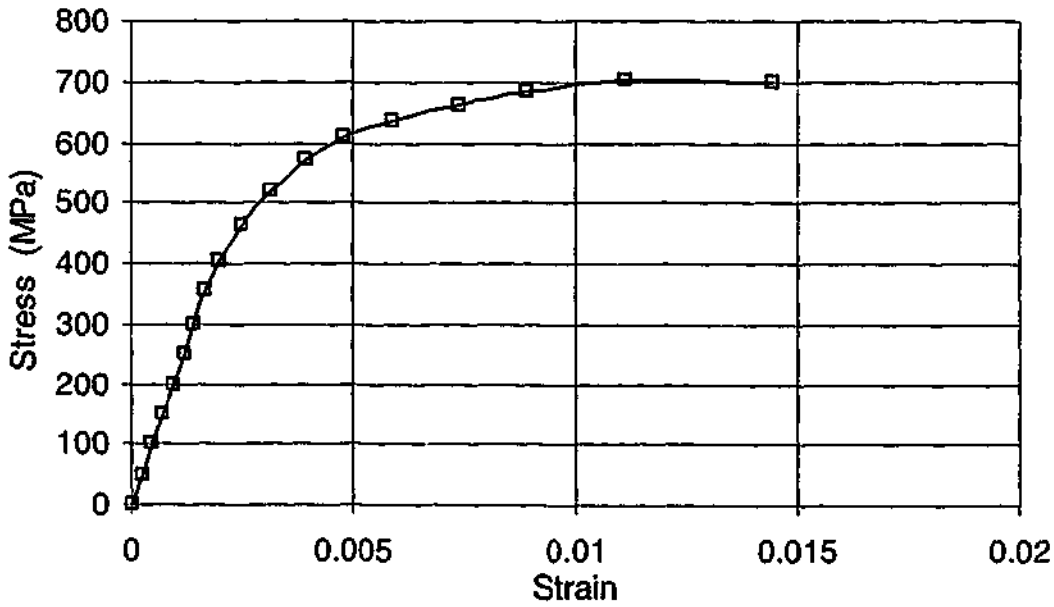

Figure C.2-2: Stress-strain curves of specimen FWS4

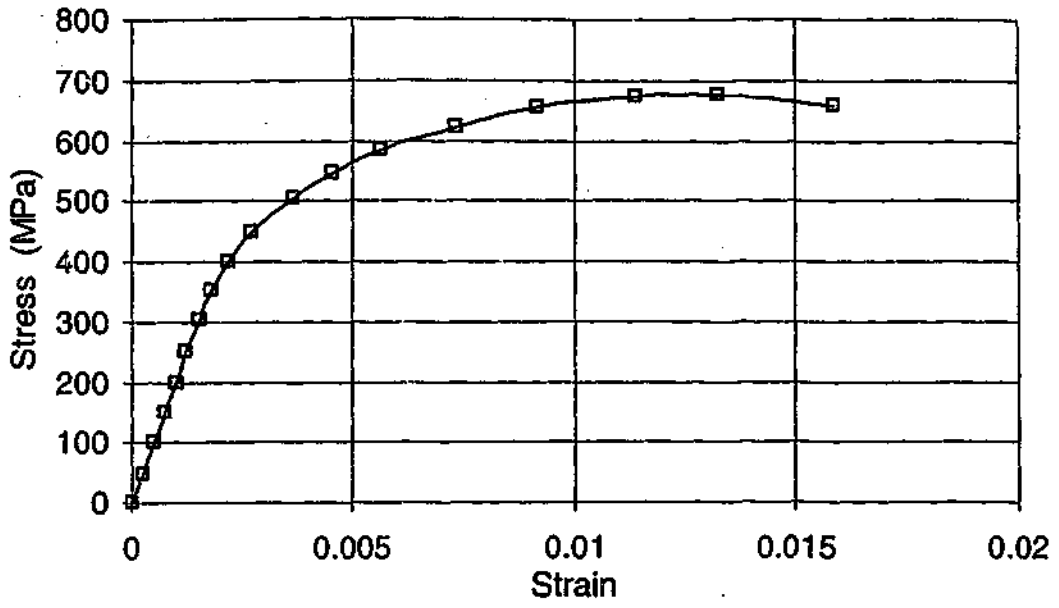

Figure C.2-3: Stress-strain curves of specimen FWS5

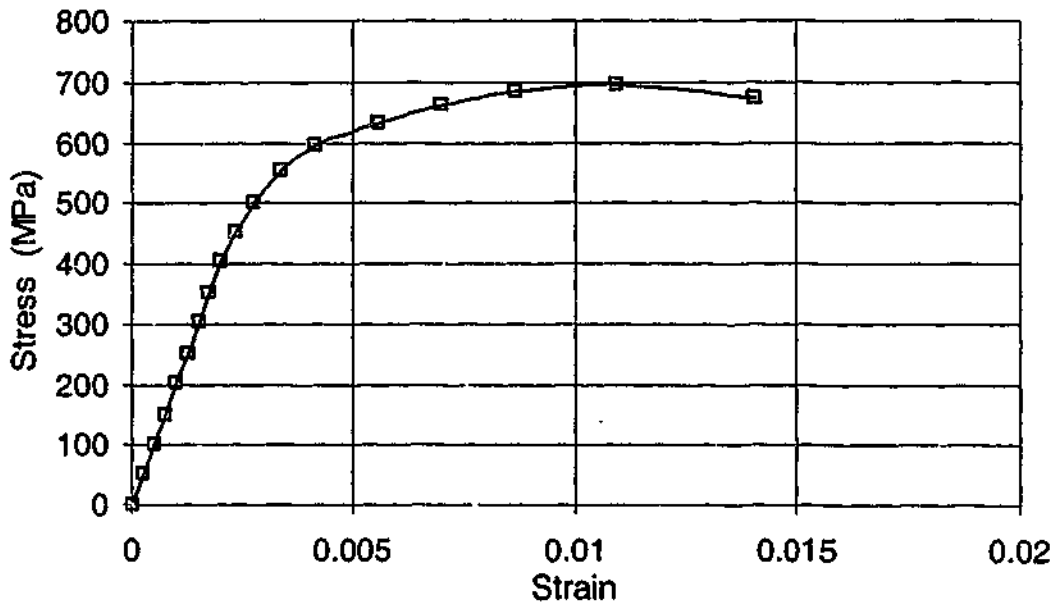

Figure C.2-4: Stress-strain curves of specimen FWS6

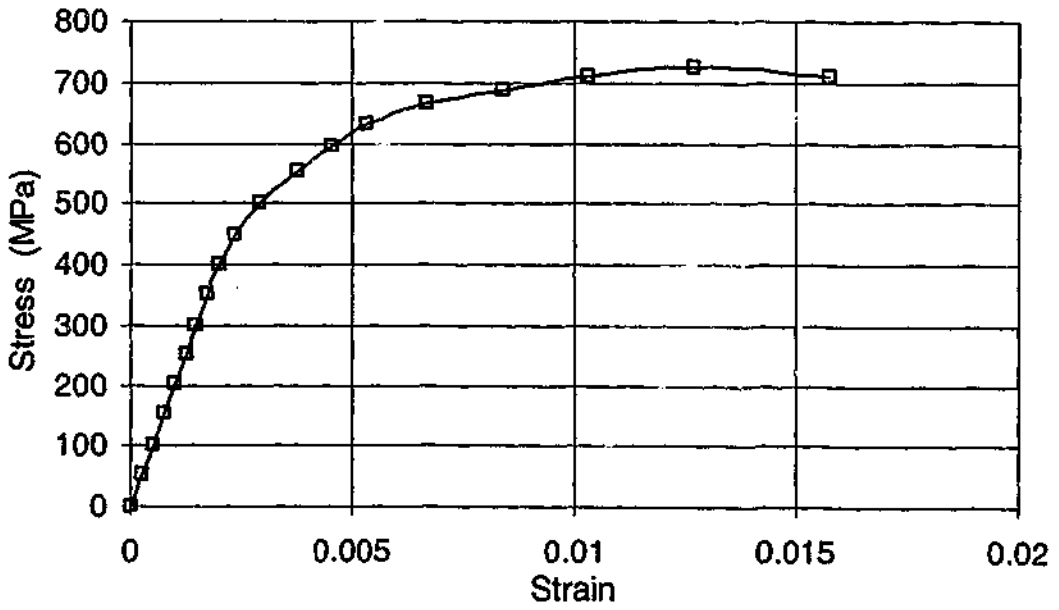

Figure C.2-5: Stress-strain curves of specimen FWS7

APPENDIX D

D.1 RESIDUAL STRESS MEASUREMENT

The measurement of residual stress of VHS and non-heat-treated (NHT) tubes are shown in the following tables. Strains were measured using the strain gauge measurement device, MCM1, which is shown in Figure D.2-2.

Table D.1-1: Residual stress measurement of VHS tubes from the strain gauges mounted in position (a) of Figure D.1-1.

Strain gauge Number	1	2	3	4
Initial strain (From MCM1)	67	2084	1592	1554
Final Reading (From MCM1)	617	2390	1745	1694
Strain ($\times 10^{-6}$)	550	306	153	140
Residual Stress (MPa)	-110.0	-61.2	-30.6	-28.0
Position of strain gauge (From seam)	0°	90°	180°	270°

Table D.1-2: Residual stress measurement of VHS tubes from the strain gauges mounted in position (b) of Figure D.1-1.

Strain gauge Number	1	2	3	4
Initial strain (From MCM1)	817	2374	1816	460
Final Reading (From MCM1)	1054	2515	1936	539
Strain ($\times 10^{-6}$)	237	141	120	79
Residual Stress (MPa)	-47.4	-28.2	-24.0	-15.8
Position of strain gauge (From seam)	0°	90°	180°	270°

Table D.1-3: Residual stress measurement of VHS tubes from the strain gauges mounted in position (c) of Figure D.1-1

Strain gauge Number	1	2	3	4
Initial strain (From MCM1)	732	254	1003	612
Final Reading (From MCM1)	1034	490	1171	856
Strain ($\times 10^{-6}$)	302	236	168	244
Residual Stress (MPa)	-60.4	-47.2	-33.6	-48.8
Position of strain gauge (From seam)	0°	90°	180°	270°

Table D.1-4: Residual stress measurement of VHS tubes from the strain gauges mounted in position (d) of Figure D.1-1

Strain gauge Number	1	2	3	4
Initial strain (From MCM1)	735	928	943	657
Final Reading (From MCM1)	488	657	746	363
Strain ($\times 10^{-6}$)	-247	-271	-197	-294
Residual Stress (MPa)	49.4	54.2	39.4	58.8
Position of strain gauge (From seam)	0°	90°	180°	270°

Table D.1-5: Residual stress measurement of VHS tubes from the strain gauges mounted in position (e) of Figure D.1-1

Strain gauge Number	1	2	3	4
Initial strain (From MCM1)	1160	1087	1056	1298
Final Reading (From MCM1)	1493	1464	1335	1552
Strain ($\times 10^{-6}$)	333	377	279	254
Residual Stress (MPa)	-66.6	-75.4	-55.8	-50.8
Position of strain gauge (From seam)	0°	90°	180°	270°

Table D.1-6: Residual stress measurement of VHS tubes from the strain gauges mounted in position (f) of Figure D.1-1

Strain gauge Number	1	2	3	4
Initial strain (From MCM1)	787	831	972	522
Final Reading (From MCM1)	645	628	917	401
Strain ($\times 10^{-6}$)	-142	-203	-55	-121
Residual Stress (MPa)	28.4	40.6	11.0	24.2
Position of strain gauge (From seam)	0°	90°	180°	270°

Table D.1-7: Residual stress measurement of NHT tubes from the strain gauges mounted in position (a) of Figure D.1-2

Strain gauge Number	1	2	3	4
Initial strain (From MCM1)	1388	2061	1118	959
Final Reading (From MCM1)	938	1651	633	538
Strain ($\times 10^{-6}$)	-450	-410	-485	-421
Residual Stress (MPa)	90.0	82.0	97.0	84.2
Position of strain gauge (From seam)	0°	90°	180°	270°

Table D.1-8: Residual stress measurement of NHT tubes from the strain gauges mounted in position (b) of Figure D.1-2

Strain gauge Number	1	2	3	4
Initial strain (From MCM1)	1742	2106	1274	982
Final Reading (From MCM1)	107	616	-121	-388
Strain ($\times 10^{-6}$)	-1635	-1490	-1395	-1370
Residual Stress (MPa)	327.0	298.0	279.0	274.0
Position of strain gauge (From seam)	0°	90°	180°	270°

Table D.1-9: Residual stress measurement of NHT tubes from the strain gauges mounted in position (c) of Figure D.1-2

Strain gauge Number	1	2	3	4
Initial strain (From MCM1)	740	1120	450	1004
Final Reading (From MCM1)	424	846	203	645
Strain ($\times 10^{-6}$)	-316	-274	-247	-359
Residual Stress (MPa)	63.2	54.8	49.4	71.8
Position of strain gauge (From seam)	0°	90°	180°	270°

Table D.1-10: Residual stress measurement of NHT tubes from the strain gauges mounted in position (d) of Figure D.1-2

Strain gauge Number	1	2	3	4
Initial strain (From MCM1)	2130	1609	1625	1538
Final Reading (From MCM1)	2668	2169	2055	2182
Strain ($\times 10^{-6}$)	538	560	430	644
Residual Stress (MPa)	-107.6	-112.0	-86.0	-128.8
Position of strain gauge (From seam)	0°	90°	180°	270°

Table D.1-11: Residual stress measurement of NHT tubes from the strain gauges mounted in position (e) of Figure D.1-2

Strain gauge Number	1	2	3	4
Initial strain (From MCM1)	1049	1335	1725	1400
Final Reading (From MCM1)	-466	-45	660	220
Strain ($\times 10^{-6}$)	-1515	-1380	-1065	-1180
Residual Stress (MPa)	303.0	276.0	213.0	236.0
Position of strain gauge (From seam)	0°	90°	180°	270°

Table D.1-12: Residual stress measurement of NHT tubes from the strain gauges mounted in position (f) of Figure D.1-2

Strain gauge Number	1	2	3	4
Initial strain (From MCM1)	398	1384	1054	1140
Final Reading (From MCM1)	1761	2440	2026	1887
Strain ($\times 10^{-6}$)	1363	1056	972	747
Residual Stress (MPa)	-272.6	-211.2	-194.4	-149.4
Position of strain gauge (From seam)	0°	90°	180°	270°

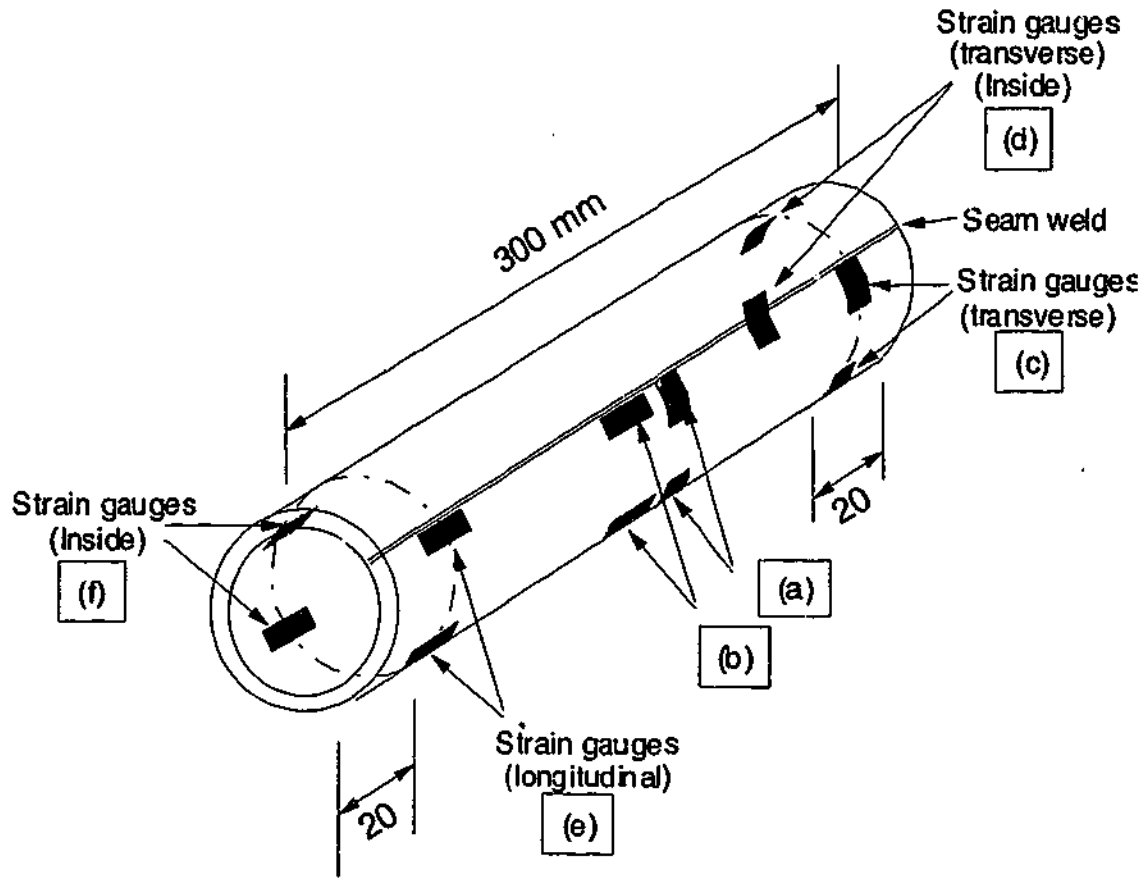

Figure D.1-1: Positions of strain gauges mounted on **VHS tube**

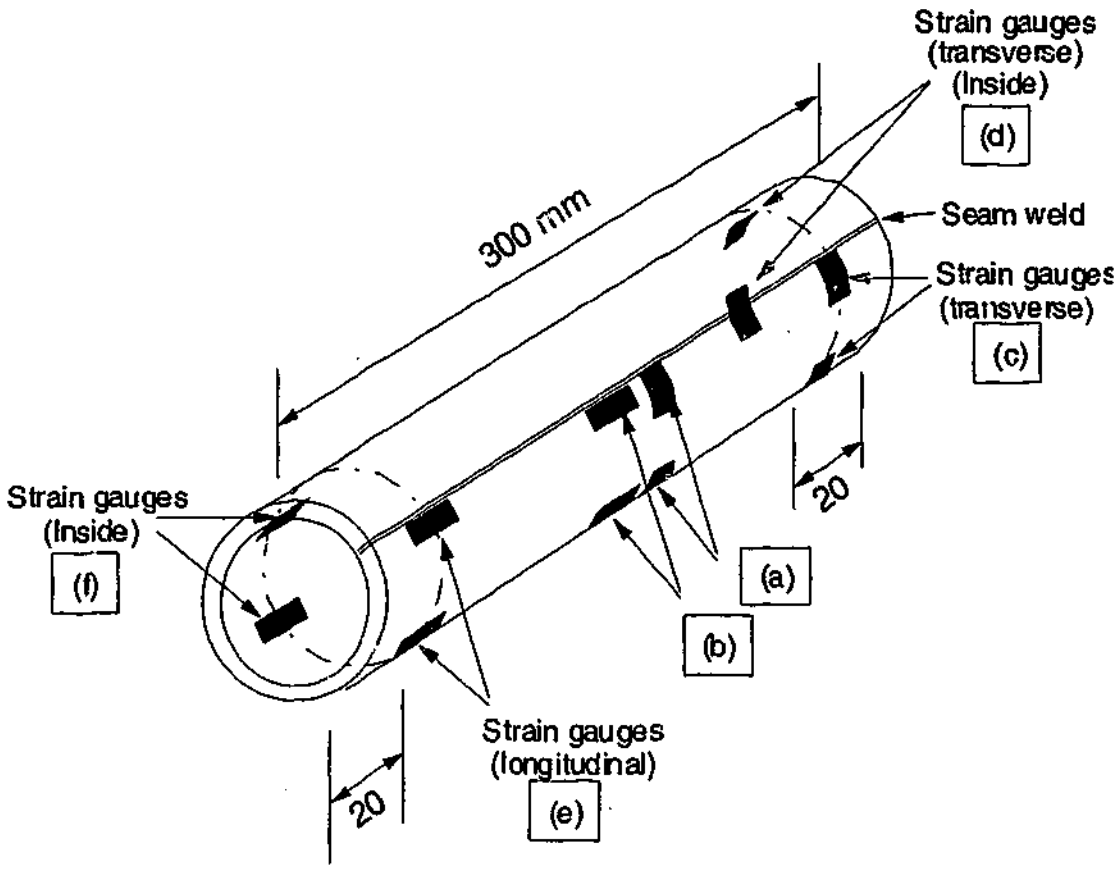

Figure D.1-2: Positions of strain gauges mounted on **NHT tube**

D.2 PHOTOS OF RESIDUAL STRESS MEASUREMENT

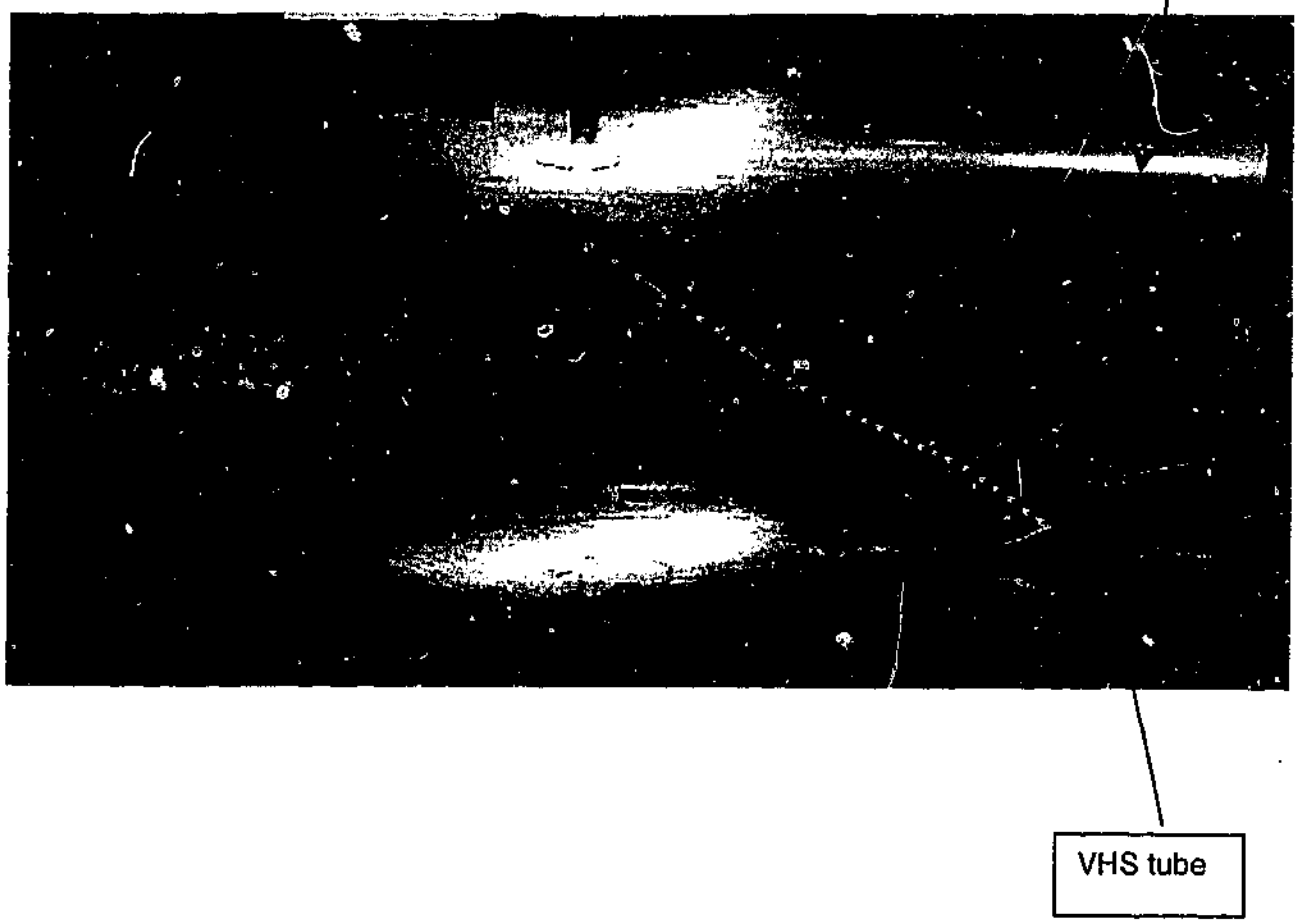

Figure D.2-1: Strain gauges were mounted on tube surface in transverse and longitudinal directions.

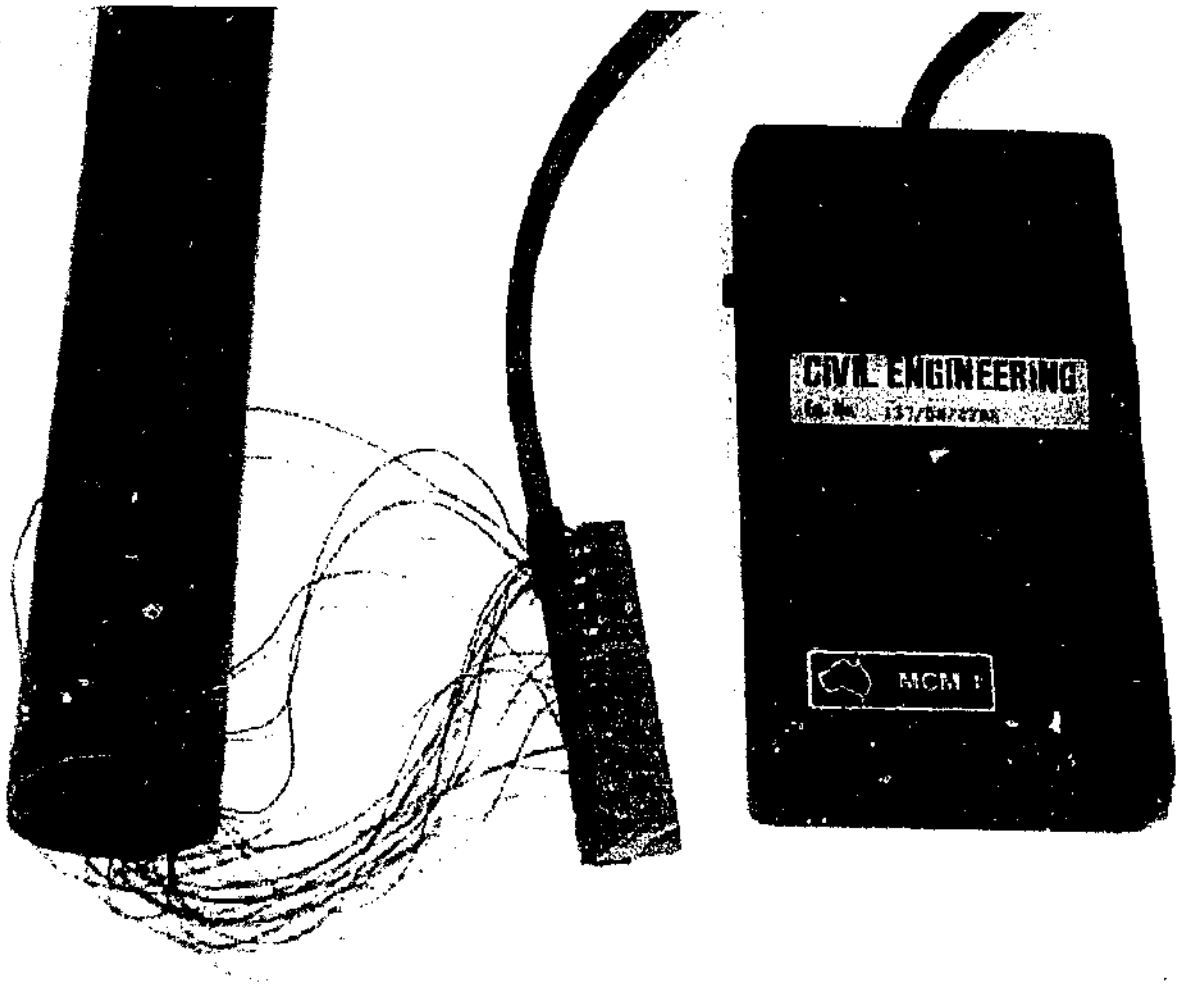

Figure D.2-2: Strains were measured with the strain measurement device (MCM1)

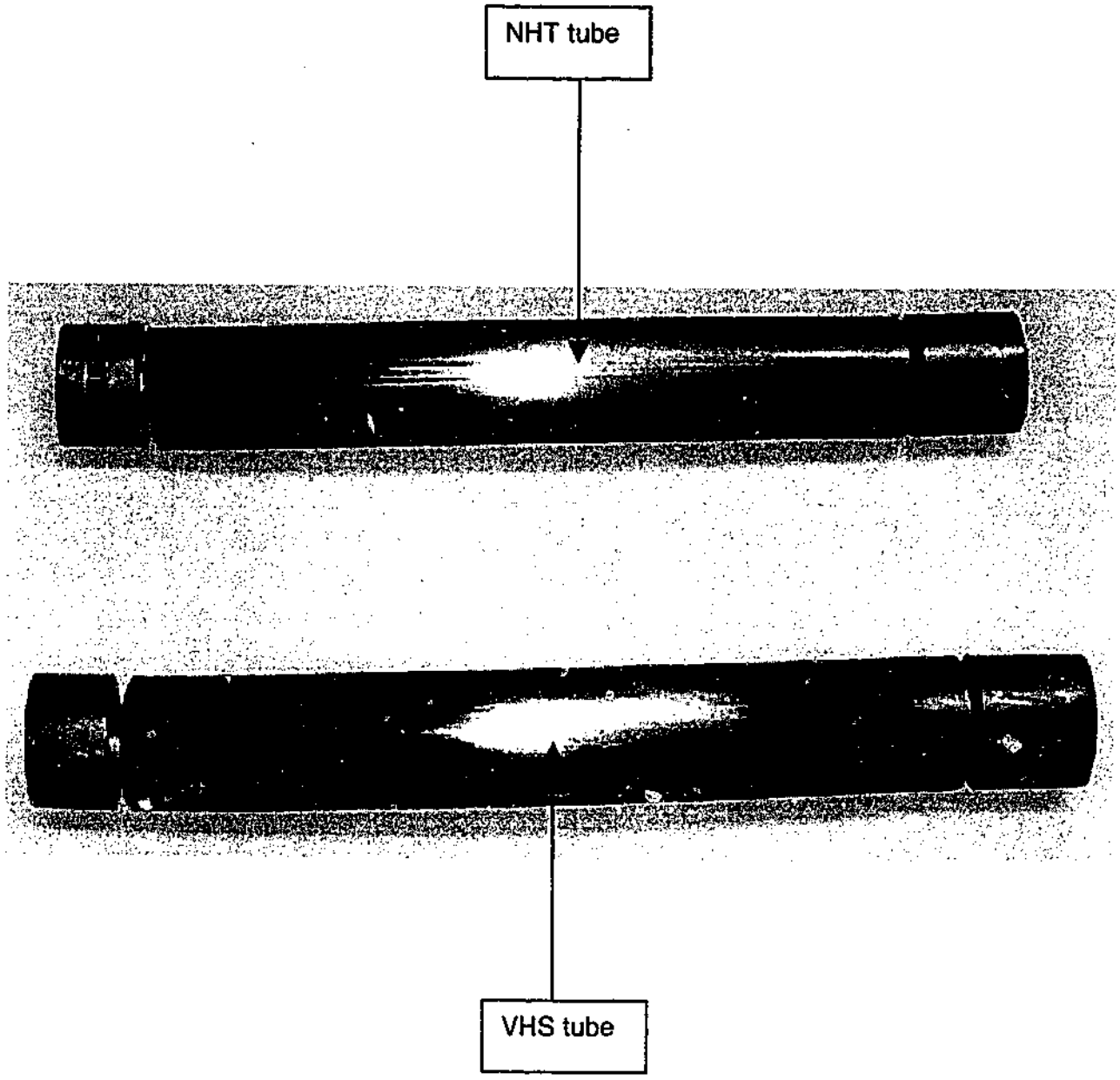

Figure D.2-3: Tubes were cut with a handsaw

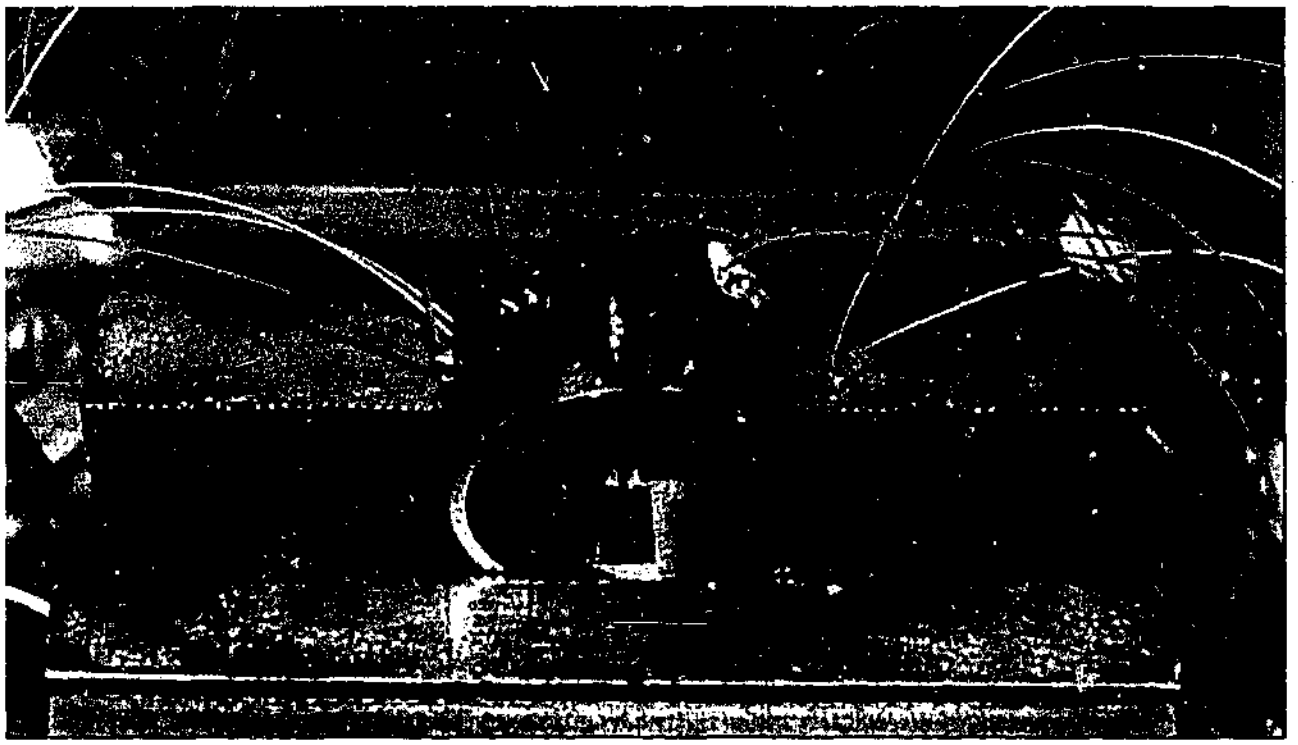

Figure D.2-4: A specimen was to be cut (Strain gauge in longitudinal direction)

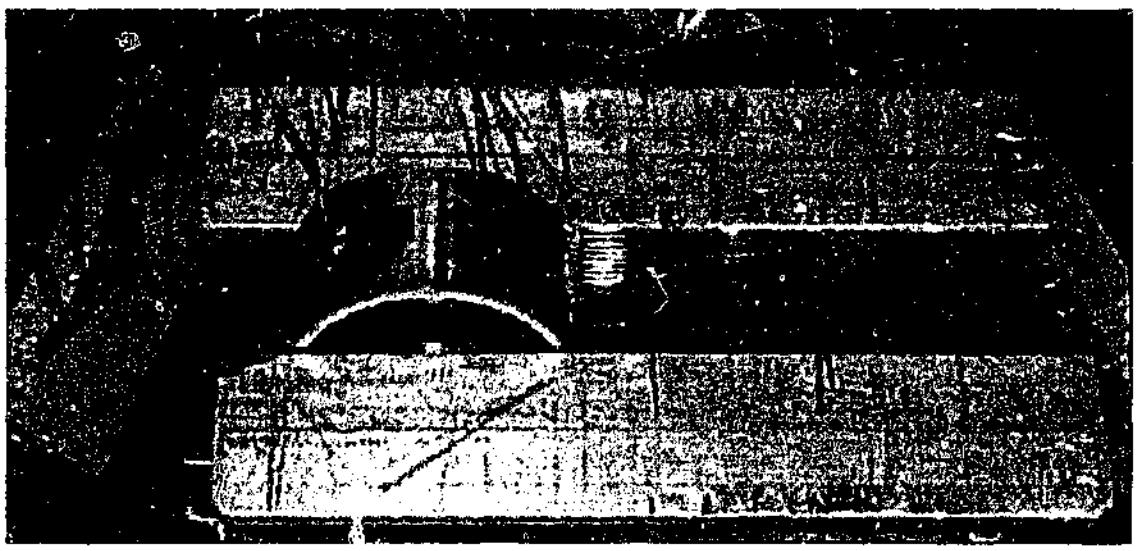

Figure D.2-5: A specimen was to be cut (Strain gauge in transverse direction)

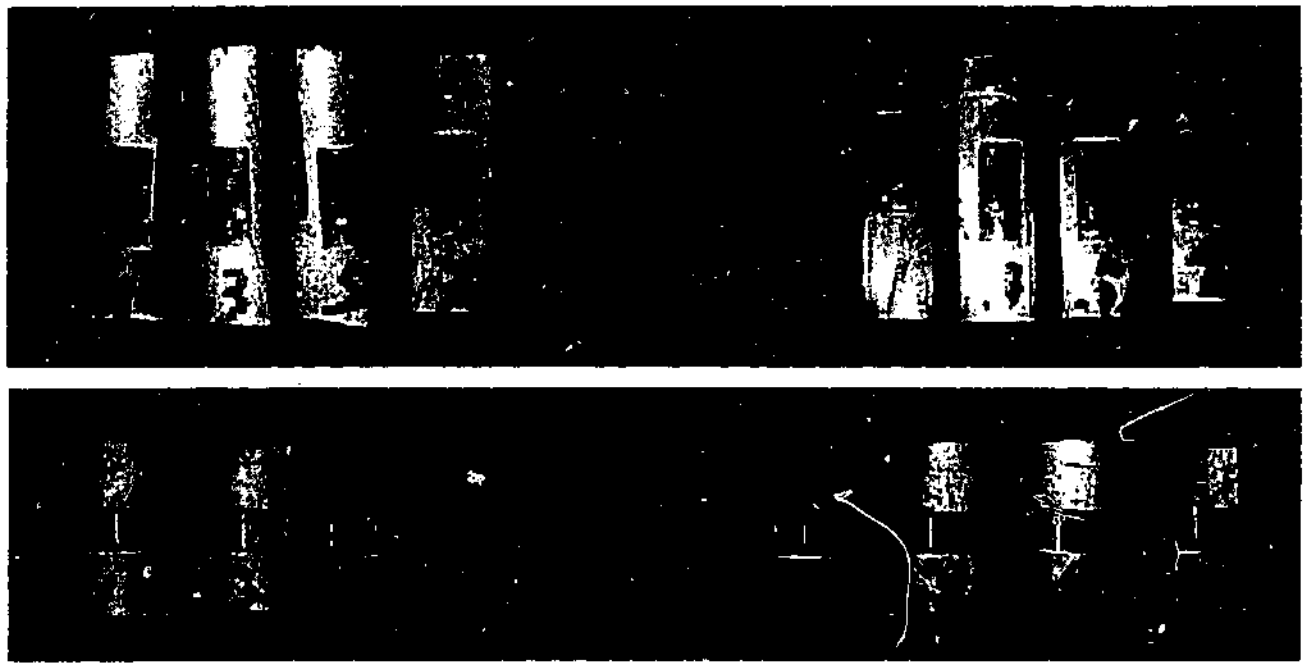

Figure D.2-6: Tubes were cut into small pieces

APPENDIX E

E.1 ADES'S OVALISATION THEORY

For a circular hollow section under pure bending, the section will flatten. Three assumptions were made for the ovalisation by Ades (1957): (1) The ovalled shape was assumed to be elliptical. (2) The circumference remained the same for the ellipse and the initial circular cross section. (3) The material was isotropic with the same stress-strain curves in tension and compression. In addition, Ades (1957) also assumed that the tube was subjected to pure bending and the tube was long enough that the end effect could be ignored.

The basic expressions needed for the calculation of the strain energy for an ovalled tube were given by Ades (1957) and are repeated as follows:

In the elastic range, the work per unit length of a small element (dW) can be expressed as:

$$dW = (\frac{1}{2}\sigma_L \varepsilon_L + \frac{1}{2}\sigma_T \varepsilon_T) d\zeta ds \qquad \text{(E.1-1)}$$

where σ_L, ε_L and σ_T, ε_T are the stress and strain in the longitudinal and transverse directions; $d\zeta$ and ds are the unit length of a small element shown in Figure E.1-1.

With the relationship between σ and ε:

$$\sigma_L = \frac{E}{1-\mu^2}(\varepsilon_L + \mu\varepsilon_T) \qquad \text{(E.1-2)}$$

$$\sigma_T = \frac{E}{1-\mu^2}(\varepsilon_T + \mu\varepsilon_L) \qquad \text{(E.1-3)}$$

Eq. (E.1-1) can be expressed as:

$$dW = \frac{E}{2(1-\mu^2)}(\varepsilon_L^2 + \varepsilon_T^2 + 2\mu\varepsilon_L\varepsilon_T)d\zeta ds \qquad \text{(E.1-4)}$$

If the strain intensity e_i is used, in that,

$$e_i = \sqrt{\frac{1}{1-\mu^2}(\varepsilon_L^2 + \varepsilon_T^2 + 2\mu\varepsilon_L\varepsilon_T)} \qquad \text{(E.1-5)}$$

Eq. (E.1-4) can be written as:

$$dW = \frac{E}{2}e_i^2 d\zeta ds = \frac{1}{2}(Ee_i)e_i d\zeta ds = \frac{1}{2}\sigma_i e_i d\zeta ds \qquad \text{(E.1-6)}$$

where σi is the stress intensity. The work is the area under the stress intensity-strain intensity curve. In elastic range, $\sigma_i = Ee_i$.

In plastic range, the work can still be given by the area under the stress intensity-strain intensity curve with the secant modulus E_s instead of Young's modulus E. The conventional stress-strain curve in an axial tension test was used as the stress intensity-strain intensity curve by Wilhoit and Merwin (1971). Poisson's ratio was taken as 0.25 and 0.5 in the elastic and plastic ranges respectively. The strains of ε_L and ε_T were expressed as:

$$\varepsilon_L = y/\rho = (y_m + \zeta\cos\alpha)/\rho \qquad \text{(E.1-7)}$$

$$\cos\alpha = \pm\{1 + \frac{b^2}{a^2}(1 - \frac{y_m^2}{b^2})/(y_m^2/b^2)\}^{-\frac{1}{2}} \qquad \text{(E.1-8)}$$

$$\varepsilon_T = \zeta(\frac{1}{\rho_T} - \frac{1}{r}) - \mu\frac{y_m}{\rho} \qquad \text{(E.1-9)}$$

where, r is the radius of the circular tube; ρ is the radius of the tube bending curvature; ρ_T is the radius of the ovalisation; α, y_m, ζ, a and b are illustrated in Figure E.1-1.

The principle of least work was used to determine the ovalled dimension of a/r. At a tube curvature of $1/\rho$, the total work was calculated for resumed different ovalled shapes of a/r. By comparing those works at the curvature of $1/\rho$, the target ovalisation of a/r would be corresponding to the tube section that had the least work.

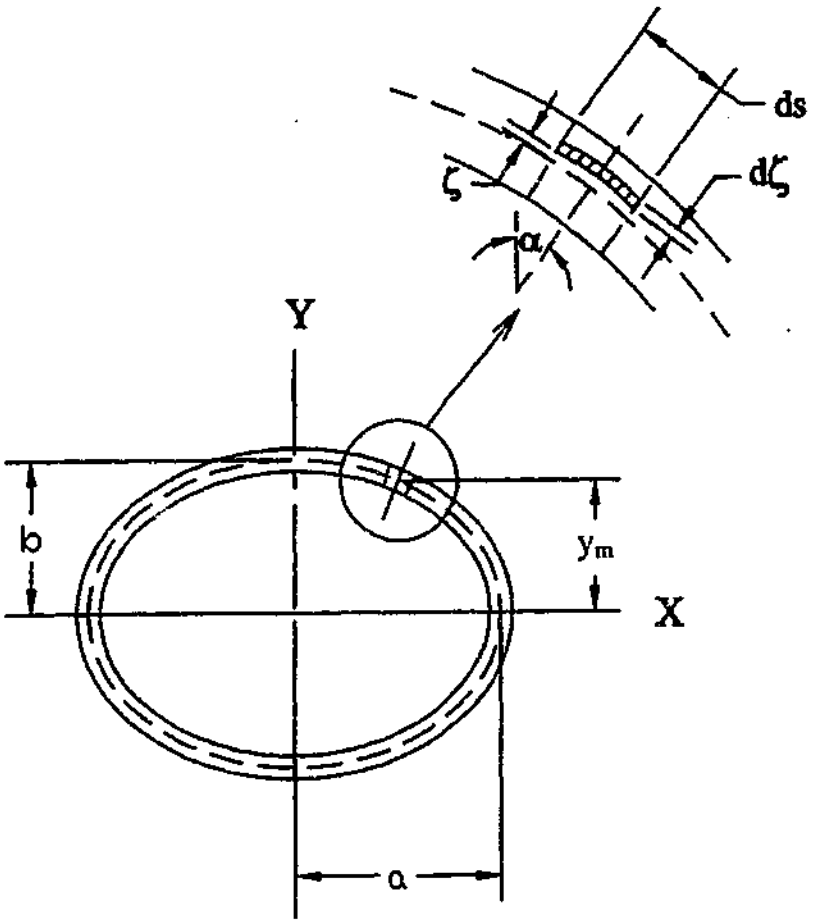

Figure E.1-1: A unit length on the ovalled tube

E.2 OVALISATION ANALYSIS OF VHS TUBES

Ades's ovalisation theory could be accomplished by writing a computer program (See Appendix E.3). The calculating process is explained as follows:

(1) Assume a curvature of 1/ρ;

(2) Assume a certain ovalisation of a/r;

(3) Calculate the intensive strain (e_i) at the five points on each of the 13 positions shown in Figure E.2-1. The half ellipse is equally divided into 12 sections. The integration is performed by using Simpson's rule (Gellert et al. 1977) as:

$$\int_a^b f(x)dx \approx \frac{h}{3}\sum_{i=0}^{m-1}(f(a+2ih)+4f(a+(2i+1)h)+f(a+2(i+1)h)) \qquad \text{(E.2-1)}$$

here m is the number of divisions between a and b; and h can be expressed as:

$$h = \frac{b-a}{2m} \qquad \text{(E.2-2)}$$

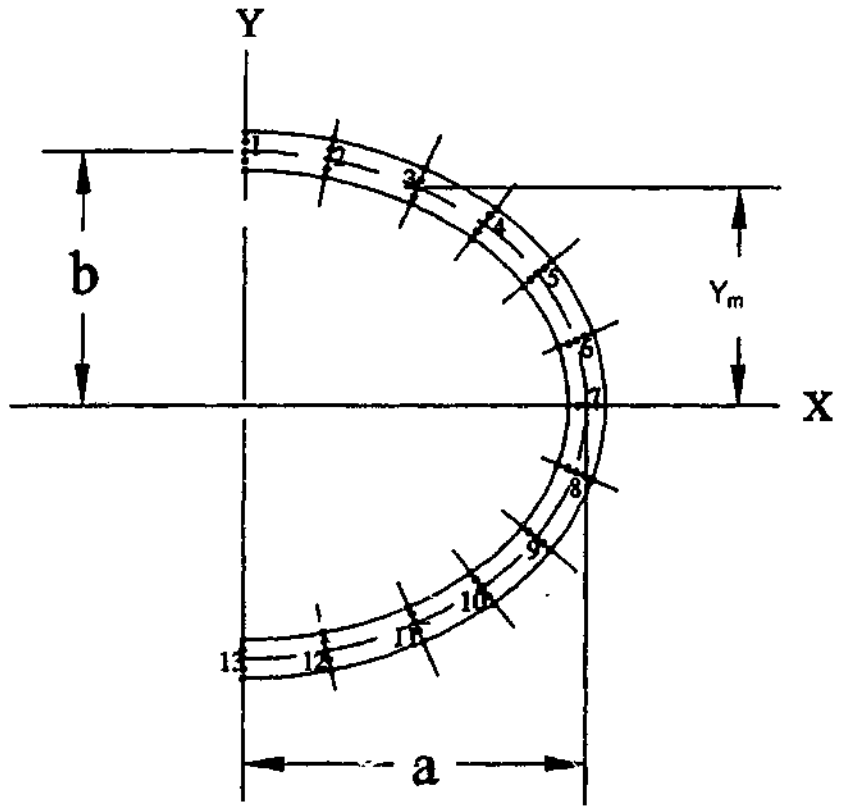

Figure E.2-1: Illustration of points on the ovalled tube section for calculation

(4) Calculate the total work. The arc length on the ellipse is calculated by using elliptic integral of the second kind. The arc length s was expressed by Gellert et al. (1977) as:

$$s = a\int_0^{\phi}\sqrt{1-k^2\sin^2\phi}\,d\phi = a(\varphi - \frac{k^2}{2}\int_0^{\phi}\sin^2\phi d\phi - \frac{k^4}{2\cdot 4}\int_0^{\phi}\sin^4\phi d\phi - \cdots)$$
$$= a(\phi - \frac{k^2}{2}(\frac{\phi}{2} - \frac{1}{4}\sin 2\phi) - \frac{k^4}{2\cdot 4}(\frac{3}{8}\phi - \frac{\sin 2\phi}{4} + \frac{\sin 4\phi}{32}) - \cdots) \qquad \text{(E.2-3)}$$

where ϕ is the angle shown in Figure E.2-2.

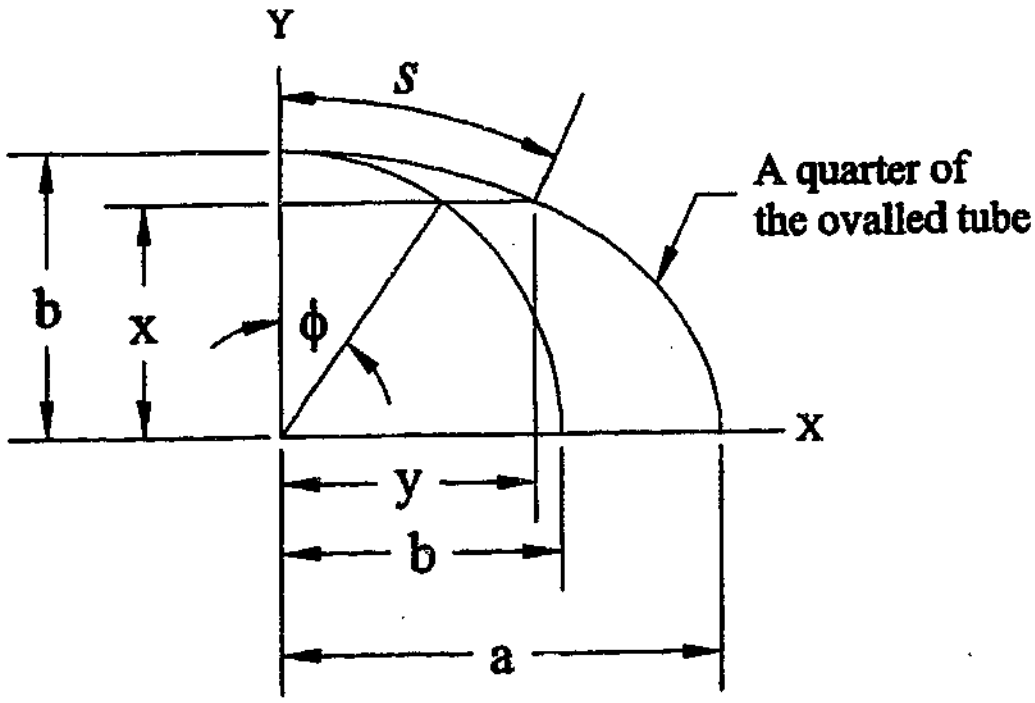

Figure E.2-2: Illustration of elliptic integral for the arc length

The Ramberg-Osgood expression proposed by Ramberg and Osgood (1943) was used for the stress-strain relations of VHS tubes:

$$\varepsilon = \frac{\sigma}{E_0} + 0.002(\frac{\sigma}{\sigma_{0.2}})^n \qquad \text{(E.2-4)}$$

here E_o is the Young's modules. Based on the test results in Chapter 3, E_o=198 GPa and n=22 was selected. The experimental stress-strain curves and the curve of Ramberg-Osgood expression are shown in Figure E.2-3.

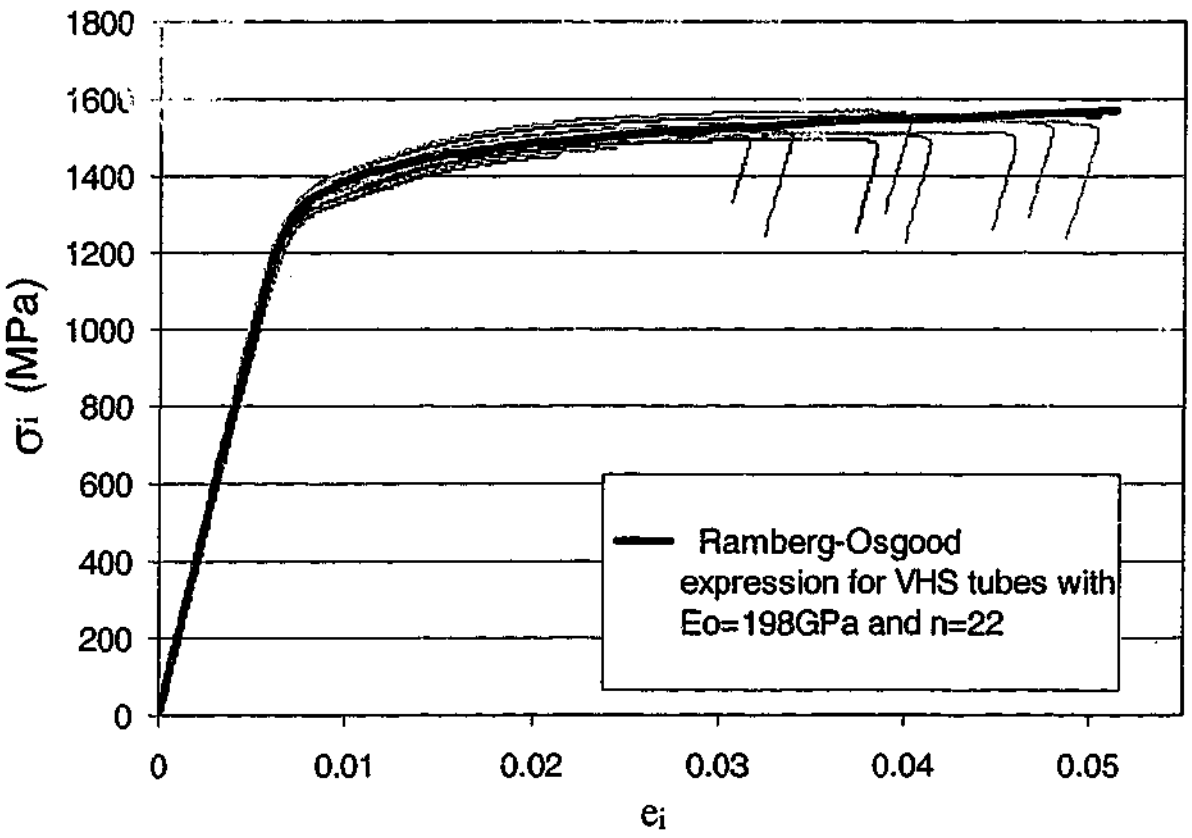

Figure E.2-3: The experimental stress strain curves and the Ramberg-Osgood expression of stress-strain curve for VHS tubes

Poisson's ratio μ is defined as:

$$\mu = -\frac{\varepsilon_x}{\varepsilon_y} \qquad \text{(E.2-5)}$$

Based on the strains of ε_x and ε_y measured from the strain rosette in section (8.2-2), the Poisson's ratio of VHS tubes is plotted in Figure E.2-4 against the stress. It can be seen from Figure E.2-4 that in the elastic range, i.e. σ_i less than 1200MPa, μ is about 0.25. However, in the plastic range, it increases with the increase of the stress. A linear expression is used to simplify the relationship between Poisson's ratio and the stress in the plastic range as:

$$\mu = 0.00049\sigma_i - 0.3622 \qquad (\sigma_i > 1248\text{MPa}) \qquad \text{(E.2-6)}$$

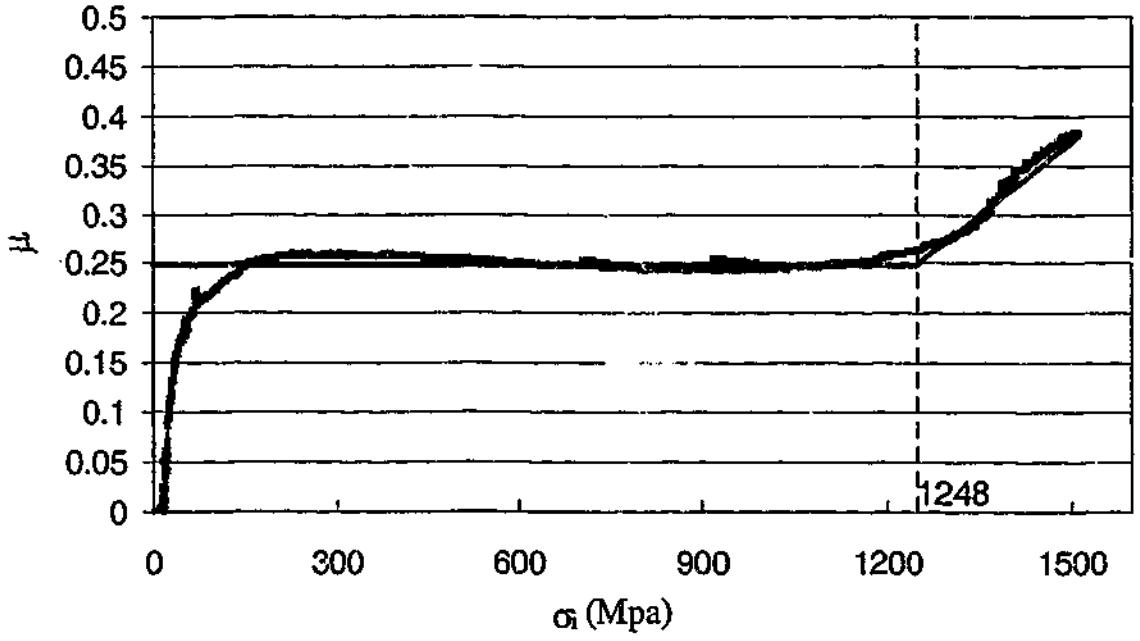

Figure E.2-4: Poisson's ratio versus stress (σ_i)

The correct ovalisation for the given ρ is obtained when the work is minimum. Therefore, the above process is repeated until the minimum is obtained. The calculated ovalisation of VHS tubes is shown in Figure 8.5-2 of Chapter 8.

E.3 COMPUTER PROGRAM CODE TO PERFORM OVALISATION OF VHS TUBES IN BENDING.

The following computer program is written in Java language – Java Development Kit 1.3.1 to perform the ovalisation of VHS tubes in pure bending:

```
import java.io.*;
/**
 * This is the controller class for Ovalisation analysis
 * of VHS tubes in pure bending.
 * Input variables: tube diameter, wall thickness and
 * the largest bending curvature.
 * Output: the ovalled dimensions of VHS tubes (a and b)
 * @
 * PUBLIC FEATURES:
 *  // Methods:
 *  public static void main(String [] args)
 *        public static void elipseModel()
 *        public static double b(double r, double a)
 *        public static double pointWork(double r, double a,double b,
 *                                       double rou, double l,double ksi,boolean up)
 *        public static double simpson(double [ ] value, double h)
 *        public static double stress(double e)
 *        public static final void writeToTextFile(String out)
 * * COLLABORATORS:
 * Utils.
 * @version 1.0,
 *
 */

public class Arc
{
        private static String eei;
        private static int failedPos1=0, failedPos2=0;
        private static StringBuffer buf = new StringBuffer();
        private static double [] r={ 18.188, 18.037, 27.787, 37.180};
        //radius of VHS tube
        private static double [] ksi={ 0.445, 0.496, 0.394, 0.397};
        //one forth of wall thickness
        private static double [] rouMin={ 420.2, 382.7, 1094.1, 1919.4};
        //minimum radius of curvature
        private static double bB;//length of short axis of elipse
        public static void main(String [] args)
        {
                elipseModel();
        }

  /**
   * Start the analysis process
   * The total curvature is divided into 10 increments.
   * For each given curvature, the total work is calculated
   * The ellipse dimension a and b that corresponding to the
   * minimum work are obtained.
   * The accuracy for the work calculation is 0.00001.
   */
        public static void elipseModel()
```

```
{
        double [] aA=new double[9];
        double rou, a, l, wholeWork, firstWork, secondWork;
        for(int i=0; i<4; i++)      //4 tubes
        {
                buf.append("Tube number "+(i+4)+"\n");
                buf.append("k/ku     a       b      RL
                   RS      DD  "+"\n");
                eei=null;
                l=Math.PI*2*r[i]/24;
                for(int j=1; j<10; j++)
                //10 Curvature-Ovalisation values are calculated
                {

                        int jj=1;
                        if(j==1)
                        a=r[i]+0.1;
                        else
                        a=r[i]+0.1;
                        rou=rouMin[i]*10/j;
                        wholeWork=1000000.0;
                        do
                        {
                                aA[j-1]=a;
                                bB=Arc.b(r[i],a);
                                firstWork=wholeWork;
                                wholeWork=wholeElipseWork(a, i, l, rou, bB);
                                if(wholeWork<0.0){
                                buf.append("Tube failed at curvature "+Utils.
                                format(rouMin[i]/rou,5,2)+
                                        "at position "+failedPos1+", "+failedPos2+", at
                                        "+eei+"\n");
                                        firstWork=wholeWork;
                                }
                                else
                                {
                                        if(wholeWork<firstWork)
                                        a=a+0.1/jj;
                                        else
                                        {
                                                a=a-0.1/jj+0.01/jj;
                                                secondWork=wholeElipseWork(a,   i,   l,
rou, bB);

                                                if(secondWork>firstWork)
                                                a=a-0.1/jj;
                                                jj=jj*10;
                                        }
                                }
                        }while(Math.abs(firstWork-wholeWork)>0.00001);
                        if(eei!=null)
                        {
                                j=10;
                        }
                        else
                        buf.append(Utils.format(rouMin[i]/rou,3,1)+Utils.format(
                                aA[j-1],10,2)+Utils.format(bB,10,2)+Utils.format((
                                        aA[j-1]+ksi[i]*2.0)*2.0,10,2)+Utils.format((bB+
                                        ksi[i]*2 0)*2.0,10,2)+Utils.format((100.0*((aA[j-
1]+
                                ksi[i]*2.0)*2.0-(bB+ksi[i]*2.0)*2.0)/(r[i]+ksi[i]*2.0)/
                                2.0),10,2)+"\n");


                                Appendix E
```

```
                    }
                    writeToTextFile(buf.toString());

                }

        }

/**
 * Calculate the work of the whole ellipse at given curvature
 * @param a and b of the ellipse, tube number i, arc length and
 * radius of curvature
 * @return the whole work
 */

        private static double wholeElipseWork(double a, int i, double l,
        double rou, double bB)
        {
                double [] workSection= new double[5];
                double [] workElipse=new double[14];
                double [][] work=new double[5][13];
                for(int k=0; k<7; k++)      //7 sections for each up quauter of elipse
                {
                        for(int kk=0; kk<5; kk++)//5 points on each section
                        {
                                work[kk][k]=Arc.pointWork(r[i], a, bB, rou, l, ksi[i]*(kk-2), true);
                                if(work[kk][k]<0)
                                {
                                        failedPos1=k;
                                        failedPos2=kk;
                                        eei="Up compression side";
                                        return -1.0;
                                }
                        }
                }
                for(int k=6; k<13; k++)    //7 sections for each down quauter of elipse
                {
                        for(int kk=0; kk<5; kk++)//5 points on each section
                        {
                                work[kk][k]=Arc.pointWork(r[i], a, bB, rou, l, ksi[i]*(kk-2), false);
                                if(work[kk][k]<0)
                                {
                                        failedPos1=k;
                                        failedPos2=kk;
                                        eei="Down Tension side";
                                        return -1.0;
                                }

                        }
                }
                for(int k=0; k<13; k++)    // quauter of elipse
                {
                        for(int kk=0; kk<5; kk++)
                        {
                                workSection[kk]=work[kk][k];

                        }
                        workElipse[k]=Arc.simpson(workSection, ksi[i]);
                }
                return simpson(workElipse, l)*2;
        }
```

```
/**
 * Calculate the angle (from the short axis to the position of arc length l
 * @param arc length l, radius of tube, long axis length a of the ellipse
 * @return the angle f
 */

        public static double angle(double l, double r,double a)
        {
                double fi, s, angle;
                fi=0.1;
                int i=1;
                do
                {
                        s=l(r,a,fi);
                        angle=fi;
                        if(l-s<0)
                        {
                                fi=fi-0.1/i+0.01/i;
                                i=i*10;
                        }
                        else
                        fi=fi+0.1/i;
                }while(Math.abs(l-s)>0.00001);
                return angle;
        }

/**
 * Calculate the length of the short axis, b of the ellipse
 * @param radius of tube, long axis length a of the ellipse
 */


        public static double b(double r, double a)
        {
                double cc, b, bb=0.0,h2, c;
                int i=1;
                b=r;
                do
                {
                        c=2*Math.PI*r;
                        h2=1-b*b/a/a;
                        cc=Math.PI*2*a*(1.0-h2/4.0-3.0/64.0*h2*h2-5.0/256.0*h2*h2*h2-
                                89.0/8192.0*h2*h2*h2*h2-231.0/32768.0*h2*h2*h2*h2*h2);
                        bb=b;
                        if(c-cc>0)
                        {
                                b=b+1.0/i-0.1/i;
                                i=i*10;
                        }
                        else
                        b=b-1.0/i;
                }while(Math.abs(c-cc)>0.00001);
                return bb;

        }

/**
 * Calculate the arc length of a ellipse
 * @param radius of tube, long axis length a of the ellipse
 * the angle ϕ
 */
```

```
    private static double l(double r, double a, double fi)
    {
            double s,b,kk,ss,k;
            double [] sinNx=new double[100];
            b=Arc.b(r,a);
            k=Math.sqrt(1-b*b/a/a);
            sinNx[0]=-Math.cos(fi)+(Math.pow(Math.cos(fi),3))/3.0;
            sinNx[1]=fi*3/8-(Math.sin(fi*2))/4+(Math.sin(fi*4))/32;
            for(int i=2;i<100;i++)
            {
                    sinNx[i]=-(Math.pow(Math.sin(fi),1+2)*Math.cos(fi)/(i+3))+
                    sinNx[i-2]*(i+2)/(i+3);
            }
            kk=k*k*k*k/2/4;
            ss=fi-k*k/2*(fi/2-(Math.sin(fi*2))/4)-kk*sinNx[1];
            for(int i=1;i<50;i++)
            {
                    kk=kk*(2*i+1)/(2*i+4)*k*k;
                    ss=ss-kk*sinNx[2*i+1];
            }
            s=a*ss;
            return s;
    }

/**
 * Calculate stress based on the given strain for VHS tube
 * @param strain e
 */


    public static double stress(double e)
    {
            double stress, ei, f, si;
            int i=1;
            si=0.0;
            do
            {
                    ei=si/198400+0.002*Math.pow((si/1365),22);
                    f=e-ei;
                    stress=si;
                    if(f<0)
                    {
                            si=si-10.0/i+1.0/i;
                            i=i*10;
                    }
                    else
                    si=si+10.0/i;
            } while(Math.abs(f)>0.00001);
            return stress;
    }

/**
 * Calculate the work of one point
 * @param radius of tube, long axis length a and short length b
 * of the ellipse, radius of curvature, arc length l, a quarter
 * of the wall thickness
 */

    public static double pointWork(double r, double a,double b,
```

```
                                                    double rou, double l,double ksi,boolean
up)
{
        double ym, eL, eT, mu, ei, muu, stress1 ,stress2;
        mu=0.25;
        muu=0.25;
        ym=b*Math.cos(Arc.angle(l,r,a));
        if(up)
        eL=-(ym+ksi*1.0/Math.sqrt((b*b/a/a+1)*(1.0-ym*ym/b/b)/(ym*ym/b/b)))/rou;
        else
        eL=(ym+ksi*1.0/Math.sqrt((b*b/a/a+1)*(1.0-ym*ym/b/b)/(ym*ym/b/b)))/rou;
        do
        {
                eT=ksi*(a*b/Math.pow(b*b-ym*ym+a*a/b/b*ym*ym,1.5)-1.0/r)-mu*eL;
                ei=Math.sqrt(1.0/(1.0-mu*mu)*(eL*eL+eT*eT+2.0*mu*eL*eT));

                if(ei>0.006539344)
                {
                        muu=mu;
                        mu=0.000485*(Arc.stress(ei)-1245)+0.25;
                }
        }while(Math.abs(mu-muu)>0.00001);
        if(eL>0.05 ||eT>0.05)
        {
                return -1.0;
        }
        else
        {
        stress1=Arc.stress(Math.abs(eL));
        stress2=Arc.stress(Math.abs(eT));
        return stress1*stress1*(1.0/198400/2+0.002*22/23/Math.pow(
                1365,22)*Math.pow(stress1,21))+
        stress2*stress2*(1.0/198400/2+0.002*22/23/Math.pow(1365,22)
        *Math.pow(stress2,21));
                }
        }


        /**
         * Simpson's rule of integration
         * @param the interval of h
         */
        public static double simpson(double [] value, double h)
        {
                int j=value.length;
                double sum=0.0;
                for(int i=0; i<(j-1)/2; i++)
                {
                        sum=sum+value[2*i]+value[2*i+1]*4+value[2*i+2];
                }
                return sum*h/3;

        }

public static final void writeToTextFile(String out)
{
   PrintWriter output;
   try
   {
      output = new PrintWriter(new FileWriter("out.txt"));
      output.println(out);
```

```
            output.close();
        }
        catch (IOException e)
        {
        }
    }
}
```

The collaborating class, Utils, for formatting the output numbers in the above program was written by Allen et al. (2000). The Java code of Utils (Allen et al. 2000) is listed as follows:

```
/** Utils
 *  String and number formatting utlities
 *  (vsn 1.3) format (double ..) corrected for large numbers
 *  (vsn 1.4) format (double ..): suppress decimal point if decimals==0
 * @
 *
 * PUBLIC FEATURES:
 *  // Data
 *  public final static int intNaN   // -2^31
 *  public final static long longNaN  // -2^63
 *
 *  // Methods
 *  public static String pad(String str, int width)
 *  // if str.length < width then returns str padded with spaces
 *  // on the right, else returns str truncated. result.length = width
 *  // Pre: width > 0
 *
 *  public static String format(long num, int width)
 *  // Returns decimal string representation of num, right-justified
 *  // in a field with preferred width 'width' characters.
 *  // Can be used with any integral data type
 *  // Pre: width > 0
 *
 *  public static String format(double num, int width, int decimals)
 *  // Returns a decimal string representation of num, right-justified
 *  // in a field with preferred width 'width' characters and 'decimals'
 *  // digits after a decimal point.  No point shown if 'decimals' is 0.
 *  // For huge numbers result is E-format.
 *  // Pre: 0 <= decimals. 0 <= width
 *
 *  public static int toInt(String str)
 *  // Converts str to an integer
 *  // Returns an integer or intNaN if string is not a valid
 *  // integer representation
 *
 *  public static long toLong(String str)
 *  // Converts str to a long integer
 *  // Returns a long integer or longNaN if string is not a valid
 *  // integer representation
 *
 *  public static float toFloat(String str)
 *  // Converts str to a floating point number
 *  // Returns a float or Float.NaN if string is not a valid
 *  // floating point representation
```

```
 *
 *  public static double toDouble(String str)
 *  // Converts str to a double precision floating point number
 *  // Returns a double precision float or Double.NaN if string is not a valid
 *  // floating point representation
 *
 * COLLABORATORS:
 * -
 * MODIFIED:
* @version 1.6, 8 February 2000
*/

public class Utils
{
  // Instance Variables
  public final static int  intNaN  = Integer.MIN_VALUE;
  public final static long longNaN = Long.MIN_VALUE;

  // Methods

  /**
   if str.length < width then returns str padded with spaces
   on the right, else returns str truncated. result.length = width
   Pre: width > 0
   */
  public static String pad(String str, int width)
  {
    StringBuffer buffer = new StringBuffer(str);

    buffer.setLength(width);
    for (int i = str.length(); i < width; i++)
    {
      buffer.setCharAt(i, ' ');
    }
    return buffer.toString();
  }

  /**
   Returns decimal string representation of num, right-justified.
   Can be used with any integral data type
   Pre: width > 0
   @param num the number to convert
   @param width preferred number of characters, ie length of result.
  */
  public static String format(long num, int width)
  {
    StringBuffer buffer = new StringBuffer();
    int numOfSpaces;
    buffer.insert(0, num);  //calls toString

    numOfSpaces = width - buffer.length();
    for (int i = 1; i <= numOfSpaces; i++)
    {
      buffer.insert(0, ' ');
    }
    return buffer.toString();
  }

  /**
   Returns a decimal string representation of num, right-justified
   with decimal places.
```

```
  (If num cannot be treated internally as a long then only 6 significant
  digits will be shown using e notation.[16 digits JDK1.1])
  ([version 1.5, 3 May 1999 rka: preserve NaN).
<br>Pre: 0 <= decimals, 0 <= width
  @param num the number to convert
  @param width is preferred number of characters, ie length of result.
  @param decimals is number of digits after decimal point.  if zero then
   no point will be shown  [version 1.4]
 */
public static String format(double num, int width, int decimals)
{
   StringBuffer buffer;
   String       temp;
   int expIndex;
   int pointIndex;
   int numDecimals;
   int numOfSpaces;
   double exp, number;

   if (num == Double.NaN)
   {
      return pad("NaN", width);
   }
   exp = Math.pow(10.0, decimals);
   if (num*exp <= Long.MIN_VALUE/2 || num*exp >= Long.MAX_VALUE/2)
   {
      temp = Double.toString(num);
      // Exponent form, do not modify representation
      buffer = new StringBuffer(temp);
   }
   else
   {
      // Round to required decimal places by scaling up
      if (num < 0.0)
         number = -Math.round(-(num * exp));
      else
         number = Math.round(num * exp);
      long n = (long)number;

      long iexp = (long)Math.round(exp);
      long frac = (n < 0 ? -n%iexp : n%iexp);  // >=0

      buffer = new StringBuffer();
      buffer.insert(0, n / iexp);      // whole number part
      if (n / iexp == 0 && n < 0)
         buffer.insert(0, '-');
      if (decimals > 0)
         buffer.append('.');

      while (iexp > 1)                 // loop for decimals
      {
         iexp = iexp / 10;
         buffer.append(frac / iexp);   // single digit
         frac = frac % iexp;
      }
   }

   // Add leading spaces if required
   numOfSpaces = width - buffer.length();
   for (int i = 0; i < numOfSpaces; i++)
   {
```

```
      buffer.insert(0, ' ');
    }
    return buffer.toString();
}


/**
 * Converts str to an integer
 * @return an integer or intNaN if string is not a valid integer representation
 */
public static int toInt(String str)

{
    int     result;

    try
    {
        result = Integer.parseInt(str);
    }
    catch(NumberFormatException e)
    {
        result = intNaN;
    }
    return result;
}

/**
 * Converts str to a long integer
 * @return a long integer or longNaN if string is not a valid
 * integer representation
 */
public static long toLong(String str)
{
    long result;

    try
    {
        result = Long.parseLong(str);
    }
    catch(NumberFormatException e)
    {
        result = longNaN;
    }
    return result;
}

/**
 * Converts str to a floating point number
 * @return a float or Float.NaN if string is not a valid
 * floating point representation
 */
public static float toFloat(String str)
{
    Float num;
    float result;

    try
    {
        num = new Float(str.trim());
        result = num.floatValue();
    }
```

```
        catch(NumberFormatException e)
        {
          result = Float.NaN;
        }
        return result;
      }

      /**
       * Converts str to a double precision floating point number
       * @return a double precision float or Double.NaN if string is not a valid
       *  floating point representation
       */
      public static double toDouble(String str)
      {
        Double num;
        double result;

        try
        {
          num = new Double(str.trim());
          result = num.doubleValue();
        }
        catch(NumberFormatException e)
        {
          result = Double.NaN;
        }
        return result;
      }
    } // end Utils
```

E.4 DESCRIPTION OF THE PROGRAM

The following description about the above computer program is generated by Java document tool.

Public class **Arc** extends java.lang.Object

This is the controller class for Ovalisation analysis of VHS tubes in pure bending. Input variables: tube diameter, wall thickness and the largest bending curvature. Output: the ovalled dimensions of VHS tubes (a and b)

Constructor Summary
Arc()

Method Summary	
static double	**angle**(double l, double r, double a) Calculate the angle (from the short axis to the position of arc length l
static double	**b**(double r, double a) Calculate the length of the short axis, b of the ellipse

static void	**elipseModel**() Start the analysis process The total curvature is divided into 10 increments.
static void	**main**(java.lang.String[] args)
static double	**pointWork**(double r, double a, double b, double rou, double l, double ksi, boolean up) Calculate the work of one point
static double	**simpson**(double[] value, double h) Simpson's rule of integration
static double	**stress**(double e) Calculate stress based on the given strain for VHS tube
static void	**writeToTextFile**(java.lang.String out)

Methods inherited from class java.lang.Object
clone, equals, finalize, getClass, hashCode, notify, notifyAll, toString, wait, wait, wait

Constructor Detail

Arc

public **Arc**()

Method Detail

main

public static void **main**(java.lang.String[] args)

---

elipseModel

public static void **elipseModel**()

Start the analysis process. The total curvature is divided into 10 increments. For each given curvature, the total work is calculated The ellipse dimension a and b that corresponding to the minimum work are obtained. The accuracy for the work calculation is 0.00001.

---

angle

public static double **angle**(double l, double r, double a)

Calculate the angle (from the short axis to the position of arc length l

Parameters: arc - length l, radius of tube, long axis length a of the ellipse

Returns: the angle f

---

b

public static double **b**(double r, double a)

Calculate the length of the short axis, b of the ellipse

Parameters: radius of tube, long axis length a of the ellipse

---

stress

public static double **stress**(double e)

Calculate stress based on the given strain for VHS tube

Parameters: strain ε

---

pointWork

public static double **pointWork**(double r, double a, double b, double rou, double l, double ksi, boolean up)

Calculate the work of one point

Parameters: radius of tube, long axis length a and short length b of the ellipse, radius of curvature, arc length l, a quarter of the wall thickness

---

simpson

public static double **simpson**(double[ ] value, double h)

Simpson's rule of integration

Parameters: the interval of h

---

writeToTextFile

public static final void **writeToTextFile**(java.lang.String out)

The description of Class Utils generated by Java document tool is listed as follows:

---

public class **Utils**

extends java.lang.Object

Utils String and number formatting utlities (vsn 1.3) format (double ..) corrected for large numbers (vsn 1.4) format (double ..): suppress decimal point if decimals==0

Field Summary	
static int	**intNaN**
static long	**longNaN**

Constructor Summary	
Utils()	

Method Summary	
static java.lang.String	**format**(double num, int width, int decimals) Returns a decimal string representation of num, right-justified with decimal places.
static java.lang.String	**format**(long num, int width) Returns decimal string representation of num, right-justified.
static java.lang.String	**pad**(java.lang.String str, int width) if str.length < width then returns str padded with spaces on the right, else returns str truncated.
static double	**toDouble**(java.lang.String str) Converts str to a double precision floating point number
static float	**toFloat**(java.lang.String str) Converts str to a floating point number

static int	**toInt**(java.lang.String str) Converts str to an integer
static long	**toLong**(java.lang.String str) Converts str to a long integer

Methods inherited from class java.lang.Object
clone, equals, finalize, getClass, hashCode, notify, notifyAll, toString, wait, wait, wait

Field Detail

intNaN

public static final int intNaN

---

longNaN

public static final long longNaN

Constructor Detail

Utils

public Utils()

Method Detail

pad

public static java.lang.String pad(java.lang.String str, int width)

if str.length < width then returns str padded with spaces on the right, else returns str truncated. result.length = width Pre: width > 0

---

format

public static java.lang.String format(long num, int width)

Returns decimal string representation of num, right-justified. Can be used with any integral data type Pre: width > 0

Parameters:

num - the number to convert

width - preferred number of characters, ie length of result.

---

format

public static java.lang.String format(double num, int width, int decimals)

Returns a decimal string representation of num, right-justified with decimal places. (If num cannot be treated internally as a long then only 6 significant digits will be shown using e notation.[16 digits JDK1.1]) ([version 1.5, 3 May 1999 rka: preserve NaN). Pre: 0 <= decimals, 0 <= width

Parameters:

num - the number to convert

width - is preferred number of characters, ie length of result.

decimals - is number of digits after decimal point. if zero then no point will be shown [version 1.4]

---

toInt

public static int toInt(java.lang.String str)

Converts str to an integer

Returns:

An integer or intNaN if string is not a valid integer representation

---

toLong

public static long toLong(java.lang.String str)

Converts str to a long integer

Returns:

A long integer or longNaN if string is not a valid integer representation

---

toFloat

public static float toFloat(java.lang.String str)

Converts str to a floating point number

Returns:

A float or Float.NaN if string is not a valid floating point representation

---

toDouble

public static double toDouble(java.lang.String str)

Converts str to a double precision floating point number

Returns:

A double precision float or Double.NaN if string is not a valid floating point representation

APPENDIX F

F.1 SPECIMEN DESIGN DRAWINGS

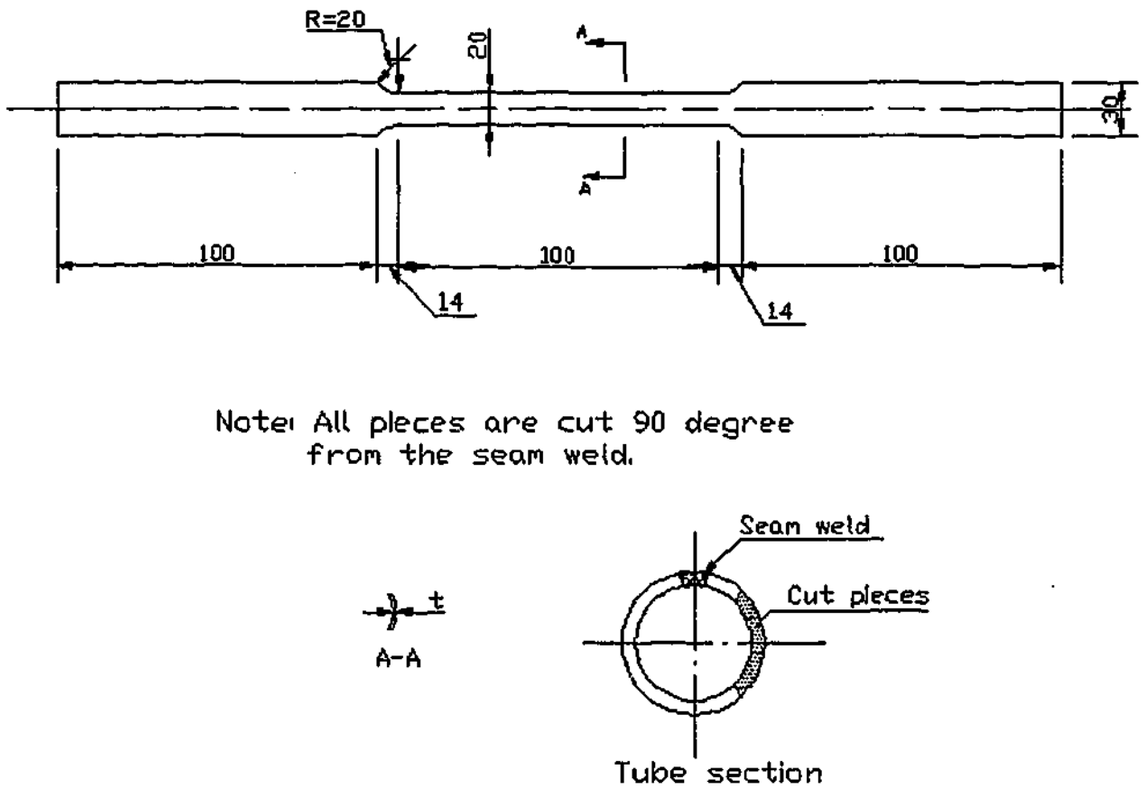

Figure F.1-1: Design of tensile coupon specimen

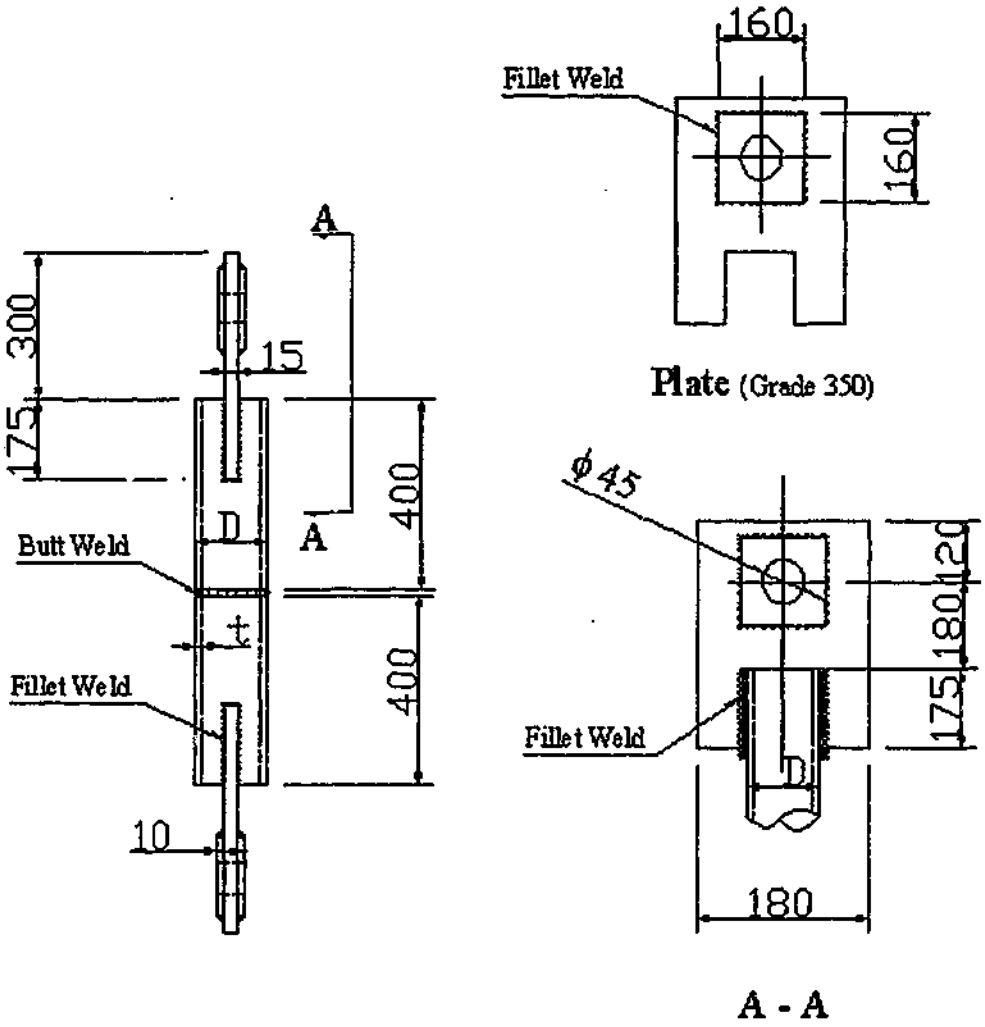

Figure F.1-2: Design of butt-welded VHS tubes with a diameter over 38mm

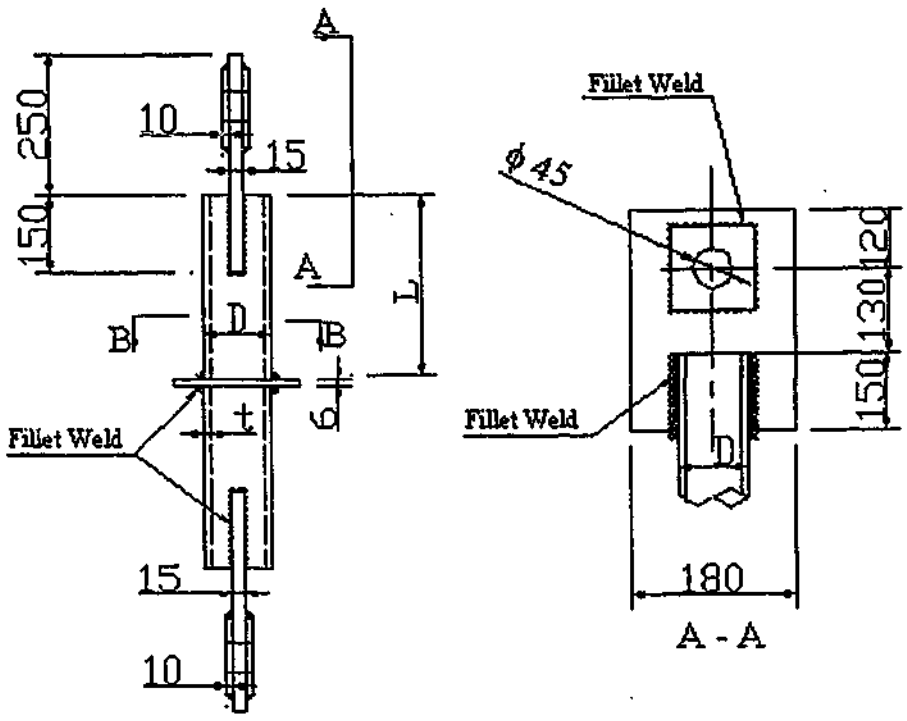

Figure F.1-3: Design of transverse fillet welded VHS tubes with a diameter over 38mm

F.2 EXPERIMENTAL PHOTOGRAPHS

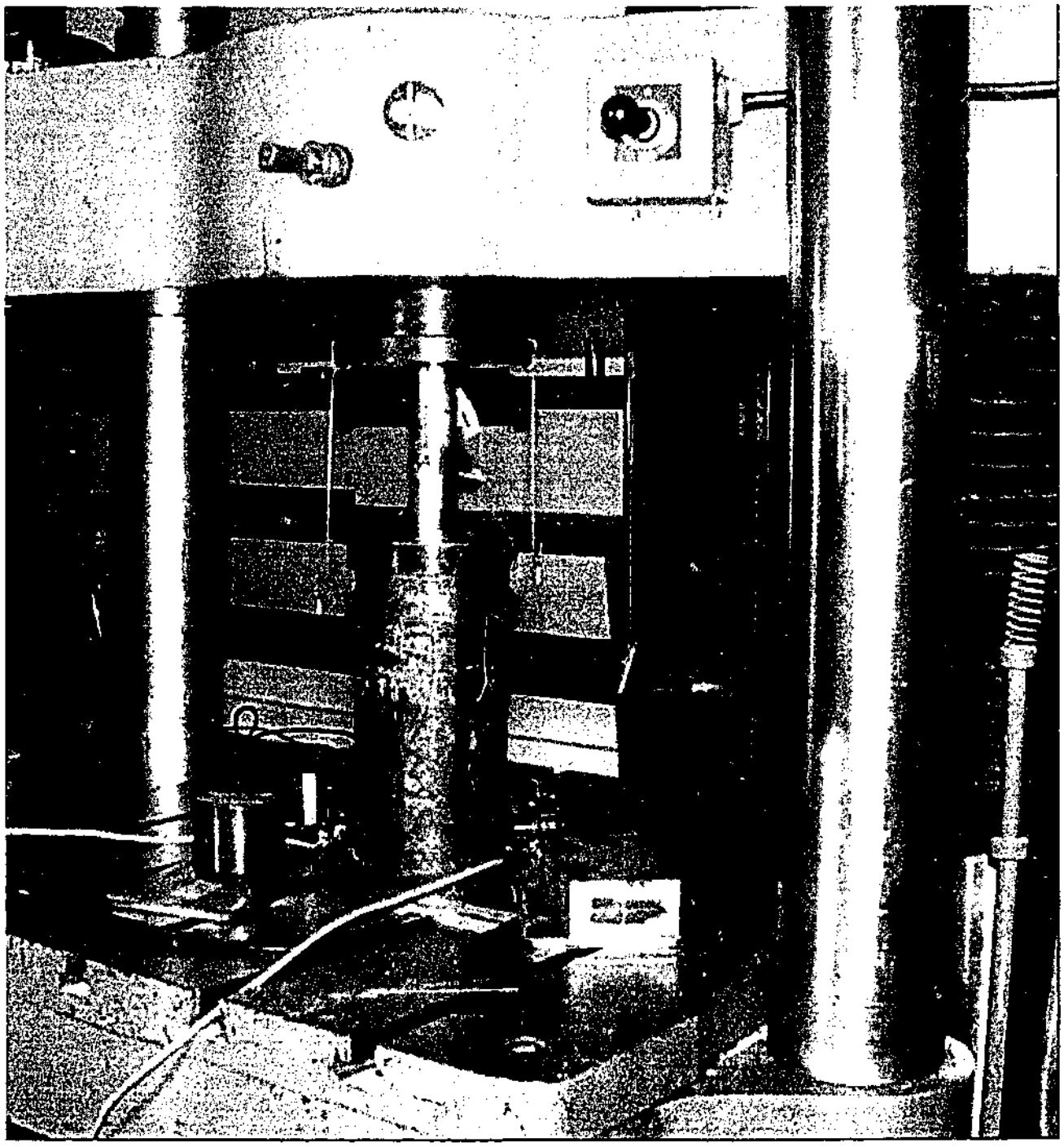

Figure F.2-1: A stub column under compression test

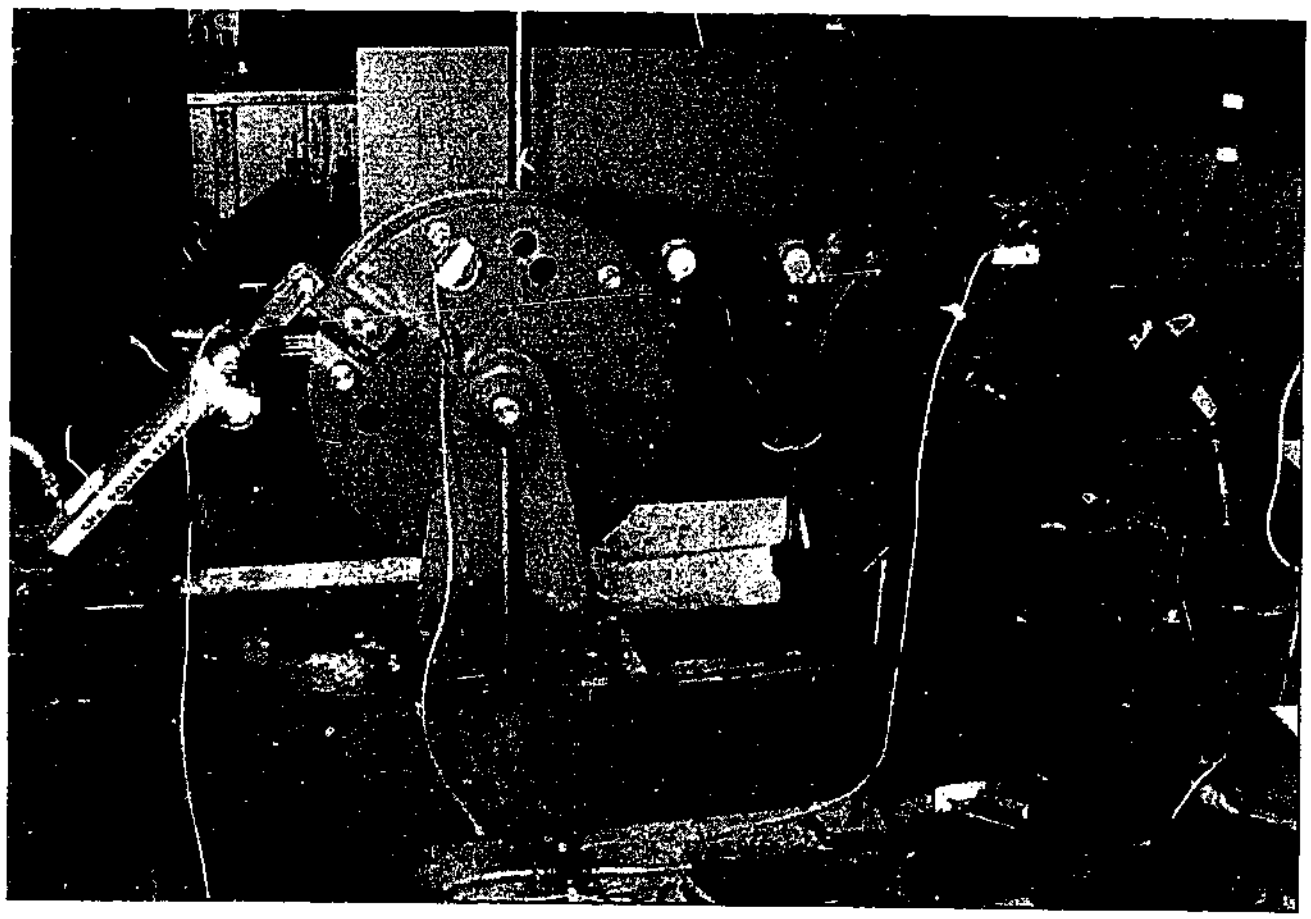

Figure F.2-2: A VHS tube in the pure bending rig

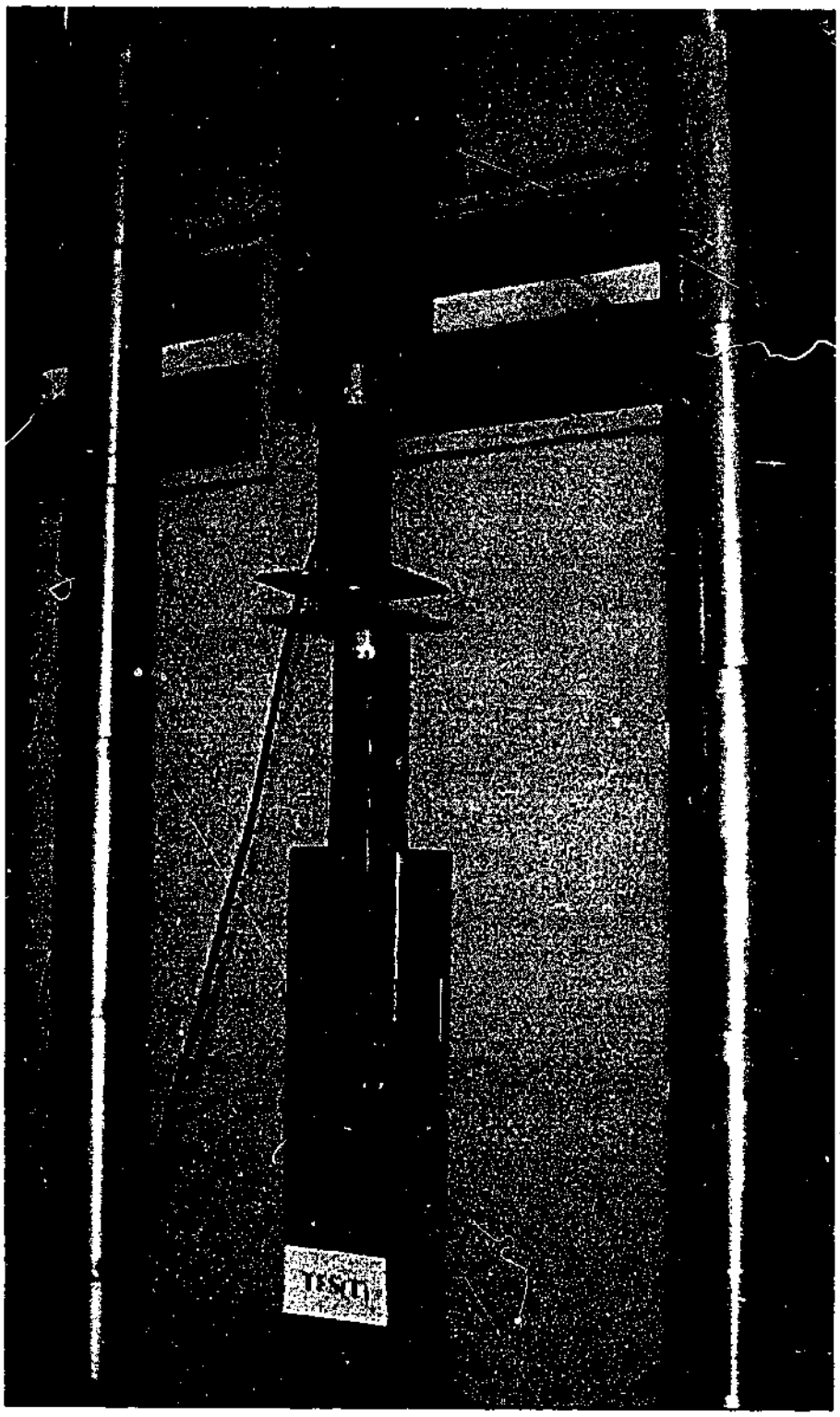

Figure F.2-3: A transverse fillet welded specimen during test

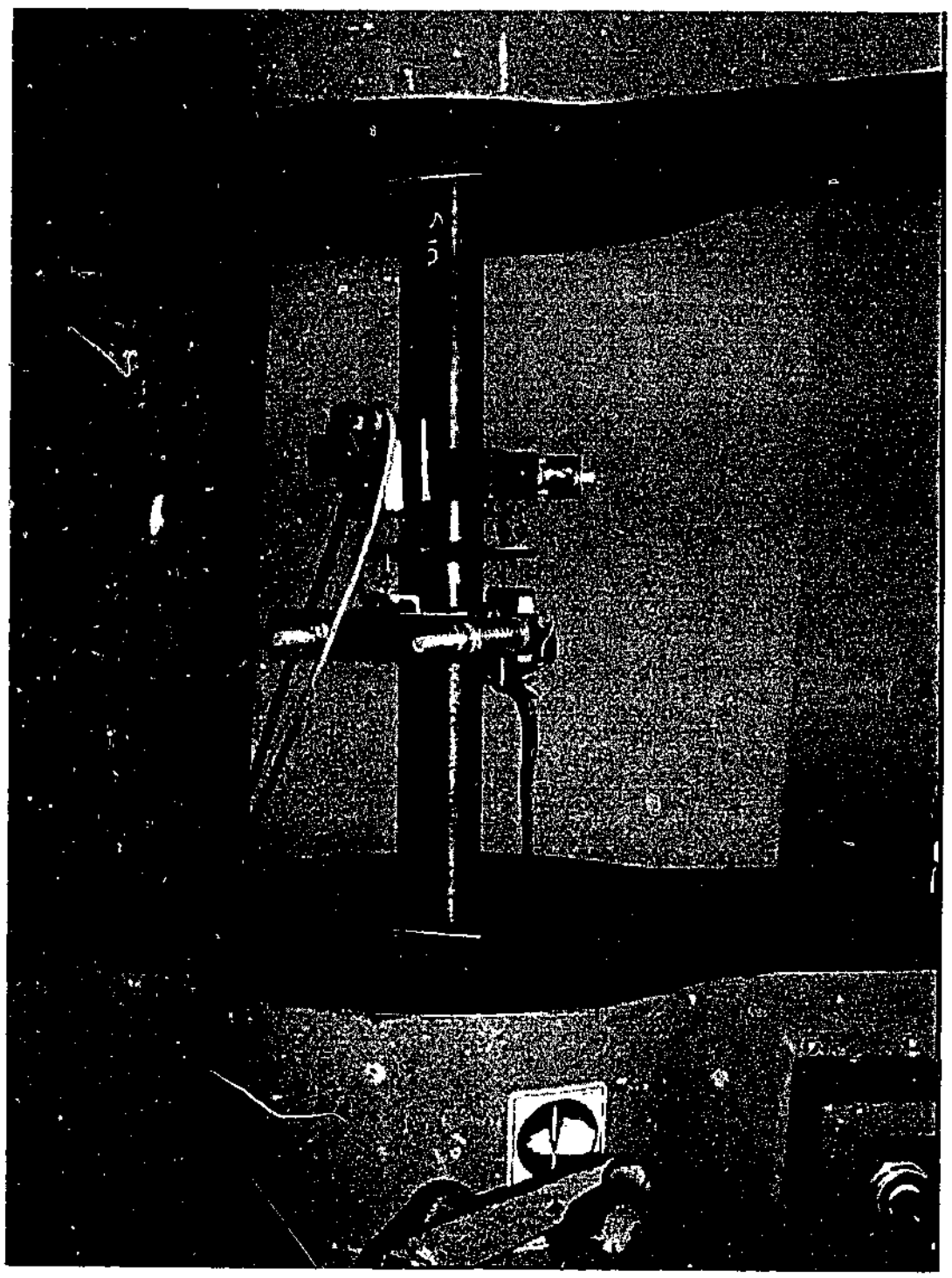

Figure F.2-4: A transverse fillet welded VHS tube in the Baldwin testing machine with the displacement measurement device made by Civil Engineering Department.

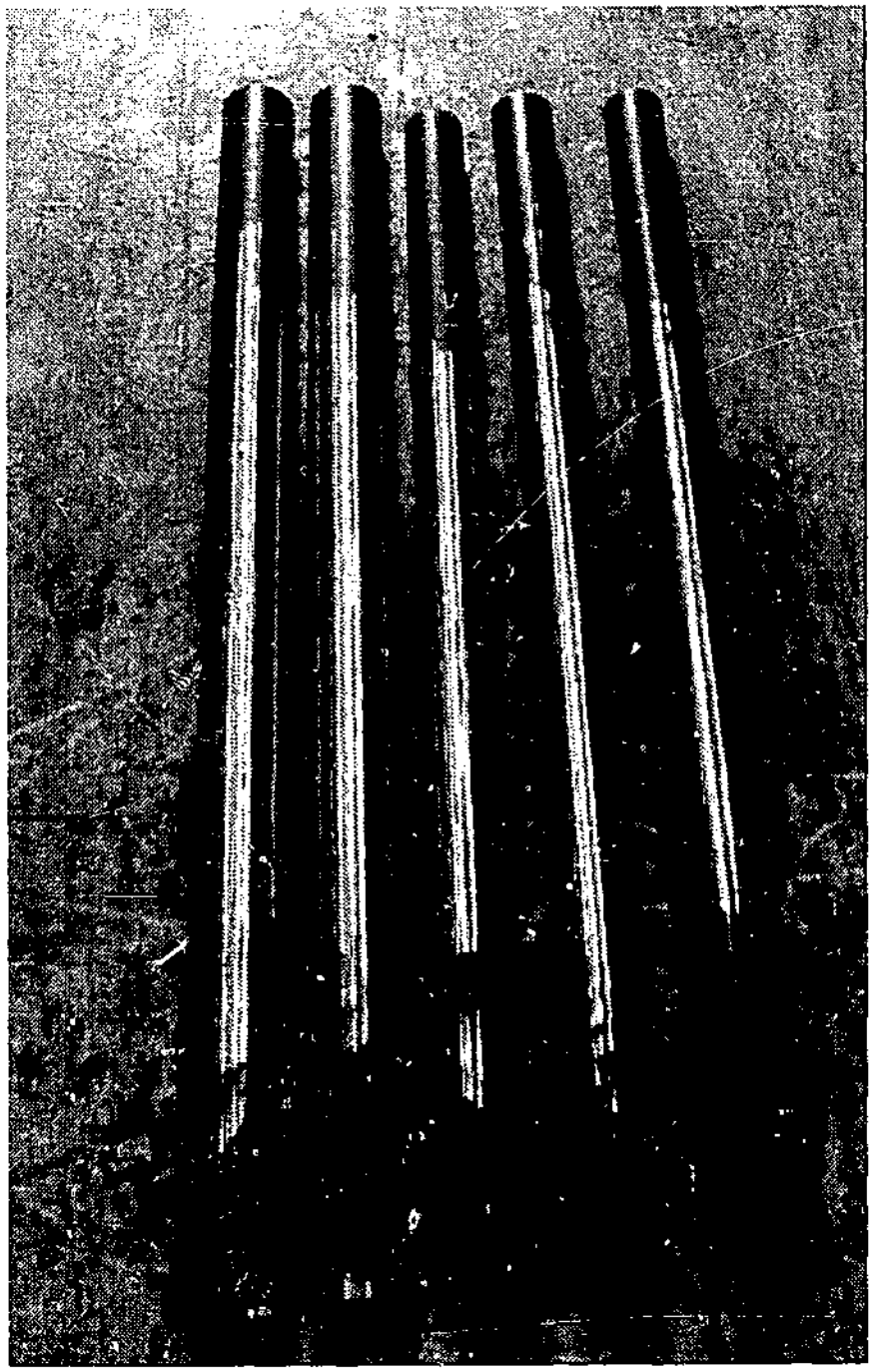

Figure F.2-5: The Surface of VHS tubes were abraded with emery cloth before applying CFRP and epoxy resin

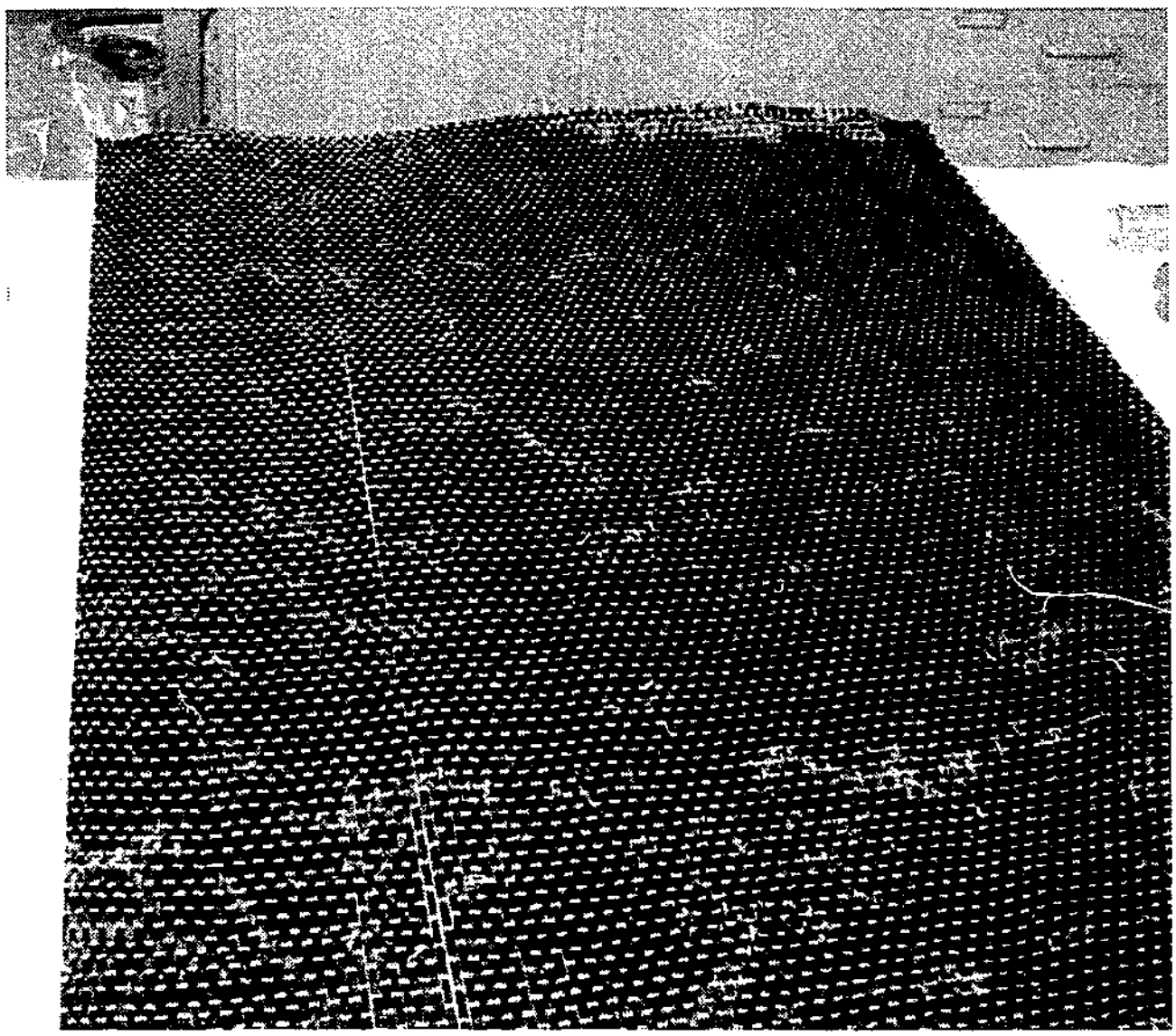

Figure F.2-6: A layer of CFRP produced by Sika Pty. Ltd. Australia for strengthening butt-welded VHS tubes